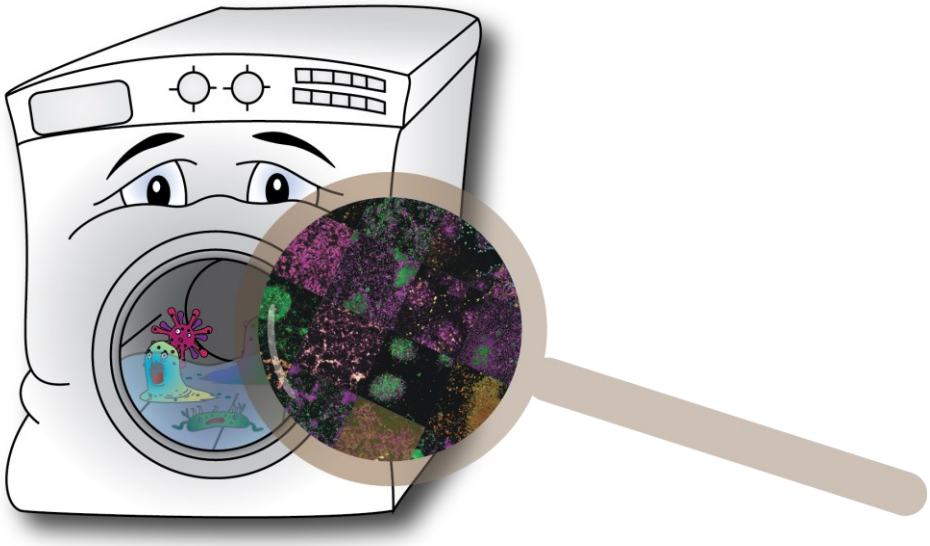
Investigating microbial biofilms within washing machines: Novel nanosensor technology enables insights into pH gradients of *Pseudomonas aeruginosa* biofilms



Birte Hollmann

Thesis submitted to the University of Nottingham

for the degree of Doctor of Philosophy

September 2020

Declaration

I hereby declare that this thesis is my own work unless otherwise acknowledged. The thesis has not been submitted in whole or in part for any other degree to another University.



Abstract

Biofilms are communities of microorganisms that attach to various surfaces and are widely associated with infections in animals and plants. This investigation is focussed on a current and growing concern: the distribution and formation of biofilms in washing machines. Many countries wash clothes at reduced temperatures around 30°C to 40°C rather than at higher temperatures above 60°C that would kill many bacteria. Survival of the bacteria is associated with biofouling, malodour and an increased infection risk due to the distribution of human pathogens such as *Pseudomonas aeruginosa* into the environment. *P. aeruginosa* is one of the predominant bacteria found in washing machines and is highly resistant to many antibiotics.

Little is known about environmental microniches present in biofilms. This work focuses on the pH variation throughout *P. aeruginosa* biofilms knowing that the pH can influence biofilm formation and could be an important aspect for the prevention of biofilm formation. Novel pH-sensitive optical nanosensors were used that penetrate *P. aeruginosa* biofilms and emit fluorescence in response to variation in pH. Using time-lapse imaging, pH changes were tracked in real time at a microcolony and single cell level, which will ultimately facilitate monitoring of environmental changes induced as biocides penetrate biofilms. Furthermore, confocal laser scanning microscopy (CLSM) was used to reveal pH variation within single microcolonies where the core of the microcolonies was more acidic than the outside. Furthermore, a set of *P. aeruginosa* strains was isolated from household washing machines and identification confirmed by matrix-assisted laser desorption/ionization. Whole genome analysis was performed to identify different genomic features relevant to antimicrobial resistance (AMR) and biofilm formation. CLSM revealed an increased propensity of these isolates to form biofilms compared to the laboratory strain PAO1-N. In addition, the washing machine isolates had a decreased susceptibility to benzalkonium chloride, a biocide used in cleaning products as well as an increase in production of pyocyanin, a toxic substance mainly produced by *P. aeruginosa*. Furthermore, testing of different washing detergent formulations revealed that they possessed a range of abilities to disrupt biofilm formation or kill *P. aeruginosa,* which will facilitate the development of more effective washing agents to limit the emergence of AMR within biofilms resident in domestic appliances.

Acknowledgements

Above all, I would like to express my deep gratitude to my main supervisors Kim Hardie and Jon Aylott for their support and guidance over the last four years. Thank you for all your time and advice both on a professional and personal level and for providing me the opportunity to grow as a research scientist. Your advice, knowledge, ideas, and overall support have been invaluable, and I could not have asked for more supportive guidance. I would also like to acknowledge my other mentors Miguel Cámara, Paul Williams, and my industrial collaborator Katherine Thompson as well as Sara Martinez for their scientific insights, input, and support throughout my PhD. I also have to thank Unilever plc. and the University of Nottingham; without whose funding this project would not have been possible.

I would like to give special thanks to Mark and Dean for all their support and friendship as well as for all the laughs and deep discussions about sciences and more we had together. I am grateful that we started this journey together and I am sure our YouTube channel will become famous one day. In addition, I want to thank my colleague Veeren, who introduced me to the world of nanosensors and who was always up for some exciting discussions and future ideas. A big thank-you to all my other colleagues in CBS and Boots, and especially in Kim's lab, for all the support, discussions, helpful tips, and fantastic conferences we spent together. Particular thanks include Elena and James for their technical expertise and suggestions as well as my master students Jenny, Laura, and Victoria, who really helped with my project. It was a great pleasure to meet and work with you all.

I would also like to thank Karen Swift who always makes sure that our lab is running smoothly and especially Sarah English for all her help with organisation and administration issues, you are really great. I would like to acknowledge all the technical staff and in particular Robert Markus for his help with all sorts of imaging questions.

Finally, I would like to thank all my friends and family for accompany me on my way and to encourage me in all my decisions, in particular Alicia, Carina, Anne, Kushal, Calvin, and Dave. You have supported and motivated me and the friendships we have are very precious to me. Most importantly, I want to give the greatest thanks to my family, my partner, sister, brother-in-law, and especially mum and dad, for all their continuous support. I owe a lot to my family who are always there for me and who helped me at every stage of my personal and academic life. I am very thankful for that (and all the supplies of chocolate and German products), and I could not have done this work without you.

Table of Contents

Declaration ..... **i**

Abstract ..... **ii**

Acknowledgements ..... **iii**

Table of Contents ..... **iv**

List of Figures ..... **x**

List of Tables ..... **xvi**

List of Publications and Preprints ..... **xvii**

Abbreviations ..... **xviii**

Chapter 1 Introduction **1**

1.1 *Pseudomonas aeruginosa* 1

1.1.1 Virulence 2

1.1.2 Quorum sensing 6

1.2 Biofilms of *P. aeruginosa* 10

1.2.1 Formation of biofilms 12

1.2.2 Extracellular matrix 14

1.2.3 The role of biofilms in pathogenesis 19

1.2.4 Biofilm formation in washing machines 24

1.2.5 Microniches within biofilms 30

1.2.6 pH-sensitive nanosensors 32

1.2.7 Different biofilm models 37

1.3 Thesis aims 42

Chapter 2 Materials and Methods **45**

2.1 Chemicals 45

2.2 Minimal medium (M9) and lysogeny broth (LB) 45

2.3 Buffer solutions for pH-sensitive nanosensors 45

2.4 Bacterial strains and growth culture 46

2.5 Nanosensor preparation 47

2.6 Nanosensor characterisation and calibration 49

2.7 Nanosensor filter assay 51

2.8 Sampling of strains from washing machines 51

2.9 Matrix-assisted laser desorption/ionisation (MALDI) time of flight mass spectrometry (TOF-MS) strain identification 52
2.10 Whole genome sequencing 52
2.11 Whole genome sequence analysis 53
2.12 Optical density ($OD_{600\,nm}$) measurement 53
2.13 DNA extraction 53
2.14 Polymerase chain reaction (PCR) 54
2.15 Agarose gel electrophoresis 55
2.16 Phenotypic assays 55
2.16.1 Gram staining 55
2.16.2 Oxidase 55
2.16.3 Catalase 56
2.16.4 Swarming motility 57
2.16.5 Swimming motility 57
2.16.6 Protease production 58
2.16.7 Crystal violet (CV) attachment assay 59
2.16.8 Pyocyanin production 59
2.16.9 Minimal inhibitory concentration (MIC) 60
2.16.10 Growth measurement of planktonic cells 60
2.16.11 pH measurement of planktonic cells 60
2.16.12 Sugar challenge 61
2.17 Viability assay 62
2.18 Biofilm formation 62
2.18.1 Static biofilm formation 62
2.18.1.1 Supplements were added at the beginning of the experiment 63
2.18.1.2 Supplements were added after 48 h of biofilm formation during the imaging 64
2.18.2 Flow-cell biofilm formation using the BioFlux system 65
2.18.3 ConA and YOYO™-1 staining 66
2.18.4 Colony forming unit (CFU) experiments of static biofilms 67
2.19 Structured illumination microscopy (SIM) of planktonic cells 68
2.20 Scanning electron microscopy (SEM) to investigate initial attachment of bacteria 69

2.21 Widefield microscopy 69
2.22 Confocal laser scanning microscopy (CLSM) 70
2.23 Image analysis using Zen and ImageJ 70
2.24 Automated image analysis using MATLAB 70
2.25 Statistical analysis 71
Chapter 3 Preparation and characterisation of fluorescent, pH-sensitive polyacrylamide nanosensors for the use in planktonic and biofilm models of *P. aeruginosa* 72
3.1 Introduction 72
3.1.1 Background 72
3.1.2 Aims of this chapter 73
3.2 Results 74
3.2.1 Preparation and characterisation of different kinds of fluorescent polyacrylamide nanoparticles 74
3.2.2 The planktonic growth of PAO1-N is unaffected by the presence of neutral or positively charged nanosensors 77
3.2.3 Neutral and positively charged nanosensors do not enter PAO1-N cells during incubation 79
3.2.4 Depending on their charge and concentration, polyacrylamide nanoparticles affect biofilm thickness and structure differently 81
3.2.5 Both neutral and positive nanosensors can penetrate already established biofilms in a static as well as a flow-cell model 87
3.2.6 Positively charged polyacrylamide nanoparticles show interaction with biofilm components 92
3.3 Discussion 99
3.3.1 Different kinds of neutral and positively charged polyacrylamide nanoparticles can be produced in a reproducible manner 99
3.3.2 Polyacrylamide nanosensors neither influence planktonic growth of PAO1-N nor do they get internalised by the cells 100
3.3.3 Neutral and positive nanosensors show incorporation within the biofilm matrix of PAO1-N, with positively charged nanosensors promoting biofilm formation 102
3.3.4 Positively charged nanoparticles show interaction with various biofilm components 105
3.4 Conclusion 108

Chapter 4 Analysis of pH changes within planktonic cell cultures and biofilms of *P. aeruginosa* 109

4.1 Introduction 109

4.1.1 Background 109

4.1.2 Aims of this chapter 110

4.2 Results 112

4.2.1 pH-sensitive fluorescent nanosensor pH measurements are equivalent to those of commercially available devices, and are responsive to induced pH changes within biofilms 112

4.2.2 The addition of glucose reduces the pH of the growth medium when added to planktonic PAO1-N 115

4.2.3 pH changes can be observed during biofilm formation in a flow-cell system at a microcolony level using polyacrylamide nanosensors and time-lapse imaging 118

4.2.4 Examination of the pH independent dye rhodamine B as alternative to TAMRA 121

4.3 Discussion 124

4.3.1 Polyacrylamide nanosensors are pH responsive in planktonic and biofilm studies 124

4.3.2 Alternative pH-independent dyes to replace TAMRA 129

4.4 Conclusion 131

Chapter 5 Isolation and characterisation of bacteria from washing machines with a focus on *P. aeruginosa* 132

5.1 Introduction 132

5.1.1 Background 132

5.1.2 Aims of this chapter 134

5.2 Results 135

5.2.1 Various bacterial species were isolated and identified from different sections of household washing machines 135

5.2.2 Phenotypes such as growth, attachment, and antimicrobial resistance differ between washing machine isolates and the lab strain PAO1-N 138

5.2.3 Washing machine isolate WMB1.3 shows elevated pyocyanin production and biofilm formation 144

5.2.4 Whole genome sequencing reveals genotypic differences between strains 148

5.3 Discussion 160

5.3.1 A variety of bacteria was successfully isolated from three different sites of domestic washing machines 160
5.3.2 Selected *P. aeruginosa* strains exhibit different phenotypes such as production of virulence factors and antimicrobial resistance 163
5.3.2.1 Motility 164
5.3.2.2 Protease production 170
5.3.2.3 Attachment and biofilm formation 170
5.3.2.4 Antimicrobial resistance 172
5.3.2.5 Pyocyanin production 177
5.3.2.6 Lipopolysaccharides 179
5.3.2.7 pH variation within biofilms 182
5.3.3 Genome analysis reveals that different *P. aeruginosa* strains co-develop within the same washing machine 183
5.4 Conclusion 185
Chapter 6 Laundry formulations and ingredients including the antimicrobial BKC differ in their ability to inhibit growth and viability of *P. aeruginosa* 186
6.1 Introduction 186
6.1.1 Background 186
6.1.2 Aims of this chapter 188
6.2 Results 189
6.2.1 The planktonic growth of *P. aeruginosa* is inhibited by the addition of powder detergent 192
6.2.2 The addition of powder and liquid detergent to cells of *P. aeruginosa* can reduce biofilm formation, both in a static and a flow-cell model 194
6.2.3 Addition of powder and liquid detergent to an established biofilm affects cells of *P. aeruginosa* 199
6.2.4 Free BKC prevents biofilm formation of *P. aeruginosa* more than encapsulated BKC 207
6.2.5 Different materials used for the coating of glass disks can reduce initial attachment of PAO1-N 224
6.3 Discussion 227
6.3.1 Various laundry products have different effects on growth, biofilm formation and biofilm killing of *P. aeruginosa* 227

6.3.2 Encapsulated BKC as alternative to free BKC does not show enhanced biocidal effects 235
6.3.3 Surface coating with anti-attachment materials could be a valid alternative to biocides to prevent biofilm formation in washing machines 242
6.4 Conclusion 245
Chapter 7 Final Conclusion and Future Aspects 246
7.1 Summary 246
7.2 Future aspects 252
References 256
Appendices 293
Appendix A Base formulations of laundry products 293
Appendix B Addition of powder detergent to an established biofilm of PAO1-N. 295
Appendix C Single dye staining (SYTO 9 and PI) of biofilms grown in M9S with or without the addition of liquid detergent, powder detergent, or fabric conditioner. 296
Appendix D CLSM imaging of biofilms grown with eBKC A or eBKC B does not reveal any fluorescein signal of the eBKC samples. 297
Appendix E Size and ζ-potential of encapsulated BKC samples. 298

List of Figures

Figure 1.1: Schematic representation of virulence factors produced by *P. aeruginosa* during acute and chronic infections. 3

Figure 1.2: Schematic representation of quorum sensing in *Vibrio fischeri*. 7

Figure 1.3: Schematic representation of the four known quorum sensing systems in *P. aeruginosa* and their regulation with each other. 9

Figure 1.4: Spatial distribution of a biofilm of different species. 12

Figure 1.5: Schematic representation of biofilm development. 13

Figure 1.6: Schematic representation of a cystic fibrosis lung and dental plaque. 20

Figure 1.7: Schematic representation of various methods used for antifouling coatings. 23

Figure 1.8: Ownership rate of washing machines. 24

Figure 1.9: Overview about laundry process and the environmental impact. 25

Figure 1.10: Transmission routes of infection involving clothing and household linens. 27

Figure 1.11: Different derivates of fluorescein exhibit multiple, pH-dependent ionic equilibria 35

Figure 1.12: Schematic representation of extended dynamic range pH-sensitive nanosensors encapsulated in a matrix. 36

Figure 1.13: Schematic representation of peg lids. 38

Figure 1.14: Schematic representation of the BioFlux flow-cell system. 40

Figure 2.1: Schematic representation of nanosensor preparation. 49

Figure 2.2: Schematic representation of the strain sampling from household washing machines. 52

Figure 2.3: Schematic representation of oxidase assay using oxidase strips. 56

Figure 2.4: Schematic representation of catalase assay using hydrogen peroxide. 56

Figure 2.5: Schematic representation of swarming motility. 57

Figure 2.6: Schematic representation of swimming motility. 58

Figure 2.7: Schematic representation of protease assay. 58

Figure 2.8: Schematic representation of 48-well BioFlux plate (top) and 24-well plate (bottom). 66

Figure 2.9: Schematic representation of colony forming unit experiments 68

Figure 3.1: Emission scans and pH calibration of pH-sensitive neutral and positive polyacrylamide nanosensors. 76

Figure 3.2: Nanosensors at concentrations below 25 mg mL^{-1} have no effect on the growth of PAO1-N. 78

Figure 3.3: Representative images of PAO1-N show some leftover positive nanosensors stuck between cells after being washed but no fluorescence inside the cells. 80

Figure 3.4: The charge of nanosensors can influence the biofilm formation of PAO1-N. 82

Figure 3.5: Enhanced PAO1-N biofilm formation as a result of positively charged nanosensors is concentration dependent. 84

Figure 3.6: Positively charged amidine beads can lead to enhanced biofilm formation of PAO1-N. 86

Figure 3.7: Positively charged nanosensors do not alter biofilm formation of PAO1-N in a flow-cell system. 87

Figure 3.8: Neutral as well as positive nanosensors can penetrate established PAO1-N biofilms under static conditions. 89

Figure 3.9: Time-lapse images reveal interaction of nanosensors with biofilms of PAO1-N. 90

Figure 3.10: Penetration of established PAO1-N biofilms by nanosensors under flow conditions was independent of the charge of the nanosensors. 91

Figure 3.11: Positive polyacrylamide nanoparticles do not directly interact with the exopolysaccharide Psl within biofilms of PAO1-N 93

Figure 3.12: Altered synthesis of the exopolysaccharide Psl has no effect on nanosensor interaction with biofilms of PAO1-N. 94

Figure 3.13: Positive polyacrylamide nanoparticles co-localise with eDNA of PAO1-N biofilms. 96

Figure 3.14: Enhanced PAO1-N biofilm formation as a result of positively charged nanosensors is independent of eDNA presence. 97

Figure 4.1: Microsensors and nanosensors determine the same pH of a liquid sample over time. 113

Figure 4.2: pH-sensitive fluorescent polyacrylamide nanosensor respond to induced pH changes within their environment. 114

Figure 4.3: The pH of M9S during planktonic growth of PAO1-N increases over time whereas the pH of M9G slightly decreases. 116

Figure 4.4: Fermentation of glucose but not lactose or saline by PAO1-N visualised with pH-sensitive nanosensors. 117

Figure 4.5: A streamer of acidic pH is evident in the downstream flow of PAO1-N biofilm microcolonies. 119

Figure 4.6: PAO1-N microcolonies in flow biofilms have an acidic centre. 121

Figure 4.7: Fluorescence intensity of Rhodamine Red™-X stays constant over time when present in a range of pH buffers. 123

Figure 4.8: Glucose and succinate metabolism pathways in *P. aeruginosa*. 127

Figure 5.1: Chemical structure of BKC. 133

Figure 5.2: Distribution of bacterial samples isolated from different sites of 22 household washing machines. 136

Figure 5.3: Phenotypic distribution of strains used for *P. aeruginosa* identification by three assays. 136

Figure 5.4: Distribution of *P. aeruginosa* strains isolated from different washing machines and sites. 137

Figure 5.5: Overview about the selection process from the washing machine sampling-up until the strain identification using MALDI-TOF MS. 138

Figure 5.6: Two washing machine isolates show reduced growth compared to PAO1-N, whereas all other isolates only show minor reduction or equal growth. 139

Figure 5.7: Representative images show swarming, swimming, and protease production for PAO1-N, whereas WM01D1 shows negative results for all three assays. 140

Figure 5.8: Selected washing machine isolates show enhanced attachment abilities in 96-well plates. 142

Figure 5.9: Selected strains isolated from washing machines show reduced susceptibility against BKC. 143

Figure 5.10: The washing machine isolate WMB1.3 shows increased production of the toxic substance pyocyanin. 145

Figure 5.11: The washing machine isolate WMB1.3 grows thicker biofilms under static conditions than the lab strain PAO1-N. 146

Figure 5.12: The presence of positive nanosensors does not influence the density of biofilms grown by WMB1.3. 147

Figure 5.13: pH maps of biofilms grown under flow conditions show similarities between the two different *P. aeruginosa* strains, PAO1-N and WMB1.3. 148

Figure 5.14: Phylogenetic tree showing the relationship between nine washing machine isolates, the lab strain PAO1-N, the reference genome PAO1, PA14, LESB65, and LESB58. 150

Figure 5.15: Proteome comparison of PAO1-N, WMB1.3, WM02F1, WM01D1, WM05D1, WM05D1R, WM05F1, WM05F1R, WM07C1 and WM07D1. 151

Figure 5.16: Overview about protein families and SNPs found in the sequences of PAO1-N and nine washing machine isolates. 152

Figure 5.17: Protein heat maps of Pil, MorA and Fli/Flg show sequence differences between strains. 154

Figure 5.18: Multiple sequence alignment of FliP shows missing start of the protein in WM02F1, WM07C1 and WM07D1. 155

Figure 5.19: Protein heat maps of Bfm and Arr show sequence differences between strains. 156

Figure 5.20: Protein heat map of Phz cluster shows sequence differences between strains. . 157

Figure 5.21: Protein heat map of Wbp cluster shows sequence differences between strains. 158

Figure 5.22: Protein heat maps of Mex and Pmr clusters show sequence differences between strains. 159

Figure 5.23: Flagellar apparatus consisting of its three main components (i) filament, (ii) hook, and (iii) basal flagellar motor. 165

Figure 5.24: Schematic representation of type IV pili. 168

Figure 5.25: Phenazine biosynthesis pathway in *P. aeruginosa* PAO1. 178

Figure 5.26: Schematic representation of rough and smooth LPS, with the B-band O antigen of the O5 serotype of *P. aeruginosa*. 181

Figure 6.1: Schematic representation of eBKC containing zein protein. 191

Figure 6.2: The addition of powder detergent reduces the growth of PAO1-N and WMB1.3 in M9S whereas liquid detergent and fabric conditioner only have minimal effects. . 193

Figure 6.3: Representative images of PAO1-N and WMB1.3 show reduced biofilm formation when grown statically in M9S LD or PD, whereas no difference is apparent for the addition of FC..... 195

Figure 6.4: CFUs of PAO1-N and WMB1.3 biofilms show a reduction in viable cells for PAO1-N biofilms grown in M9S powder detergent under static conditions. 197

Figure 6.5: Representative images of PAO1-N and WMB1.3 show reduced biofilm formation when grown in M9S with liquid or powder detergent in a flow-cell system whereas no reduction is shown for the addition of fabric conditioner..... 198

Figure 6.6: Representative images of PAO1-N and WMB1.3 show liquid or powder detergent added to established biofilms kill bacteria, whereas fabric conditioner does not..... 201

Figure 6.7: CFUs of PAO1-N and WMB1.3 biofilms reveal that bacterial viability in established biofilms is not altered by the addition of laundry supplements. 202

Figure 6.8: Fewer viable planktonic PAO1-N cells detected following exposure to powder detergent..... 203

Figure 6.9: Fluorescence intensity measurement shows SYTO 9 and PI fluorescence for medium with and without laundry supplements..... 204

Figure 6.10: Representative images of PAO1-N cells stained with SYTO 9 show loss of fluorescence signal over time when liquid detergent is added to the cells. 206

Figure 6.11: Addition of free BKC or eBKC A-H prevents the growth of PAO1-N in M9S, whereas the addition of eBKC I (control without BKC) shows normal growth. 209

Figure 6.12: Representative images of PAO1-N show altered biofilm formation when grown statically in M9S with the addition of free BKC or different eBKC samples..... 212

Figure 6.13: CFUs of PAO1-N biofilms show reduced number of viable cells for all biofilms grown with the addition of free BKC or eBKC apart from eBKC I (control) under static conditions. 213

Figure 6.14: Representative images of PAO1-N show killing effects at different intensities when free BKC or eBKC was added to established biofilms for 30 min. 216

Figure 6.15: CFUs of PAO1-N biofilms show killing activity when free BKC or eBKC A, C, G, or H was added to established biofilms for 30 min. 217

Figure 6.16: Representative images of PAO1-N biofilms show increased killing effects of selected eBKC samples when added to established biofilms for 24 h. 220

Figure 6.17: CFUs of PAO1-N biofilms show increased killing activity when eBKC D was added to established biofilms for 24 h. 221

Figure 6.18: Representative images of PAO1-N show no increased killing effects of selected eBKC samples when added together with liquid detergent to established biofilms for 30 min. 223

Figure 6.19: CFUs of PAO1-N biofilms show no killing activity when eBKC was added to the biofilms together with liquid detergent for 30 min. 224

Figure 6.20: Representative SEM images show different attachment of PAO1-N to various coatings. 225

Figure 7.1: Schematic model of static biofilm formation of *P. aeruginosa* with positive (top) or neutral (bottom) pH-sensitive nanosensors. 249

Appendix Figure A: Representative images of PAO1-N cells stained with SYTO 9 show slight loss of fluorescence signal over time when powder detergent is added to the cells.. 295

Appendix Figure B: Representative images of PAO1-N show reduction of viable cells when grown statically in M9S with liquid or powder detergent, whereas no reduction is apparent for the addition of fabric conditioner for biofilms either stained with SYTO 9 or PI. 296

Appendix Figure C: Representative images of PAO1-N grown with eBKC A or eBKC B do not show any fluorescein signal of the eBKC samples. 297

List of Tables

Table 1.1: Roles of major biofilm matrix components in *P. aeruginosa*. 18

Table 2.1: pH buffer preparation using 0.2 M sodium phosphate and 0.1 M citric acid. 46

Table 2.2: Bacterial strains used in this work. 47

Table 2.3: Excitation and emission settings for emission scans of nanosensors. 50

Table 2.4: Excitation and emission settings for pH calibration using a Tecan plate reader. 50

Table 2.5: Components of GoTaq® PCR reaction and adjustment of the programme. 54

Table 2.6: Oligonucleotide primers used to amplify 16S rRNA of *P. aeruginosa*. 54

Table 2.7: Initial and final concentrations of supplements added to biofilm growth medium. . 63

Table 2.8: Sample composition for static biofilm assays using M9 medium, normalised cells and M9 medium containing different supplements. 63

Table 2.9: Initial and final concentrations of supplements prepared in M9S, which were added to an established biofilm during the imaging process. 65

Table 3.1: Size, PDI and ζ-potential of polyacrylamide nanoparticles used in this study. 75

Table 3.2: Minimal loss occurs during filter sterilisation of neutral and positive nanosensor preparations. 77

Table 3.3: Size, PDI and ζ-potential of amidine latex beads used in this study. 85

Table 4.1: Size, PDI and ζ-potential of polyacrylamide nanosensors using Rhodamine Red™-X. 122

Table 5.1 Overview of swarming motility, swimming motility, and protease production of PAO1-N and nine washing machine isolates. 141

Table 5.2 PAO1-N and nine washing machine isolates show phenotypic variation. 144

Table 5.3: Genome analysis information for all ten sequenced genomes. 149

Table 6.1: Composition of encapsulated BKC samples. 190

Table 6.2: Overview about the presence or absence of zein protein, epoxy-silica and glutaraldehyde used for the outer coating of the eBKC samples. 239

Appendix Table A: Base formulations of laundry products. 293

Appendix Table B: Size and ζ-potential of encapsulated BKC samples used in this study. 298

List of Publications and Preprints

Brown, J. M., Blunk, B., Williams, P. and Hardie, K. R. 2019. Microfluidic-based growth and imaging of bacterial biofilms. *Bio-Protocol*, 9, doi: 10.21769/BioProtoc.3460

Blunk, B., Perkins, P., Chauhan, V. M., Aylott, J. W., Hardie, K. R. 2020 Fluorescent nanosensors reveal dynamic pH gradients during biofilm formation. *bioRxiv preprint*, doi: https://doi.org/10.1101/2020.07.31.230474

Abbreviations

%	percent
% (v/v)	volume/volume percent
% (w/v)	weight/volume percent
°C	degree Celsius
µg	microgram
µL	microlitre
µm	micrometre
µM	micromolar
1OH-PHZ	1-hydroxyphenazine
3D	3 dimensional
6PG	6-phosphogluconate
a x b	number of biological replicates x number of technical replicates
A. baumannii	*Acinetobacter baumannii*
AFM	atomic-force microscopy
Ag	silver
AHL	*N*-acylated homoserine lactone
AI	autoinducer
AI-2	autoinducer-2 furanosyl borate diester
AIP	cyclic thiolactone
AMR	antimicrobial resistance
AOT	Dioctyl sulfosuccinate sodium salt
APMA	N-(3-Aminopropyl) methacrylamide hydrochloride
APS	ammonium persulfate
APTAC	3-acrylamidopropyl)trimethylammonium chloride
arr	aminoglycoside response regulator
ATP	adenosine triphosphate
BDMA	benzyl dimethylamine
Bfm	biofilm maturation factor
BHL	*N*-butyrylhomoserine lactone
BKC	benzalkonium chloride
bp	basepair
ca	circa
c-di-GMP	cyclic di-guanosine monophosphate
CDS	coding sequence
CF	cystic fibrosis
CFTR	cystic fibrosis transmembrane conductance regulator protein
CFU	colony forming units
CLSM	confocal laser scanning microscopy/microscope
cm	centimetre
CM	cytoplasmic membrane
ConA	concanavalin A
COPD	chronic obstructive pulmonary disease
C-SNARF	seminaphthorhodafluor-4F 5-(and-6) carboxylic acid
CV	crystal violet
DAPI	4’,6-Diamidin-2-phenylindol
DLS	dynamic light scattering

DNA	deoxyribonucleic acid
DSF	methyl dodecenoic acid
E. coli	*Escherichia coli*
EB	ethidium bromide
eBKC	encapsulated BKC
eDNA	extracellular DNA
EDTA	ethylenediaminetetraacetic acid
EPS	extracellular polymeric substances
et al.	*latin: et alii, et aliae,* and others
EU	European Union
F	forward
FAM	5-(and-6)-carboxyfluorescein
FC	fabric conditioner
FITC	fluorescein isothiocyanate
FRET	fluorescence resonance energy transfer and quenching
g	gram
g	acceleration caused by gravity
gDNA	genomic DNA
GFP	green fluorescence protein
GO	graphene oxide
h	hour(s)
H_2O	water
H_2O_2	hydrogen peroxide
HCl	hydrochloric acid
HPTS	trisodium 8-hydroxypyrene-1,3,6-trisulfonate
IQS	2-(2-hydroxyphenyl)-thiazole-4-carbaldehyde
K. oxytoca	*Klebsiella oxytoca*
kb	kilo base pair
KEGG	Kyoto Encyclopedia of Genes and Genomes
L	litre
LAS	linear alkyl benzene sulphonate
lab	laboratory
LB	lysogeny broth, also known as Luria-Bertani broth
LD	liquid detergent
LES	Liverpool epidemic strain
LPS	lipopolysaccharide
M	molar
M9G	M9 glucose
M9S	M9 succinate
M. luteus	*Micrococcus luteus*
MALDI	matrix-assisted laser desorption/ionization
mAmp	milliampere
Mb	megabasepair
MBEC	minimal biofilm eradication concentration
Mex	multiple efflux
MFP	membrane fusion protein
mg	milligram
MH	Mueller Hinton broth
MIC	minimal inhibitory concentration
min	minute(s)
mL	millilitre
mM	millimolar
mm	millimetre

mmol	millimole
MRD	modified Robbins device
MRSA	multi resistant *Staphylococcus aureus*
MS	mass spectrometry
MSA	multiple sequence alignment
MTP	microtiter plate
mV	millivolt
NaCl	sodium chloride
ng	nanogram
nm	nanometre
NMR	nuclear magnetic resonance
OD	optical density
OdDHL	*N*-(3-oxododecanoyl) homoserine lactone
OG	Oregon Green
OM	outer membrane
OMF	outer membrane factor
P. aeruginosa	*Pseudomonas aeruginosa*
P. alcaliphila	*Pseudomonas alcaliphila*
P. fluorescence	*Pseudomonas fluorescens*
P. nitroreducens	*Pseudomonas nitroreducens*
P. stutzeri	*Pseudomonas stutzeri*
P-123, Pluronic-123	triblock poly(ethylene oxide) 18-poly(propylene oxide) 62-poly(ethylene oxide) 18 copolymer
P19	poly(ethylene glycol methacrylate 350)-PEG500) 29:1 copolymer
PAME	hydroxypalmitic acid methyl ester
PATRIC	Pathosystems Resource Integration Center
PBS	phosphate buffered saline
PCA	phenazine-1-carboxylic acid
PCN	phenazine-1-carboxamide
PCR	polymerase chain reaction
PD	powder detergent
PDC	phenazine-1,6 dicarboxylate
PDI	polydispersity index
PDMS	polydimethylsiloxane
PEG	poly(-ethylene glycol)
pel	*pellicle locus*
PEOX	poly(2-ethyl-2-oxazoline)
PES	polyethersulfone
PI	propidium iodide
PIA	*Pseudomonas* isolation agar
pK_a	negative logarithm (to the base 10) of the acid dissociation constant
PMS	peptide mass fingerprint
PQS	2-heptyl-3-hydroxy-4-quinolone
psl	*polysaccharide synthesis locus*
QAC	quaternary ammonium compounds
QS	quorum sensing
R	reverse
Rho	rhodamine B
RITC	rhodamine B isothiocyanate
RNA	ribonucleic acid
RND	resistance-nodulation-cell division

rpm	rounds per minute
rRNA	ribosomal ribonucleic acid
S. aureus	*Staphylococcus aureus*
S. epidermidis	*Staphylococcus epidermidis*
Se. marcescens	*Serratia marcescens*
sec	second(s)
SEM	scanning electron microscopy
SERS	surface-enhanced Raman scattering
SIM	structured illumination microscopy
SIMS	secondary-ion mass spectrometry
SNP	single nucleotide polymorphism
T1SS	type I secretion system
T2SS	type II secretion system
T3SS	type III secretion system
T5SS	type V secretion system
T6SS	type VI secretion system
TAMRA	5-(and-6)-carboxytetramethylrhodamine
TCA	tricarboxylic acid cycle
TEMED	tetramethylethylenediamine
TMR	tetramethylrhodamine
TOF	time of flight
TPE	two-photon excitation microscopy
TRITC	tetramethylrhodamine
TSB	tryptic soy broth
UK	United Kingdom
USA	United States of America
UV	ultraviolet
V. fisheri	*Vibrio fisheri*
VBNC	viable but non culturable
WM	washing machine
WT	wild type
YOYO	(1,1'-(4,4,8,8-tetramethyl-4,8-diazaundecamethylene)bis[4-[(3-methylbenzo-1,3-oxazol-2-yl)methylidene]-l,4-dihydroquinolinium] tetraiodide), homodimer of **O**xazole **Y**ellow
ζ-potential	zeta potential

Chapter 1 Introduction

1.1 *Pseudomonas aeruginosa*

Pseudomonas aeruginosa is a Gram-negative, highly adaptive, ubiquitous bacterium that can be found in a range of environments including water, soil, plants, and animals (Kung *et al.*, 2010; Diggle and Whiteley, 2020). *P. aeruginosa* is a ~2 µm long, rod shaped bacterium and belongs to the largest genus of Gram-negative bacteria, *Pseudomonas*, with more than 144 different species (Gomila *et al.*, 2015). As an opportunistic pathogen, *P. aeruginosa* can cause infections in immunocompromised patients including those suffering from burns, AIDS, wounds, urinary tract infections, and respiratory infections such as bronchiectasis, chronic obstructive pulmonary disease (COPD), and cystic fibrosis (CF), whereas infections of healthy individuals are rare (Kossel, 1908; Cross *et al.*, 1980; Schimmelbusch, 1993; Gellatly and Hancock, 2013; Al-Wrafy *et al.*, 2017). These infections are challenging to treat, due to the intrinsic antibiotic resistance, which contributes to *P. aeruginosa* infections being the leading cause of morbidity for CF sufferers. *P. aeruginosa* belongs to the ESKAPE pathogens, a group of pathogens compromising *Enterococcus faecium, Staphylococcus aureus, Klebsiella pneumoniae, Acinetobacter baumanii, P. aeruginosa* and *Enterobacter* species, that are responsible for most nosocomial infections by “escaping” antibiotic treatments due to resistance mechanisms (Rice, 2008). Because *P. aeruginosa* is prevalent in the environment, numerous potential reservoirs of infection exist. *P. aeruginosa* exerts its pathogenicity through the production of several virulence factors including those shown to play a key role in biofilm attachment such as extracellular DNA (eDNA) or polysaccharides (O'Toole and Kolter, 1998; Whitchurch *et al.*, 2002; Rasamiravaka *et al.*, 2015; Cai *et al.*, 2016). To regulate the large number of virulence factors and to enable the adaptation to the various environments that *P. aeruginosa* can inhibit, the genome is relatively large (5-7 Mb), with 5,570 predicted open reading frames for strain PAO1 and a high proportion of regulatory genes (~10%). Many genes involved in transport and efflux of organic compounds,

chemotaxis, and catabolism provide the basis of its adaptability. Furthermore, a large amount of gene rearrangement and acquisition facilitates the high adaptability of the bacterium (Stover *et al.*, 2000; Williams, 2007). *P. aeruginosa* strains produce multiple secondary metabolites and polymers and can use various carbon sources and electron acceptors, underlying its metabolic capacity to adapt to diverse environments (Moradali *et al.*, 2017).

1.1.1 Virulence

P. aeruginosa produces many cell-associated and extracellular virulence factors that are associated with its pathogenicity during acute and chronic infections and facilitate host colonisation and damage. Most of these virulence factors are secreted by various secretion pathways, including the type I secretion system (T1SS), type II secretion system (T2SS), type III secretion system (T3SS), type V secretion system (T5SS), type VI secretion system (T6SS), efflux pumps, Sec pathway, Tat system, and diffusion (Moradali *et al.*, 2017). Virulence factors include proteases, phenazines, siderophores, exoenzymes, exotoxins, rhamnolipids, pili, flagella, lipopolysaccharide (LPS), and exopolysaccharides. The regulation of the diverse virulence factors is complex and differs between acute and chronic infections, as shown in Figure 1.1. Phenotypes of acute infections are generally associated with motility and virulence (top panel), whereas chronic infections are associated with increased antibiotic resistance and biofilm formation (bottom panel). Following, some of the virulence factors will be outlined in more detail.

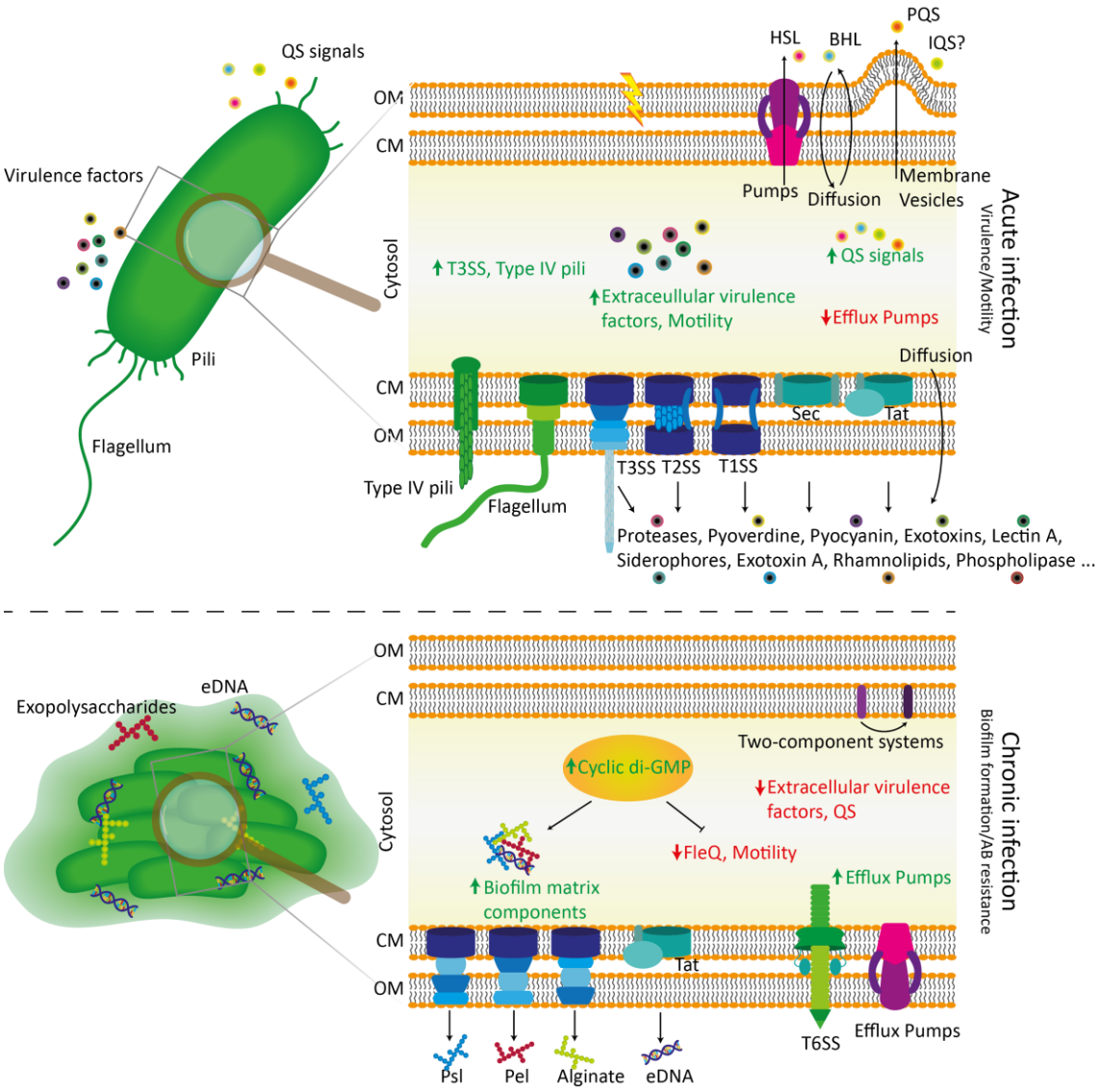


Figure 1.1: Schematic representation of virulence factors produced by *P. aeruginosa* during acute and chronic infections. Top: Acute infection involves the synthesis of flagella, type IV pili, secretion systems including T1SS, T2SS, T3SS, Sec and Tat, quorum sensing signals, and upregulation of extracellular virulence factors such as proteases, pyoverdine, pyocyanin, exotoxins, lectin A, siderophores, exotoxin A, rhamnolipids, and phospholipases. Bottom: Of importance for chronic traits are efflux pumps, the T6SS (biofilm associated and delivery of toxins to other bacteria), and the production of exopolysaccharides such as Psl, Pel, and alginate that are required for biofilm matrix production. Green and red arrows indicate up and down regulation, respectively. CM = cytoplasmic membrane, OM = outer membrane.

P. aeruginosa is known to produce at least four different proteases: (i) Alkaline protease, a zinc metalloprotease that can degrade host complement protein and host fibronectin and furthermore helps to avoid host immune systems by degrading flagellin monomers (Kipnis *et al.*, 2006; Bardoel *et al.*, 2011; Laarman *et al.*, 2012), (ii) Protease IV, which is involved in the

degradation of host lung surfactant proteins A, B and D during respiratory infections, which can inhibit the association of *P. aeruginosa* with host macrophages (Kipnis *et al.*, 2006; Ben Haj Khalifa *et al.*, 2011; Gellatly and Hancock, 2013), (iii) and (iv) the two elastases LasA and LasB that are both regulated by the *las* quorum sensing (QS) system (Toder *et al.*, 1994; de Kievit and Iglewski, 2000). Both elastases can destroy host tissue and play a role in acute lung infections and burned wound infections (Bielecki *et al.*, 2008; Rocha *et al.*, 2019). LasA can enhance the activity of LasB, that is furthermore involved in host protein degradation, inactivation of immune systems, and is crucial for tissue invasion and infection (Toder *et al.*, 1994; Hoge *et al.*, 2010). In addition, another protease, Lon, produced by *P. aeruginosa*, was investigated, which is not secreted but degrades proteins inside the *P. aeruginosa* cells and has also roles in virulence (Marr *et al.*, 2007; Breidenstein *et al.*, 2012; Moradali *et al.*, 2017). Generally, protease-deficient strains are less virulent than protease producers, especially in burn models (Holder and Haidaris, 1979).

Pyocyanin is a secondary metabolite and belongs to the phenazines. As a redox-active zwitterion, it can easily penetrate biological membranes to cause cellular damage and disrupt enzyme and ion balances (Lau *et al.*, 2004a; Lau *et al.*, 2004b). Furthermore, pyocyanin targets the host cell immune response and can induce neutrophil apoptosis (Mavrodi *et al.*, 2001; Lau *et al.*, 2004a).

Pyoverdines and pyochelin are two kinds of siderophores produced by *P. aeruginosa* that are involved in iron scavenging and transport. Iron transport is important for both growth and biofilm formation, with pyoverdine mutants showing defective biofilms under iron starvation (Banin *et al.*, 2005; Lamont *et al.*, 2009). Furthermore, iron starvation is associated with changes in QS and twitching motility, which are important for biofilm formation (Patriquin *et al.*, 2008). Pyoverdine is the primary siderophore of *P. aeruginosa*, with three different types of pyoverdines that can be produced (Meyer *et al.*, 1997). Pyochelin has a lower affinity for iron than pyoverdine but was shown to also chelate other ions such as zinc and copper (Brandel *et*

al., 2012). However, pyochelin production is increased in the absence of pyoverdine, suggesting a supportive role of pyochelin.

The four exoenzymes ExoS, ExoT, ExoY and ExoU are known virulence factors secreted by the T3SS of *P. aeruginosa* (Finck-Barbançon *et al.*, 1997; Yahr *et al.*, 1998; Sato *et al.*, 2003). ExoS, ExoT and ExoY are involved in altering cellular cytoskeletal components, cell rounding and detachment, and inhibition of bacterial uptake and phagocytosis (Sato *et al.*, 2003). In addition, ExoU possesses a unique cytotoxic effect, making *P. aeruginosa* strains capable of destroying cellular monolayers (Finck-Barbançon *et al.*, 1997). Furthermore, ExoU is associated with lung injury and seems to play a role in the development of septic shock. The reference strain PAO1 only contains *exoS, exoT* and *exoY*, but lacks *exoU* (Stover *et al.*, 2000).

Exotoxin A belongs to the two-component AB toxin family and is secreted by T2SS (Pillar and Hobden, 2002). It is composed of an A domain carrying enzymatic activity and a B domain that serves as cell binding subunit (Odumosu *et al.*, 2010). Exotoxin A is the most toxic virulence factor of *P. aeruginosa* and can disrupt protein synthesis and lead to cell death (Iglewski and Kabat, 1975; Iglewski *et al.*, 1977; Daddaoua *et al.*, 2012; Michalska and Wolf, 2015). The production of exotoxin A is highly dependent on iron availability (Pillar and Hobden, 2002).

Furthermore, *P. aeruginosa* produces rhamnolipids that primarily function as surfactant. However, they are also associated with antimicrobial activity, immune system modulation, biofilm formation, and surface motility (Van Delden and Iglewski, 1998; Davey *et al.*, 2003; Moradali *et al.*, 2017). Also involved in motility of *P. aeruginosa* are type IV pili and flagella, with type IV pili allowing twitching motility and flagella being important for swimming and swarming motility (O'Toole and Kolter, 1998; Köhler *et al.*, 2000; Rashid and Kornberg, 2000; Persat *et al.*, 2015). Both virulence factors also have a role in biofilm formation, with flagella being involved in the initial biofilm formation, whereas type IV pili play a role in downstream events, for example during microcolony formation (O'Toole and Kolter, 1998). However, flagella can trigger host cell immune systems, which can help to clear cells (Amiel *et al.*, 2010). Thus, flagella

mutants seem to have selection advantage during chronic infections, for example during CF (Luzar *et al.*, 1985; Feldman *et al.*, 1998).

LPS forms the outer membrane permeability barrier in Gram-negative bacteria and promotes resistance to phagocytosis and serum. It typically consists of three parts, named lipid A, a core and O antigen chains (Rocchetta *et al.*, 1999). However, CF isolates often show absence of O antigen and altered lipid A types, suggesting that the loss of O antigen chains reduces the activation of immune systems during invasion (Hancock *et al.*, 1983; Lam *et al.*, 1988; Rocchetta *et al.*, 1999). Exopolysaccharides, such as Pel, Psl and alginate, form a major part of the extracellular biofilm matrix (Elder *et al.*, 1995; Harmsen *et al.*, 2010; Høiby *et al.*, 2010; Kunacheva and Stuckey, 2014). The primary function of extracellular polysaccharides includes adhesion and protection of cells and will be discussed in more detail further on.

Production of virulence factors is metabolically costly and is therefore under control of complex regulation systems. Many of the virulence factors are regulated by QS, including motility, motility-sessility switch and biofilm formation, antibiotic resistance mechanisms, and stress response, highlighting the important role of QS in *P. aeruginosa*, which will be discussed below (Williams and Camara, 2009; Moradali *et al.*, 2017).

1.1.2 Quorum sensing

Cell-cell communication between bacteria allows the regulation of many different biological processes that are important for bacterial adaptation. QS pathways are one example of regulation that controls microbiological functions, with more than 10% of genes regulated by QS in *P. aeruginosa* (Moradali *et al.*, 2017). During infections of *P. aeruginosa*, QS is critical for survival and host colonisation by coordinating phenotypic changes, for example after the initial attachment to host cells (González and Keshavan, 2006). A typical QS system consists of a signalling molecule called autoinducer (AI) and a receptor and can be described as the regulation of gene expression in response to a critical threshold of AI. Bacterial cooperation was first

discovered 50 years ago in *Vibrio fischeri* mediated through the induction of bioluminescence (Nealson *et al.*, 1970). A schematic representation of quorum sensing in *V. fischeri* is shown in Figure 1.2.

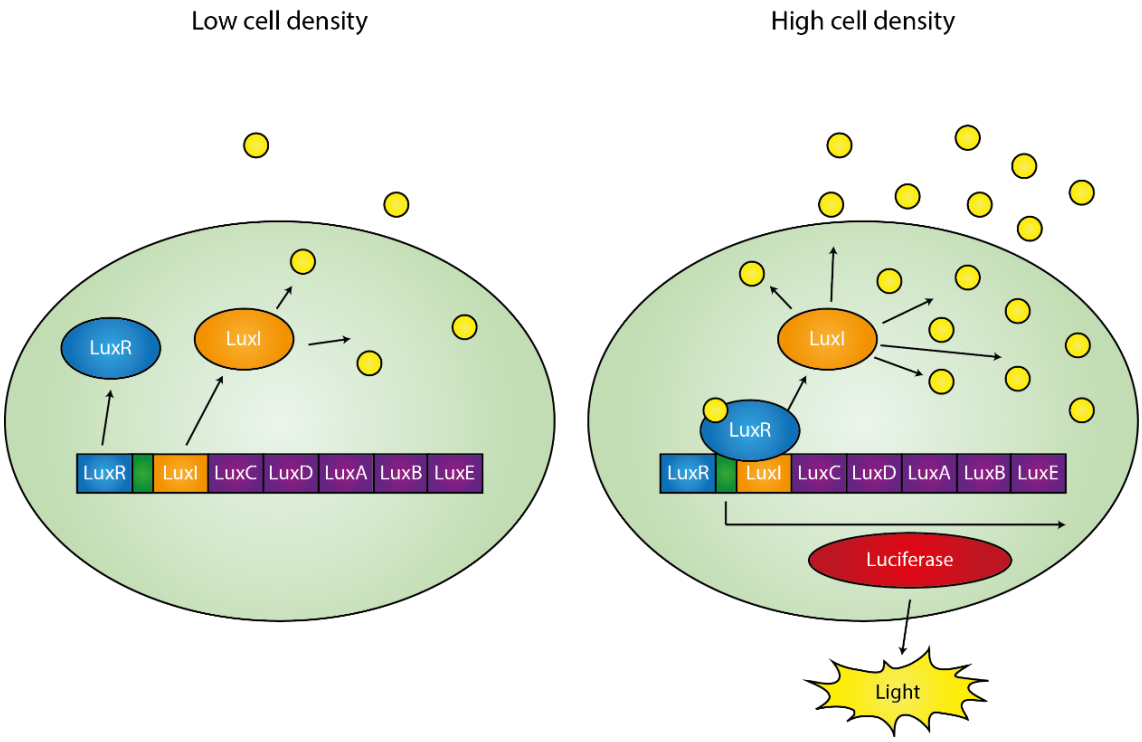


Figure 1.2: Schematic representation of quorum sensing in *Vibrio fischeri*. The left part represents low cell density, at which the level of the autoinducer acylated homoserine lactone (AHL) (yellow) synthesised by LuxI (orange) is below the threshold to activate the receptor LuxR (blue). AHL acts as a transcriptional activator of the luciferase genes *luxICDABE*. The right part represents high cell density, at which LuxI is upregulated and more autoinducer is produced. The threshold for the autoinducer is reached so that it binds to LuxR initiating the transcription of the *lux* operon and producing even more AHL. This autoinduction positive feedback of LuxI exponentially increases AHL levels leading to bioluminescence. Adapted from Bellezza *et al.* (2014).

Involved in the regulation of bioluminescence in *V. fischeri* is the Lux pathway. At low cell density, the level of the AI synthesised by LuxI is small so that LuxR is not activated. At high cell density, more of the autoinducer is produced until a threshold is reached leading to the binding of the autoinducer to LuxR. This binding initiates the transcription of the *lux* operon resulting in bioluminescence (Bellezza *et al.*, 2014). The responsible substance is *N*-Acyl homoserine lactone (AHL) (Eberhard *et al.*, 1981). Bacteria are using AHL-signals to observe the density of their own

population and to selectively synchronise their gene expression. Other cell-cell communication signals of Gram-negative bacteria apart from AHL include the autoinducer-2 furanosyl borate diester (Al-2), cyclic thiolactone (AIP), hydroxypalmitic acid methyl ester (PAME), and methyl dodecenoic acid (DSF) (Pesci *et al.*, 1999; Oh *et al.*, 2001; Whitehead *et al.*, 2001; Federle and Bassler, 2003; Zhang, 2003; Wang *et al.*, 2004; Diggle *et al.*, 2007; Kalia, 2013). Some bacteria host a complex hierarchical QS circuitry that are often composed of more than one QS system. For instance, *P. aeruginosa* possesses at least four different QS systems: (i) The *las* system at the top of the hierarchy including the LasR receptor and its AI *N*-(3-oxododecanoyl) homoserine lactone (OdDHL), (ii) the *rhl* system with the RhlR receptor and the AI *N*-butyrylhomoserine lactone (BHL), (iii) the *pqs* system, consisting of the receptor PqsR and the AI 2-heptyl-3-hydroxy-4-quinolone (PQS), and (iv) the *iqs* system with IqsR as receptor and 2-(2-hydroxyphenyl)-thiazole-4-carbaldehyde (IQS) as AI. All four systems were found to be involved in the pathogenicity of *P. aeruginosa*, including the regulation of virulence factor gene expression such as proteases, rhamnolipids, and pyocyanin (Lee and Zhang, 2015). However, it should be noted that the *iqs* system is controversial. In a short comment, Cornelis points out that IQS is a by-product of the siderophore pyochelin or a degradation product rather than an autoinducer synthesised by the *ambABCDE* genes (Cornelis, 2019).

As mentioned, the *las* system is on top of the hierarchy and activates the expression of the *rhl*, *pqs* and *iqs* systems in addition to positively activating its own regulon (Winson *et al.*, 1995; Latifi *et al.*, 1996; Pesci *et al.*, 1997; Gallagher *et al.*, 2002; Kiratisin *et al.*, 2002; Déziel *et al.*, 2004). Although the *las* system is often described as the most important QS system in *P. aeruginosa*, many QS-dependent virulence factors are predominantly activated by *rhl* (Latifi *et al.*, 1995; Whiteley *et al.*, 1999; Winzer and Williams, 2001; Schuster and Greenberg, 2007). Furthermore, PQS is able to enhance expression of the *rhl* QS system, but is negatively regulated by *rhl*, suggesting that the concentration of the AI OdDHL and BHL are important for the position of *pqs* (Pesci *et al.*, 1999; Cao *et al.*, 2001). *Iqs*, the most recent identified and controversial QS system,

is also regulated by *las*, although it was shown that environmental conditions such as phosphate depletion or oxygen deprivation can influence the hierarchy and can overcome non-functional *las* systems (Lee *et al.*, 2013; Lee and Zhang, 2015). This is particularly interesting as a number of clinical isolates of *P. aeruginosa* from CF patients were found to have loss-of-function mutations within the *las* system (Hamood *et al.*, 1996; Dénervaud *et al.*, 2004; Schaber *et al.*, 2004; Smith *et al.*, 2006; Wang *et al.*, 2018). *Las* and *rhl* systems both mediate QS signalling at early stages of growth whereas the *pqs* pathway is active at late exponential growth phase (Choi *et al.*, 2011). All four QS systems and their correlations are presented in Figure 1.3.

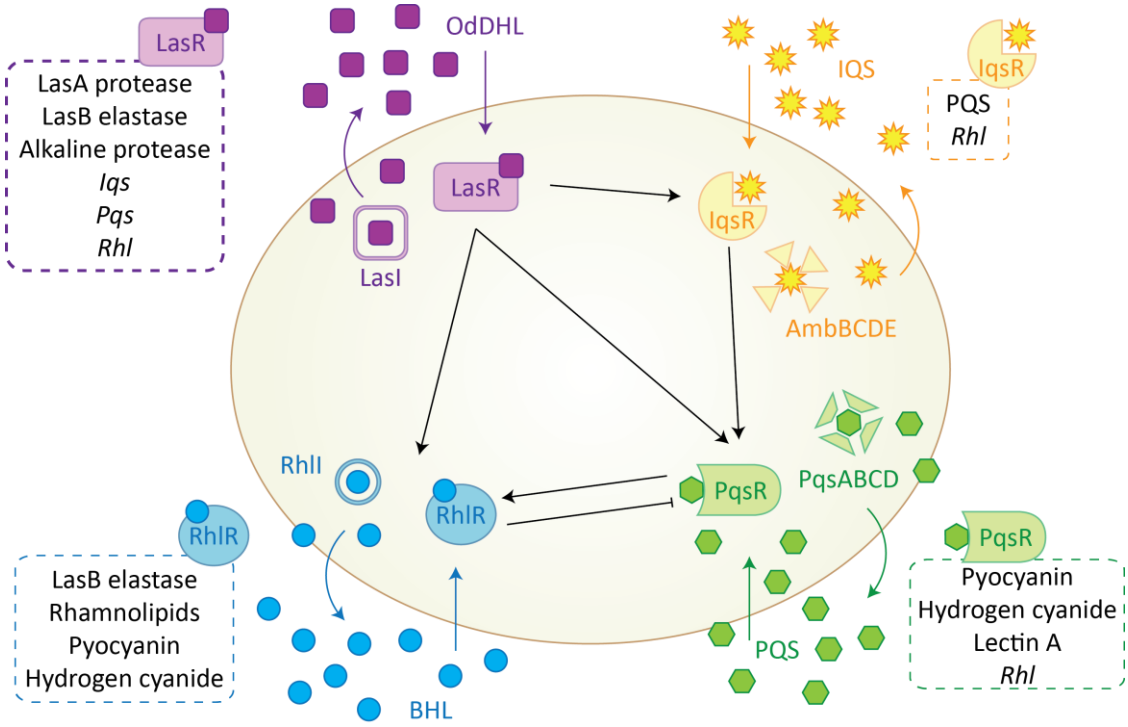


Figure 1.3: Schematic representation of the four known quorum sensing systems in *P. aeruginosa* and their regulation with each other. Arrows indicate regulation (positive or negative). Additional systems that are regulated by one or more of the QS systems are listed in boxes next to the QS regulator. The AIs are synthesised by enzymes including LasI, RhlI, PqsABCD, and AmbBCDE, respectively. OdDHL = *N*-(3-oxododecanoyl) homoserine lactone, BHL = *N*-butyrylhomoserine lactone, PQS = 2-heptyl-3-hydroxy-4-quinolone, IQS = 2-(2-hydroxyphenyl)-thiazole-4-carbaldehyde. Adapted from Lee and Zhang (2015).

As already mentioned, QS is influenced by environmental effects such as heat, oxygen, or starvation. Another factor that can affect AHL signal molecules is the surrounding pH. Uroz *et al.* for example found that AHLs are rapidly inactivated by pH-dependent lactonolysis (Yates *et al.*,

2002; Uroz *et al.*, 2005). It was shown that during growth of *Yersinia* and *Pseudomonas*, AHLs are inactivated and accumulated in an open-ring form as a consequence of a pH-dependent hydrolysis of the lactone ring due to an alkaline pH occurring during the stationary phase of the growth. Providing a pH of 2.0 or lower by acidifying the culture, the AHLs could be recovered (Yates *et al.*, 2002). In contrast, Tinh *et al.* investigated the activity of a recombinant AHL-lactonase originated from a *Bacillus* species under different pH and reported on optimal activity from pH 6 to pH 8, whereas there was a marked reduction at pH values below pH 6 and no activity below pH 4 (Tinh *et al.*, 2013). In agreement with those findings, Pedroza *et al.* presented results indicating that a recombinant AHL lactonase showed an optimum activity at pH 8 but a reduced catalytic activity at decreasing pH indicating a change in the conformational structure of the AHL lactonase at low pH (Pedroza *et al.*, 2014). These findings show that the environmental pH may play an important role in the pathogenesis of *P. aeruginosa* and should be kept in mind.

In addition to the regulation of virulence factors, QS was also shown to play a role in biofilm development and maturation, with the *las* system being necessary for the establishment of differentiated *P. aeruginosa* biofilm (Davies *et al.*, 1998) and the *rhl* system being activated during the maturation stage (De Kievit *et al.*, 2001a). Furthermore, release of eDNA is controlled by the *pqs* QS system (Allesen-Holm *et al.*, 2006). Biofilm formation by *P. aeruginosa* is particularly important for it to establish chronic infections for example within CF lungs and has therefore been studied intensively.

1.2 Biofilms of *P. aeruginosa*

A common misconception of microbial living is that bacteria exist as individual organisms in a “planktonic state”. Rather, microorganisms have been shown to naturally accumulate on a wide variety of surfaces, where they form sessile, sedentary communities. Those surfaces include household and industrial pipes, (bio)materials such as contact lenses, medical devices including implants and urinary catheters, as well as plant and animal tissues (Elder *et al.*, 1995; Cortés *et*

al., 2011; Gupta *et al.*, 2016). These accumulations of microorganisms of mono- or poly-microbial aggregates are commonly referred to as a biofilm and can consist of diverse communities of bacteria and fungi (Elias and Banin, 2012). The close proximity of the microorganisms enables substrate exchange, distribution of metabolic products, and removal of toxic end products so that the different species can support each other (Davey and O'Toole, 2000a). *P. aeruginosa* exerts its pathogenicity through several components that have been proven to have a key role in biofilm formation, for example eDNA or type IV pili (O'Toole and Kolter, 1998; Whitchurch *et al.*, 2002; Klausen *et al.*, 2003b; Fuxman Bass *et al.*, 2010; Gloag *et al.*, 2013; Jennings *et al.*, 2015). Moreover, the structure of biofilm communities can protect the bacteria from attack by antimicrobials, sheer forces, and the immune system of host cells during infection (Lewis, 2001). It was shown that microorganisms located in a biofilm exhibited higher metabolic functional diversity and metabolic cooperation than those living in planktonic form (Tribedi *et al.*, 2015). One example for the collaborating network between different organisms in a biofilm is the degradation of complex organic matter into methane and carbon dioxide during anaerobic digestion, which requires the involvement of at least three types of bacteria (Davey and O'Toole, 2000a; Gupta *et al.*, 2016). This process is a type of symbiosis called syntrophism, where two metabolically distinct bacteria depend on each other to utilise certain substrates for their energy source (Davey and O'Toole, 2000a). Figure 1.4 shows three different options for the spatial distribution of a biofilm consisting of different species and their option for communication. In part a, the different species of the biofilm are separated. Part b shows a co-aggregation and part c the distribution in layers. The variable distribution affects the communication of the cells (Elias and Banin, 2012).

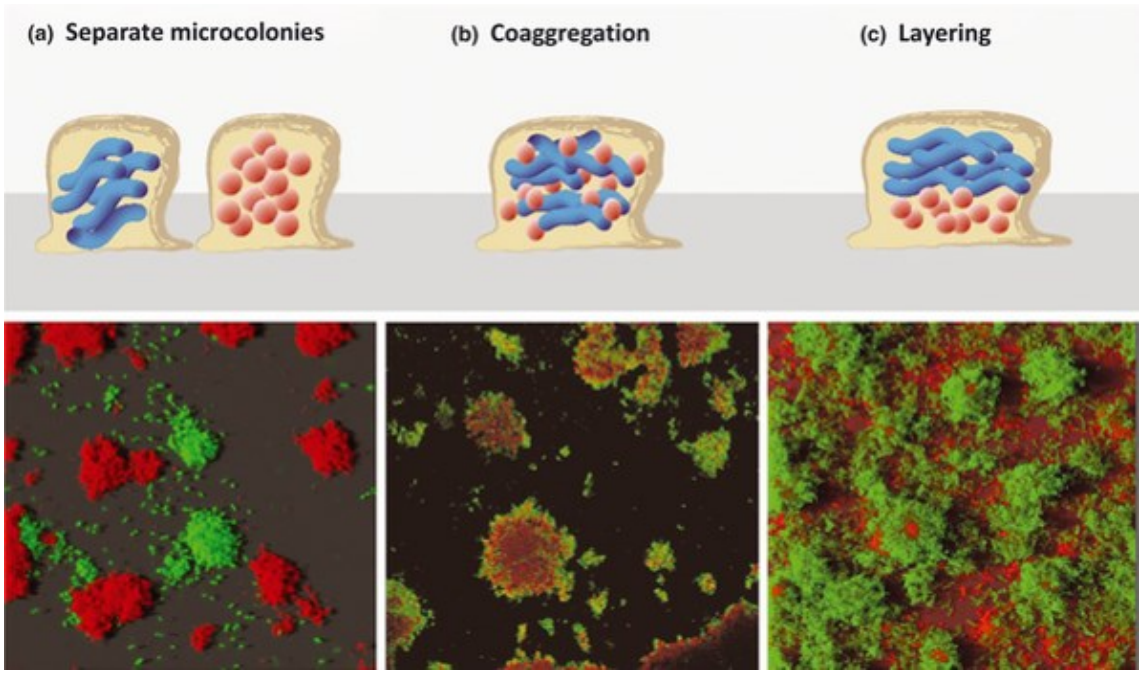


Figure 1.4: Spatial distribution of a biofilm of different species. The pictures were taken using confocal laser scanning microscopy. **(a)** Separate one-species microcolonies (*Burkholderia* sp. and *Pseudomonas* sp.) (Nielsen *et al.*, 2000), **(b)** Co-aggregation of the species (*Streptococcus oralis* and *Actinomyces naeslundii*) (Rickard *et al.*, 2006), **(c)** Distribution of the species in layers (*Acinetobacter* sp. and *Pseudomonas putida*) (Hansen *et al.*, 2007). Taken from Elias and Banin (2012).

1.2.1 Formation of biofilms

Biofilm formation starts with the switch from a motile to a sessile state of bacteria. The whole process can be divided into five stages: (i) Initial reversible attachment, (ii) irreversible attachment, (iii) microcolony formation, (iv) maturation, and (v) dispersion (Sauer *et al.*, 2002; Stoodley *et al.*, 2002b). The initial contact of the moving planktonic bacteria with the surface is the starting point, which is still reversible at this stage. The bacteria will then start to form a monolayer and will produce an extracellular matrix or "slime" for protection. The matrix consists of polysaccharides, structural proteins, cell debris, and nucleic acids; referred to as extracellular polymeric substances (EPS). The initial steps of the matrix formation are dominated by eDNA, whereas polysaccharides and structural proteins take over later. In these stages, the formation of microcolonies takes place, which exhibit significant growth and cell-cell communication such as QS. The biofilm grows in a three-dimensional manner and the attachment is now irreversible.

In the last stage, some cells of the mature biofilm start to detach and disperse into the environment as planktonic cells again to potentially start a new cycle of biofilm formation. During this stage, different saccharolytic enzymes are produced by the organisms inside the biofilm, which break the biofilm stabilising polysaccharides so that these planktonic cells can attach to new surfaces. *Pseudomonas fluorescens* and *P. aeruginosa* for example release alginate lyase, *Escherichia coli* releases *N*-acetyl-heparosan lyase and *Streptococcus equi* produces hyaluronidase enzymes that help to break down the biofilm matrix (Sutherland, 1999). Additionally, the microorganisms start to upregulate flagella protein production to regain motility and attach to new surfaces (Gupta *et al.*, 2016). It is also possible, that whole parts of the cell aggregate detach or a movement of the complete biofilm takes place (Tolker-Nielsen *et al.*, 2000; Sauer *et al.*, 2002). The typical biofilm formation is illustrated in Figure 1.5.

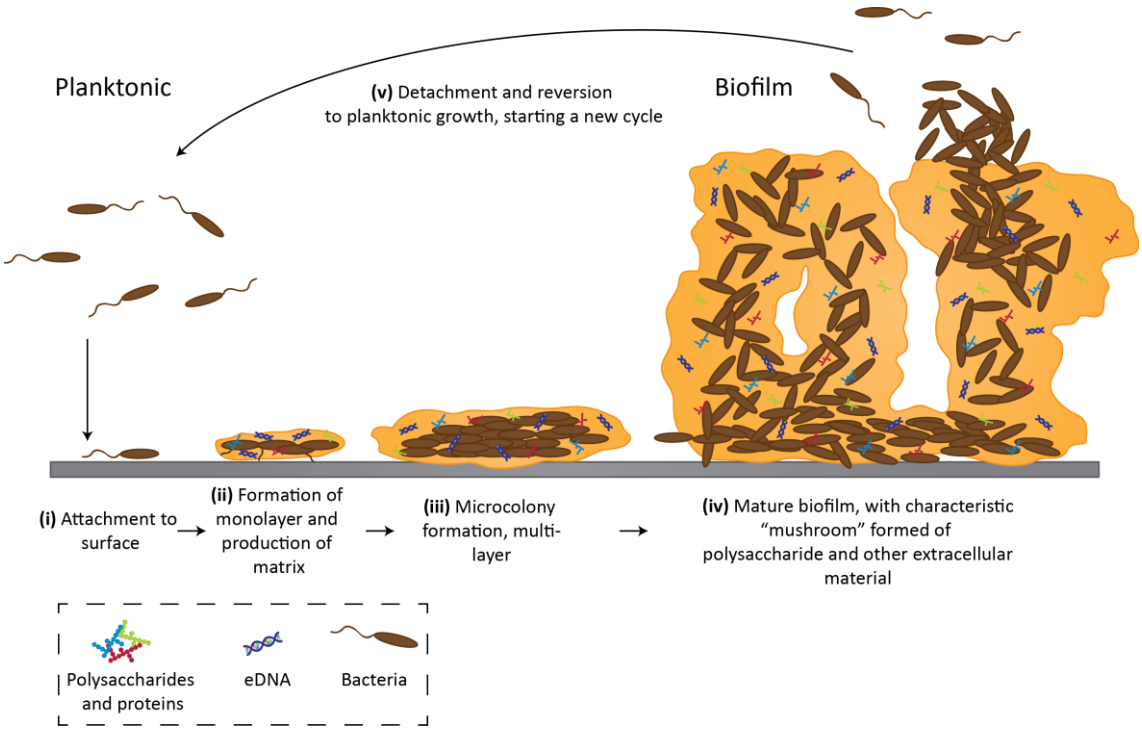


Figure 1.5: Schematic representation of biofilm development. The formation begins with attachment of the planktonic cells followed by the adhesion to the surface. The bacteria then form a monolayer and start to produce an extracellular matrix. Next, a microcolony is formed where multilayers appear. During the final stage, cells start to detach, and the biofilm will disperse starting a new cycle. Adapted from Vasudevan (2014).

Movement of bacteria is a crucial part of biofilm formation and is dependent on environmental conditions, for example by consuming glucose as a carbon source, *P. aeruginosa* settles initially as a non-motile subpopulation (Klausen *et al.*, 2003a). In contrast, using citrate as a carbon source, differentiation occurs into a motile phase (Klausen *et al.*, 2003b). It has furthermore been described that twitching motility is favoured under iron limitation conditions (Singh *et al.*, 2002). Additionally, it has been reported that a rhamnolipid source results in increased hydrophobicity which enhances adhesiveness critical for biofilm formation (Zhang and Miller, 1994). The nutritional conditions like carbon sources and iron level present in the growth medium also influence the shape of the formed biofilm of *P. aeruginosa*. Under some conditions, *P. aeruginosa* forms a flat biofilm without separate microcolonies whereas under different conditions it develops mushroom-shaped microcolonies composed of stalk and cap subpopulations (Klausen *et al.*, 2003a; Klausen *et al.*, 2003b; Yang *et al.*, 2009a). Those subpopulations are in different physiological conditions and therefore have different tasks like producing “public goods” or expression of QS genes (De Kievit *et al.*, 2001a; West *et al.*, 2007). In addition, biofilm formation is largely strain dependent, for example the development of mushrooms or the formation of mucoid versus non-mucoid biofilms.

1.2.2 Extracellular matrix

After forming a biofilm, the microorganisms are located in a distinct extracellular matrix. Among other things, the matrix consists of extracellular polysaccharides, structural proteins, cell debris, and nucleic acids summarised as EPS (Elder *et al.*, 1995; Harmsen *et al.*, 2010; Høiby *et al.*, 2010; Kunacheva and Stuckey, 2014). It was found that 75% of the extracted polymers of water-soluble EPS consisted of proteins, followed by eDNA and polysaccharides (Jahn *et al.*, 1999). Overall, the amount of microorganisms only accounts for 10% of dry mass in most biofilms, with the other 90% consisting of matrix components (Flemming and Wingender, 2010). However, the composition varies over time during the biofilm development depending on the production of EPS.

The extracellular matrix provides an increased tolerance against antimicrobials and a protection against the depletion of the biofilm. EPS retard the diffusion of antibiotics through the biofilm and can therefore increase drug resistance (Crossley *et al.*, 2009). Due to the composition of EPS, biofilms are found to be hydrogels that exhibit viscoelastic behaviours allowing biofilms to withstand mechanical stress (Stoodley *et al.*, 2002a; Hall-Stoodley *et al.*, 2004). The viscoelastic properties of the biofilm affects its structure and adhesive properties (Peterson *et al.*, 2015). *P. aeruginosa* and other biofilm-producing bacteria use biofilms as a mechanism of defence, for example against phagocytes (Jesaitis *et al.*, 2003), osmotic and oxidative stress (Hall-Stoodley and Stoodley, 2009), antibiotics (Hassett *et al.*, 2002), or antibodies (Cerca *et al.*, 2006). The formation of a biofilm can furthermore facilitate gene transfer among bacteria leading to an increase of virulent strains (Lewis, 2001). The composition of the EPS varies between biofilms and is important for the attachment of the microorganisms, for example the EPS layer of *P. aeruginosa* has an increased adhesion strength when compared to *B. subtilis* because of the bigger portion of carbohydrate components like LPS, alginate, and Pel and Pls polysaccharides (Harimawan and Ting, 2016). The EPS content of the biofilm is influenced by environmental factors and conditions like sheer forces, high levels of oxygen (Bayer *et al.*, 1990), limited availability of nitrogen (Jarman *et al.*, 1978), desiccation (Ophir and Gutnick, 1994), low temperature (Junkins and Doyle, 1992), and low pH (Ryu and Beuchat, 2004).

An important role is played by eDNA, which provides structural stability but does not carry any genetic information (Mann and Wozniak, 2012). The eDNA of *P. aeruginosa* is involved in the cellular communication and stabilisation of biofilms (Gloag *et al.*, 2013). It was suggested that eDNA is generated from random chromosomal DNA and can be directly secreted through secretion systems, by lysis of sub-populations of the biofilm or by the release of small membrane vesicles (Spoering and Gilmore, 2006). Additional roles of eDNA include the contribution to cation gradients, genomic DNA release, antibiotic resistance, and activation of neutrophils during infection (Finkel and Kolter, 2001; Mulcahy *et al.*, 2008; Fuxman Bass *et al.*, 2010). eDNA

can cause cell lysis by chelating cations that under normal conditions stabilise LPS and the outer membrane and has therefore antimicrobial activity (Mulcahy *et al.*, 2008). The anionic nature of eDNA can also cause binding of cationic antimicrobials to directly reduce the diffusion rate of antimicrobials through the biofilm matrix. However, this mechanism only provides a short-term protective effect until the matrix becomes saturated. During long-term antibiotic exposure, DNA chelation of cations such as Mg^{2+}, Ca^{2+}, or Mn^{2+} was shown to induce the *PA3552-PA3559* operon via a PhoPQ and PmrAB-controlled response to cation limitations, which encode an LPS modification pathway that reduces the permeability of the outer membrane to cationic antimicrobial peptides leading to resistance. The minimal inhibitory concentration values for polymyxin B and aminoglycosides were up to 2560-fold and 640-fold increased within DNA-enriched biofilms, respectively, as a result of DNA-induced expression of *PA3552-PA3559* (Mulcahy *et al.*, 2008). The expression of the *PA3552-PA3559* operon can also be induced by an acidic environment even in the presence of Mg^{2+}, with an accumulation of eDNA being responsible for the acidification of the biofilm environment (Wilton *et al.*, 2016). During starvation, eDNA as well as other components of the EPS can serve as nutrient source (Finkel and Kolter, 2001). In addition to eDNA, lipids, LPS as well as polymers like glycopeptides form a scaffold and hold the biofilm together (Flemming and Wingender, 2010).

For *P. aeruginosa*, it has been reported that it produces three major polysaccharides, namely alginate, Pel (*pellicle locus*) and Psl (*polysaccharide synthesis locus*) that provide further stability to the biofilm (Gupta *et al.*, 2016). Alginic acid is a heteropolymer of mannuronic and guluronic acids and is suggested to be the major polymeric substance component in mucoid *P. aeruginosa* biofilms, for example during chronic infections like CF, whereas Pel and Psl are primarily utilised by non-mucoid strains. PAO1 that is commonly used as laboratory (lab) strain does not produce alginate under normal conditions (Hunter and Beveridge, 2005). Alginate interacts with nutrients and water and is responsible for the supply of the nutrients to the biofilm (Rasamiravaka *et al.*, 2015). Furthermore, alginate is involved in persistence and immune

evasion as well as the scavenge of free radicals released from neutrophils and macrophages (Simpson *et al.*, 1989). Alginate is involved in the establishment of microcolonies as well as being involved in stability of mature biofilms.

The glucose rich polysaccharide Pel and the mannose- and galactose rich pentasaccharide Psl act as scaffold for the biofilm structure and are mainly synthesised during *in vitro* biofilm formation (Govan and Deretic, 1996; Colvin *et al.*, 2011; Franklin *et al.*, 2011). The *pel* locus contains seven genes encoding proteins that are involved in synthesis and export of the polysaccharide (Franklin *et al.*, 2011). It was first identified in mutants showing loss of pellicle formation, a form of biofilms at the air-liquid interface of static cultures but was also shown to be required for the formation of solid surface-associated biofilms (Friedman and Kolter, 2004). Experiments using non-piliated *P. aeruginosa* strains revealed that *pel* mutations have defects in the initial attachment process, suggesting that Pel is involved in the attachment process of early biofilm formation especially in the absence of other adhesins such as type IV pili (Vasseur *et al.*, 2005). More recent studies revealed that Pel is a major structural component of the biofilm stalk where it cross-links eDNA (Jennings *et al.*, 2015). Additionally, Pel is involved in antibiotic resistance of biofilms, especially aminoglycosides (Colvin *et al.*, 2011).

The *psl* locus includes 15 genes, although only 11 were found to be necessary for Psl synthesis and export (Jackson *et al.*, 2004; Ma *et al.*, 2007; Byrd *et al.*, 2009; Ma *et al.*, 2009). Overproduction of Psl leads to increased cell-surface and intercellular adhesion, underlying the importance of this polysaccharide in adhesion, initiation, and maintenance of biofilm structure (Ma *et al.*, 2006; Byrd *et al.*, 2009). Psl is anchored around cells in a helical arrangement during biofilm initiation in early stages of biofilm formation (Ma *et al.*, 2009; Moradali *et al.*, 2017). This arrangement enables cell-cell-interaction and cell-surface adhesion. During later stages of biofilm formation, Psl is accumulated on the periphery of 3D-structured microcolonies to provide structure support and subsequent biofilm dispersion (Ma *et al.*, 2009). Furthermore, Psl can have a signalling role for two diguanylate cyclase enzymes to enhance intracellular cyclic

diguanylate monophosphate (c-di-GMP) production. C-di-GMP is a second messenger molecule involved in biofilm formation, and increased c-di-GMP concentration leads to a positive feedback in elevated Psl production (Irie *et al.*, 2012). Additionally, Psl has roles in pathogenesis, antibiotic resistance, and protection against the immune system (Wei and Ma, 2013). An overview about the major components of *P. aeruginosa* biofilm matrix is listed in Table 1.1.

Table 1.1: Roles of major biofilm matrix components in *P. aeruginosa*. Taken from Wei and Ma (2013).

Component	Role	Property
Psl	Initial attachment and adhesion Primary biofilm scaffold Proinflammatory signalling Antibiotic resistance Avoidance of host defence Signalling molecule to stimulate biofilm formation	Neutral charge
Pel	Pellicle formation and solid surface-associated biofilm formation Aggregation of bacterial cells Antibiotic resistance Initial attachment in the absence of type IV pili	Positively charged
Alginate	Persistence and immune evasion Antibiotic resistance ROS scavenges Mucoid phenotype Water and nutrient source	Negatively charged
eDNA	Nutrient source Scaffold Antibiotic resistance Major proinflammatory component	Negatively charged
Flagella	Initial cell-to-surface interactions	-
Type IV pili	Formation of mushrooms	-

1.2.3 The role of biofilms in pathogenesis

Microbial biofilms occur in many different areas and can have positive impact, for example in microbial bioelectrochemical systems. Another positive occurrence of biofilms is in rhizospheric soil, where it has been found to increase the soil fertility and plant growth (Qurashi and Sabri, 2012). Because of the poly anionic nature of EPS, biofilms can form complexes with positively charged metal cations and were therefore used to support the remediation of heavy metals (Pal and Paul, 2008). It was also reported that the degradation of polymer is more efficient if biofilms are present (Balasubramanian *et al.*, 2010; Tribedi *et al.*, 2015). Another example of a positive effect includes the biofilms of commensal bacteria such as *Staphylococcus epidermidis*, which can impede the colonisation of potentially pathogenic bacteria through the stimulation of host-cell immune defences and the prevention of adhesion. However, biofilms are more often associated with many pathogenic forms of human diseases and plant infections. The biofilm population contributes to around 80% of the total microbial infection (Cortés *et al.*, 2011). One common example is CF, the most frequently passed genetic disorder in Western Europe. CF patients have a defect in the cystic fibrosis transmembrane conductance regulator protein (CFTR), which results in a defective secretion system in the respiratory epithelium of the lung. When infecting the CF lung, *P. aeruginosa* undergoes a characteristic transition from an acute virulent pathogen to a CF-adapted pathogen, allowing it to persist in the lung for years or even decades. This is due to the overproduction of the matrix polysaccharide alginate, leading to the formation of a mucoid biofilm that tolerates antibiotics, components of both the innate and adaptive immune response, and resists phagocytosis. The persistence of these mucoid biofilms within the CF lung leads to the development of a distinct antibody response. This prompts chronic inflammation mediated by granulocytes, and results in severe damage to the lung tissue of CF patients (Figure 1.6a). A second example of biofilms in human health is dental plaque potentially leading to dental caries. The consumption of fermentable carbohydrates such as sugary treats or drinks causes an increase in the production and secretion of organic acids by

the bacteria found in dental plaque. If left untreated, the increased acidification of the biofilm leads to the demineralisation of the enamel and the formation of dental caries (Figure 1.6b). Both examples refer to polymicrobial biofilms.

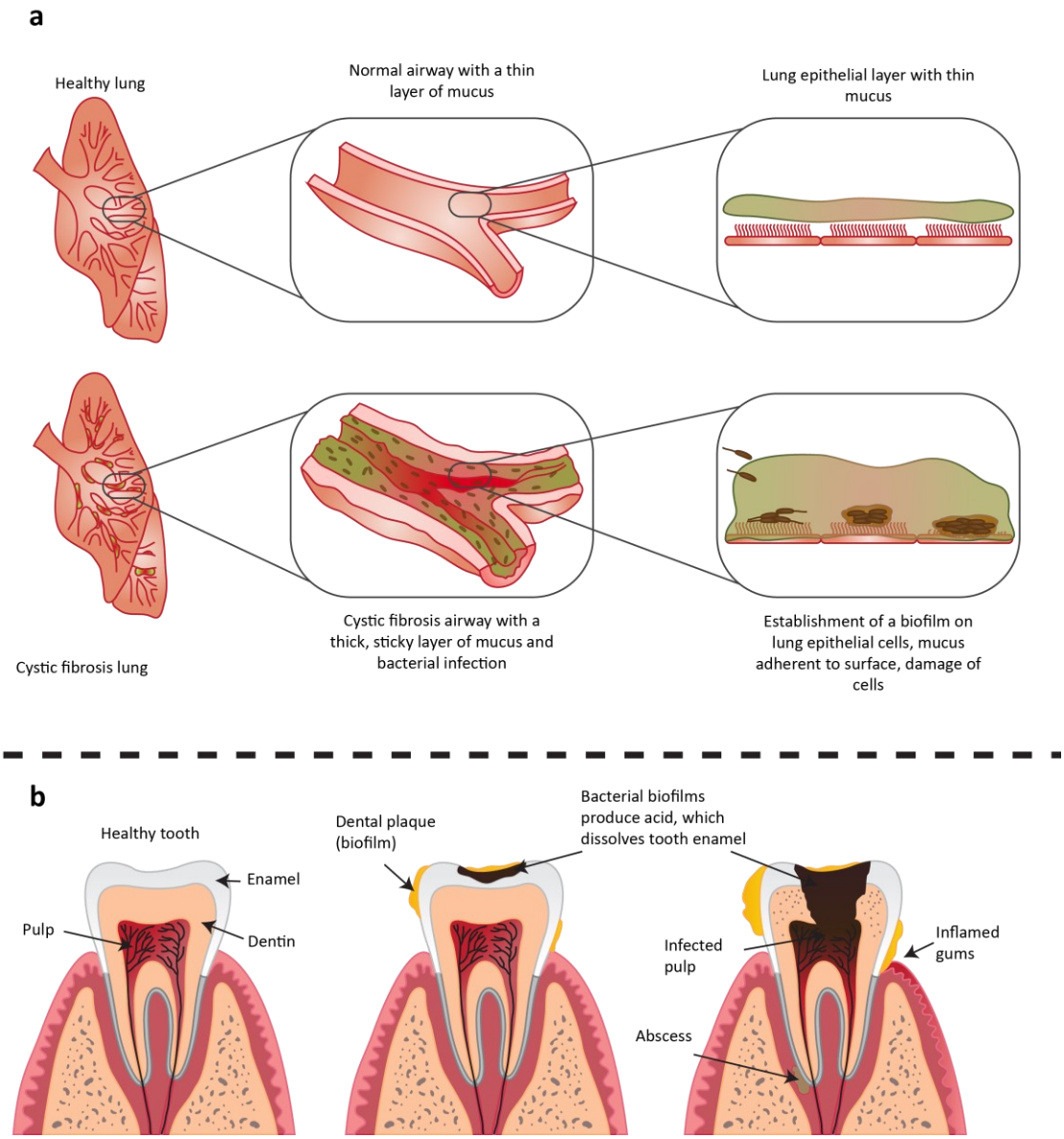


Figure 1.6: Schematic representation of a cystic fibrosis lung and dental plaque. (a) In a healthy lung, the epithelial cells of the airway are covered with a thin layer of mucus whereas the airway of a CF lung contains a thick, sticky mucus including bacterial biofilms leading to damaging of the cells and breathing problems. **(b)** Dental plaque is formed on top of the teeth where acid produced by the bacteria dissolves the tooth enamel leading to infections and dental caries.

Other examples for the occurrence of biofilm forming bacteria include chronic wounds like diabetic foot ulcer, pressure sores, and venous ulcers where the infections are leading to a

persistence of the wounds (Bjarnsholt, 2013; Alhede and Alhede, 2014). As wounds usually involve loss of the skin integrity, it is easy for microbes to enter the wound and colonise the wet, warm, and often nutrient-rich environment (Alhede and Alhede, 2014). *S. aureus* and *P. aeruginosa* colonisation is found in many of those infections leading to a delay of the healing process (Bowling *et al.*, 2009; Bjarnsholt, 2013).

In addition to those diseases, biofilms are also found in device-related infections, were the biofilms form on foreign surfaces (Bjarnsholt, 2013). A common example are urinary catheters made of either latex or silicone. Bacteria involved in the contamination include *S. epidermidis*, *E. coli*, *Proteus mirabilis*, *P. aeruginosa*, *K. pneumoniae*, *Enterococcus faecalis* and other Gram-negative bacteria. In addition, implants, artificial heart valves, teeth, contact lenses and other surfaces may involve chronic infections (Bjarnsholt, 2013). Furthermore, biofilms can also be found within the household environment, for example within dish washers or washing machines, causing potential infection risks due to the distribution of human pathogens as described in 1.2.4.

Because of the increasing number of biofilms associated with diseases, the control of biofilms has high priority. The most efficient way to treat a biofilm infection is to remove the infected area if possible, for example dental caries, contaminated catheters, or infected organs. In cases where a removal is not possible, early aggressive antibiotic treatment before formation of a biofilm and suppressive antibiotic treatment should be considered (Bjarnsholt, 2013). However, as mentioned previously, the extracellular matrix is used as a diffusion barrier against antibiotics and other bactericidal substances (Fux *et al.*, 2005; Hall-Stoodley and Stoodley, 2009). Therefore, preventing the initial attachment of the bacteria at the beginning so that no biofilm can be formed might be preferable. Several approaches are currently under investigation, for example the prevention of communication channels by QS signals or antibacterial coatings applied to indwelling surfaces. These approaches have already been investigated in various areas, including antimicrobial treatment on dental material surfaces or coating of biomedical

devices such as catheters (Danese, 2002; Li *et al.*, 2010; Hook *et al.*, 2012; Hook *et al.*, 2013; Wang *et al.*, 2014; Junter *et al.*, 2016; Magennis *et al.*, 2016; Zaltsman *et al.*, 2017; Singh *et al.*, 2019). Surface colonisation as a result of bacterial attachment occurs through various mechanisms, such as hydrophobic and electrostatic interactions (Park *et al.*, 1998; Ostuni *et al.*, 2001; Roosjen *et al.*, 2004; Tedjo *et al.*, 2007). Reducing the initial attachment of bacteria will prevent infection and reduce the necessity of antibiotic treatment and hence reduce the spread of antibiotic resistance. Bacterial attachment on surfaces can also occur through conditioning of a substrate that enhances bacterial attachment properties. Thus, surfaces that resist protein adsorption could also help prevent bacterial colonisation (Ostuni *et al.*, 2001). Therefore, much research is directed toward preventing attachment and biofilm formation through either the development of anti-adhesive or bactericidal surfaces (Junter *et al.*, 2016). Bactericidal coatings traditionally involved agents like antibiotics, copper, silver, and quaternary ammonium salts, that would subsequently be released into the environment causing antibiotic- and metal-resistant bacteria and is therefore not favourable (Banerjee *et al.*, 2011). Methods to improve the anti-adhesive properties of materials include modification of surface topography (roughness), enzymes, nanomaterials, photoactive agents, and physiochemistry such as hydrophilic or hydrophobic and cationic or anionic behaviour (Katsikogianni and Missirlis, 2004; Teughels *et al.*, 2006; Banerjee *et al.*, 2011; Zhang *et al.*, 2013). An overview of various approaches to fabricate antifouling surfaces is given in Figure 1.7.

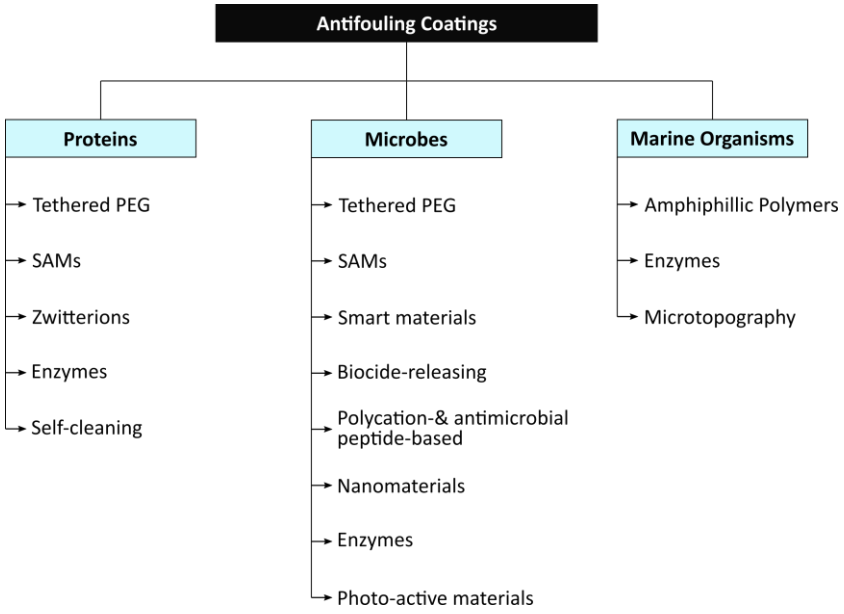


Figure 1.7: Schematic representation of various methods used for antifouling coatings. Different approaches are used to prevent protein fouling, bacterial attachment and specifically colonisation of marine organism. SAMs = self-assembled monolayers, PEG = poly(ethylene glycol) Figure taken from (Banerjee *et al.*, 2011).

One polymer that has been used for surface coating by many researchers is poly(ethylene glycol) (PEG) (Park *et al.*, 1998; Ostuni *et al.*, 2001; Roosjen *et al.*, 2004). PEG can induce protein resistance to a substrate, possibly due to the large steric repulsion forces that impede the approach of bacteria towards surfaces (Banerjee *et al.*, 2011). However, PEG undergoes oxidation and is therefore not suitable for long term use (Ostuni *et al.*, 2001; Roosjen *et al.*, 2004). Other materials under investigation include chitosan or biological molecules like albumin or heparin, which are based on surfactants (Arciola *et al.*, 2005; Banerjee *et al.*, 2011). Additionally, combinatorial polymer microarrays are used to discover novel materials consisting of a broad resistance to bacterial attachment (Hook *et al.*, 2013). A different approach to the use of polymers is the coating of materials by incorporating enzymes that either generate antimicrobial agents to prevent bacterial colonisation or that kill the bacteria directly on contact (Banerjee *et al.*, 2011). However, stability and self-degradation of enzymes are major disadvantages for this method. Another focus lies on the development of surfaces consisting of various topographies. The microstructures lead to resistance of the surfaces to biofouling but

seems to be species dependent (Efimenko *et al.*, 2009). Overall, a combination of surface topography and chemical composition seems to be a good approach for future antifouling materials.

1.2.4 Biofilm formation in washing machines

Communities of microorganisms can colonise humanmade inventions that incorporate water reservoirs, such as drains, water fountains, transvaginal ultrasound probes, urinary catheters, dishwashers, showerheads, household surfaces, or washing machines (WM) to form highly resilient biofilms (Rayner *et al.*, 2004; Feazel *et al.*, 2009; Gattlen *et al.*, 2010; Zalar *et al.*, 2011; Gupta *et al.*, 2016). Since its invention in 1851 by James King, the drum-based WM has spread all over the world and is still in wide use today. In Germany and the UK, 95% and 93% of the households own their own WM, respectively (Pakula and Stamminger, 2010; Statistisches Bundesamt, 2017). In other regions like China, Turkey and East Europe, the ownership rate of WMs is lower (Figure 1.8).

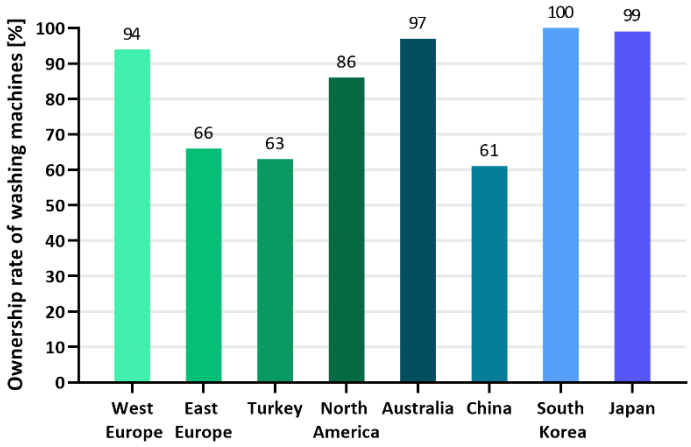


Figure 1.8: Ownership rate of washing machines. Taken from Pakula and Stamminger (2010).

Overall, laundering clothes is one of the most widespread housework worldwide and is responsible for 4% and 4.2% of electricity consumption for clothes washing in relation to total electricity consumption per household in Germany and the UK, respectively. The water consumption accounts for 9.8% in Germany, whereas no value is available for UK (Pakula and

Stamminger, 2010). Over the past decades, it has become apparent that clothes and laundry have the potential to be a part in the chain of infection transmission during normal daily activities similar to other hand contact sites (Bloomfield *et al.*, 2011). Therefore, the important aspect of laundering to fight against bacteria that colonise textiles came into focus in addition to the removal of stains and dirt from clothes (Arild *et al.*, 2003). The three main routes of reducing soil and microbial contamination of clothes include: (i) physical removal, (ii) thermal inactivation, and (iii) chemical inactivation (Arild *et al.*, 2003; Bloomfield *et al.*, 2013). During the physical removal, soil and microorganisms are suspended and the majority of microorganisms will be drained off during one of the multiple rinse steps. In addition to physical removal, microorganisms can be killed by heat achieved at high temperature washes, leading to thermal inactivation. Chemical inactivation can be obtained using detergents and bleaching agents (Arild *et al.*, 2003). An overview about the process and the environmental aspects is presented in Figure 1.9.

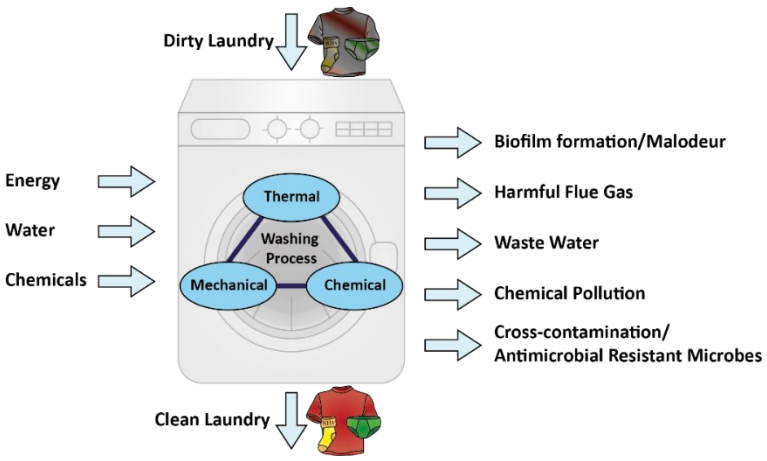


Figure 1.9: Overview about laundry process and the environmental impact. Adapted from Bao *et al.* (2017).

The washing procedures in different countries vary in temperature and show differences between the use of washing detergents. While eastern countries like China, South Korea, and Japan as well as the USA mainly use cold water, European countries wash at 30°C to 40°C, which offers favourable growth conditions for bacteria (Arild *et al.*, 2003; Brusdal, 2003; Pakula and

Stamminger, 2010). Multiple studies have shown that temperatures below 60°C result in significant reduction of sterilisation (Raschle, 1983; Davis and Ainsworth, 1989; Perenich and Wilkinson, 1993; Terpstra, 1998). Mainly because of environmental reasons, the washing process has been adapted to sustain energy in order to conserve resources and reduce costs, which negatively impacts laundry hygiene by enabling the survival of microorganisms inside the WM and the washed laundry (Munk *et al.*, 2001). Lower washing temperatures as well as lower rinsing efficiency to reduce water consumption have been reported to facilitate bacterial survival and even growth within WMs. In addition to reducing the thermal inactivation of microbes, lowering the temperature also diminishes the effectiveness of bleach agents of the detergents (Davis and Ainsworth, 1989). Additional energy saving steps has been introduced by shortening the overall wash cycles, leading to reduced soil removal and resulting in diminished hygienic quality (Terpstra, 1998; Munk *et al.*, 2001). Furthermore, it was previously common to dry laundry outside, enabling an increased microbiocidal effect achieved from sunlight. Additional ironing caused reduction of the microbial load, both of which have largely disappeared in many households (Bloomfield *et al.*, 2011). Therefore, steps have to be taken to ensure hygienic standards as the reduction of washing temperature increases the risk of bacterial survival and therefore results in cross-contamination of clothing in almost all performed washing procedures with pathogenic and non-pathogenic bacteria like *P. aeruginosa* (Davis and Ainsworth, 1989).

There exist two main sources from which microorganisms enter and contaminate the WMs and clothes: On the one hand, the human body consists of diverse microbiota on the skin and on the other hand, the environment is colonised with ubiquitous terrestrial water- and airborne microbes. A higher risk is described for laundry worn during contact with pathogens like hospital uniforms as well as work clothing being in direct contact with soil (Kagan *et al.*, 2002; Wilson *et al.*, 2007; Bockmühl, 2011). In addition, interactions with animals and pets can contribute to the

contamination of household textiles (Bockmühl, 2011). Various routes of transmission are presented in Figure 1.10.

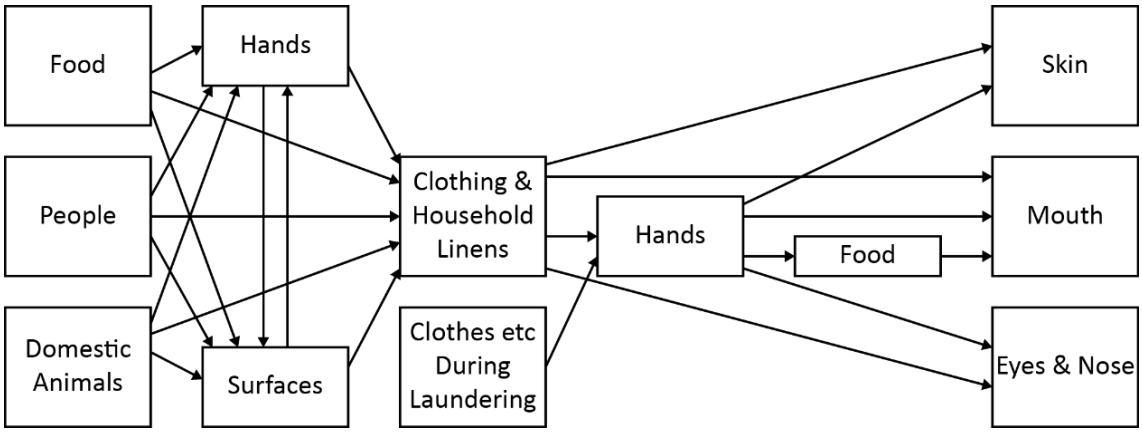


Figure 1.10: Transmission routes of infection involving clothing and household linens. Taken from Bloomfield *et al.* (2011).

Biofilms can be formed on almost all surfaces that come into contact with an aqueous environment. WMs provide an optimal environment for biofilm formation, especially on the parts consisting of plastic such as the detergent drawer, which is favourable for adhesion of bacteria and therefore for the development of biofilms (Sheane, 2000). Nutrition for bacteria is supplied by the dirty laundry in the form of sweat and dead skin cells as well as by water (Munk *et al.*, 2001; Nix *et al.*, 2015).

In a study by Gattlen *et al.*, eleven different WMs from four different countries and three different continents were sampled, showing that amongst the 94 isolated strains, 30% were potential human pathogens (Gattlen *et al.*, 2010). In contrast, Egert *et al.* only found 3.6% potential pathogens in toilet bowls (Egert *et al.*, 2010b). Further studies investigated the microbial transfer within WMs showing that even sterile samples were cross-contaminated during wash steps by other laundry textiles, with a higher cross-contamination at lower temperatures (Arild *et al.*, 2003; O'Toole *et al.*, 2009). In a study by Callewaert *et al.*, almost all bacterial genera that have been found on the initial cotton sample were still present after the wash procedure. The main bacterial isolates were proteobacteria, including *Pseudomonas*

species (Callewaert *et al.*, 2015). Another study by Egert *et al.* also identified alpha-proteobacteria as the main bacterial isolates (Egert *et al.*, 2010a). Proteobacteria are known for their predominant presence in drinking water supplies, suggesting that cleaning-water is the main source of bacteria in WMs (Egert *et al.*, 2010a; Bockmühl, 2011; Kwon *et al.*, 2011).

All those studies were based on traditional culturing methods. However, in the 1980s, the property of bacteria to be viable, but non culturable (VBNC) was identified with the potential to act as hidden reservoirs of infection (Xu *et al.*, 1982). More recent studies therefore use culture-independent techniques such as 454 pyrosequencing. Using this technique, Nix *et al*. have stated that different locations in twelve different WMs were highly colonised by biofilm-forming bacteria including VBNC microorganisms (Nix *et al.*, 2015). Furthermore, thirteen domestic WMs were sampled at four different sites (detergent drawer, door seal, sump, and fibres collected from washing solution) using 16S rRNA gene pyrosequencing. The bacterial community was found to be significantly site-dependent with the highest diversity found inside the detergent drawer (Jacksch *et al.*, 2019). In both studies, the majority of bacteria belonged to phylum of Proteobacteria as noted previously, with *Pseudomonas* identified as the predominant genera (Nix *et al.*, 2015; Jacksch *et al.*, 2019).

The increase of bacterial population in the WM has been identified as the main reason for malodour even in freshly washed clothing (Gattlen *et al.*, 2010; Kubota *et al.*, 2012; Takeuchi *et al.*, 2012). Additionally, laundry has been found as a route for potential disease development following infection outbreaks such as meningitis, Q-fever, and ringworm (Shah *et al.*, 1988; Aleraj *et al.*, 1990; Barrie *et al.*, 1994; Standaert *et al.*, 1994; Nguyen *et al.*, 2005; Dohmae *et al.*, 2008; Elias *et al.*, 2010). More recently, infection risks from WMs were demonstrated when thirteen new-borns and one child were colonised with *Klebsiella oxytoca* within a paediatric hospital in Germany between April 2012 and May 2013. *K. oxytoca* was isolated from the detergent drawer and the rubber door seal of a domestic WM that was used to wash laundry for the new-borns (Schmithausen *et al.*, 2019). Only after the WM was removed, further

colonisation could be stopped. It was suggested that the strain was introduced by residual water, which reaches a much lower temperature in the area of the rubber door seal and the detergent drawer than the 65°C used for the laundry. Although the current focus is on resistant superbugs within hospital environments, infection risks has also become a rising concern in domestic areas (Bloomfield *et al.*, 2011). For example, the number of persons being cared for in domestic settings is rising as well as the spread of multi resistant pathogens (Bockmühl, 2011). Additionally, fewer hospitals now launder staff uniforms. Instead, the staff is expected to use their own domestic machines to clean their uniforms, which mostly run at 40°C (Patel *et al.*, 2006).

However, to safeguard our planet, it has become clear long ago that the water consumption and pollution as well as the energy usage has to be reduced (Terpstra, 1998). The reasons for this include (i) increased environmental awareness, (ii) economic reasons based on the report of the Club of Rome 1967, and (iii) the energy crisis. Therefore, laundry liquid and powder composition has been adjusted and temperature profiles of WMs have adapted. These adaptions are based in part on recent developments in the reduction of wash temperatures, the use of enzymes to achieve visible stain removal, and to enable hygiene during cold washes, reduced water usage, and the removal of bleaching agents, which is driven by the trend for liquid products, where bleaches cannot be stably incorporated (Terpstra, 1998; Munk *et al.*, 2001; Laitala and Jensen, 2010; Niehaus *et al.*, 2011; Vojcic *et al.*, 2015). However, as already stated, temperatures below 60°C as well as reduced water consumption result in significant reduction of sterilisation (Raschle, 1983; Davis and Ainsworth, 1989; Ainsworth and Fletcher, 1993; Perenich and Wilkinson, 1993; Terpstra, 1998; Hall *et al.*, 2009; Lakdawala *et al.*, 2011; Honisch *et al.*, 2014). Peroxidic bleach systems used in powder products are also less effective for bleaching and hygiene at lower temperatures. Therefore, higher temperatures above 60°C have been recommended for thermal disinfection of textiles, but are only applied to a limited selection of clothing due to the stress on the fibres (Munk *et al.*, 2001; Bjarnsholt and Givskov, 2007; Gerba

and Kennedy, 2007; Department of Health, 2016). The International Scientific Forum of Home Hygiene Report in 2018 concluded that although lower temperatures are advisable in energy terms, steps have to be taken to ensure hygienic standards because the reduction of washing temperature increases the risk of bacterial survival resulting in cross-contamination of clothing in almost all performed washing procedures leading to the spread of antibiotic resistant strains such as MRSA (Davis and Ainsworth, 1989; International Scientific Forum on Home Hygiene, 2018).

1.2.5 Microniches within biofilms

As already mentioned, bacteria are able to rapidly adapt to environmental changes by fine-tuning their physiology and metabolism dependent on available resources and fluctuations. Within a biofilm, different microenvironments are likely to emerge with various characteristics such as the lack of oxygen, low pH, and high level of hydrogen peroxide (Moriarty *et al.*, 2007; Jensen *et al.*, 2017). These gradients can for example occur due to varied fermentation processes of different species within mixed biofilms, influences from outside of the biofilm that mainly affects the cells located close to the surface, or nutrient availability (Stewart and Franklin, 2008). Different growth rates could furthermore lead to heterogeneity of microniches within biofilms (Davey and O'Toole, 2000b). For instance, oxygen depletion by bacterial biomass and transfer limitation of the diffusive oxygen from the surrounding medium can lead to a decline in aerobic growth at the bottom of a biofilm (de Beer *et al.*, 1993; Kühl *et al.*, 2007; Jensen *et al.*, 2017).

In the literature, the observations of the relationship between pH and biofilm formation differ. For example, Ahmed *et al.* demonstrated that a trigger of biofilm formation in some bacteria, autoinducer-2-signalling (AI-2), is temperature dependent in *Streptococcus intermedius* but not pH-dependent (Vendeville *et al.*, 2005; Ahmed *et al.*, 2008; Hardie and Heurlier, 2008). In contrast, Sun *et al.* showed that a low pH together with glucose could improve AI-2 activity and that the addition of a low concentration of boric acid induces the synthesis of AI-2 (Sun *et al.*, 2016). Although this could be relevant for some bacteria, *P. aeruginosa* does not synthesize AI-2.

However, like many other bacteria, some of the molecules *P. aeruginosa* produces are AHLs, signal molecules for QS to mediate population density-dependent cell-cell communication. AHLs have been implicated in biofilm formation for many bacterial species. For instance, Yates *et al.* showed that the lactonolysis of AHLs is pH-dependent, with ring closure only taking place at reduced pH levels (Yates *et al.*, 2002), whereas Hostacka *et al.* demonstrated an accelerated biofilm production for *P. aeruginosa* at pH 7.5 and pH 8.5 in comparison to pH 5.5 using crystal violet quantification (Hoštacká *et al.*, 2010). A similar behaviour was described by Stoodley *et al.* who observed that *P. aeruginosa* biofilm thickness fell to 68% at a low pH of 3 (Stoodley *et al.*, 1997).

In contrast, studying the Gram-positive bacteria *S. aureus* and *S. epidermidis*, Nostro *et al.* found biofilms were 2.5 to 3 times thinner at high pH levels suggesting this to be a possible way to control biofilm formation in this species (Nostro *et al.*, 2012). Studies of *Streptococcus agalactiae*, whose infection can result in meningitis, have shown an accelerated biofilm formation in highly acidic conditions (D'Urzo *et al.*, 2014). For other group B streptococcal isolates, the same behaviour was found in vaginal infections of pregnant women where clinical isolates showed a higher biofilm formation rate at a vaginal pH of 4.5 in comparison to pH 7 (Ho *et al.*, 2013).

Although biofilm microenvironments are good targets for specific diagnosis and treatment of biofilm related infection diseases, metabolic changes and environmental microniches within biofilms are still poorly characterised as the development of appropriate techniques is challenging (Benoit and Koo, 2016; Benoit *et al.*, 2019). There exist various methods to measure intracellular pH, such as nuclear magnetic resonance spectroscopy (NMR), microelectrodes, surface-enhanced Raman scattering (SERS) and two-photon excitation microscopy (TPE) (Ramsing *et al.*, 1993; Vroom *et al.*, 1999; Kulichikhin *et al.*, 2007; Søndergaard *et al.*, 2014). NMR was used by Kulishikhin *et al.* to determine the effect of oxygen concentration on the intracellular pH of root tips of rice and wheat and can discriminate between cytoplasmic and

vacuolar pH (Kulichikhin *et al.*, 2007; Søndergaard *et al.*, 2014). Microelectrodes can also measure pH very accurately and have been used on a large variety of biological systems (Ramsing *et al.*, 1993; Hidalgo *et al.*, 2009). However, the resolution of microelectrode-based techniques is restricted for example by the tip size (Hunter and Beveridge, 2005; Hidalgo *et al.*, 2009). Furthermore, microelectrodes may only be used for larger tissues or whole small animals and not at a single-cell level as the insertion of the microelectrode can disturb the surroundings (Hunter and Beveridge, 2005; Søndergaard *et al.*, 2014). SERS is another promising tool to measure intracellular pH at a single-cell level but the resolution is not yet comparable to fluorescence-based measurements (Søndergaard *et al.*, 2014). TPE was described to provide images of biofilms four times deeper than CLSM without loss of contrast (Vroom *et al.*, 1999). However, those technologies are not accessible to all laboratories. Therefore, most recently, fluorescent nanosensors are most widely implemented in approaches to pH measurement (Søndergaard *et al.*, 2014; Elsutohy *et al.*, 2017; Fulaz *et al.*, 2019).

1.2.6 pH-sensitive nanosensors

Unlike metal nanoparticles, fluorescent nanoparticles exhibit higher hydrophilicity, biocompatibility, and stability under physiological conditions (Bae *et al.*, 2012). With a size of <100 nm, the use of nanosensors enables insertion into biofilms without disrupting the biofilm structure or other physical perturbation. Typically, nanosensors are devices that can measure a variety of chemical or biological events with a subsequent release of signals as result of the interaction between analyte and nanosensor. For instance, optical nanosensors use fluorescence signals, as fluorescence is sensitive and easy to visualise. Studies have already used nanosensors to look at oxygen concentration, glucose, or pH.

Different fluorophores are used to detect various pH levels in the neutral to acidic pH range, for example Oregon Green (OG), seminaphthorhodafluor-4F 5-(and-6) carboxylic acid (C-SNARF-4) and 5-(and-6)-carboxyfluorescein (FAM) (Hunter and Beveridge, 2005; Chauhan *et al.*, 2013). However, it has been reported that free fluorophores can interact with their environment and

therefore influence the emission characteristics (Večeř *et al.*, 2001). pH indicators like carboxyfluorescein can be affected by self-quenching and protein binding (Graber *et al.*, 1986). Vecer *et al.* described changes of photophysical characteristics resulting from an interaction of the probe carboxy SNARF-1 with cell constituents like proteins, lipids or nucleic acids after exposure of the dye to the intracellular environment (Večeř *et al.*, 2001). Furthermore, toxicity to cells, intracellular sequestration, and photo bleaching have been reported and must be considered (Graber *et al.*, 1986; Morelle *et al.*, 1994; Overly *et al.*, 1995; Cohen-Kashi *et al.*, 1997). Therefore, publications focus on nanosensors where the indicator dyes are entrapped within a protective polymer matrix to minimise the undesired side effects and interactions between the fluorophores and cells (Conway *et al.*, 1997; Panova *et al.*, 1997; Clark *et al.*, 1999; Søndergaard *et al.*, 2014; Chauhan *et al.*, 2016; Elsutohy *et al.*, 2017; Fulaz *et al.*, 2019). Incorporation of different pH-sensitive fluorophores in the correct ratio in a single nanosensor can enable the detection of the full physiological pH spectrum from pH 3.5 to pH 7.5 (Benjaminsen *et al.*, 2011; Chauhan *et al.*, 2011; Sun *et al.*, 2011). The nanosensor matrix enables the diffusion of ions to bind with the probe but prevents the release of the probe into the cell to reduce potentially harmful effects to the cells as well as protecting the dyes (Clark *et al.*, 1999; Desai *et al.*, 2014). The non-toxic matrix can consist either of silica or polyacrylamide, which is covalently bound to the fluorophores (Desai *et al.*, 2014). Polyacrylamide and silica are both inert, hydrophilic, porous, and inexpensive to produce (Aylott, 2003). Polyacrylamide nanosensors reach sizes between 30 to 100 nm whereas silica sol-gel particles have a slightly larger size up to 300 nm (Aylott, 2003; Desai *et al.*, 2014). Due to the small size, high quantities can be delivered with minimal cell perturbations (Clark *et al.*, 1999). Although it is possible to only use one pH-sensitive fluorophore for the nanosensors, a combination of one (or more) pH-sensitive dyes as indicator together with a pH-insensitive probe is often used. The pH-insensitive fluorophore acts as internal standard and is referred to as reference dye (Graber *et al.*, 1986; Clark *et al.*, 1999; Burns *et al.*, 2006; Chauhan *et al.*, 2013). The reference fluorophore constantly emits in a wavelength different to the analyte fluorophore and independent of the analyte

concentration (Desai *et al.*, 2014). The use of both a pH-sensitive and a pH-insensitive fluorophore increases the accuracy of ratiometric pH measurements as the analyte concentration is measured independently of changes in the sensor concentration, whereas single-color sensor imaging can only give a qualitative description of the local environment (Clark *et al.*, 1999; Sarkar *et al.*, 2010). Examples for reference dyes include Cy5, rhodamine B, and 5-(and-6)-carboxytetramethylrhodamine (TAMRA) (Burns *et al.*, 2006; Chauhan *et al.*, 2011; Sun *et al.*, 2011).

From the repertoire of pH-sensitive nanosensors available, polyacrylamide-based nanoparticles were selected in this study due to their small size and biocompatibility. To enable a physiological range between pH 3 and pH 8 to be measured and visualised, two pH-sensitive fluorophores, OG and FAM, were used. OG is pH-sensitive between pH 3.5 to 6.0, whereas FAM covers the range between pH 5.0 and 7.5. The excitation and emission spectra of both fluorophores lie at 488 nm (excitation) and 520 nm (emission) and do not overlap with the emission spectra of TAMRA (580 nm) used as reference dye. Therefore, the fluorescence intensity at 580 nm remains the same while the fluorescence intensity measured at 520 nm decreases with increasing protonation, thus decreasing pH, enabling ratiometric measurements of the surrounding pH at high resolution (+/- 0.17 pH units) (Chauhan *et al.*, 2013). The different stages of protonation are described in Figure 1.11, representative for FAM (fluorescein). The introduction of fluorine, an electron-withdrawing group, into fluorescein generates OG and lowers the pKa of the phenolic group (pKa = 3.3-6.1 for OG instead of pKa = 6.5 for fluorescein), leading to ionisation at lower pH (Sun et al., 1997).

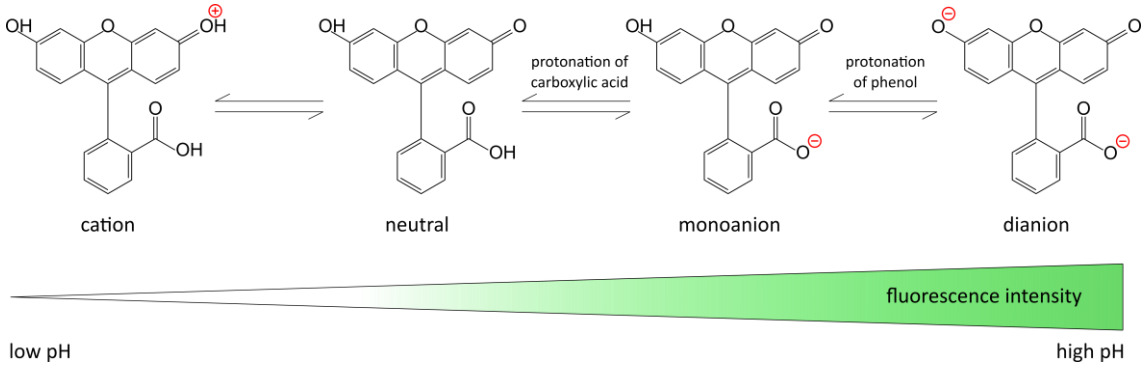


Figure 1.11: Different derivates of fluorescein exhibit multiple, pH-dependent ionic equilibria. At high pH, the fluorescein dianion is fluorescent with both the phenol and the carboxylic acid functional groups being ionised. Acidification of the dianion protonates the phenol, resulting in the monoanion, before the carboxylic acid becomes protonated to produce the neutral derivate of fluorescein. At very low pH, further acidification generates the fluorescein cation. Both the neutral and the cation are not fluorescent (Thermo Fisher Scientific, 2010b)**.**

All three fluorophores, OG, FAM and TAMRA, were covalently linked to a polyacrylamide nanoparticle matrix using APMA to synthesise ratiometric pH-sensitive nanosensors as described by Chauhan *et al.* (2013). APMA is used to conjugate the fluorophores to the polyacrylamide matrix formed of acrylamide and bisacrylamide. A schematic representation of the nanosensors can be found in Figure 1.12.

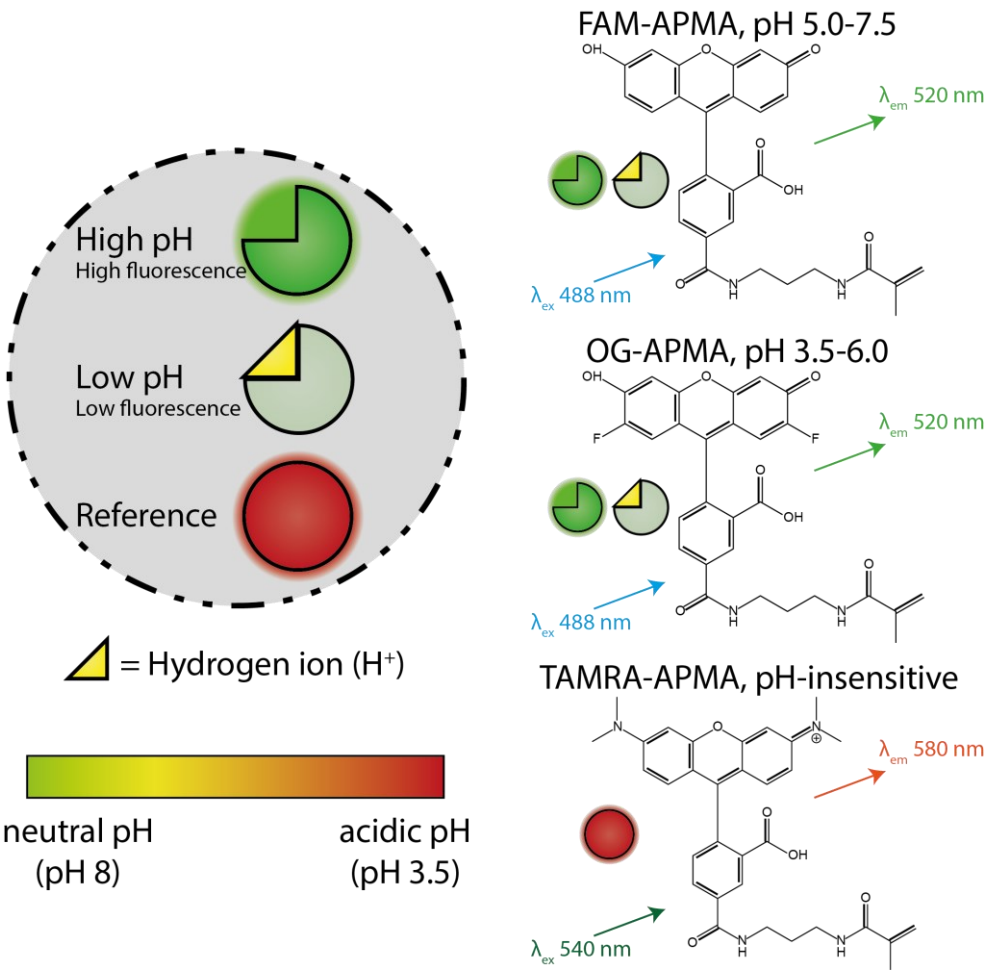


Figure 1.12: Schematic representation of extended dynamic range pH-sensitive nanosensors encapsulated in a matrix. The pH-sensitive dyes OG and FAM are both excited at 488 nm and show an emission peak at ~520 nm whereas the pH-insensitive dye TAMRA excites at 540 nm giving an emission peak at ~580 nm. Adapted from (Chauhan *et al.*, 2013)

This nanosensor design furthermore enables the simultaneous measurement of different analytes at the same time. Chauhan *et al.* constructed quadruple labelled oxygen and pH-sensitive nanosensors using the cationic Pt porphyrin, the two pH-sensitive dyes FAM and OG and the reference fluorophore TAMRA (Chauhan *et al.*, 2016). Those combined nanosensors were able to measure 0 to 100% oxygen content and a pH range from pH 3.5 to pH 7.5 (Chauhan *et al.*, 2016). The nanosensors in this study were synthesised via an inverse nanoemulsion polymerisation reaction performed by using water and oil. Tetramethylethylenediamine (TEMED) and ammonium persulfate (APS) were used to catalyse the polymerisation of acrylamide and bisacrylamide to create the polyacrylamide matrix. The two pH-sensitive dyes as

well as the reference dye were encapsulated by conjugation to the N-(3-aminopropyl) methacrylamide (APMA) matrix. The quaternary ammonium cationic monomer (3-acrylamidopropyl)trimethylammonium chloride (APTAC) was used to give a slight positive charge to the particles that are subsequently named positive nanoparticles/nanosensors as opposed to neutral nanosensors.

1.2.7 Different biofilm models

Most biofilm studies in the literature use *in vitro* biofilm models, as studying *in vivo* biofilms cause many difficulties. However, differences between laboratory and naturally occurring biofilms are likely to exist and require further comparison (Lebeaux *et al.*, 2013; Roberts *et al.*, 2015). For example, *in vitro* biofilms of *P. aeruginosa* were shown to be very different to biofilms grown *in vivo* within CF patients, with *in vitro* biofilms being denser in contrast to only relatively small aggregates within the infected CF lung (Jensen *et al.*, 2017).

Nevertheless, there exist many different *in vitro* biofilm models that are used for research in various areas. In general, the *in vitro* models can be divided into closed static models and open dynamic systems (Lebeaux *et al.*, 2013). Closed systems typically provide limited nutrients and aeration, but enable rapid quantification of biomass, for example using crystal violet or LIVE/DEAD staining. One of the most popular static models are microtiter plate (MTP)-based systems, where biofilms are grown on the bottom and walls of MTPs, mostly 96-well plates (O'Toole, 2011). Other popular systems include the Calgary Biofilm Device that is commercially available as minimal biofilm eradication concentration (MBEC) assay, where pegs are attached to the lids of 96-well MTPs (De Kievit *et al.*, 2001b). While the lid is closed, the biofilm will form on the surface of the pegs and can subsequently be transferred to a second plate containing various solutions, for example different antibiotic concentrations. After the treatment, the lid can be transferred to a third plate containing growth medium to allow regrowth or the biomass attached to the lids can directly be quantified. This system enables simple evaluation of effects

of different antimicrobial agents on biofilm eradication. A schematic representation is shown in Figure 1.13.

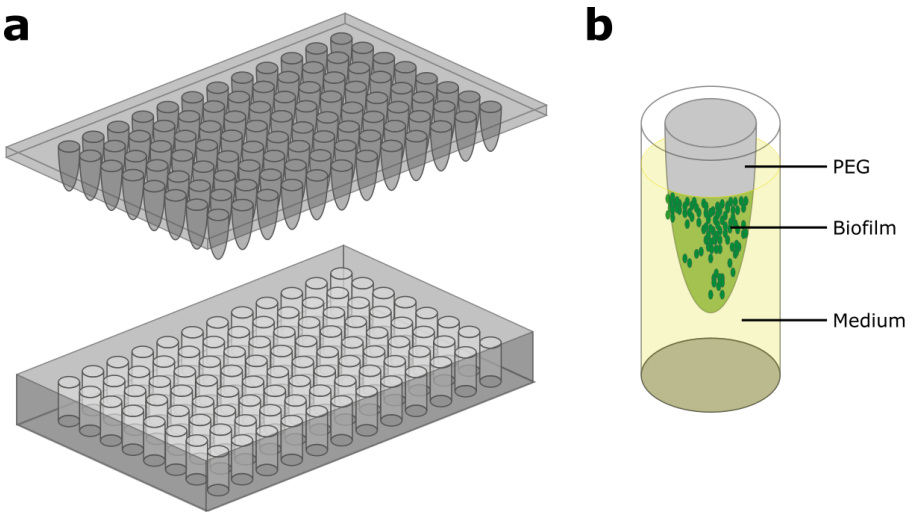


Figure 1.13: Schematic representation of peg lids. (a) Peg lid with 96-well plate below. **(b)** Biofilms grown on pegs within 96-well plate showing bacteria in dark green, biofilm matrix in pale green and medium in beige.

These closed systems are very user friendly because they are relatively cheap, only require small volumes of reagents, provide the opportunity to screen for large numbers of tests simultaneously, and enable the change of multiple parameters such as medium, incubation temperatures, humidity, and O_2 and CO_2 concentrations. However, closed systems are prone for environmental changes because of depleted nutrients and accumulation of molecules unless the medium is regularly replaced.

In contrast to static models, open systems allow a continuous exchange of medium (fresh and waste) to provide fresh nutrients at the same time as removing waste and planktonic cells. One example is the modified Robbins device (MRD) that can be constructed from plastic or stainless steel and consists of several individual ports arranged in a row (Coenye and Nelis, 2010). Each port can be modified with a disc made of different materials on which the biofilm will form. After initial attachment of the cells to the discs, a continuous flow of growth medium is applied to allow biofilm formation. At the end of the experiment, the discs can be detached to evaluate the effect of the material on biofilm formation. Other open systems include flow-cells that

typically consists of a glass chamber connected to a pump to circulate the growth medium, a container with fresh medium, and another container to collect the waste. An advantage of these type of chambers is the use of glass channels that can be used for real-time non-destructive microscopic analysis during biofilm formation. In addition, biofilms within microfluidic devices are usually grown under more physiologically relevant conditions than using static models. As a result of the continuous flow of fresh medium, the chemical microenvironment can be maintained, leading to a distribution of nutrients and metabolites within the biofilm (Jensen *et al.*, 2017). These gradients result in adaptation of the bacteria according to the actual chemical microenvironment leading to different growth zones and modes of metabolism. However, these simple customised chambers are often very limited in sample size and are therefore not ideal choices for larger screens. The more recently developed well plate microfluidic device called BioFlux (available through Fluxion Biosciences) allows high-throughput screening of biofilms under controlled environmental conditions using multi-channel plates that typically allow 12 (24-well plate) or 24 (48-well plate) different biofilm set-ups in one experiment. The system uses pneumatic pressure to push fresh medium through microchannels from an inlet containing the fresh medium to an outlet to collect the waste. Special design of the 24-well plates may allow a switch of flow medium during the experiment, for example to enable the addition of antimicrobials or other supplements to the biofilm during maturation. This can be achieved by providing two separate inlet wells with fresh medium that are connected with one outlet well (waste collection) through a channel where the biofilms will grow. The inlet chamber can be switched during the experiment to change the medium or concentration of supplements, for example. In contrast, a 48-well plate only consists of one inlet connected with one outlet chamber. With its portable heating plate, the whole system can be applied to a microscope to visualise biofilm formation in real-time (Brown *et al.*, 2019). A schematic figure of the BioFlux system using a 48-well plate with a single inlet is presented in Figure 1.14.

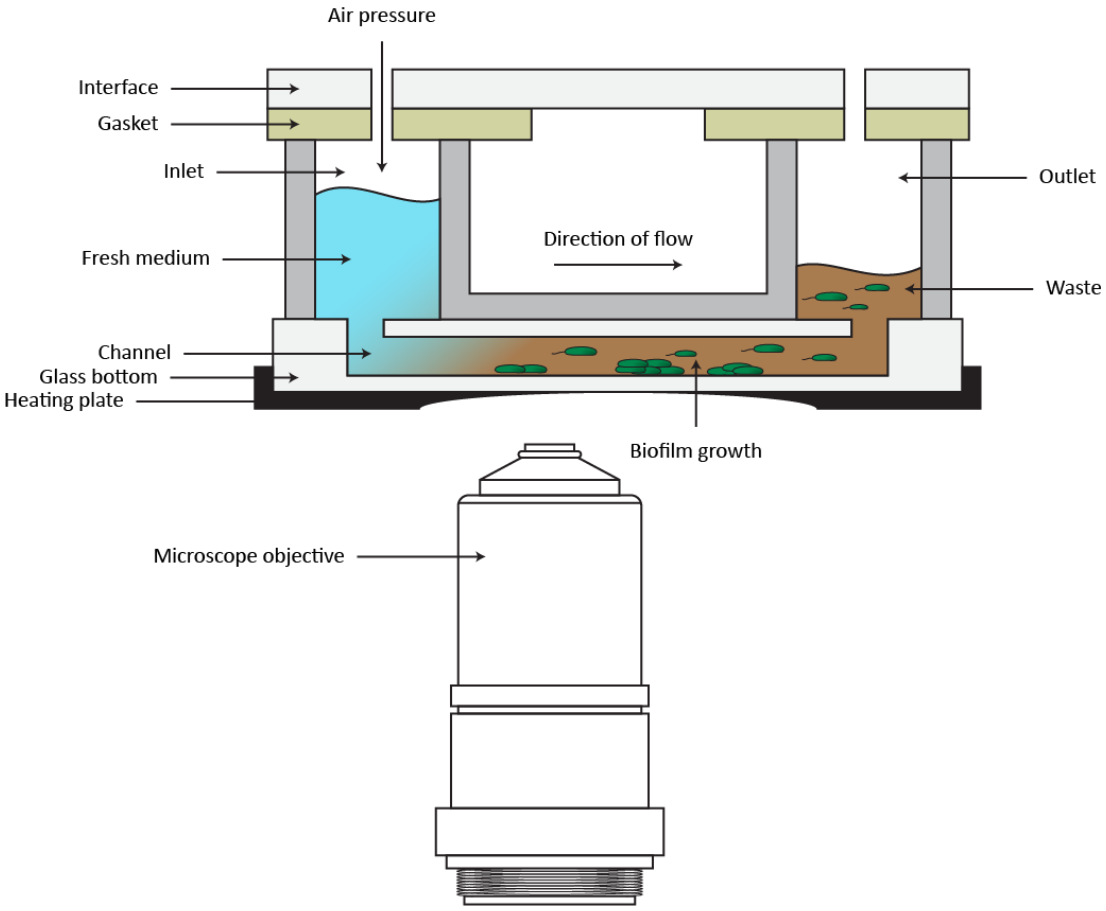


Figure 1.14: Schematic representation of the BioFlux flow-cell system. The system consists of the well plate, where each biofilm set-up includes an inlet well with fresh medium, the connected channel where the biofilm formation takes plate, and an outlet well to collect the waste. Air pressure is used to enable a continuous flow of fresh medium. The plate can be placed on a heating plate to allow temperature control, which consists of holes to enable real-time microscopy during the biofilm formation.

Although all the mentioned *in vitro* biofilm models can be used to test effects of simple parameters on biofilm formation and structure, it is not possible to mimic the complex host environment where biofilms naturally occur (Bjarnsholt *et al.*, 2013). Therefore, *in vivo* models were also developed, including *Caenorhabditis elegans* (round worm), *Galleria mellonella* (wax moth caterpillar), rats, mice, and guinea pig models (Lebeaux *et al.*, 2013). However, the use of *in vivo* models involving animals should always be kept to a minimum. One workaround is the use of cell-culture models and *ex vivo* models, in which tissues or organs are extracted from organisms and placed in an artificial environment, such as the polymicrobial biofilm skin model by Jordana-Lluch *et al.* or the *ex vivo* lung model by Harrison and Diggle (Lebeaux *et al.*, 2013;

Roberts *et al.*, 2015; Harrison and Diggle, 2016; Jordana-Lluch *et al.*, 2020). That way, a more controlled *in vivo* like environment can be provided.

The variety of available biofilm models all have their advantages and disadvantages. A detailed description of methods can for example be found in Roberts *et al.* (2015), (Franklin *et al.*, 2015), Lebeaux *et al.* (2013), or Coenye and Nelis (2010). It should be noted that several studies have shown that the choice of the biofilm system influences the outcome of experiments, for example when looking at the efficacy of antimicrobials on biofilm treatment (Coenye and Nelis, 2010). In addition, the method of choice to analyse the biofilm formation should carefully be considered, for instance time of flight-secondary ion mass spectrometry (TOF-SIMS) can visualise small molecules and biochemical gradients within bacterial biofilms, such as antimicrobials to determine penetration (Davies *et al.*, 2017). However, TOF-SIMS usually requires ultrahigh-vacuum conditions so that biofilm samples must be fixed and cannot stay hydrated, which can impact the biofilm structure and the molecular information obtained. As an alternative, it was shown that cryo-OrbiSIMS can be used to image biofilm samples consisting of >90% of water by preserving the native state using cryogenic sample handling and high-pressure freezing (Zhang *et al.*, 2020). Confocal laser scanning microscopy (CLSM) using a variety of different fluorescent labels is another popular technique to study biofilm formation without disturbing the environment. However, this technique requires labelling and cannot provide detailed information on small molecules such as QS signals (Zhang *et al.*, 2020). Alternatively, atomic-force microscopy (AFM) could be used to image microbial communities to give high-resolution insights into the topography and material properties of biofilm matrix without the need for labelling, staining, or other sample preparations and therefore enables detailed analysis under physiological conditions (Gazze *et al.*, 2016). In addition, many different methods exist to quantify *in vitro* biofilms using various (bio-)chemical/microbiological reference parameters, such as LIVE/DEAD fluorescence staining, standard plate counting (CFU method), a resazurin based assay, the BacTiter-Glo™ assay, and CV staining (Doll *et al.*, 2016). Previous studies have

proven that LIVE/DEAD staining in combination with CLSM is a valid method for reproducible quantification of bacterial adhesion and biofilm formation (Doll *et al.*, 2016). The kit combines two nucleic acid stains, SYTO 9 and PI, which compete for the same target areas. PI is excluded from cells with structurally intact cytoplasmic membranes because of the size and charge, whereas SYTO 9 can cross intact membranes to stain intracellular DNA (Hewitt and Nebe-Von-Caron, 2004). Thus, the LIVE/DEAD kit enables differentiation between bacteria with intact or damaged cytoplasmic membranes, but bacterial metabolic activity cannot be assessed (Doll *et al.*, 2016). Yet, cellular and membrane integrity can be used as one criterion to distinguish between viable and dead cells, as viable cells are assumed to have intact cell membranes that cannot be penetrated by staining compounds (Gregori *et al.*, 2001; Stiefel *et al.*, 2015). However, under some conditions, cells could be metabolically inactive while maintaining an intact cell membrane, whereas other cells could show reduced membrane integrity despite being viable, for example during exponential growth (Joux and Lebaron, 2000; Nebe-von-Caron *et al.*, 2000; Shi *et al.*, 2007; Trevors, 2012; Stiefel *et al.*, 2015). Therefore, it should be considered that the environment and the physiological status of the cells can influence the outcome of the viability staining when analysing the results (Shi *et al.*, 2007). It is therefore important to know the limitations of the systems and to choose a model that produces biofilms under conditions that are similar to the *in vivo* environment, where possible, and to use analysis techniques that enable appropriate examination of the sample. Additionally, different models should be used to confirm observations.

1.3 Thesis aims

Although biofilms have been studied extensively over the last decades, little is known about the miconiches that form within biofilms, mostly because of the lack of suitable analytical tools. The major aim of this work is to extend the understanding and characterisation of environmental microniches within biofilms to identify potential points of application for biocide penetration within the environment of washing machines by addressing the following questions:

- Can optical pH-sensitive polyacrylamide nanosensors be produced and used within planktonic as well as static and flow-cell biofilm models of *P. aeruginosa*?
- How does the pH change over time within planktonic cells as well as biofilms and can those changes and gradients be measured and visualised using the pH-sensitive nanosensors?
- How do bacteria isolated from household washing machines differ in their phenotypes and genotypes and are those strains better adapted to their environment within washing machines compared to lab strains?
- What effects do commercially available laundry products have on biofilm formation of *P. aeruginosa* and can encapsulated biocides improve the hygienic effect?

To answer these questions, established biofilm analysis will be combined with novel optical nanosensor technology. Initially, a system to monitor microniche pH in biofilms will be set up using *P. aeruginosa* as model organism. *P. aeruginosa* is involved in many biofilm-associated infections, is highly resistant to various antibiotics and has been shown to be the predominant organism found in biofilms grown in washing machines. In addition, there exist many robust, well characterised biofilm models for *P. aeruginosa*, making it an ideal choice for this study. One of the two most common lab strains, PAO1, was used as reference strain. PAO1 was originally isolated from a skin infection (chronic wound) in the 1950s and was the first sequenced *P. aeruginosa* strain (Stover *et al.*, 2000). The biofilms grown in static and flow conditions on abiotic surfaces and their pH-microniches will be examined by CLSM. Fluorescently labelled pH-sensitive nanosensors will be incorporated to detect pH changes in real time. Furthermore, the microbial ecology and environmental microniches of biofilms in washing machines will be characterised. Biofilms grown *in situ* within washing machines will be analysed using different methods to identify the organisms present. In addition, strains isolated from household washing machines will be included in this study to investigate phenotypic and genotypic diversity of environmental strains that act as a potential infection risk in naturally occurring biofilms.

Furthermore, commercially available laundry products to reduce microbial contamination and biofouling in washing machines will be evaluated to investigate the design of on-demand biocides that react upon pH changes to release formulations that can subsequently prevent biofouling. In summary, this work will advance knowledge in the field by elucidating pH-microniches within biofilms of *P. aeruginosa*. These findings will eventually help to produce on-demand biocides that respond to pH changes to reduce biofouling in washing machines and biofilm formation in general.

Chapter 2 Materials and Methods

2.1 Chemicals

Most chemicals used in this study were purchased from Sigma Aldrich if not stated otherwise. Oregon Green® 488 carboxylic acid (OG), 5-(and-6)-carboxyfluorescein (FAM), 5-(and-6)-carboxytetramethylrhodamine (TAMRA), CellMask™ Deep Red, 4',6-diamidino-2-phenylindole (DAPI), YOYO™-1, Concanavalin A Tetramethylrhodamine conjugate (ConA-TRITC), LIVE/DEAD™ BacLight™ Bacterial Viability Kit, hexane, ethanol absolute (99.5%), and phosphate buffer saline (PBS) were obtained from Invitrogen™ by Thermo Fisher Scientific. N-(3-Aminopropyl) methacrylamide hydrochloride (APMA, >98%) was obtained from Polysciences Inc. The liquid detergent, powder detergent, fabric conditioner and encapsulated benzalkonium chloride were provided by the industry partner Unilever. The composition can be found in Appendix A.

2.2 Minimal medium (M9) and lysogeny broth (LB)

Minimal medium (M9) was prepared by using 200 mL of 5x M9 salts (purchased by Sigma Aldrich), 2 mL $MgSO_4$ (1M), 100 µL $CaCl_2$ (1M) and 40 mL carbon source (0.5 M of glucose or succinate) in a total of 1 L. If not stated otherwise, succinate salt was used as sole carbon source (M9S). The initial pH at room temperature of M9 succinate was ~5.5, the pH of M9 glucose ~6.5.

Lysogeny broth, (LB, Bertani (1951)) was prepared by using 10 g tryptone, 10 g sodium chloride and 5 g yeast extract in a total of 1 L. If LB agar was prepared, 15 g agar was added to the medium prior to autoclaving. The pH was adjusted to pH 7.

2.3 Buffer solutions for pH-sensitive nanosensors

Buffer solutions with a pH ranging from 3.0 to 8.0 in 1.0 steps were prepared using 0.2 M Sodium phosphate (Na_2HPO_4) and 0.1 M Citric acid ($C_6H_8O_7$) as indicated in Table 2.1. The pH was adjusted using 0.2 M Sodium phosphate and 0.1 M Citric acid.

Table 2.1: pH buffer preparation using 0.2 M sodium phosphate and 0.1 M citric acid.

pH	Na_2HPO_4 [mL]	$C_6H_8O_7$ [mL]	H_2O [mL]
2.5	1.08	8.92	10
3.0	2.04	7.96	10
3.5	3.02	6.98	10
4.0	3.86	6.14	10
4.5	4.5	5.45	10.05
5.0	5.14	4.86	10
5.5	5.68	4.32	10
6.0	6.42	3.58	10
6.5	7.1	2.9	10
7.0	8.72	1.3	9.98
7.5	8.99	1.015	9.99
8.0	9.765	0.24	9.99

Na_2HPO_4 0.2 M sodium hydrogen phosphate, $C_6H_8O_7$ 0.1 M Citric acid, H_2O water

2.4 Bacterial strains and growth culture

LB medium was used as standard growth medium (liquid or solid as agar plate) with the addition of gentamicin at 20 µg mL^{-1}, where appropriate. *P. aeruginosa* was grown on plate or in liquid medium at 37°C for 16-20 h. Liquid cultures were prepared in 5 mL liquid media, inoculated with a single bacterial colony and shaken at 200 rpm. Strains were stored for the longer term as glycerol cultures that were made by using 500 µL overnight culture with 500 µL sterile 50% (v/v) glycerol and stored at -80°C. The bacterial strains used in this study are listed in Table 2.2.

Table 2.2: Bacterial strains used in this work.

Strain	Genotype/Notes	Source
Pseudomonas aeruginosa PAO1 Nottingham WT	Wild type, originally a wound isolate from Australia with a chloramphenicol resistance	(Klockgether *et al.*, 2010)
PAO1 Δ*psl*	Mutant derived from PAO1 with deletion of gene *psl*	unpublished, Hardie lab
PAO1 Δ*pel*	Mutant derived from PAO1 with deletion of gene *pel*	unpublished, Hardie lab
PAO1 Δ*tatA*	Mutant derived from PAO1 with deletion of gene *tatA*	unpublished, Hardie lab
WMB1.3, WM01D1, WM02F1, WM05D1, WM05D1R, WM05F1, WM05F1R, WM07C1, WM07D1	*P. aeruginiosa* strains isolated from household washing machines	unpublished, Hardie lab

2.5 Nanosensor preparation

Nanosensors were prepared as reported by Chauhan *et al.* (2013).

Conjugation of the three fluorophores OG, FAM and TAMRA to APMA

A 50 mM (pH 9.5) sodium tetraborate buffer in water was prepared and used to make a 0.002 mM APMA solution (5 mg APMA in 2.5 mL buffer). For each fluorophore (OG, FAM and TAMRA), 1 mg was weighed out in separate vials and suspended in 200 µL of the APMA solution. The mixtures were sonicated for 5 min before being incubated on an oscillator at room temperature for 24 h in the dark to allow conjugation of the fluorophores to the APMA. The dyes were stored in the dark at -20°C for further use.

Synthesis of polyacrylamide pH-sensitive fluorescent nanosensors

For the synthesis of the nanosensors, 1.59 g dioctyl sulfosuccinate sodium salt (AOT) and 3.08 g Brij L4 were weighed out, mixed in a 250 mL round bottom flask, and deoxygenated for 15-20 min using argon while being stirred. A 500 mL round-bottom flask was used to deoxygenate 100 mL hexane for 30 min using argon before 42 mL of the deoxygenated hexane was added to

the AOT and Brij solution. The flask was sealed with a stopper and a balloon under an argon atmosphere with continuous stirring as shown in Figure 2.1. For the synthesis of neutral polyacrylamide nanosensors, 540 mg acrylamide and 160 mg bisacrylamide were dissolved in 1.5 mL deionised water, whereas 513 mg acrylamide, 152 mg bisacrylamide and 119 µL (3-acrylamidopropyl) trimethylammonium chloride (APTAC) were used for the preparation of positively charged polyacrylamide nanosensors. The APMA-fluorophore conjugates were added to the acrylamide solution using 15 µL OG-APMA, 15 µL FAM-APMA and 60 µL TAMRA-APMA. The mixture was deoxygenated and added to the flask containing the surfactants and hexane using a syringe. After 10 min, 30 µL of ammonium persulfate (APS, 10% (w/v)) and 15 µL tetramethylethylenediamine (TEMED) were added to initiate the polymerisation. The flask was deoxygenated again, sealed, wrapped in aluminium foil, and incubated on the stirrer for 2 h. After the incubation, the hexane was removed using a rotary evaporator at 30°C and 30 mL of ethanol (100%) was added. The mixture was transferred to a 50 mL falcon tube and spun down at 3800 x *g* for 3 min using a Hermle centrifuge (Z300). The supernatant was discarded, and the pellet re-suspended in 30 mL of ethanol (90% in water). The mixture was spun down again at 3800 x *g* for 3 min and washed twice in 30 mL ethanol (100%) and then suspended in 10 mL of ethanol (100%). The mixture was transferred into a clean 250 mL flask and the ethanol was removed using the rotary evaporator at 30°C before the nanosensors were collected and stored at -20°C in the dark until further use.

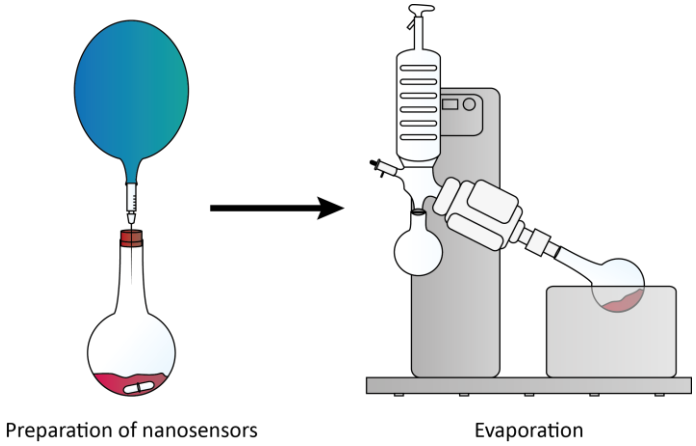


Figure 2.1: Schematic representation of nanosensor preparation. Left = Suspension sealed under argon atmosphere. Right = Evaporation.

2.6 Nanosensor characterisation and calibration

Size and ζ-potential determination

Dynamic light scattering (DSL) was performed using a Malvern Zetasizer Nano ZS. For the size determination of polyacrylamide nanosensors, 1 mg mL^{-1} nanosensors were prepared in PBS (10% (v/v)) and transferred into a cell disposable cuvette (Sarstedt). The mean diameter of the nanosensors was calculated from the intensity of scattered light measured by the Zetasizer. For the determination of the zeta potential (ζ-potential), 1 mg mL^{-1} nanosensors were prepared in PBS (10% (v/v) in water) and transferred into a disposable folded capillary cell (DTS1070, Malvern Panalytical) using a 2 mL syringe. Measurements were made at room temperature (25°C).

Emission scans and calibration of nanosensors

Polyacrylamide nanosensors were suspended in deionised water to a concentration of 2 mg mL^{-1}. Four-clear-sided cuvettes were prepared by adding 500 µL of buffer solution (see 0, Table 2.1) and 500 µL of the nanosensors to make a final concentration of 1 mg mL^{-1}. The cuvettes were sealed with parafilm and inverted prior to each measurement. Emission scans were performed with an Agilent Fluorescence Spectrometer for each sample for OG-FAM and TAMRA using the settings indicated in Table 2.3.

Table 2.3: Excitation and emission settings for emission scans of nanosensors.

	OG-FAM	TAMRA
Excitation wavelength	488 nm	540 nm
Emission wavelength	500 to 555 nm	560 to 620 nm

The ratio between OG-FAM and TAMRA was calculated using the highest fluorescence intensity for the emission scan at 520 nm and 580 nm, respectively. The linear part of the resulting sigmoid curve was taken to generate a linear regression, which was subsequently used to calculate the surrounding pH of nanosensors within biofilms or planktonic culture.

Alternatively, the nanosensors were calibrated using a black 96-well plate (Greiner Bio-one CELLSTAR® F-bottom) with a Tecan plate reader (Infinite® 200 PRO, Tecan). For each pH buffer, 200 µL containing 1 mg mL^{-1} polyacrylamide were added to a well. Single reads were taken with the settings as indicated in Table 2.4.

Table 2.4: Excitation and emission settings for pH calibration using a Tecan plate reader.

	OG/FAM	TAMRA
Excitation wavelength	488 nm	540 nm
Emission wavelength	520 nm	580 nm

For the nanosensor calibration using the Zeiss CLSM, polyacrylamide nanosensors were suspended in water and mixed with each of the individual buffers to make a final concentration of 5 mg mL^{-1}. The suspensions were placed in an 8-well glass bottom chamber (Ibidi) with 200 µL in each well and imaged using the CLSM. Image acquisition settings for the microscope were set on the brightest fluorescent intensity sample from the corresponding experiment and were kept constant throughout the measurement. OG and FAM were excited using the laser at 488 nm and TAMRA at 555 nm. The fluorescence intensities were measured for each buffer using ImageJ. A ratiometric curve was produced and used as described above.

2.7 Nanosensor filter assay

Neutral and positively charged polyacrylamide nanosensors were suspended in water at concentrations of 25 mg mL^{-1}, 20 mg mL^{-1}, 15 mg mL^{-1}, 10 mg mL^{-1}, 5 mg mL^{-1} and 1 mg mL^{-1}. An Agilent Fluorescence Spectrometer was used to measure the fluorescence intensity of OG-FAM and TAMRA (Table 2.4) before the solutions were filter sterilised using 0.22 µm polyethersulfone (PES) filters (Minisart®, starlab). As the fluorescence intensity is proportional to the nanosensor concentration, a linear regression was calculated. After the filtration, the fluorescence intensity of the nanosensor solutions was measured again and the resulting concentration was calculated with the help of the linear regression.

2.8 Sampling of strains from washing machines

Sterile plastic loops were used to streak samples from the drum, the detergent drawer, and the rubber seal of 19 different household washing machines onto LB plates (Figure 2.2). Three of the washing machines were resampled again after six weeks. The plates were sealed with parafilm and incubated at 37°C overnight. Single colonies were picked and streaked onto fresh LB plates, grown overnight, and subcultured onto *Pseudomonas* isolation agar (PIA). Colonies grown on PIA were considered possible *P. aeruginosa* strains and taken forward for strain identification and characterisation.

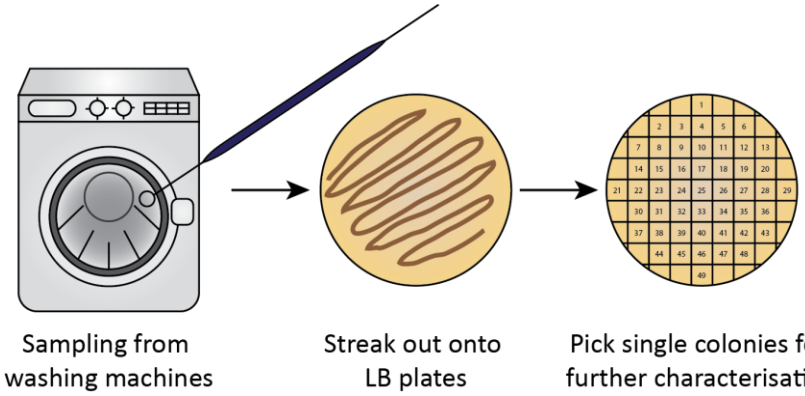


Figure 2.2: Schematic representation of the strain sampling from household washing machines.

2.9 Matrix-assisted laser desorption/ionisation (MALDI) time of flight mass spectrometry (TOF-MS) strain identification

Bacteria isolated from washing machines were streaked from -80°C glycerol stocks onto LB plates and incubated overnight. A single colony was selected and restreaked onto LB for another incubation overnight. Plates were sent to the Nottingham Analytical and Scientific Service, University of Nottingham, and matrix-assisted laser desorption/ionisation (MALDI) coupled with time of flight mass spectrometry (TOF-MS) on single colonies of the plates to identify bacterial species was carried out.

2.10 Whole genome sequencing

Preparation of strains for whole genome sequencing was done in accordance with the guidelines provided by MicrobesNG, Birmingham. A single colony of the strain to be sequences was picked from a fresh LB plate, mixed in 100 µL PBS and streaked onto another fresh LB plate. Around 1/3 of the plate was made a lawn of bacteria. After incubation of the plate at 37°C overnight, a large sterile loop was used to take all bacteria off the plate and mix into the barcoded bead tubes provided by MicrobesNG. The tubes were inverted ten times and sent off to MicrobesNG. DNA extraction and sequencing were performed by MicrobesNG and the sequences can be accessed following this link: https://microbesng.com/portal/projects/4EBB2167-5692-46DE-B2F9-40C0BD349F31/.

2.11 Whole genome sequence analysis

Trimmed raw reads of genomes provided by MicrobesNG were submitted to the Pathosystems Resource Integration Center (PATRIC) online platform (https://www.patricbrc.org/) (Wattam *et al.*, 2017). Several services from PATRIC were used for further analysis of the genomes, including the comprehensive genome analysis, the construction of a phylogenetic tree, the variation analysis to identify single nucleotide polymorphisms (SNPs), the proteome comparison, and the integrated BLAST service (Boratyn *et al.*, 2013). The phylogenetic tree was adjusted using iTOL 5.6.2 (Ciccarelli *et al.*, 2006). Variation analysis was performed using the aligner BWA-MEM with Free-Bayes as SNP caller and default parameters. Sequences of genes that were identified with SNPs were extracted from pseudomonas.com (Winsor *et al.*, 2016) and inserted into the PATRIC BLAST service to identify sequence identity between genomes. Multiple sequence alignments (MSA) were generated to investigate the location and impact of the mutations.

2.12 Optical density ($OD_{600\ nm}$) measurement

A Thermo Fisher Scientific spectrometer was used to measure the optical density (OD) of planktonic cultures prior to normalisation. A volume of 1 mL was prepared in a 1:10 dilution of the overnight culture (900 µL medium with 100 µL culture) and placed into a clear disposable cuvette. OD readings were measured at 600 nm if not stated otherwise. OD measurements using a spectrometer are not directly comparable with OD measurements taken with a Tecan plate reader (Infinite® 200 PRO, Tecan), which is described in 2.16.10.

2.13 DNA extraction

Overnight cultures of *P. aeruginosa* strains of interest were prepared from fresh LB plates and DNA extraction was performed using the QIAmp DNA Mini Kit (QIAGEN) according to manufacturer's instructions. Elution of the final DNA was carried out in 50 µL elution buffer instead of 200 µL to increase the final concentration. DNA concentration was measured using a Nanodrop and the extracted DNA was stored at -20°C until further use.

2.14 Polymerase chain reaction (PCR)

Polymerase chain reactions (PCR) were carried out according the manufacturer's instructions (GoTag® Green Master Mix Usage Information by Promega) using a Geneflow SensoQuest Lab Cycler. The composition of a 25 µL reaction using GoTag® Green Master Mix (Promega) and the standard programme are listed in Table 2.5.

Table 2.5: Components of GoTaq® PCR reaction and adjustment of the programme.

Component	Volume (µL)	PCR programme	
GoTaq® Green Master Mix	12.5	1) Initial denaturation	95°C, 5 min
Forward primer (10 µM)	0.5	2) Denaturation	95°C, 1 min
Reverse primer (10 µM)	0.5	3) Annealing	58°C, 30 sec
DNA template (≤ 250 ng)	1-3	4) Elongation	72°C, 40 sec
H_2O	8.5-10.5	*Repeat step 2) - 4) 35 times*	
	25	5) Final elongation	72°C, 10 min

P. aeruginosa specific 16S rRNA primers were used on extracted DNA to identify potential strains as *P. aeruginosa*. The sequences for primers can be found in Table 2.6 and were designed in a previous PhD project by Dina Lary.

Table 2.6: Oligonucleotide primers used to amplify 16S rRNA of *P. aeruginosa*.

Name	**Description**	**Sequence 5' – 3'**
PA-16SrRNA/F	16S rRNA *P. aeruginosa*	ATCCAGCTTCTTCATAAGCTCC
PA-16SrRNA/R		GCGCTTCTTCACTTGACC

2.15 Agarose gel electrophoresis

DNA molecules were separated in 1% (w/v) agarose gels in 1x TAE buffer (40 mM Tris, 20 mM acetic acid, and 1 mM EDTA) at 100 V by gel electrophoresis. SYBR™ Safe (Bio-Rad) was added to the gels for the detection of DNA via ultraviolet (UV) light. For PCR samples, the loading buffer was already included in the GoTaq® Green Master Mix (Promega) and 6 µL of each sample could be loaded directly to the gel. The 100 bp DNA ladder (New England Biolabs) was used for size determination. DNA fragments were visualised using the UV-trans illuminator (Bioline).

2.16 Phenotypic assays

2.16.1 Gram staining

A sterile plastic loop was used to pick a single colony from a fresh LB plate, which was suspended in 0.9% (v/v) saline on a microscope slide. After air drying, the cells were fixed on the plate using a Bunsen burner. Gram staining was performed based on Smith and Hussey (2005). Carbol fuchsin was used as counterstain and stains were left for 30 sec. After successful staining, the slides were analysed using a Nikon Eclipse widefield microscope with a 100x objective. Gram-negative bacteria were decolorized after the treatment and shown in pink whereas the thick layers of peptidoglycan of Gram-positive bacteria were stained in blue/violet.

2.16.2 Oxidase

Oxidase strips (Sigma Aldrich) were used on single colonies grown on LB plates. The colony to be tested was touched with the oxidase strip and observed for one minute. In presence of the enzyme cytochrome oxidase, the N,N-dimethyl-p-phenylenediamine and alpha-naphthol react to indophenol blue (dark purple colour), giving a positive result while no colour change indicates a negative result (Figure 2.3).

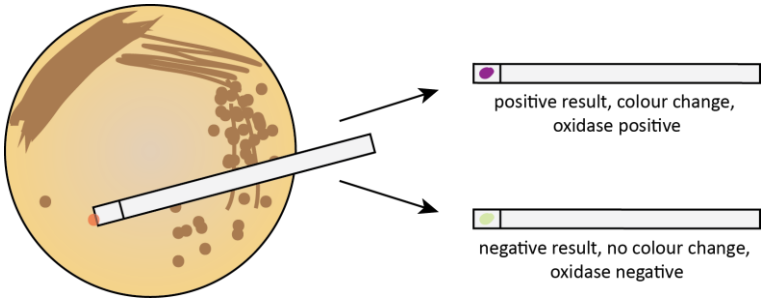


Figure 2.3: Schematic representation of oxidase assay using oxidase strips.

2.16.3 Catalase

Overnight cultures were normalised to an OD_{600} of 1 and 100 µL of culture was mixed with 100 µL of 1% Triton X-100 and 100 µL hydrogen peroxide (H_2O_2). Samples are catalase positive if immediate bubble formation can be observed as a result of the catalase enzyme hydrolysing the hydrogen peroxide (Figure 2.4).

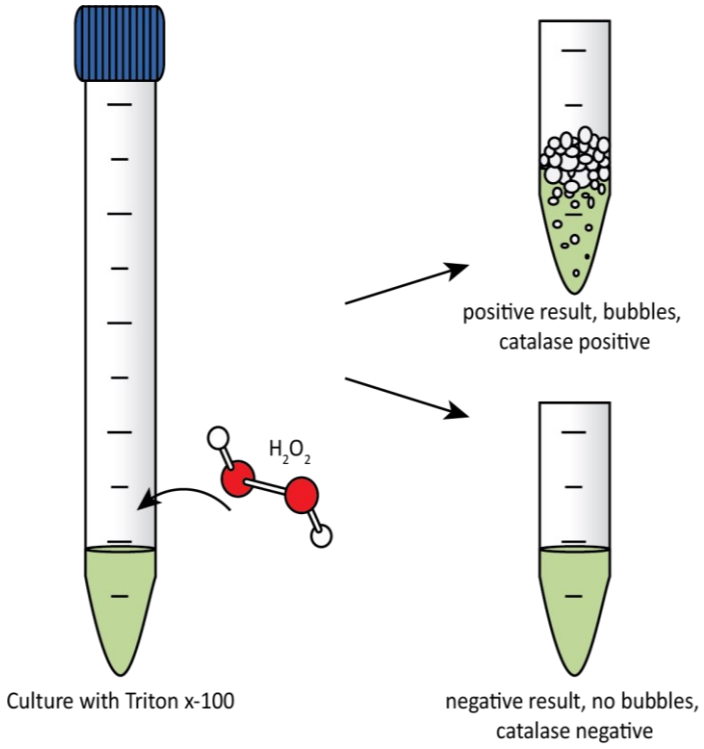


Figure 2.4: Schematic representation of catalase assay using hydrogen peroxide.

2.16.4 Swarming motility

Agar was prepared using 2 g Bactoagar and 3.2 g nutrient broth powder in 400 mL distilled water (0.5% agar). After autoclaving, 20 mL of 20% (w/v) glucose was added, and 20 mL was used for each plate. Plates were left to set for 30 min with the lid on before the lid was removed until the agar was completely set (safety cabinet). Overnight cultures were normalised to an OD_{600} of 1 and 3 µL were pipetted into the middle of the plate. Plates were incubated at 37°C overnight and motility observed by eye (Figure 2.5).

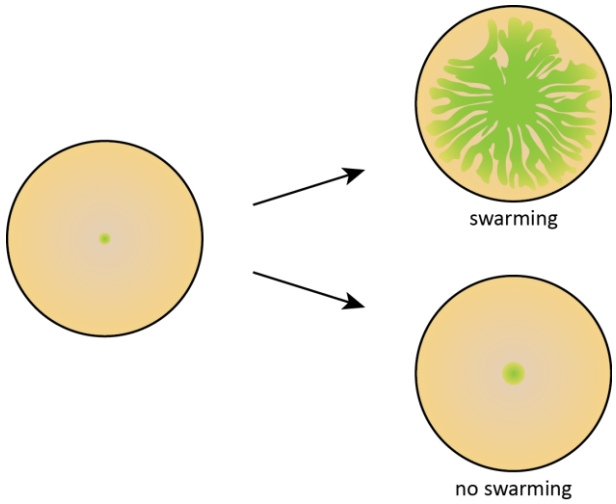


Figure 2.5: Schematic representation of swarming motility.

2.16.5 Swimming motility

Agar was prepared using 4 g tryptone, 2 g yeast extract, 4 g natrium chloride (NaCl) and 3 g agar technical in 400 mL distilled water (0.75% agar). After autoclaving, 20 mL was used for each plate. Plates were left to set for 30 min with the lid on. Overnight cultures were normalised to an OD_{600} of 1 and 1 µL was pipetted into the middle of the plate. Plates were incubated at 37°C for 6 h and motility observed by eye (Figure 2.6).

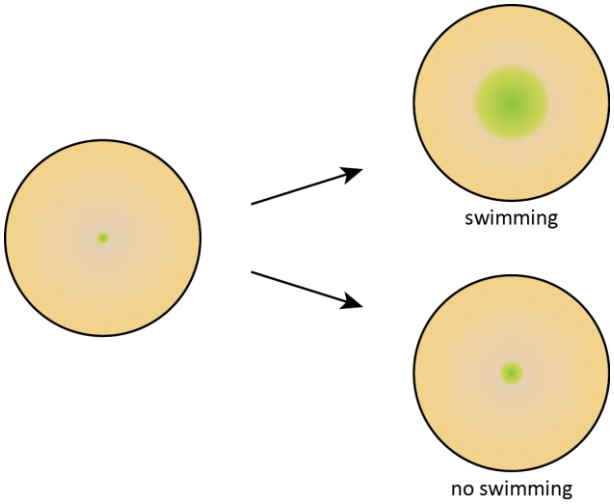


Figure 2.6: Schematic representation of swimming motility.

2.16.6 Protease production

Agar was prepared using 3.6 g of Bactoagar in 255 mL distilled water. After autoclaving, 45 mL skimmed milk was added, which has been sterilised by exposure to UV light for five minutes prior to addition, and 20 mL was used for each plate. Plates were left to set with the lids off until completely set. Overnight cultures were normalised to an OD_{600} of 1 and 10 µL were pipetted to the middle of the plate. Plates were incubated at 37°C overnight and protease activity determined by measuring the diameter of clearance (Figure 2.7).

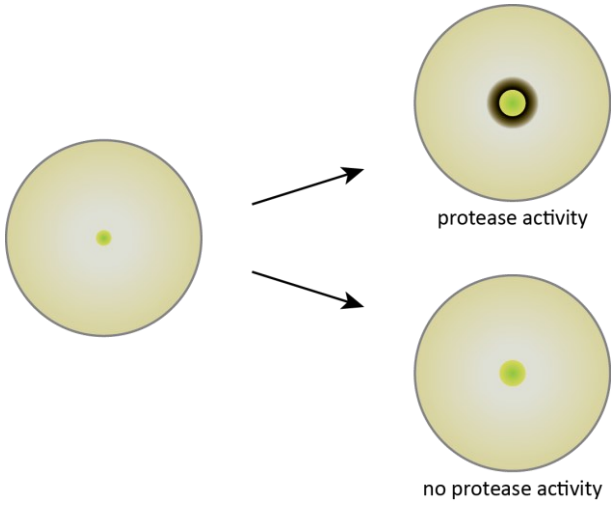


Figure 2.7: Schematic representation of protease assay.

2.16.7 Crystal violet (CV) attachment assay

Attachment of bacteria was assessed using crystal violet (CV) staining as reported by O'Toole (2011). Briefly, overnight cultures of strains of interest were normalised to an OD_{600} of 1 and diluted 1:100 in LB broth. For each strain, 100 µL culture was added to the well of a clear 96-well plate (Nunc™ MicroWell™ 96-Well Microplates, polystyrene, Thermo Fisher Scientific). Following 24 h of static incubation at 37°C, the medium was poured off and the wells were washed three times with water to remove any planktonic cells. Wells were air dried before being stained with 125 µL of 0.1% (w/v) CV for 10 min at room temperature. Any free CV was poured off and wells were washed two times with water. After air drying of the plates, the remaining CV bound to the attached bacteria was released by adding 150 µL of 30% (v/v) acetic acid for 10 min at room temperature before 125 µL was transferred to a new 96-well plate. The OD_{590} was measured using a Tecan plate reader (Infinite® 200 PRO, Tecan) indicating the amount of CV and hence the amount of bacteria attached to the wells.

2.16.8 Pyocyanin production

Pyocyanin levels were measured based on the absorbance of pyocyanin at 520 nm as described by Essar *et al.* (1990). Briefly, overnight cultures were normalised to an OD_{600} of 1 and diluted 1:100 in 16 mL Mueller Hinton broth (MH, cation adjusted, Sigma Aldrich) using 100 mL shaking flasks. The flasks were incubated statically for 24 h at 37°C. After the incubation, 2 x 5 mL were removed and spun down at 10.000 rpm for 5 min. The supernatant was filter sterilised and 3 mL chloroform was added. The mixture was vortexed, and the bottom blue coloured chloroform layer was transferred to a fresh tube. The tubes were vortexed again with 1 mL of 0.2 M hydrochloric acid (HCl) and spun down at 10.000 rpm for 5 min. The top pink layer containing the HCl and pyocyanin was transferred into a disposable cuvette and the OD_{520} was measured using a spectrophotometer. Pyocyanin concentration in µg mL^{-1} was calculated by multiplying the measured OD by 17.072 as described in Essar *et al.* (1990).

2.16.9 Minimal inhibitory concentration (MIC)

Overnight cultures of strains of interest were normalised to an OD_{600} of 1 and diluted 1:10 in Mueller Hinton broth (MH, cation adjusted, Sigma Aldrich). Benzalkonium chloride (BKC) was prepared in MH broth to obtain concentrations twice as high as the desired final concentration. For each of the concentrations, 100 µL was mixed with 100 µL of prepared cells in 96-well plates (Nunc™ MicroWell™ 96-Well Microplates, Thermo Fisher Scientific) to obtain final BKC concentrations and a start OD_{600} of 0.05. Plates were incubated statically for 24 h at 37°C before the OD_{600} was measured using a Tecan plate reader (Infinite® 200, Tecan).

2.16.10 Growth measurement of planktonic cells

Selected media were prepared with the addition of different supplements at selected concentrations (nanosensors = 1 mg mL^{-1} unless otherwise stated, liquid detergent = 2.9 mg mL^{-1}, powder detergent = 2.0 mg mL^{-1}, fabric conditioner = 2.9 mg mL^{-1}, BKC = 0.2 mg mL^{-1}, eBKC A and E = 0.51 mg mL^{-1}, eBKC B, C, D, F, G, H, I = 0.55 mg mL^{-1}). Concentrations of laundry product were selected in conjunction with Unilever to achieve concentrations comparable to a normal wash step in washing machines. Overnight cultures of *P. aeruginosa* grown in LB and adjusted to an OD_{600} of 0.05 in selected media were used to compare growth in clear 96-well plates (Nunc™ MicroWell™ 96-Well Microplates, polystyrene, Thermo Fisher Scientific). Each well was filled with 200 µL of the diluted culture. The plates were incubated at 37°C using a Tecan plate reader (Infinite® 200 PRO, Tecan) for 12 h to 20 h. The plates were shaken every 15 min for 10 sec with a settle time of 5 sec before the OD_{600} was measured.

2.16.11 pH measurement of planktonic cells

For the pH determination of planktonic cultures, nanosensors were filter sterilised (0.22 µm PES filter, starlab) before being added to the growth medium at a final concentration of 1 mg mL^{-1}. The fluorescence intensity for OG-FAM and TAMRA was taken every 15 min together with the OD_{600} during the growth measurement (2.16.10). Fluorescence was measured using the

following excitation and emission wavelengths: OG-FAM = 488 nm/ 520 nm, TAMRA = 540 nm/ 580 nm. Black 96-well plates (CELLSTAR® F-bottom, Greiner Bio-one) were used to reduce crosstalk between wells. The excitation and emission settings can be found in Table 2.4. A Tecan plate reader (Infinite® 200 PRO, Tecan) was used for the measurement. To determine the pH, wells were included containing nanosensors suspended in pH buffers, which were used to generate a calibration curve (see 2.6). With the help of the calibration, the pH of the samples was determined taking the fluorescence intensity ratio of OG-FAM and TAMRA.

2.16.12 Sugar challenge

An overnight culture of *P. aeruginosa* in LB was spun down and re-suspended in PBS for 30 min as a starvation step. The cells were spun down again and re-suspended in saline before being mixed with filter sterilised (0.22 µm PES filter, starlab) positively charged nanosensors in saline to obtain an OD_{600} of 1 and a nanosensor concentration of 1 mg mL^{-1}. The suspension was aliquoted into a black 24-well plate (PS, flat glass bottom, Greiner Bio-one) using 400 µL per well. Imaging was performed using a Nikon Eclipse Ti2-U inverted fluorescence microscope with a 40x/0.6 lens (see 2.21). An image was taken for time point 0 min before 20 µL of either glucose, lactose, or saline to a final concentration of 1% (v/v) was added to their respective wells. Images were taken every 5 min for 30 min (see 2.21). Additional controls with glucose, lactose, and saline solution added to 1 mg mL^{-1} positively charged nanosensors in saline without bacteria were also imaged to confirm the absence of any pH change brought on by the solutions themselves.

The calibration was performed using a fresh 24-well plate where pH buffers from pH 8 to pH 2.5 were mixed with positively charged polyacrylamide nanosensors for a final concentration of 1 mg mL^{-1}. Images were taken from each pH using the same exposure settings as for the experiment. The fluorescence intensity ratio from each pH buffer was plotted and the equation of the linear regression calculated to determine the pH values from the fluorescence intensities generated during the experiment.

2.17 Viability assay

BacTiter-Glo™ Microbial Cell Viability Assay (Promega) was performed according to the manufacturer's instructions (Promega, 2019). Overnight cultures of *P. aeruginosa* were normalised to an OD_{600} of 1 in 1 mL LB medium containing no supplement, 2.9 mg mL^{-1} liquid detergent, 2 mg mL^{-1} powder detergent or 2.9 mg mL^{-1} fabric conditioner. After incubation at room temperature for 30 min, 100 µL were transferred into wells of a white 96-well plate (non-treated, Thermo Fisher Scientific). To each of the wells, 100 µL of the provided BacTiter-Glo™ Reagent was added and mixed with the cells. After incubation for 5 min at room temperature, the luminescence intensity was measured using a Tecan plate reader (Infinite® 200 PRO, Tecan).

2.18 Biofilm formation

2.18.1 Static biofilm formation

Overnight cultures of *P. aeruginosa* grown in LB were used to spin down 1 mL of cells in a fresh Eppendorf tube at 1000 x *g* for 1 min. The pellet was re-suspended in 1 mL PBS, spun down again at 1000 x *g* and re-suspended in 1 mL of minimal medium (M9S). The OD_{600} was taken and the cells normalised to an OD_{600} of 0.5 in 1 mL of minimal medium. Depending on the experiment, the following steps are described in 2.18.1.1 and 2.18.1.2.

2.18.1.1 Supplements were added at the beginning of the experiment

Medium was prepared with the addition of supplements as shown in Table 2.7.

Table 2.7: Initial and final concentrations of supplements added to biofilm growth medium.

Supplement	Initial concentration	Final concentration
Nanosensors	1.5 mg mL^{-1}	1 mg mL^{-1}
Liquid detergent	4.35 mg mL^{-1}	2.9 mg mL^{-1}
Powder detergent	3.0 mg mL^{-1}	2.0 mg mL^{-1}
Fabric conditioner	4.35 mg mL^{-1}	2.9 mg mL^{-1}
BKC	0.4 mg mL^{-1}	0.2 mg mL^{-1}
eBKC A, E	1.02 mg mL^{-1}	0.51 mg mL^{-1}
eBKC B-D, F-I	1.11 mg mL^{-1}	0.55 mg mL^{-1}

To obtain the desired final concentration of supplements and a starting OD_{600} of 0.05, the normalised cells (OD_{600} of 0.5) were combined with the prepared media suspensions as listed in Table 2.8.

Table 2.8: Sample composition for static biofilm assays using M9 medium, normalised cells and M9 medium containing different supplements.

Supplement	M9 [µL]	Cells (OD_{600} 0.5) [µL]	M9 containing supplement [µL]
Control	675	75	-
Nanosensors	175	75	500
Liquid detergent	175	75	500
Powder detergent	175	75	500
Fabric conditioner	175	75	500
BKC	637.5	75	37.5
eBKC A, E	300	75	375
eBKC B-D, F-I	300	75	375

To each well of an 8-well glass bottom chamber (Ibidi), 300 µL of the suspension was added in duplicates before the chamber was set in a box wrapped in aluminium foil to prevent bleaching of nanosensors and placed in a static incubator at 37°C. After an incubation of 48 h, the medium was carefully removed and replaced by 200 µL fresh medium containing 3.34 mM SYTO 9 and 20 mM propidium iodide (PI, Thermo Fisher Scientific) to stain live and dead cells or 2.5 µg mL^{-1} CellMask™ Deep Red (Thermo Fisher Scientific) to stain the cell membrane. Experiments that included laundry products did not include the wash step, instead fresh medium containing SYTO 9 and PI was directly added to the wells. Chambers were incubated for 10 min at 37°C in the dark before the biofilms were imaged using a Zeiss CLSM and the appropriate laser settings for the fluorescence channels (see 2.22).

2.18.1.2 Supplements were added after 48 h of biofilm formation during the imaging

Dilutions of cells were prepared using 675 µL of medium and 75 µL normalised cells to obtain a starting OD_{600} of 0.05. To each well of an 8-well glass bottom chamber (Ibidi), 300 µL of the suspension was added before the chamber was placed in a static incubator at 37°C. After an incubation of 48 h, the medium was carefully removed and replaced by 200 µL fresh medium containing 3.34 mM SYTO 9 and 20 mM PI (Thermo Fisher Scientific) to stain live and dead cells or 2.5 µg mL^{-1} CellMask™ Deep Red (Thermo Fisher Scientific) to stain the cell membrane. Medium was prepared with the addition of supplements at initial concentrations as shown in Table 2.9.

Table 2.9: Initial and final concentrations of supplements prepared in M9S, which were added to an established biofilm during the imaging process.

Supplement	Initial concentration	Final concentration	Volume added [µL]
Nanosensors	3 mg mL^{-1}	1 mg mL^{-1}	100
Liquid detergent	14.5 mg mL^{-1}	2.9 mg mL^{-1}	50
Powder detergent	10 mg mL^{-1}	2.0 mg mL^{-1}	50
Fabric conditioner	14.5 mg mL^{-1}	2.9 mg mL^{-1}	50
BKC	2.2 mg mL^{-1}	0.2 mg mL^{-1}	20
eBKC A, E	5.61 mg mL^{-1}	0.51 mg mL^{-1}	20
eBKC B-D, F-I	6.05 mg mL^{-1}	0.55 mg mL^{-1}	20

The biofilms were imaged using a Zeiss CLSM and the appropriate excitation and emission settings for the fluorescence channels (see 2.22). After the initial image, the appropriate amount of the prepared solution (given in Table 2.9) was added to the well and the same spot as before was imaged every 5 min for 30 min.

2.18.2 Flow-cell biofilm formation using the BioFlux system

Liquid cultures of *P. aeruginosa* were prepared in 5 mL LB using a 1:100 dilution from an overnight culture and incubated at 37°C, 200 rpm until an OD_{600} of 0.4-0.6 was reached. The cells were normalised in 1 mL M9S to an OD_{600} of 0.05. The BioFlux channels were coated with 100 µL medium at a flow of 2 dyn cm^{-2} for 4 min before they were seeded with 50 µL of normalised cells for 3 sec at 2 dyn cm^{-2} (from the outlet to the inlet) and left for incubation on the heating plate at 37°C for at least 45 min. M9S with supplements at selected concentrations was prepared (nanosensors = 5 mg mL^{-1}, liquid detergent = 2.9 mg mL^{-1}, powder detergent = 2.0 mg mL^{-1}, fabric conditioner = 2.9 mg mL^{-1}, BKC = 0.2 mg mL^{-1}) and 1 mL was used for the inlet of a 48-well plate or for inlet 2 of a 24-well plate. If a 24-well plate was used, 1 mL of plain M9S medium was

added to inlet 1. The BioFlux (Fluxion Biosciences) was run from the inlet to the outlet at a flow of 0.2 dyn cm^{-2} for 24 h (48-well plate) or for 12 h using inlet 1 with a following switch to inlet 2 for up to 12 h (24-well plate). A Nikon Eclipse Ti2-U fluorescent microscope was used for time-lapse imaging every 15 min with the appropriate settings (see 2.21). End point images were taken using the Zeiss CLSM (see 2.22). A schematic view of the 48-well plate and 24-well plate is given in Figure 2.8.

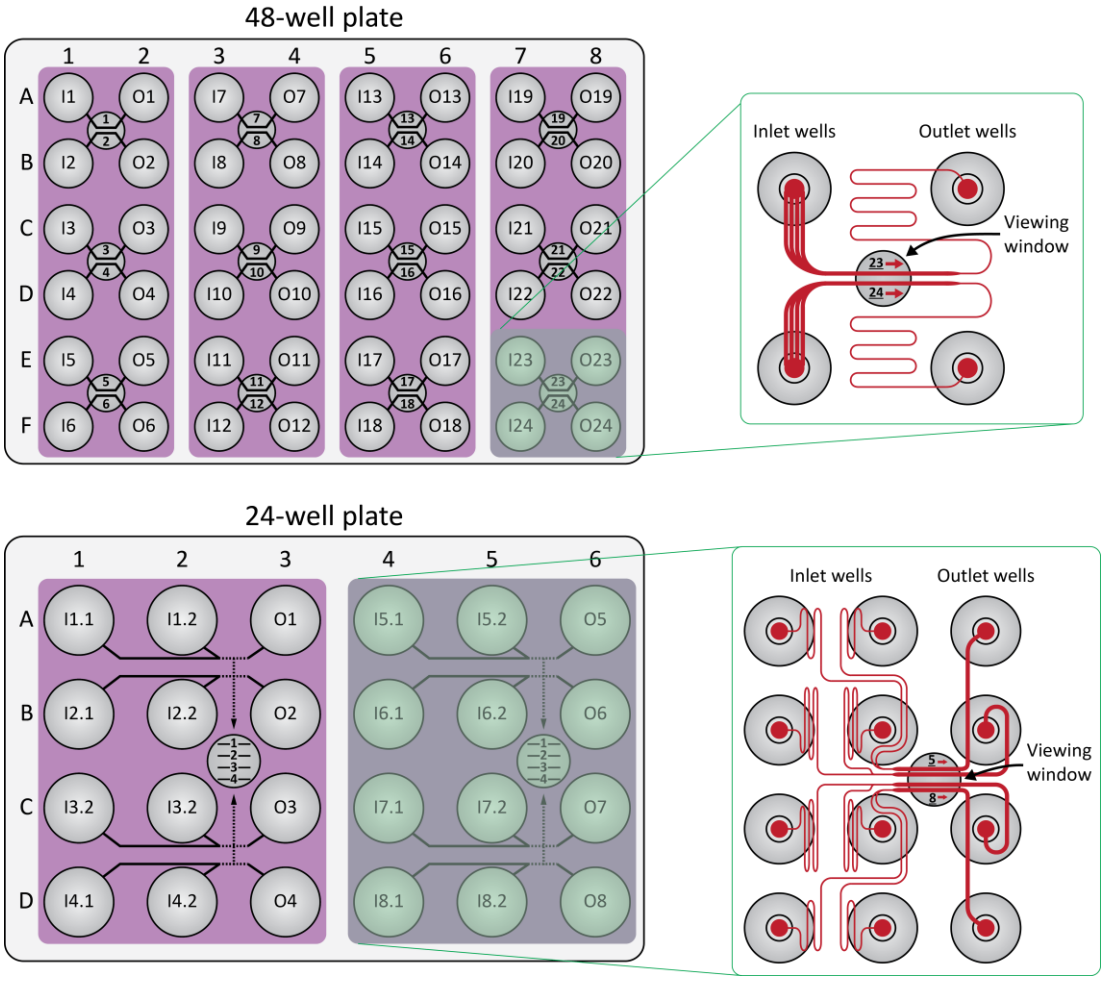


Figure 2.8: Schematic representation of 48-well BioFlux plate (top) and 24-well plate (bottom). 48-well plates consist of one inlet that is connected to one outlet, whereas 24-well plates have two inlets that are connected with one outlet.

2.18.3 ConA and YOYO™-1 staining

The concanavalin A-tetramethylrhodamine (ConA-TRITC, Thermo Fisher Scientific) conjugate was used at a concentration of 50 µg mL^{-1} to stain the exopolysaccharide Psl, whereas YOYO™-1

(Thermo Fisher Scientific) was used at 0.1 µM to stain extracellular DNA. The dyes were added to established static biofilms during the wash step or were directly added to the flow medium in flow-cell experiments. Red (ConA-TRITC) and green (YOYO™-1) filter settings were used for the widefield microscopy (see 2.21) and the 555 nm laser and 488 nm laser for the CLSM (see 2.22).

2.18.4 Colony forming unit (CFU) experiments of static biofilms

P. aeruginosa biofilms were set up as described in 2.18.1. Instead of 8-well glass bottom chambers (Ibidi), clear 24-well plates (Corning® Costar® TC-Treated Multiple Well Plates, Sigma Aldrich, CLS3526) were used to increase sample throughput, with each well containing 1 mL of culture with or without the addition of laundry products or BKC/eBKC (see 2.18.1 for final concentrations). After 48 h of static incubation at 37°C, the remaining growth medium was removed, and 1 mL of PBS was added to each well. If the growth medium contained laundry products, the medium was not removed, and 1 mL of PBS was directly added to the biofilms. If established biofilms were treated with laundry products or BKC/eBKC after the 48-h growth, the remaining growth medium was removed and replaced with medium containing the supplement at the desired concentration for 30 min. Following, the plate was sonicated for 30 sec (Ultrasonic cleaning unit Elmasonic S) before the biofilm was scratched from the surface and resuspended using 1 mL pipette tips. Dilutions (1:10) were prepared in PBS (10^{-1} to 10^{-8}) and 5 µL of each dilution was pipetted onto fresh LB plates in triplicates. Plates were incubated overnight at 37°C and single colonies were counted for the dilution in which single colonies were countable (Figure 2.9).

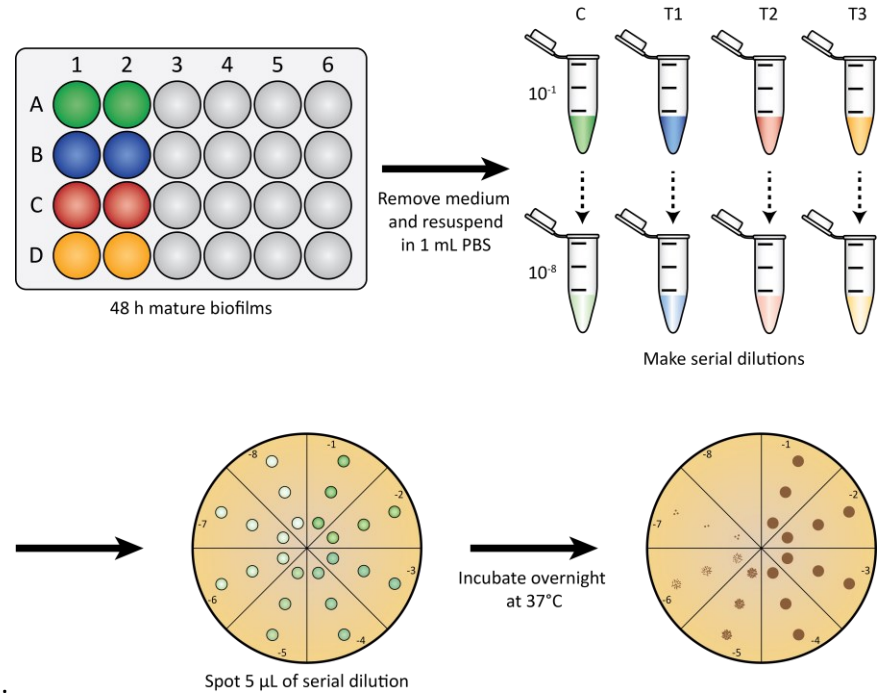


Figure 2.9: Schematic representation of colony forming unit experiments. Two replicates for the control (wells A1 and A2 (C)) and each treatment (wells B1 and B2 (T1), wells C1 and C2 (T2) and wells D1 and D2 (T3)) are presented in the same colour displayed in the 24-well plate. One replicate is taken as representation for the preparation of the dilutions. Subsequently, the dilutions of the control are taken forward for the plating. C = control, T = treatment

2.19 Structured illumination microscopy (SIM) of planktonic cells

Overnight cultures of *P. aeruginosa* were prepared in 5 mL LB broth with and without the addition of 1 mg mL^{-1} positive or neutral nanosensors. For all three overnight cultures, 1 mL was taken, spun down at maximum speed and resuspended in fresh LB broth. The wash step was performed twice to remove all nanosensors. Agarose pads were prepared by adding 1% (w/v) molten agarose in water to a fresh squared petri dish plate (~5 mm thick). Once the agarose was set, small cubes (~0.5 cm x 0.5 cm) were cut out of the gel to be used as base for the cells to prevent movement of bacteria. Fluorescent TetraSpeck™ Microspheres (0.1 µm, Thermo Fisher Scientific) were vortexed and diluted 1:10 in sterile MiliQ water before 0.5 µL were applied to an agarose cube and mixed with 4.5 µL cells (washed or unwashed). Once the cells were soaked into the agarose, the cube was placed into a glass bottom dish (Matek Life Sciences, 35 mm dish with 20 mm glass microwell, coverslip no. 1.5) upside down with the cell surface facing the

bottom of the plate. A Zeiss Elyra PS.1 with structured illumination microscopy was used with a Zeiss C-Apochromat 63x/1.2 W Korr M27 water objective lens. Images were processed using Zen black and blue software.

2.20 Scanning electron microscopy (SEM) to investigate initial attachment of bacteria

Differently coated glass disks (round, 1.5 cm diameter, Unilever) were transferred to a clear 12-well plate (Thermo Fisher Scientific), one per well. Overnight cultures of *P. aeruginosa* were normalised to an OD_{600} of 0.05 in tryptic soy broth (TSB, Sigma Aldrich) and 2 mL of the culture were added per well to completely cover the glass disk. The plate was incubated at 37°C for 3 h. For the fixation of the cells, 2 mL of 2.5% glutaraldehyde (Sigma Aldrich) were transferred into the wells of a fresh 12-well plate and glass disks were transferred into the new wells for 2 h at 4°C. During the incubation, Ethanol was prepared in different concentrations (20%, 40%, 60%, 80% and 100% (v/v)) and 2 mL were added to wells of a fresh plate (one plate for each concentration). The glass disks were transferred to each concentration for ½ h, starting with the lowest concentration going upwards to enable dehydration of the sample. Following, the glass disks were transferred to an empty plate and stored at 4°C until further use.

For the imaging, the glass disks were mounted on aluminium stubs using silver (Acheson Silver DAG 1415M, agar scientific) and stored in a desiccator overnight. The samples were sputtered with chromium for 10 sec at 120 mAmp (Quorum Q150T, Quorum Technologies). A Hitachi S-4800 scanning electron microscope was used for the imaging.

2.21 Widefield microscopy

To generate widefield images, a Nikon Eclipse Ti2-U inverted fluorescence microscope was used fitted with a 10x Plan Fluor DIC L N1 lens, a 20x/0.45 S Plan Fluor ELWD lens, or a 40x/0.6 S Plan Fluor ELWD lens. Images were captured by using a Photometrics CoolSNAP MYO camera connected to the NIS-Elements software. Excitation and emission wavelength were used as

follows: OG-FAM, SYTO 9 or YOYO™-1 = 460/525 nm, TAMRA, PI or ConA = 550/620 nm, and CellMask™ Deep Red = 550/650 nm.

2.22 Confocal laser scanning microscopy (CLSM)

To generate detailed images, a Zeiss LSM 700 compact CLSM was used fitted with a HAL 100C lamp for light illumination and a Zeiss Plan-Apochromat 63x/1.40 Oil DIC M27 objective or a C-Apochromat 40x/1.20 W Korr M27. Images were captured by using an AxioCam digital microscope camera connected to ZEN software and analysed using Zen black and blue software. Lasers were used as follows: SYTO 9 or YOYO™-1 = 488 nm, PI or ConA = 555 nm, CellMask™ Deep Red = 639 nm, OG-FAM = 488 nm, and TAMRA = 555 nm.

2.23 Image analysis using Zen and ImageJ

Image analysis was performed using Zen blue/black (CLSM, Zeiss) and ImageJ/FIJI (Abràmoff *et al.*, 2004).

2.24 Automated image analysis using MATLAB

Automated pH analysis of CLSM images using MATLAB (MathWorks) was based on a previously reported protocol by our research group (Chauhan *et al.*, 2013). Biofilms consisting of nanosensors were imaged using a Zeiss CLSM with an image size of 1024 × 1024 pixels (see 2.22). For the calibration of the nanosensors, fluorescent images of nanosensors in pH buffers (see 0) and background images (buffer without nanosensors) were taken for each corresponding pH value. Background-corrected ratiometric images were generated automatically using MATLAB after subtraction of the background images from the corresponding ratiometric fluorescent images. The calibration curve was constructed using the mean of the pixel ratios of two background-corrected images. The biofilm images were processed in the same way. ImageJ was used to construct a false colour heat map of the pH images as well as a 3D rendering of the biofilms.

2.25 Statistical analysis

Statistical analysis was preformed using GraphPad Prism. Prior to a significance test, all data was tested for normal distribution using a Kolmogorov-Smirnov test. If the data passed the normality test with alpha = 0.05, the results were classified statistically significant or not significant using an ordinary one-way ANOVA or two-way ANOVA with Sidak's multiple comparison test. Unpaired t-tests were used if only two conditions were compared. If data could not be considered normal distributed, a non-parametric Mann-Whitney test was used for grouped data or if only two conditions were compared. Otherwise, a non-parametric Kruskal-Wallis test was performed. Although testing for normal distribution was performed for each data set, only the subsequently applied significance test was stated in each figure legend based on the outcome of the normality test.

Significance levels were given as follows: $p<0.05$ (indicated as *), $p<0.01$ (indicated as **), $p<0.001$ (indicated as ***), and $p<0.0001$ (indicated as ****).

Number of replicates were indicated as n = **a** x **b**, with **a** specifying biological replicates and **b** technical replicates for each biological replicate. If only technical replicates were available or the differentiation was difficult, the number was indicated as n = **a**.

Chapter 3 Preparation and characterisation of fluorescent, pH-sensitive polyacrylamide nanosensors for the use in planktonic and biofilm models of *P. aeruginosa*

3.1 Introduction

3.1.1 Background

The biofilm communities that bacteria form on surfaces are dynamic and complex. The architecture of biofilms and the identity of extracellular components have been characterised *in vitro* for a variety of biofilms, although there is discussion in the literature about how representative this is of *in vivo* bacterial communities (Lebeaux *et al.*, 2013; Chua *et al.*, 2015; Roberts *et al.*, 2015; Brackman and Coenye, 2016; Fernandez-Barat *et al.*, 2018). Whilst there is evidence for fluid channels and microcolonies within *in vitro* biofilms, the characterisation of the environmental microniches these create has been limited due to the absence of analytical tools that are suitably sensitive at the required resolution. In this work, the application of fluorescent nanosensors capable of dynamic pH monitoring of the environmental microniches within biofilms is demonstrated using the model organism *P. aeruginosa*.

Nanoparticles have the potential for applications in the prevention of some disease if employed at early stages (Bae *et al.*, 2012). Biodegradable polymer based nano- and microparticles can, for example, be used to encapsulate antibiotics to ensure a targeted release of the antimicrobial substance (Xiong *et al.*, 2014; Ikuma *et al.*, 2015; Singh *et al.*, 2019). Therefore, it is important to understand the interaction between the nanoparticles and the biofilm and to establish the penetration of nanoparticles into the biofilm. Penetration usually occurs by diffusion where the nanoparticles are interacting with either the bacteria or the biofilm matrix components (Peulen and Wilkinson, 2011; Forier *et al.*, 2014; Ikuma *et al.*, 2015). The diffusion characteristics of the

nanoparticles mostly depend on their size and charge but are also influenced by pore size of the biofilm, the charge and chemical gradient of the biofilm matrix, and the hydrophobicity of the environment (Habimana *et al.*, 2011; Peulen and Wilkinson, 2011; Sahle-Demessie and Tadesse, 2011; Ikuma *et al.*, 2015). An increasing size and negative charge of silver nanoparticles has been reported to reduce their diffusion into *P. fluorescens* biofilms (Peulen and Wilkinson, 2011). A similar behaviour was seen for anionic liposomes added to a *S. aureus* biofilm, where the liposomes could not penetrate the biofilm, possibly due to the negative surface charge of the bacteria (Ahmed and Jones, 2003). On the downside, a positive charge of particles and surfactants has been shown to play a role in antimicrobial action of these compounds (Enomoto *et al.*, 2007; J. Li *et al.*, 2018), which should be borne in mind when choosing appropriate nanosensors. As different laboratories use a variety of nanoparticles, characterisation of the interaction of nanoparticles with bacteria and biofilm components is required. For their use in biological systems, it is important that the nanoparticles do not alter the metabolism and behaviour of the cells.

3.1.2 Aims of this chapter

This chapter aimed to answer the following questions in order to develop the optical nanosensor tools for application in the mechanistic studies presented in the subsequent chapters:

- Can good quality functional pH-sensitive nanosensors be reproducibly prepared?
- Will the nanosensors inhibit planktonic cell growth?
- Do the nanosensors influence biofilm formation?
- Can the nanosensors enter *P. aeruginosa* cells during incubation?
- Do the nanosensors interact with the cells and/or biofilm components during biofilm formation?
- Can the nanosensors penetrate an already established biofilm?
- Will the nanosensors be washed away from biofilms during downstream manipulations?

3.2 Results

The penetration and interactions of the nanosensors within biofilms of *P. aeruginosa* were characterised in this chapter using different kinds of polyacrylamide nanoparticles. To evaluate the influence of charge, both neutral and positively charged versions of the nanosensors were produced. In addition, nanoparticles without fluorophores and particles consisting only the red fluorophore (TAMRA only) or green fluorophores (OG-FAM only) were prepared to investigate the effects of the nanoparticles and their charge on biofilm formation. Furthermore, preparation of single-coloured nanoparticles enabled the use of additional dyes to simultaneously stain biofilm components while being able to track the location of the nanoparticles. Two different *in vitro* biofilm models were used and compared throughout the study; one static model using glass-bottom chambers and one flow-cell model using the BioFlux flow-cell system as described in 2.18.1 and 2.18.2.

3.2.1 Preparation and characterisation of different kinds of fluorescent polyacrylamide nanoparticles

Dynamic light scattering (DLS) was performed on nanosensor preparations to determine the size and zeta potential (ζ-potential) of the nanoparticles as described in 2.6. DLS is based on the assumption that nanoparticles are a spherical shape. The ζ-potential specifies the magnitude of the charge repulsion or attraction between particles and describes the potential difference between the dispersion medium and the layer of fluid attached to the dispersed particles. For all nanoparticle batches, the average size, polydispersity index (PDI) and ζ-potential were determined using a Zetasizer (Malvern Panalytical) and are listed in Table 3.1. The PDI is used to estimate the average uniformity of the particle solution and indicates nanoparticle aggregation. The index is dimensionless; however, PDI values that fall below 0.2 are commonly deemed acceptable for polymer-based nanoparticle work, whereas values bigger than 0.7 indicate that the samples have a very broad particle size distribution and are not suitable for dynamic light scattering analysis (Danaei *et al.*, 2018).

Table 3.1: Size, PDI and ζ-potential of polyacrylamide nanoparticles used in this study. *PDI* polydispersity index, *n* number of batches analysed, +/- represents standard error between different batches of nanoparticles.

Polyacrylamide nanoparticles	Size (nm)	PDI	ζ-potential (mV)
neutral (n = 5)	38.86 +/- 1.61	0.126 +/- 0.024	-2.17 +/- 1.15
positive (n = 13)	39.9 +/- 1.48	0.186 +/- 0.02	18.26 +/- 1.66
positive no fluorophores (n = 1)	46.41	0.167	17.7
positive TAMRA only (n = 1)	46.53	0.097	13.7
positive OG-FAM only (n = 1)	39.37	0.134	18.9

All nanoparticles have a size between 38 nm and 47 nm with a PDI < 0.24. The ζ-potential of positive nanoparticles ranges between 13.7 mV and 18.26 mV, whereas the neutral nanosensors show an average ζ-potential of -2.17.

To investigate the responsiveness of the pH-sensitive, fluorescent nanosensors, emission scans were performed using a range of pH buffers and a spectrophotometer. Representative emission graphs are presented in Figure 3.1a and b and were subsequently used for the pH calibration of the nanosensors, shown in Figure 3.1c. All measurements were conducted at room temperature.

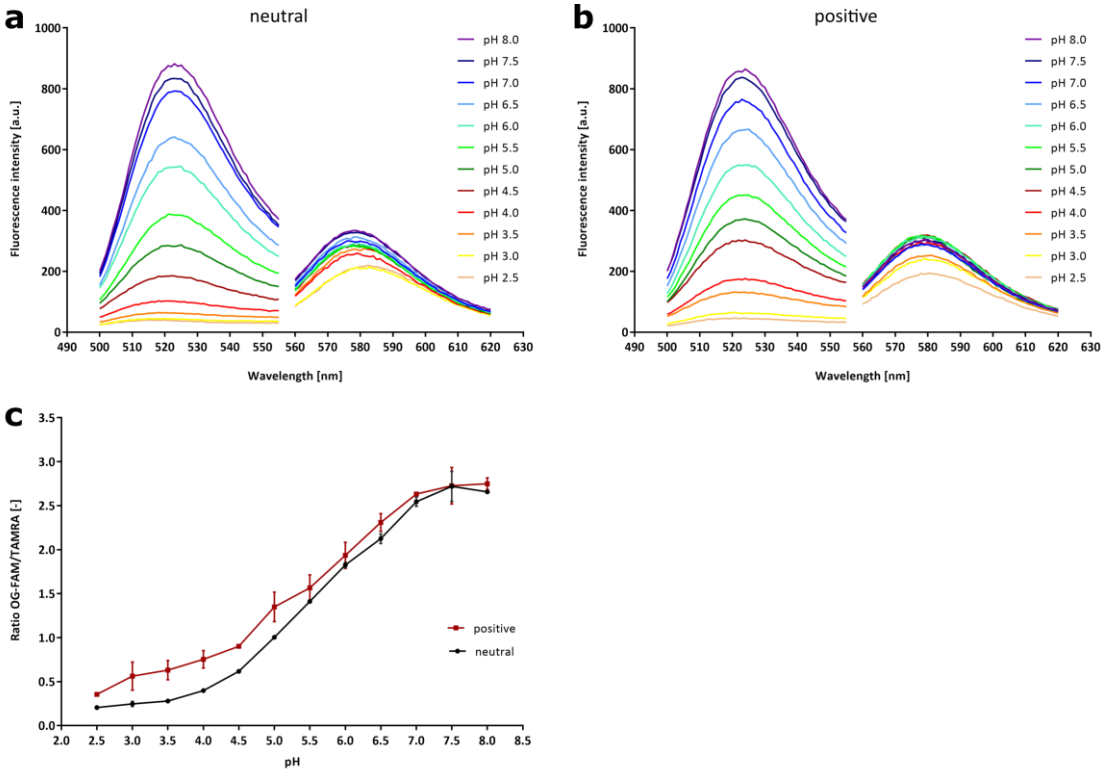


Figure 3.1: Emission scans and pH calibration of pH-sensitive neutral and positive polyacrylamide nanosensors. Fluorescence intensity of **(a)** neutral and **(b)** positive nanosensors is shown against the emission wavelength between 500 nm and 555 nm for OG-FAM (excitation wavelength = 488 nm) and between 560 nm and 620 nm for TAMRA (excitation wavelength = 540 nm). Sodium phosphate and citric acid buffer solutions with a pH ranging from 2.5 to 8.0 in 0.5 steps were used. **(c)** pH calibration of neutral and positive nanosensors was performed by calculating the fluorescence intensity ratio between OG-FAM at 520 nm and TAMRA at 580 nm. Error bars represent standard error, where n = 3. All measurements were performed at room temperature.

The emission scans for both nanosensors show the highest fluorescence intensity for OG-FAM at pH 8 with decreasing intensity when pH is descending. The TAMRA fluorescence intensity is consistent between pH buffers, with a slightly lower intensity for pH values below 3.5. For the calibration of the nanosensors, the ratio of OG-FAM to TAMRA was calculated, using the maximum intensity values of the emission scans, measured at 520 nm for OG-FAM and at 580 nm for TAMRA. The resulting pH calibration curves look very similar between nanosensors, showing a linear slope between pH 4 to 7 with plateaus at high and low pH. Instead of using a spectrophotometer, the calibration of the nanosensors can also be performed using a Tecan plate reader or a fluorescence microscope.

For most of the experiments, the nanosensors were filter sterilised with 0.22 µm polyethersulfone (PES) filters prior to the use to avoid contamination of the growth culture. Therefore, a filter assay was carried out to ensure that no significant loss of nanosensors occurs. The fluorescence intensity of nanosensors at a known concentration was measured before and after the filtration using a spectrophotometer. The concentration after the filtration was calculated based on the measured fluorescence intensity and is shown in Table 3.2.

Table 3.2: Minimal loss occurs during filter sterilisation of neutral and positive nanosensor preparations. Original concentration is shown on the left and calculated concentration after the filtration for both nanosensors on the right.

Original concentration [mg mL^{-1}]	Concentration after filtration [mg mL^{-1}]	
	Neutral	Positive
25	23.88	24.56
20	19.9	19.41
15	16.41	16.9
10	9.98	9.72
5	3.02	4.4
1	1	0.8

For both nanosensors, the loss of concentration after the filtration was low, indicating that the filtration does not affect the experiments. The increase for the concentration of 15 mg mL^{-1} is likely due to variation in the fluorescence intensity measurement.

3.2.2 The planktonic growth of PAO1-N is unaffected by the presence of neutral or positively charged nanosensors

For further experiments, it was important to examine whether the nanosensors have an effect on the bacterial growth during incubation. Therefore, a growth measurement over 24 h in 96-well plates was performed to detect any growth inhibition caused by the nanosensors in

planktonic cultures. Different concentrations of neutral and positively charged polyacrylamide nanosensors ranging from 0.1 mg mL^{-1} to 25 mg mL^{-1} were examined in liquid culture using the *P. aeruginosa* strain PAO1-Nottingham wild type (subsequently called PAO1-N) (Figure 3.2).

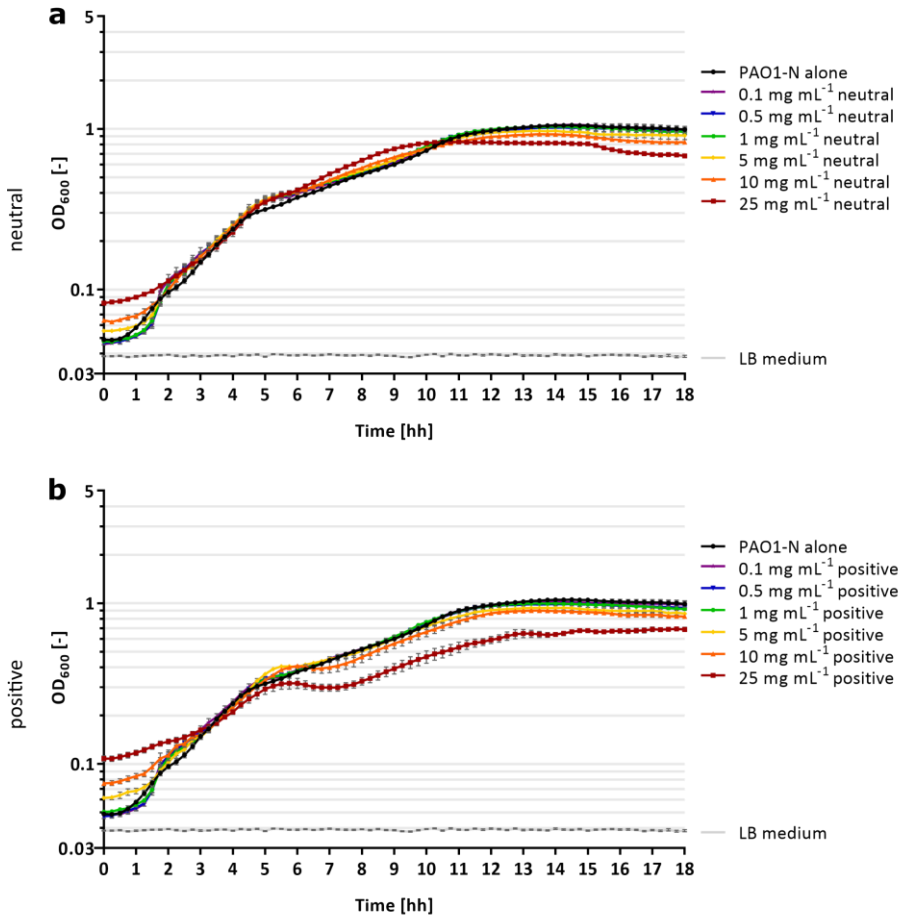


Figure 3.2: Nanosensors at concentrations below 25 mg mL^{-1} have no effect on the growth of PAO1-N. PAO1-N was inoculated into a 96-well plate at an OD_{600} of 0.05 in LB media containing 0.1 to 25 mg mL^{-1} of **(a)** neutral or **(b)** positive nanosensors and incubated for 24 h at 37°C, during which the OD_{600} was measured automatically every 15 minutes and is shown on a log scale against time. No path length correction was applied. Error bars represent standard error, where n = 3x3.

Comparing the growth of PAO1-N with different concentrations of neutral or positive polyacrylamide nanosensors, no significant difference could be detected for any concentration below 25 mg ml^{-1}. Positively charged polyacrylamide nanosensors at a concentration of 25 mg mL^{-1} showed a slight reduction in growth between 7 and 16 h, however the OD_{600} reached almost the same level as the other samples after 18 h.

3.2.3 Neutral and positively charged nanosensors do not enter PAO1-N cells during incubation

To get a better understanding of the behaviour of polyacrylamide nanosensors during incubation with overnight liquid cultures of *P. aeruginosa*, planktonic cells were examined under a Zeiss PS1 Super Resolution Microscope. In particular, the question whether the nanosensors are able to enter the cells during incubation was investigated. This is particularly important to know because uptake of the nanosensors into the cell would influence the analysis in future pH measurements as the measured pH would point to the internal cell environment rather than the pH around the cells or within the biofilms. Overnight cultures of PAO1-N without nanosensors or with either neutral or positive nanosensors were prepared and samples were taken for the microscopy on the following day as described in 2.19. Unwashed samples as well as cells washed in LB were analysed. To enable post-channel alignment of the images, 0.1 µm fluorescent beads (Thermo Fisher Scientific) were mixed with the cells prior to the imaging (Figure 3.3).

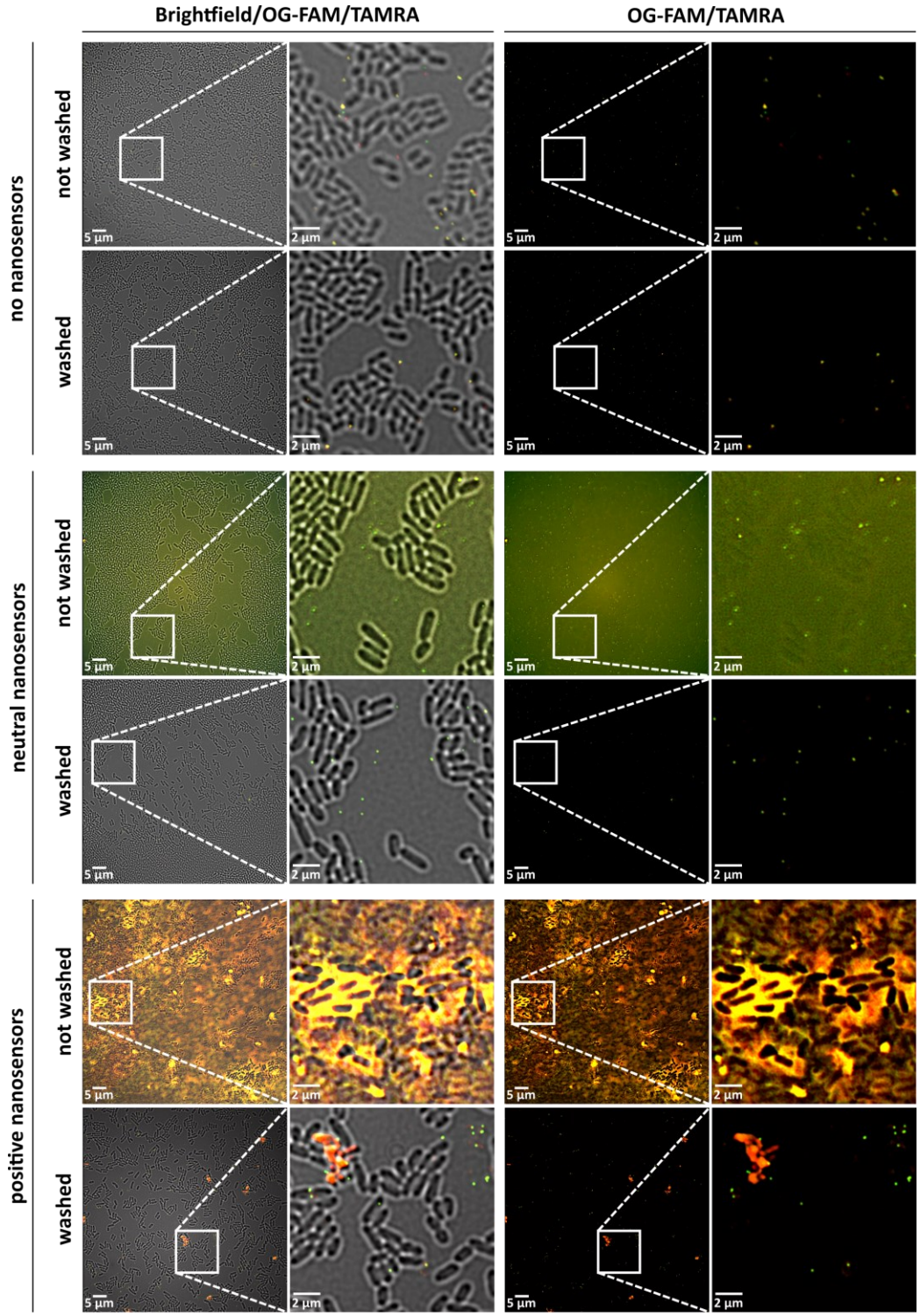


Figure 3.3: Representative images of PAO1-N show some leftover positive nanosensors stuck between cells after being washed but no fluorescence inside the cells. PAO1-N overnight cultures were incubated in LB with or without 1 mg mL^{-1} positive or neutral nanosensors at 37°C. Washed or unwashed cells were imaged using a Zeiss Elyra PS.1 with structured illumination microscopy and a 63x objective. Four coloured (green, red, blue, far-red) fluorescent TetraSpeck™ Microspheres were used for image processing.

All images show distinct green and red fluorescence spots representing the fluorescent beads that were used for the channel alignment. Other than that, no fluorescence and no differences between washed and unwashed samples were detected in the control images without nanosensors. Images taken of the unwashed sample containing neutral nanosensors show nanosensor fluorescence evenly distributed throughout the image. After the wash, no more fluorescence was detected. In contrast, the image of the sample with positive nanosensors before the wash step shows fluorescence signal within the medium and bright signals between the cells. The zoom-in view reveals that this fluorescence is present all around the cells but does not seem to be inside the cells. The sample that has been washed in LB confirms this observation, where most of the fluorescence has been removed. Only a few parts of the image still report fluorescence. Those parts indicate regions where bigger cell clumps are found as seen in the overlay images.

3.2.4 Depending on their charge and concentration, polyacrylamide nanoparticles affect biofilm thickness and structure differently

After having confirmed that the presence of the nanosensors within planktonic culture of PAO1-N has no effect, the influence of nanosensors on biofilm growth was investigated. In most cases within this study, the cells were stained with CellMask™ Deep Red (Invitrogen™), a membrane stain fluorescing in the far-red region. CellMask™ was chosen in preference to DAPI, a commonly used nucleic stain fluorescing in the blue wavelength, for two reasons: (i) CellMask™ exhibits a reduced background signal, and (ii) the blue auto fluorescence of PAO1 interferes with the DAPI stain. A few experiments carried out early in this study using DAPI however are included since the result was unequivocal.

To analyse the effects of the nanosensors on biofilm formation, the nanosensors were suspended in the culture medium prior to the incubation with bacteria as described in 2.18.1.1. The resultant biofilms, grown with and without nanosensors under static conditions, were analysed after 48 h using fluorescence CLSM. In addition to the neutral and positive pH-sensitive

nanosensors, positive nanoparticles without fluorophores were included in this study. Representative images and related quantifications are shown in Figure 3.4.

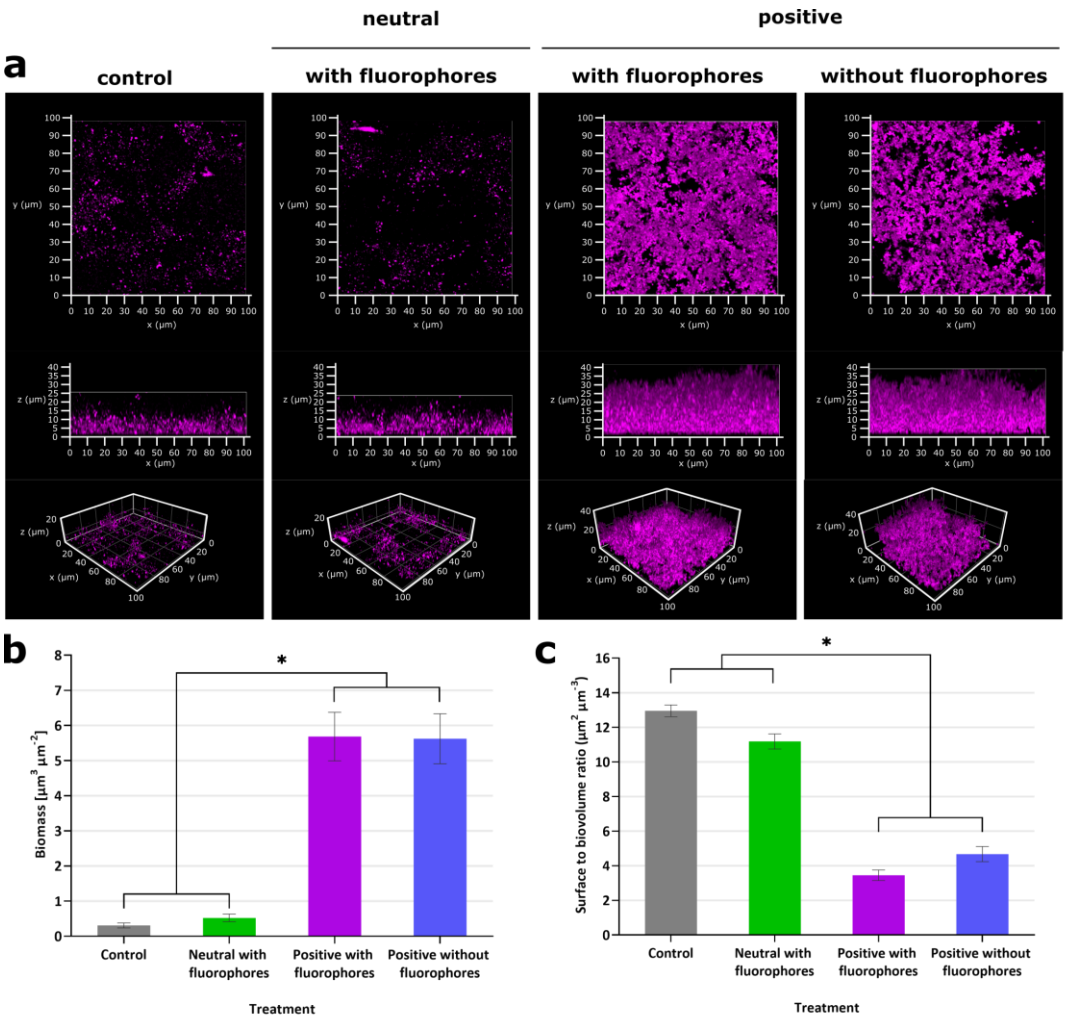


Figure 3.4: The charge of nanosensors can influence the biofilm formation of PAO1-N. PAO1-N was inoculated into an 8-well glass bottom chamber at an OD_{600} of 0.05 in M9S containing no nanoparticles (left panel), 1 mg mL^{-1} neutral polyacrylamide nanosensors (left central panel), 1 mg mL^{-1} positive nanosensors (right central panel) or 1 mg mL^{-1} positive nanoparticles containing no fluorophores (right panel). The cells were incubated at 37°C under static conditions for 48 h and stained with CellMask™. Z-stack images were taken with a Zeiss CLSM using a 63x objective. Quantitative Comstat analysis of the biofilm images was performed using ImageJ. **(a)** Representative confocal images of PAO1-N with the top row showing a 3D view from the top of the biofilm, the middle row showing a 3D view from the front of the biofilm and the bottom row representing an angled 3D view from the top. Graphs represent **(b)** biomass and **(c)** surface to biovolume ratio. Error bars represent standard error measured for different biofilm images, where n = 10 (control), n = 7 (neutral nanosensors and positive nanoparticles without fluorophores) and n = 8 (positive nanosensors), with $p<0.05$ = * (non-parametric Kruskal-Wallis test).

The neutral pH-sensitive nanosensors dispersed throughout the *P. aeruginosa* biofilm without altering their architecture or thickness. Interestingly, biofilms grown together with the positively charged pH-sensitive polyacrylamide nanosensors were approximately four times thicker (40 μm) compared to biofilms grown in the absence of nanosensors or with neutral pH-sensitive nanosensors (~10 μm) (Figure 3.4a). The general structure of the biofilms grown with positively charged pH-sensitive nanosensors was also notably different, showing a very dense structure. To exclude the possibility that the dyes incorporated within the polymer matrix of the positively charged pH-sensitive nanosensors were responsible for the enhanced biofilm formation, positively charged polyacrylamide nanoparticles featuring the same characteristics in size and charge were produced without inclusion of the fluorophores (Table 3.1). The addition of these nanoparticles led to the similar increases in biofilm thickness and robustness as the positively charged nanosensors.

Quantitative analysis of the images using Comstat, an open source programme used to analyse image stacks of biofilms, revealed that there is no significant difference between the biofilms produced in the absence of nanoparticles or with neutral nanosensors (Figure 3.4b and c). Furthermore, a significantly lower biomass for biofilms grown without nanosensors or with neutral nanosensors was confirmed compared to the positively charged particles ($p<0.05$, non-parametric Kruskal-Wallis test). In contrast, no significant difference in biofilm biomass was detected between formation in the presence of positively charged pH nanosensors and the positively charged nanoparticles without dyes. In addition, a significantly higher surface area to biovolume ratio for biofilms grown without nanosensors or with neutral nanosensors than those grown with positively charged nanosensors was observed ($p<0.05$, non-parametric Kruskal-Wallis test).

To investigate whether higher concentrations of nanosensors would lead to an even thicker biofilm than using the normal previously selected concentration of 1 mg ml^{-1}, biofilms were

grown under the same conditions using 10 mg mL^{-1} or 20 mg mL^{-1} positively charged nanosensors. Representative images and the related quantifications are shown in Figure 3.5.

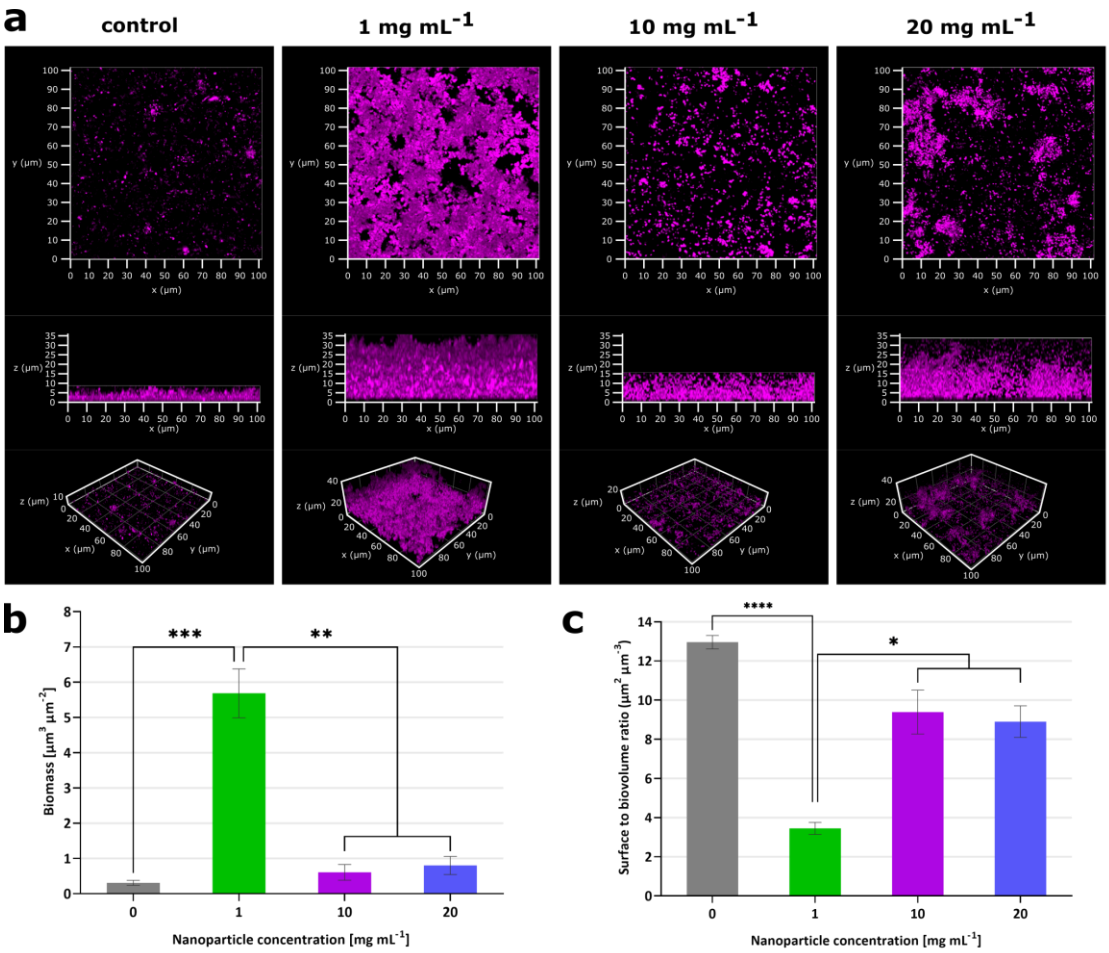


Figure 3.5: Enhanced PAO1-N biofilm formation as a result of positively charged nanosensors is concentration dependent. PAO1-N was inoculated into an 8-well glass bottom chamber at an OD_{600} of 0.05 in M9S containing no nanoparticles (left panel), 1 mg mL^{-1} positive polyacrylamide nanosensors (left central panel), 10 mg mL^{-1} (right central panel) or 20 mg mL^{-1} (right panel). The cells were incubated at 37°C under static conditions for 48 h and stained with CellMask™. Z-stack images were taken with a Zeiss CLSM using a 63x objective. Quantitative Comstat analysis of the biofilm images was performed using ImageJ. **(a)** Representative confocal images of PAO1-N with the top row showing a representative 3D view from the top of the biofilm, the middle row showing a 3D view from the front of the biofilm and the bottom row an angled 3D view from the top. Graphs represent **(b)** biomass and **(c)** surface to biovolume ratio. Error bars represent standard error measured for different biofilm images, where n = 10 (control), n = 8 (1 mg mL^{-1}), n = 12 (10 mg mL^{-1}) and n = 13 (20 mg mL^{-1}), with $p<0.05$ = *, $p<0.01$ = ** and $p<0.001$ = *** (non-parametric Kruskal-Wallis test).

CLSM revealed that a higher concentration of positively charged nanosensors does not seem to further enhance the biofilm formation, instead the thickness is reduced compared to when

1 mg mL^{-1} nanosensors were introduced. This was again underlined using Comstat for quantitative analysis of the different conditions, where a significant reduction in biomass was observed for biofilms grown with 10 or 20 mg mL^{-1} compared to 1 mg mL^{-1} nanosensors ($p<0.01$, non-parametric Kruskal-Wallis test).

Further investigation was required to confirm that the positive charge of the nanoparticles is responsible for the increase in biofilm thickness of PAO1-N. Therefore, the positively charged nanoparticles were exchanged with commercially available positively charged amidine latex beads (Invitrogen™) at a concentration of 1 mg mL^{-1}. According to the manufacturer, these beads are larger than our nanosensors with a size of 0.2 µm. To confirm the size and charge, the beads were characterised using a Zetasizer (Table 3.3).

Table 3.3: Size, PDI and ζ-potential of amidine latex beads used in this study. *PDI* polydispersity index.

	Size (µm)	PDI	ζ-potential (mV)
Amidine beads	1.56	0.78	18.1

As expected, the beads are larger than our nanoparticles, being 1.56 µm compared to ~40 nm. The PDI is also relatively high (0.78), indicating a polydispersed suspension. However, the ζ-potential of 18.1 mV is very similar to our positively charged nanoparticles.

Biofilms were grown with the addition of the amidine beads under the same conditions as before using 1 mg mL^{-1} amidine beads and representative images as well as quantification can be found in Figure 3.6.

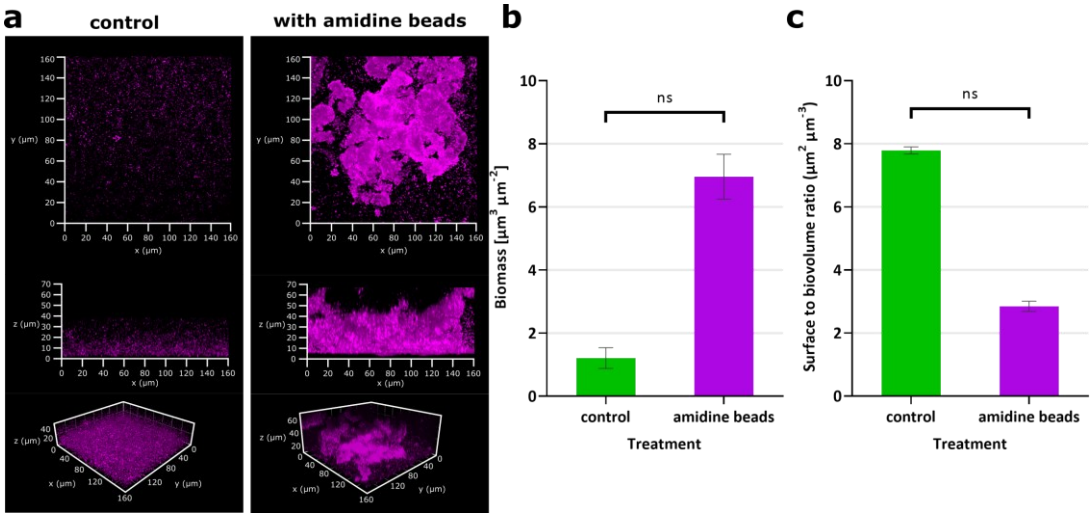


Figure 3.6: Positively charged amidine beads can lead to enhanced biofilm formation of PAO1-N. PAO1-N was inoculated into an 8-well glass bottom chamber at an OD_{600} of 0.05 in M9S containing no beads (left panel) or 1 mg mL^{-1} amidine beads (right panel). The cells were incubated at 37°C under static conditions for 48 h and stained with DAPI. Z-stack images were taken with a Zeiss CLSM using a 63x objective. Quantitative Comstat analysis of the biofilm images was performed using ImageJ. **(a)** Representative confocal images of PAO1-N with the top row showing a 3D view from the top of the biofilm, the middle row showing a 3D view from the front of the biofilm and the bottom row representing an angled 3D view from the top. Graphs represent **(b)** biomass and **(c)** surface to biovolume ratio. Error bars represent standard error measured for different biofilm images, where n = 2, with ns = not significant (non-parametric Mann-Whitney test).

As previously seen with the positively charged nanoparticles, the cationic amidine beads at a concentration of 1 mg mL^{-1} led to increased biofilm formation of PAO1-N. However, elevated levels of clumping of the bacteria in the biofilm was evident. Using a non-parametric Mann-Whitney test, the biomass and surface to biovolume was not significantly changed, probably due to the low number of replicates (n=2), but the trend was very apparent (Mann-Whitney test).

Interestingly, the increase in thickness for biofilms grown with positively charged particles was only seen with the static biofilm model but not for biofilms grown with the BioFlux flow-cell, as presented in Figure 3.7.

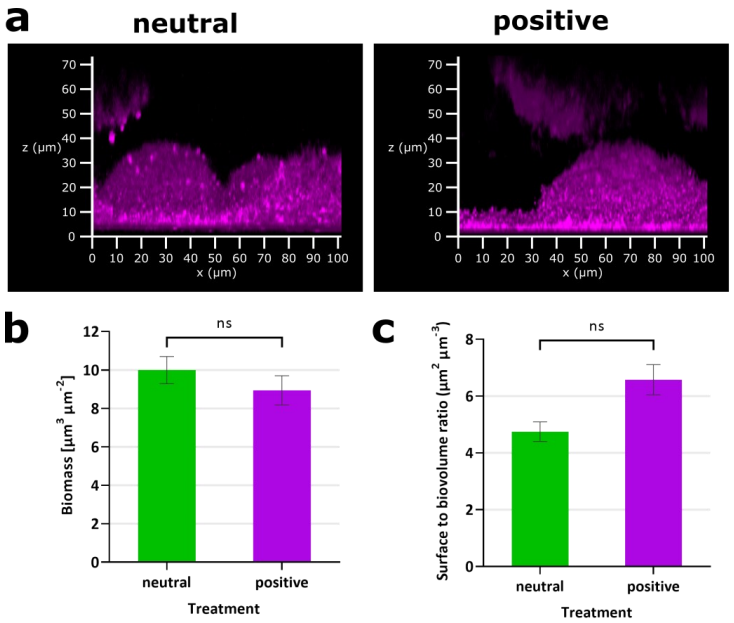


Figure 3.7: Positively charged nanosensors do not alter biofilm formation of PAO1-N in a flow-cell system. PAO1-N was inoculated into a 48-well BioFlux flow-cell plate at an OD_{600} of 0.05 in M9S containing neutral polyacrylamide nanosensors (left panel) or positive nanosensors (right panel) at 5 mg mL^{-1}. The cells were incubated at 37°C under flow conditions (0.2 dyn cm^{-2}) for 24 h and stained with CellMask™. Z-stack images were taken with a Zeiss CLSM using a 63x objective. Quantitative Comstat analysis of the biofilm images was performed using ImageJ. **(a)** Representative confocal images of PAO1-N. Images represent a 3D view from the front of the biofilm. Graphs represent **(b)** biomass and **(c)** surface to biovolume ratio. Error bars represent standard error measured for different biofilm images, where n = 3, with ns = not significant (non-parametric Mann-Whitney test).

Although no effect of nanosensors on the biofilm formation was observed, structural differences between biofilms grown under static conditions compared to flow conditions were evident. Especially striking was enhanced microcolony formation and the development of characteristic mushrooms, which was only observed when using the BioFlux flow-cell system.

3.2.5 Both neutral and positive nanosensors can penetrate already established biofilms in a static as well as a flow-cell model

To investigate if nanosensors can penetrate an already established *P. aeruginosa* biofilm, nanosensors were added to a 48-h matured biofilm. Penetration of the sensors was assessed using fluorescence CLSM. To ensure that a thick biofilm could be used for the analysis, controls were included where the bacteria were pre-grown with positively charged nanoparticles without

fluorophores. After imaging the biofilm, positively charged or neutral nanosensors were added to the cultures and the biofilms were immediately imaged again without washing (2.18.1.2). Penetration of the biofilm by the nanosensors was assessed by tracking the fluorescence of the nanosensors throughout the thickness of the biofilm. Representative images are shown in Figure 3.8.

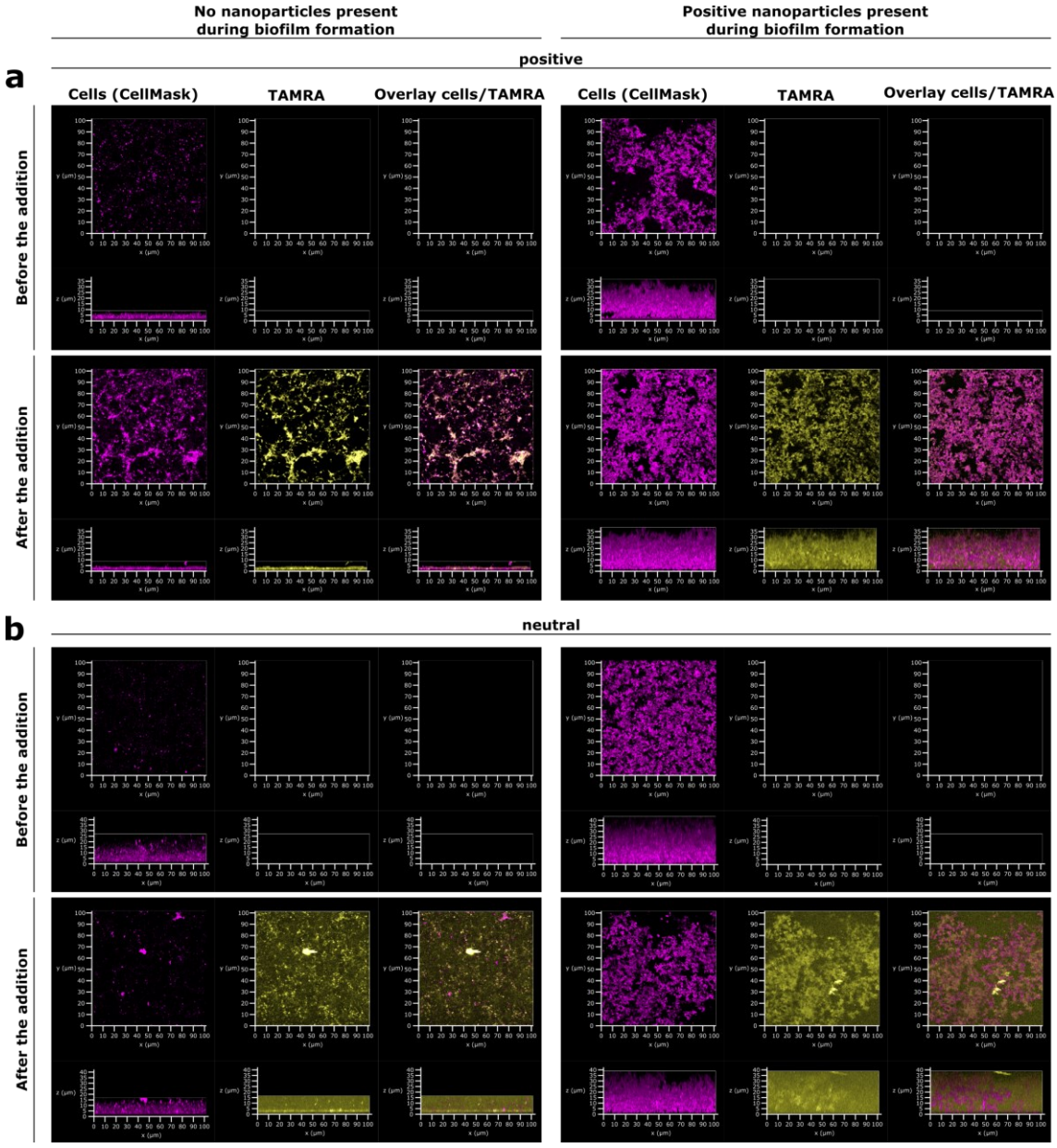


Figure 3.8: Neutral as well as positive nanosensors can penetrate established PAO1-N biofilms under static conditions. PAO1-N was inoculated into an 8-well glass bottom chamber at an OD_{600} of 0.05 in M9S containing no nanoparticles (left panel) or 1 mg mL^{-1} positive nanoparticles without fluorophores (right panel). The cells were incubated at 37°C under static conditions for 48 h and stained with CellMask™. Z-stack images were taken with a Zeiss CLSM using a 63x objective. **(a)** Representative confocal images of PAO1-N show cells stained with CellMask™ (magenta) and TAMRA fluorescence of nanosensors (yellow). For the purpose of these images, TAMRA has been false coloured to yellow to facilitate visualisation of nanoparticle distribution. Top panel = Before the addition of positively charged pH-sensitive nanosensors. Bottom panel = After the addition of positively charged pH-sensitive nanosensors to a final concentration of 1 mg mL^{-1}. **(b)** Representative confocal images of PAO1-N with same conditions as in **(a)**, but with the addition of 1 mg mL^{-1} neutral pH-sensitive nanosensors.

Fluorescence within the whole biofilms was observed after 3 min following the addition of the nanosensors suggesting that the nanosensors enter the biofilm very quickly and without obvious resistance. This behaviour was observed for both the neutral and the positively charged nanosensors. Interestingly, when the biofilms were grown initially without the positive nanoparticles, the structure of the biofilm was disrupted when positively charged nanosensors were added but not when neutral nanosensors were added, supporting the observation that growing PAO1-N together with the positive nanoparticles results in a more robust biofilm. It can also be noted, that the addition of neutral nanosensors to the biofilms led to a more even distribution of the nanosensors as opposed to the positive nanosensors, that can immediately be co-localised with the bacteria, as already observed in 3.2.2.

In addition to a static biofilm, the flow-cell BioFlux system was used to investigate penetration of biofilms by both neutral and positive nanosensors. In a first attempt, biofilms of PAO1-N were either grown with or without the addition of 5 mg mL^{-1} positively charged nanosensors for 12:30 h in a 24-well plate, before the medium was switched to medium with or without nanosensors, respectively (2.18.2). Images were taken every 15 min using a Nikon Ti Eclipse fluorescent microscope and representative images at the start (0 h) or after 12:30 h (right before the switch), 12:45 h (right after the switch) and 14:30 h are shown in Figure 3.9.

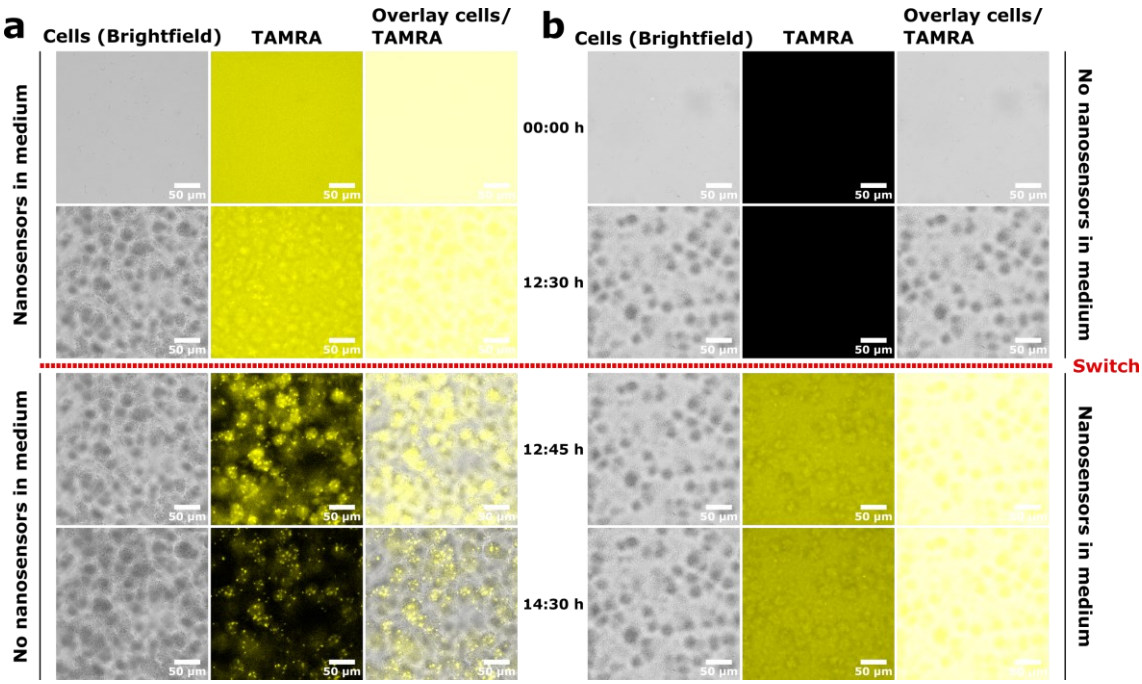


Figure 3.9: Time-lapse images reveal interaction of nanosensors with biofilms of PAO1-N. PAO1-N was inoculated into a 24-well BioFlux flow-cell plate at an OD_{600} of 0.05 in M9S. The cells were incubated at 37°C under flow conditions (0.2 dyn cm^{-2}) for 24 h. Time-lapse images were taken with a Nikon Eclipse Ti-U fluorescent microscope using a 20x objective. Representative widefield images show cells (brightfield, grey) and TAMRA fluorescence of nanosensors (yellow). For the purpose of these images TAMRA has been false coloured to yellow to facilitate visualisation of nanoparticle distribution. **(a)** PAO1-N biofilms were initially grown for 12:30 h with 5 mg mL^{-1} positive nanosensors before the medium was switched to medium without nanosensors. **(b)** PAO1-N biofilms were initially grown without nanosensors before the medium was switched to medium with 5 mg mL^{-1} positive nanosensors.

As indicated in the images in Figure 3.9a, nanosensor fluorescence was still detected after the medium was switched to a medium without nanosensors. At the same time, the overall fluorescence within the medium was greatly reduced, as expected. On the other hand, nanosensors were detected within the biofilm when introduced after 12:30 h of initial growth without nanosensors, as shown in Figure 3.9b. However, it is not possible to determine whether the nanosensors penetrated the microcolonies and interact with the biofilm or if the fluorescence that was detected only represents the nanosensors that are dispersed within the flow medium. Therefore, further experiments were conducted to confirm penetration of biofilms under flow conditions. After biofilms were initially grown for 12 h in the absence of nanosensors, the inlet of the flow medium was switched to a medium containing nanosensors

for 5 h followed by a switch back to medium without nanosensors for another 5 h. CLSM was performed at the end point and images are shown in Figure 3.10.

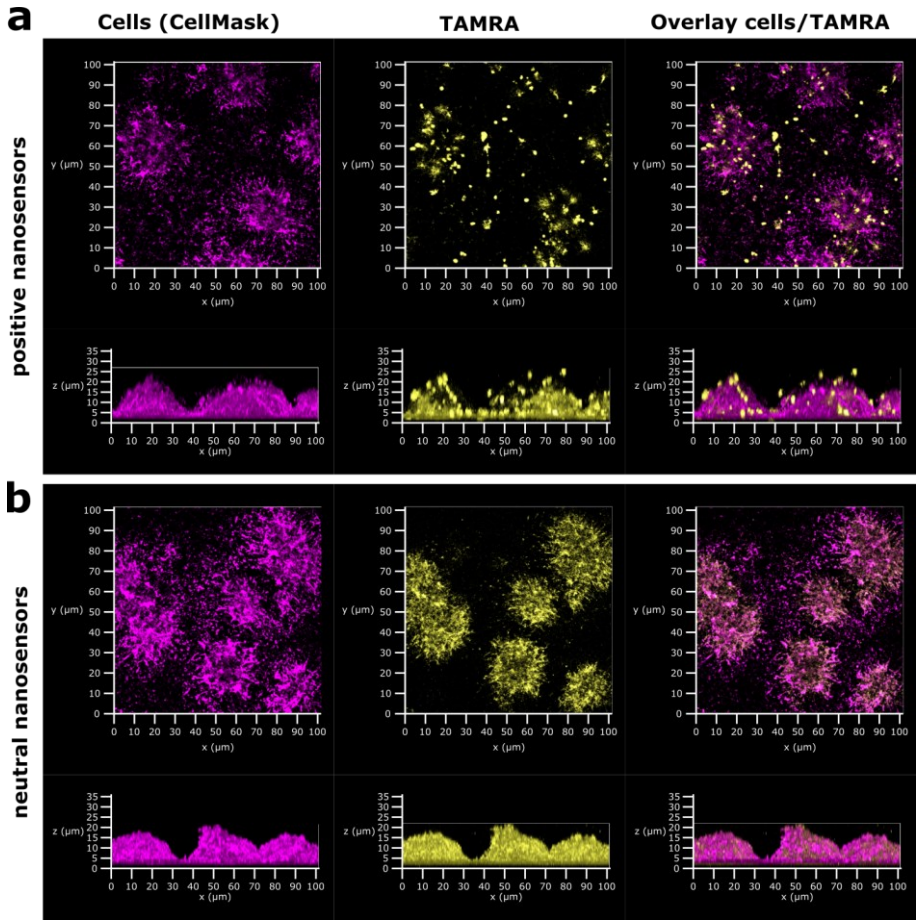


Figure 3.10: Penetration of established PAO1-N biofilms by nanosensors under flow conditions was independent of the charge of the nanosensors. PAO1-N was inoculated into a 24-well BioFlux flow-cell plate at an OD_{600} of 0.05 in M9S. The cells were incubated at 37°C under flow conditions (0.2 dyn cm^{-2}). Biofilms were initially grown for 12 h without nanosensors before the medium was switched to medium with 5 mg mL^{-1} **(a)** positive or **(b)** neutral nanosensors for 5 h followed by a switch back to medium without nanosensors for another 5 h. Z-stack images were taken with a Zeiss CLSM using a 63x objective. Representative images show cells stained with CellMask™ (magenta) and TAMRA fluorescence of nanosensors (yellow). For the purpose of these images TAMRA has been false coloured to yellow to facilitate visualisation of nanoparticle distribution.

CLSM at the end point showed that there were nanosensors incorporated within the biofilm indicating penetration of the biofilm by the nanosensors under flow conditions. Although the medium was switched back to medium without nanosensors, fluorescence was still detectable,

confirming interaction between the nanosensors and the biofilm components. No nanosensor fluorescence was detected within the medium, as expected.

3.2.6 Positively charged polyacrylamide nanoparticles show interaction with biofilm components

Previous experiments have revealed an interaction between PAO1-N biofilms and nanosensors, especially with the positively charged nanoparticles. To further investigate this interaction, single-coloured, positively charged nanoparticles containing only the green fluorophores OG and FAM or the red fluorophore TAMRA were prepared featuring the same characteristics in size and charge (Table 3.3). Combining these single-coloured nanoparticles with dyes that were used to stain specific biofilm components like exopolysaccharides or eDNA enabled identification of interactions between the nanosensors and the components.

Firstly, biofilms of PAO1-N were grown together with OG-FAM nanosensors for 48 h under static conditions or for 24 h under flow conditions. Concanavalin A, a lectin that selectively binds to α-mannopyranosyl and α-glucopyranosyl residues, was used as conjugate with tetramethylrhodamine (TRITC, orange-red dye) to stain the exopolysaccharide Psl produced by PAO1-N. Static biofilms were stained right before the imaging, whereas biofilms grown in the BioFlux system were stained from the beginning of the experiment by adding the dye to the growth medium. No membrane staining was included for the flow-cell system. Representative images for both models are presented in Figure 3.11.

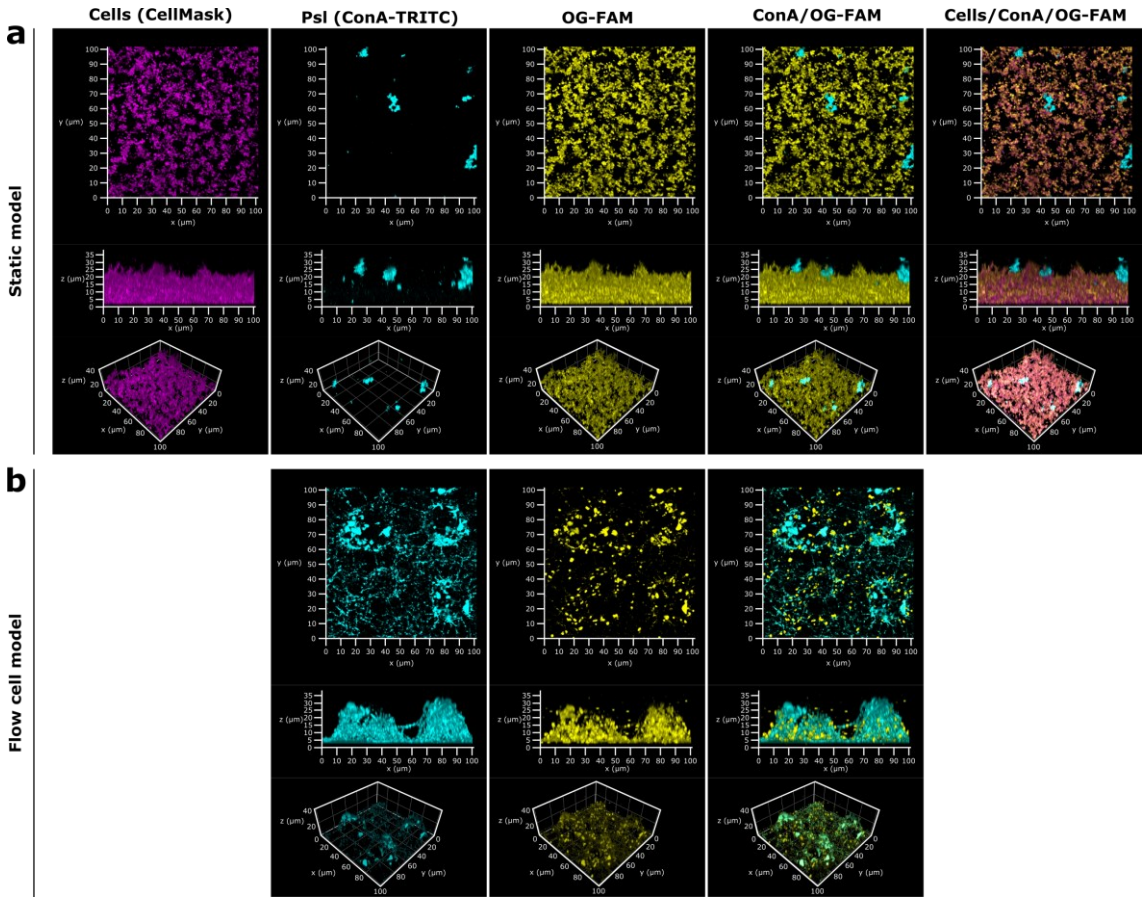


Figure 3.11: Positive polyacrylamide nanoparticles do not directly interact with the exopolysaccharide Psl within biofilms of PAO1-N. Representative images show cells stained with CellMask™ (magenta), ConA-TRITC bound to Psl (cyan) and OG-FAM fluorescence of nanoparticles (yellow). For the purpose of these images, ConA-TRITC has been false coloured to cyan and OG-FAM has been false coloured to yellow to facilitate visualisation of nanoparticle interaction. Z-stack images were taken with a Zeiss CLSM using a 63x objective. The top row is a 3D view from the top of the biofilm, the middle row shows a 3D view from the front of the biofilm and the bottom row represents an angled 3D view from the top. **(a)** PAO1-N was inoculated into an 8-well glass bottom chamber at an OD_{600} of 0.05 in M9S containing 1 mg mL^{-1} positive OG-FAM nanoparticles. The cells were incubated at 37°C under static conditions for 48 h. Staining with ConA-TRITC at 50 µg mL^{-1} was performed right before imaging. **(b)** PAO1-N was inoculated into a 48-well BioFlux flow-cell plate at an OD_{600} of 0.05 in M9S containing 5 mg mL^{-1} positive OG-FAM nanoparticles and 50 µg mL^{-1} ConA-TRITC. The cells were incubated at 37°C under flow conditions (0.2 dyn cm^{-2}) for 24 h.

Biofilms grown under static conditions (Figure 3.11a) exhibit distinct Psl staining visible as lumps within the biofilm. No direct co-localisation can be observed between the Psl and the positive nanoparticles. The biofilms grown in the BioFlux flow-cell (Figure 3.11b) show much more Psl staining distributed throughout the whole biofilm. Some co-localisation between Psl and nanoparticles was detected. To further investigate the impact of Psl on the nanosensor

interaction with the biofilm, two mutant strains were analysed, PAO1 Δ*pel* and PAO1 Δ*psl.* The first mutant, PAO1 Δ*pel*, overproduces the polysaccharide Psl, whereas the second mutant, PAO1 Δ*psl*, lacks the gene for the synthesis of Psl. Biofilms of the two strains were grown with OG-FAM nanoparticles under static conditions and stained with ConA-TRITC as previously described (Figure 3.12).

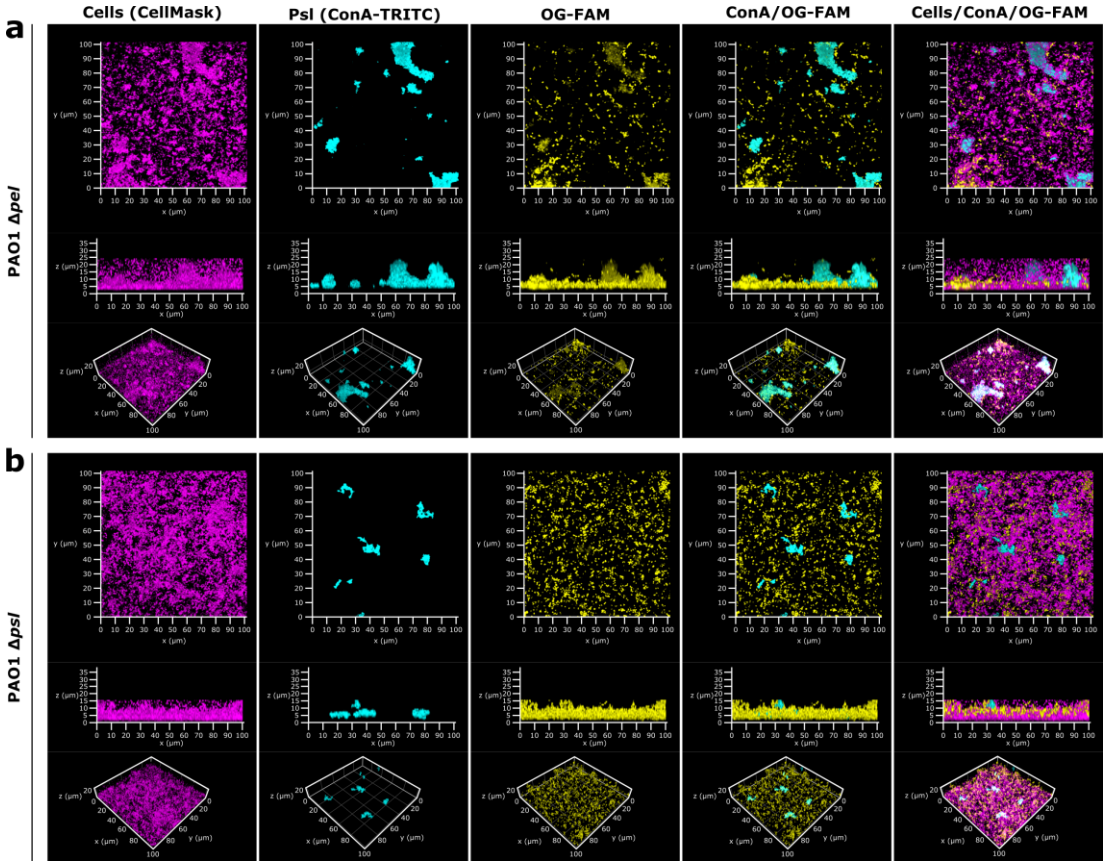


Figure 3.12: Altered synthesis of the exopolysaccharide Psl has no effect on nanosensor interaction with biofilms of PAO1-N. **(a)** PAO1 Δ*pel* and **(b)** PAO1 Δ*psl* were inoculated into an 8-well glass bottom chamber at an OD_{600} of 0.05 in M9S containing 1 mg mL^{-1} positive OG-FAM nanoparticles. The cells were incubated at 37°C under static conditions for 48 h. Staining with ConA-TRITC at 50 µg mL^{-1} was performed right before imaging. Representative images show cells stained with CellMask™ (magenta), ConA-TRITC bound to Psl (cyan) and OG-FAM fluorescence of nanoparticles (yellow). For the purpose of these images, ConA-TRITC has been false coloured to cyan and OG-FAM has been false coloured to yellow to facilitate visualisation of nanoparticle interaction. The top row is a 3D view from the top of the biofilm, the middle row shows a 3D view from the front of the biofilm and the bottom row represents an angled 3D view from the top.

Both mutants, PAO1 Δ*pel* and PAO1 Δ*psl,* show the same structure and ConA staining as previously seen for the WT. PAO1 Δ*pel* shows a slightly increased amount of Psl production, where the bigger lumps of Psl seem to be co-localised with the nanoparticles. However, the nanoparticles were detected throughout the whole biofilm and fluorescence was not restricted to regions of Psl production. Although the mutant strain PAO1 Δ*psl* is not producing any Psl, ConA-TRITC was still detected in lumps within the biofilm.

In addition to investigating the potential of an interaction between the nanosensors and polysaccharides within the biofilm, the possibility that positive nanoparticles interact with eDNA was investigated. For this purpose, single-coloured TAMRA nanoparticles were used and eDNA was stained with YOYO™-1 (green dye). Representative images for static and flow-cell biofilms of PAO1-N are shown in Figure 3.13.

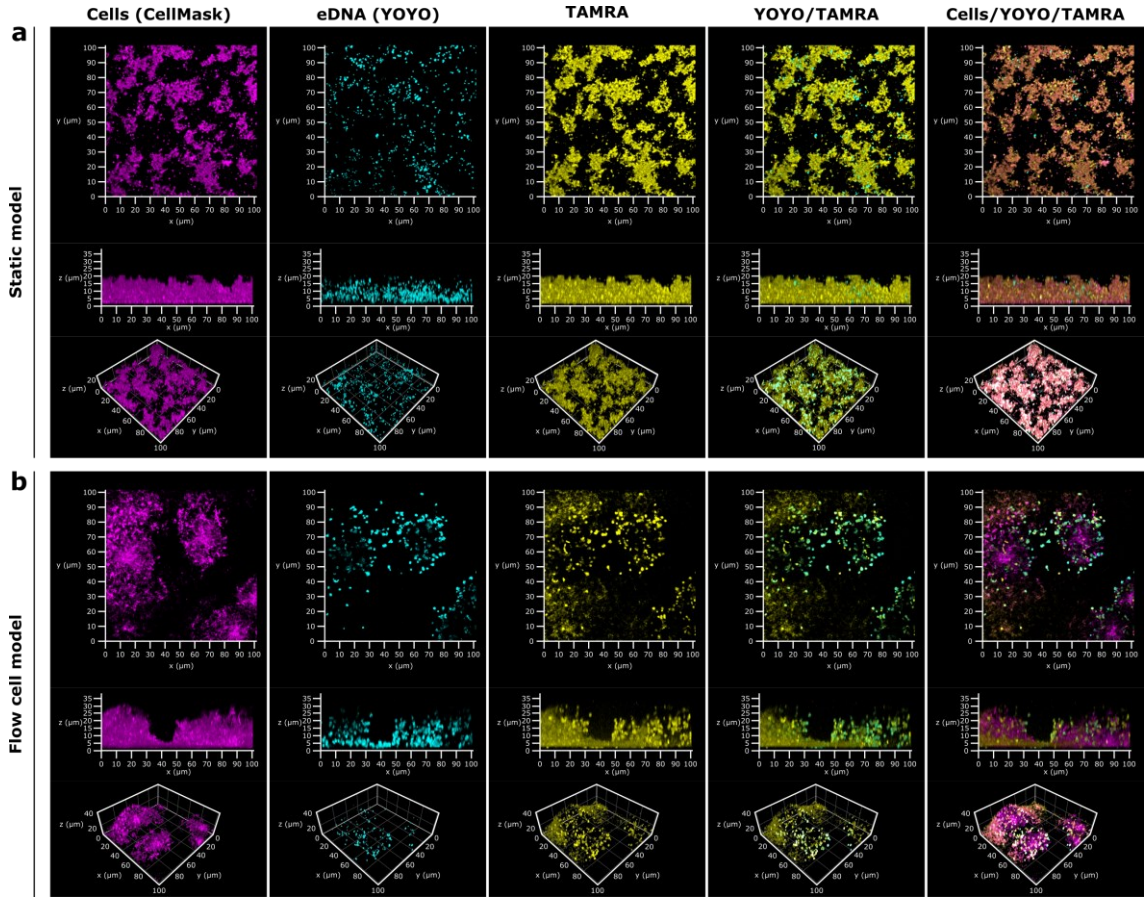


Figure 3.13: Positive polyacrylamide nanoparticles co-localise with eDNA of PAO1-N biofilms. Representative images show cells stained with CellMask™ (magenta), YOYO™-1 bound to eDNA (cyan) and TAMRA fluorescence of nanoparticles (yellow). For the purpose of these images, YOYO™-1 has been false coloured to cyan and TAMRA has been false coloured to yellow to facilitate visualisation of nanoparticle interaction. Z-stack images were taken with a Zeiss CLSM using a 63x objective. The top row is a 3D view from the top of the biofilm, the middle row shows a 3D view from the front of the biofilm and the bottom row represents an angled 3D view from the top. **(a)** PAO1-N was inoculated into an 8-well glass bottom chamber at an OD_{600} of 0.05 in M9S containing 1 mg mL^{-1} positive TAMRA nanoparticles. The cells were incubated at 37°C under static conditions for 48 h. Staining with YOYO™-1 at 0.1 µM was performed right before imaging. **(b)** PAO1-N was inoculated into a 48-well BioFlux flow-cell plate at an OD_{600} of 0.05 in M9S containing 5 mg mL^{-1} positive TAMRA nanoparticles and 0.1 µM YOYO™-1. The cells were incubated at 37°C under flow conditions (0.2 dyn cm^{-2}) for 24 h.

The resulting images look very similar between static and flow-cell model with regards to the distribution of the nanoparticles and the eDNA. Nanoparticles and eDNA were detected throughout the whole biofilm with co-localisation visible. However, nanoparticles were also located in areas where no eDNA was observed.

To investigate if an interaction between eDNA and the positive nanosensors is necessary and responsible for the enhanced biofilm formation observed in 3.2.4, the PAO1 Δ*tatA* mutant was exploited. TatA is a Sec-independent translocase protein, shown to indirectly affect the PQS-dependant release of eDNA in PAO1 but not the synthesis of PQS signal (Yang *et al.*, 2009b). Therefore, the amount of eDNA found in biofilms of this mutant is highly reduced, resulting in a very fragile biofilm formation. Biofilms were grown with and without the addition of positively charged pH-sensitive nanosensors under static condition (Figure 3.14).

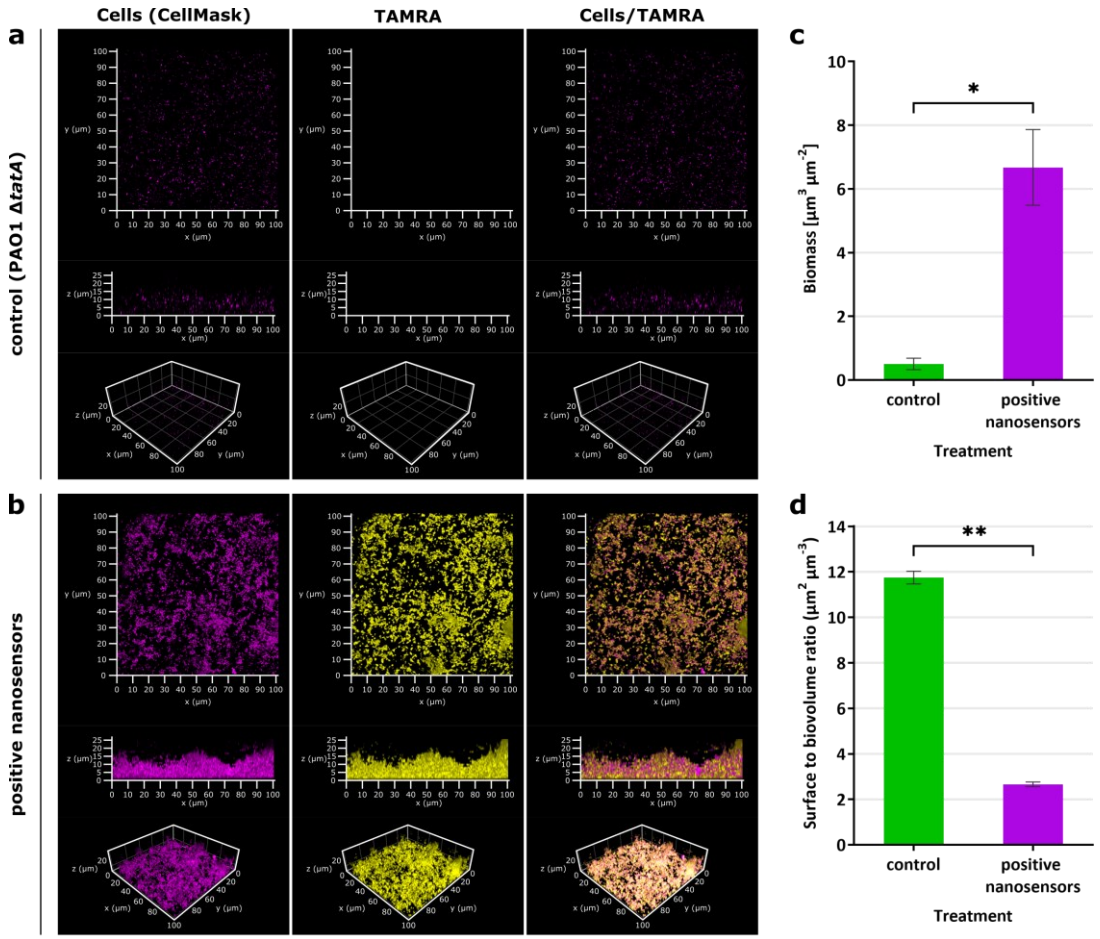


Figure 3.14: Enhanced PAO1-N biofilm formation as a result of positively charged nanosensors is independent of eDNA presence. PAO1 Δ*tatAl* was inoculated into an 8-well glass bottom chamber at an OD_{600} of 0.05 in M9S containing **(a)** no nanosensors and **(b)** 1 mg mL^{-1} positive nanosensors. The cells were incubated at 37°C under static conditions for 48 h. Representative images show cells stained with CellMask™ (magenta) and TAMRA fluorescence of nanoparticles (yellow). For the purpose of these images, TAMRA has been false coloured to yellow to facilitate visualisation of nanoparticle interaction. The top row is a 3D view from the top of the biofilm, the middle row shows a 3D view from the front of the biofilm and the bottom row represents an angled 3D view from the top. Quantitative Comstat analysis of the biofilm images was performed using ImageJ. Graphs represent **(c)** biomass and **(d)** surface to biovolume ratio. Error bars represent standard error measured for different biofilm images, where n = 3, with $p<0.05$ = * and $p<0.01$ = ** (non-parametric Kruskal-Wallis test).

Under normal conditions, PAO1 Δ*tatA* did not produce structured biofilms due to the lack of eDNA (Figure 3.14a). However, when positive nanosensors were present, a thick and dense biofilm was formed similar to the wild type PAO1-N (Figure 3.14b). The nanosensors are co-localised with the cells as already observed before. This was again underlined by Comstat quantification showing that the biomass of biofilms grown with the positive nanosensors is

significantly increased ($p<0.05$, non-parametric Kruskal-Wallis test), whereas the surface to biovolume ratio is significantly decreased ($p<0.01$, non-parametric Kruskal-Wallis test), indicating a rescue of biofilm formation for $eDNA^-$ mutants and an interaction between positive nanosensors and eDNA.

3.3 Discussion

Recent research pointed out the importance of improving the understanding of biofilm formation and its environmental microniches to enhance possible treatment options against pathogenic bacteria like *P. aeruginosa* (Hidalgo *et al.*, 2009; Bjarnsholt, 2013; Fulaz *et al.*, 2019). It has been shown that the environmental pH can influence many different physiochemical properties of bacteria and thus it is important to characterise (Hunter and Beveridge, 2005; Wilton *et al.*, 2016; Fulaz *et al.*, 2019). In this study, pH-sensitive nanosensors are used to investigate pH microniches during biofilm formation of the model organism *P. aeruginosa*.

The selection of appropriate nanosensors, especially with regards to their charge, is crucial for the analysis of microbial biofilms. For this study, fluorescently labelled, neutral and positive polyacrylamide nanosensors were manufactured, consisting of the two pH-sensitive dyes OG and FAM and the reference dye TAMRA. It was shown that pH-sensitive polyacrylamide nanosensors penetrate biofilms of *P. aeruginosa.* Moreover, in static models, nanosensors with a positive charge supported the formation of thicker *P. aeruginosa* biofilms. Interaction between positive nanosensors and the negative surface of the bacteria as well as with the negative eDNA was observed. Furthermore, different biofilm models were used and compared, revealing structural differences between static and flow-cell models.

3.3.1 Different kinds of neutral and positively charged polyacrylamide nanoparticles can be produced in a reproducible manner

The production of both neutral and positively charged polyacrylamide nanoparticle was reproducible with batches showing a size between 38 nm and 47 nm with PDIs below 0.2 (Table 3.1), which correlates with the nanoparticles reported by Chauhan *et al.* (2013). The ζ-potential was also reproducible between batches, with ~-2.17 mV for neutral nanosensors and 13 mV to 18 mV for positively charged particles (Table 3.1). The small standard errors indicate the reproducibility of the production both in size and ζ-potential. Furthermore, optical

characterisation through emission scans confirmed responsiveness of the nanosensors to their pH environment (Figure 3.1). The fluorescence intensity of the pH-sensitive dyes OG and FAM was reduced as the pH decreased from 8 to 3.5. On the other hand, the fluorescence intensity of TAMRA was not affected between pH 4 and 8, making it a useful reference fluorophore. Additionally, the excitation and emission spectra between the pH-sensitive dyes and the reference dye TAMRA are significantly different, reducing crosstalk between the fluorophores during pH measurement. However, TAMRA can become pH-sensitive at very low pH (<3.5) as observed in the scan (Thermo Fisher Scientific, 2010a). The ratio between the pH-sensitive dyes OG and FAM and the pH insensitive dye TAMRA produced a sigmoidal curve that can be used for the calibration of the nanosensors to measure pH gradients of planktonic cultures or within biofilms.

3.3.2 Polyacrylamide nanosensors neither influence planktonic growth of PAO1-N nor do they get internalised by the cells

Because of their small size and other characteristics, such as surface charge, nanoparticles can be harmful to their environment (Sajid *et al.*, 2015). For instance, the particles may (i) release toxic substances such as free Ag^+ ions from silver particles, (ii) participate in surface interactions with media to produce toxic substances such as reactive oxygen species, or (iii) interact directly with the biological targets, for example with membranes or DNA (Ma *et al.*, 2013). Cationic nanoparticles were found to be more toxic than anionic particles that were non-toxic (Goodman *et al.*, 2004; Makabenta *et al.*, 2020). Furthermore, the toxicity increased with a rising positive surface charge (El Badawy *et al.*, 2010). However, for most research on negative effects of nanoparticles to their environment, materials are used that are believed to be harmful to cells in order to identify suitable anti-bacterial materials. These materials include metals like copper, zinc, and silver, whereas the nanosensors in this study consist of polyacrylamide, which is considered to be non-toxic. To exclude influences of the nanosensors used in this study on *P. aeruginosa*, toxicity of the nanoparticles was assessed. The comparison of the growth of

PAO1-N in LB medium with different concentrations of pH-sensitive polyacrylamide nanosensors revealed that concentrations below 25 mg mL^{-1} do not have any negative effects on the planktonic growth (Figure 3.2). Higher concentrations do inhibit the growth of the bacteria, which is likely due to the accumulation of nanoparticles resulting in reduced cell wall permeability and cell death (Abbaszadegan *et al.*, 2015). The positive charge could increase this effect, as a bigger impact was seen for the cationic nanosensors at a concentration of 25 mg mL^{-1} compared to the neutral sensors. However, those high concentrations of nanosensors are not reasonable and were only tested to identify the cut off. This study was performed at working concentrations of 1 mg mL^{-1} for planktonic cultures and static biofilm formation and at 5 mg mL^{-1} for flow-cell experiments, which were proven to not harm the cells. Comparable concentrations (0.5 and 1 mg mL^{-1}) of nanosensors at similar size were used for static biofilms in other studies, justifying this choice (Fulaz *et al.*, 2019).

Apart from toxic effects due to cationic surface charges of nanoparticles, applying a positive charge to nanosensors has previously been used to facilitate the internalisation of nanoparticles to eukaryotic cells (Sun *et al.*, 2009; Elsutohy *et al.*, 2017). In order to exclude that the nanosensors enter the bacterial cells of *P. aeruginosa* during incubation, structured illumination microscopy (SIM) was performed. Imaging of samples of PAO1-N incubated overnight with neutral or positive nanosensors showed nanosensor fluorescence throughout the samples (Figure 3.3). The most apparent difference was seen between the dispersal of the nanosensors, where positive nanosensors showed increased fluorescence signal around cells and cell clusters, which was not the case for the neutral nanosensors. Most bacteria carry a negative surface charge, including *P. aeruginosa* PAO1, due to the high number of carboxylate groups present in the B-band LPS resulting in a negative charge (Jucker *et al.*, 1996; Shephard *et al.*, 2008). Therefore, the coating of the cells by the positive nanosensors suggests an interaction of the positive charge with the negative surface charge of the bacteria. This behaviour has also been described by Li *et al.*, where cationic nanoparticles diffused into biofilms of Gram-positive

bacteria, whereupon they attached to the bacteria without killing them (J. Li *et al.*, 2018). LPS mutants could help to confirm a direct interaction between the positive particles and the surface of PAO1-N.

Using SIM furthermore revealed that the polyacrylamide nanosensors do not seem to enter the *P. aeruginosa* cells, as no or only little fluorescence was detected after two simple wash steps of the cells in LB medium. This finding will be relevant when analysing the pH of biofilms as any pH variation that will be measured by the nanosensors indicate pH changes inside of the biofilm and not inside of the cells. Some fluorescence of positive nanosensors was still observed after the wash step, suggesting that the nanosensors were trapped between cell clusters, where the interaction between the sensors and bacteria was strong enough to withstand the simple wash step.

3.3.3 Neutral and positive nanosensors show incorporation within the biofilm matrix of PAO1-N, with positively charged nanosensors promoting biofilm formation

After characterisation of the neutral and positive nanosensors in planktonic cultures of *P. aeruginosa*, biofilm formation with the addition of the various nanoparticles was investigated. It was shown that biofilms grown initially with positively charged nanosensors were approximately four times thicker than biofilms grown with neutral nanosensors or without nanosensors (Figure 3.4). Due to the negative surface charge of PAO1, it is likely that the positively charged nanosensors are interacting directly with the bacteria. This interaction could facilitate the bacteria to attach to each other and form a denser biofilm as seen in this study. The positive nanosensors did in this case function as “glue”, sticking the cells together and enable biofilm development. The biofilm thickness promoting effect of the positively charged polyacrylamide nanosensors upon static PAO1-N biofilms was independent of the incorporation of fluorophores and conferred an enhanced robustness to the biofilms. Positively charged amidine beads equally promoted biofilm formation, although increased clumping of the cells

was observed, likely due to the size of the beads (>1 µm), supporting the hypothesis that the positive charge and the resulting interaction is responsible for enhanced biofilm formation (Figure 3.6).

When neutral nanosensors or negatively charged particles are used, the interaction between nanosensors and cells is non-existent, or even reversed, most likely due to the same charge of the bacteria and nanoparticles leading to repulsion instead, which has been shown for negatively charged nanoparticles (Hidalgo *et al.*, 2009). In contrast, Li *et al.* found that treatment of PAO1 biofilms with engineered silver (Ag) or graphene oxide (GO) nanoparticles led to thicker biofilms of approximately 70 µm and 60 µm, respectively, compared to the control biofilm (30 µm) (N. Li *et al.*, 2018). Both nanoparticles carried a negative surface charge of -21.35 mV and -16.4 mV, respectively, and were therefore unlikely to promote biofilm formation in the same way. Instead, Li *et al.* showed enhanced *N*-3-oxo-dodecanoyl homoserine lactone ($3OC_{12}$-HSL) production induced by Ag and GO nanoparticles as well as promoted protease production and LasR expression (N. Li *et al.*, 2018). The LasR protein is the transcriptional activator of one of the two acyl-homoserine lactone quorum sensing systems of *P. aeruginosa,* and functions jointly with its autoinducer molecule, $3OC_{12}$-HSL, to coordinate the expression of target genes, including genes that encode factors to promote biofilm formation (Kiratisin *et al.*, 2002). Therefore, induction of the QS pathway by our nanosensors should be considered and investigated in future assays.

Nanosensor-dependent enhanced biofilm formation was not observed when biofilms were grown in the BioFlux flow-cell system (Figure 3.7). Due to the constant flow of medium, it could be postulated that the bacteria are less influenced by the nanosensors and therefore their adherence to each other is not modulated by the sensors. In addition, differences in the structure between static and flow-cell biofilms were observed, with mushrooms only forming when flow conditions were applied, underlying the importance of using different biofilm models (Lebeaux *et al.*, 2013).

Furthermore, the increased thickness of static biofilms was dependent on the concentration of the nanosensors, where higher concentrations of up to 20 mg mL^{-1} did not intensify the effect, but instead led to a biofilm which was less uniform and robust compared to the biofilms incubated with the working concentration of nanosensors (1 mg mL^{-1}, Figure 3.5). Nanosensor concentrations below 20 mg mL^{-1} did not affect the growth of planktonic PAO1-N (Figure 3.2). It follows that a higher concentration could simply result in flooding of the biofilm with positively charged particles. Too many positively charged nanosensors would be predicted to lead to a repulsion between the nanosensors and possibly other positively charged biofilm components, and consequently less adherence between bacteria, which would in turn reduce the robustness of the biofilm and potentially adversely affect its uniformity.

Penetration of biofilms by nanoparticles usually occurs by diffusion, with particles interacting with the bacteria and the biofilm matrix components (Stewart, 2003; Jefferson *et al.*, 2005; Rani *et al.*, 2005; Takenaka *et al.*, 2009). When positively charged nanosensors were added to biofilms that were initially grown without nanosensors, the biofilm structure was disrupted (Figure 3.8). This behaviour was not seen when biofilms were grown with positively charged nanoparticles from the beginning. One hypothesis that could be drawn from this is that biofilms initially grown with positive nanoparticles were more robust. The less robust biofilms formed in the absence of positively charged nanoparticles might be susceptible to disruption upon introduction of positively charged nanoparticles capable of interacting with the bacterial cell surface or matrix components. This has also been observed by Li *et al.* who used positively charged block copolymer nanoparticles to disperse established biofilms of multidrug-resistant Gram-positive bacteria, probably due to the enhanced solubility of the bacteria-nanoparticle complex by the nanoparticle dextran shell (J. Li *et al.*, 2018). The situation appears to differ in flow-cell biofilms since both neutral and positively charged nanosensors were able to penetrate an already established biofilm that had been grown for 12 h without causing disruptions (Figure 3.9 and Figure 3.10). Even after changing the flow-cell back to a medium without nanosensors, the

nanosensors were still detectable and incorporated within the biofilm. This has the practical application for future investigation as it indicates that the nanosensors can be added at later timepoints for pH analysis if needed.

3.3.4 Positively charged nanoparticles show interaction with various biofilm components

Interaction of the nanosensors, especially positively charged nanoparticles, with PAO1-N biofilms was observed and described above. To investigate this interaction in more detail and to identify possible components of the biofilm that are involved in the interaction, single-coloured, positively charged nanoparticles were used together with selectively binding dyes. One of these dyes is the tetramethhylrhodamine conjugate ConA-TRITC. ConA is a lectin that selectively binds to α-mannopyranosyl and α-glucopyranosyl residues, which makes it a suitable stain for the exopolysaccharide Psl, produced by PAO1. Extracellular polysaccharides, amongst other things, account for a large proportion of biofilm matrix and function as a structural scaffold and protective barrier in *P. aeruginosa*. This study revealed no direct interaction between Psl (neutral charge) and the OG-FAM positive nanoparticles in a static biofilm model; though a partial co-localisation was observed in the flow-cell model (Figure 3.11). It is likely that the staining of the statically grown biofilm with ConA-TRITC is not optimal as it was applied after biofilm formation, whereas within the flow-cell model the staining was undertaken during biofilm growth. It is thus possible that non-uniform staining of the static biofilm occurred. Nevertheless, an interaction between Psl and the nanosensors was suggested, and requires further investigation. Another polysaccharide with important roles in biofilm formation in *P. aeruginosa* is Pel, a cationic exopolysaccharide that cross-links extracellular DNA within the biofilm matrix (Jennings *et al.*, 2015). In this study, the two mutants PAO1 Δ*psl* and PAO1 Δ*pel* were used in a static model to examine the effects of the mutations on the distribution of the positive nanosensors. It was previously shown that Pel and Psl may have redundant functions as structural scaffolds, probably to help preserve the capacity to produce biofilms (Colvin *et al.*,

2012). Consequently, the deletion of *psl* results in overproduction of Pel and *vice versa*. The imaging showed slightly increased detection of Psl within the biofilm of PAO1 Δ*pel*, as expected, with some co-localisation with the nanoparticles (Figure 3.12). However, no differences were observed regarding the general distribution of the nanoparticles within the biofilm. The mutant PAO1 Δ*psl* still showed ConA-TRIT binding although no Psl should be present, resembling the wild type strain. It would have been reasonable to expect structural changes as a result of the enhanced cationic Pel production, which could lead to a repulsion with the also positively charged nanoparticles. This finding furthermore implies that the staining with ConA is not restricted to Psl and other molecules containing α-mannopyranosyl and α-glucopyranosyl residues are present within the biofilm matrix. Strathmann *et al.* showed that alginate, the third major exopolysaccharide produced during *P. aeruginosa* biofilm formation, is involved in the interaction of ConA with the biofilm matrix (Strathmann *et al.*, 2002). Alginate is another anionic component of the biofilm and could therefore be a valid target for interaction with the positive nanoparticles. Using additional mutants such as ones capable of alginate overproduction or that are deficient, could help shed more light on this. Overall, no precise conclusion about a direct interaction between exopolysaccharides and the nanosensors can be drawn from the results and experiments involving polysaccharide mutants should be repeated and performed using a flow-cell model to enable consistent staining of the polysaccharides.

Another negatively charged component of a biofilm that plays an important role in the formation of biofilms is eDNA. The cell-impermeable nucleic stain YOYO™-1, fluorescing in green and staining eDNA, was used in combination with red fluorescing, positively charged TAMRA nanoparticles to investigate an interaction. CLSM revealed co-localisation between eDNA and positive nanoparticles within both biofilm models, suggesting that the positive nanoparticles can stick to the negatively charged eDNA (Figure 3.13). In a study using 0.2 µm positively and negatively charged fluorescent polystyrene nanoparticles with *Burkholderia cepacia* it was shown that the addition of DNase to the biofilm enhanced the diffusion coefficient of the

positively charged nanoparticles, suggesting that there is an interaction between positively charged nanoparticles and the eDNA. This could further increase the "glue" effect and enhance biofilm formation (Messiaen *et al.*, 2013). Since the polyacrylamide nanosensors used in our study penetrated biofilms so rapidly (within seconds to minutes), diffusion gradients would be challenging to measure. Instead, the eDNA deficient mutant PAO1 Δ*tatA* was used to determine if the positive nanosensors would still promote biofilm formation without or with only little eDNA being present. The amount of eDNA found in biofilms of PAO1 Δ*tatA* is highly reduced due to a mutation in the Sec-independent translocase protein TatA that is involved in the secretion of eDNA in PAO1 (Paul Williams, unpublished). Despite the lack of eDNA, biofilm formation of PAO1 Δ*tatA* was significantly enhanced, confirming that an interaction between the nanoparticles and the eDNA is not alone responsible for the biofilm promoting effect (Figure 3.14). It is more likely that the enhanced biofilm formation is a result of a combination of components including the negative surface charge of bacteria, eDNA, and other factors that were beyond this study and will form part of future investigations.

3.4 Conclusion

The selection of appropriate nanosensors, especially with regards to their charge, is crucial for the analysis of microbial biofilms. The nanosensors chosen for this work show distinct characteristics, including monodispersity, pH responsiveness, and interaction with biofilm components such as eDNA and the bacteria itself. Being able to increase the thickness of biofilms has beneficial implications. For example, the positively charged nanosensors could be employed in future studies to elucidate the mechanistic steps of biofilm formation by combining them with mutants defective in defined aspects of biofilm formation. On the other hand, neutral nanosensors could be the better choice to study biofilms that closely mimic the natural physiological or environmental conditions, as no structural change in biofilm formation behaviour was observed when they were applied to our models.

Extrapolating from the influence of nanoparticle charge on biofilm formation, it is interesting to speculate that the charge of antimicrobials could influence the structure of biofilms. For example, antimicrobials with a positive charge could not only have biocidal effects such as benzalkonium chloride (Enomoto *et al.*, 2007), but also interact with cells in a way that could enhance quorum sensing, biofilm formation, or dispersal (N. Li *et al.*, 2018). It would follow that this might affect medical treatment or anti-biofouling regimens.

Chapter 4 Analysis of pH changes within planktonic cell cultures and biofilms of *P. aeruginosa*

4.1 Introduction

4.1.1 Background

As already raised, it is important to characterise the environmental pH of microorganisms because it can influence many different physiochemical properties such as polymer-polymer, ion-polymer and macromolecule-polymer interactions (Hunter and Beveridge, 2005). pH gradients in biofilm infections together with other factors can lead to an increased degree of physiological heterogeneity, which is correlated with the susceptibility of bacterial cells to antibiotics and biocides and can lead to the development of drug resistance (Gilbert *et al.*, 2002). The formation of chemical gradients (such as pH, redox potential, and ions) within the biofilm community can provide indications about microbial metabolism (Villaverde *et al.*, 1997; Allan *et al.*, 1999; Vroom *et al.*, 1999; Williamson *et al.*, 2012; Wan *et al.*, 2018). One example of biofilm-generated chemical gradients is dental caries, where the pH drops dramatically within a dental-plaque biofilm while the pH within the saliva remains neutral. It has been reported that biofilms of plaque forming bacteria comprise of pH 5.6 to 6.5 whereas the pH of resting saliva is ca 6.7 (Kleinberg, 1970; Moreno and Margolis, 1988). Whilst the biofilm matrix creates a diffusion-limiting polymer matrix, which protects the biofilm-forming community, sugars are fermented within the matrix resulting in a highly acidic microenvironment (Vroom *et al.*, 1999; Bowen and Koo, 2011; Horev *et al.*, 2015). Dental biofilms can reach pH values of 4.5 and even lower, often after exposure to sucrose, starch and cariogenic food products (Firestone *et al.*, 1987; Fejerskov *et al.*, 1992; Lingström *et al.*, 1993; Horev *et al.*, 2015). The low pH results in acid-dissolution of tooth-enamel and eventually carious lesions (Vroom *et al.*, 1999; Koo *et al.*, 2013).

A range of different pH nanosensors has already been applied in biological research, for example in cancer research where it has been suggested that low oxygen concentration and low pH increase the potential of cancer metastasis and reduce the treatment prognosis for patients with advanced stage cancers (Höckel *et al.*, 1993). Horev *et al.* reported a low pH responsive nanoparticle approach where nanoparticles destabilise by approaching the low pH niches in dental biofilm leading to a controlled disruption of the biofilm (Horev *et al.*, 2015). Using this approach, a 4-fold enhanced disruption of *Streptococcus mutans* biofilms using the antibacterial drug farnesol loaded onto nanoparticles was achieved compared to application of free farnesol (Horev *et al.*, 2015). Within microbiology, silica based nanosensors were used to analyse pH microenvironments in microbial biofilms of *E. coli* (Hidalgo *et al.*, 2009). Hidalgo *et al.* could show local variation in pH from the neutral outside surface of the film to the acidic core. Nanosensors with a single fluorescent ratiometric pH-sensitive probe were used to reveal pH heterogeneity throughout a *P. aeruginosa* biofilm (Hunter and Beveridge, 2005). A slightly acidic biofilm environment was reported with a pH range between 5.6 within the biofilm and 7.0 in the bulk fluid (Hunter and Beveridge, 2005). More recently, Fulaz *et al.* reported the use of pH-sensitive nanosensors to detect pH gradients in biofilms, but did not extend their study to real time analysis of the environmental microniches under flow conditions (Fulaz *et al.*, 2019).

4.1.2 Aims of this chapter

Having characterised the penetration and responsiveness of pH-sensitive ratiometric polyacrylamide nanosensors in a biofilm context in Chapter 3, the goal here was to determine whether the nanosensors afford the sensitivity and resolution to accurately measure physiological pH in biofilm microniches by addressing the following questions:

- Are pH measurements of *P. aeruginosa* cultures comparable between the pH-sensitive nanosensors and devices available on the market?
- Are the nanosensors pH-responsive to induced pH changes within biofilms?
- Can pH changes be measured over time in planktonic growth experiments?

- Can pH changes within biofilms be tracked over time using a flow-cell model?
- Are real-time pH gradients within microcolonies detectable using the nanosensors?

4.2 Results

In this chapter, the fluorescent pH-sensitive polyacrylamide-based nanosensors that were introduced in Chapter 3 were used to investigate the pH microenvironments of *P. aeruginosa* liquid cultures and biofilms. The effects of various carbohydrates on the external pH of a culture was analysed. In addition, the use of nutrient flow and time-lapse imaging enabled real-time reporting of pH modulation within a biofilm to be monitored. Alternative dyes that could be used within our systems were furthermore investigated.

4.2.1 pH-sensitive fluorescent nanosensor pH measurements are equivalent to those of commercially available devices, and are responsive to induced pH changes within biofilms

Prior to further use of the nanosensors, they were compared to other devices available on the market. For this purpose, a needle-type pH microsensor NTH-HP5 (PreSens) was chosen, which is designed to measure the pH in small volumes. The microsensors are only responsive between pH 5.5 and 8.5 and cannot be easily applied to experiments where the pH should be measured continuously over time. Furthermore, although the needle is very small, there is still a chance to disrupt fragile structures such as biofilms.

The pH of M9 glucose (M9G, initially at a pH of ~6.5) incubated in falcon tubes (Greiner Bio-One, 50 mL) without bacteria was measured at the beginning (0 hours), after 10 h and after 26 h using the nanosensors and the microsensor at room temperature (Figure 4.1). The nanosensors and microsensor were calibrated at the beginning of the experiment using pH buffers.

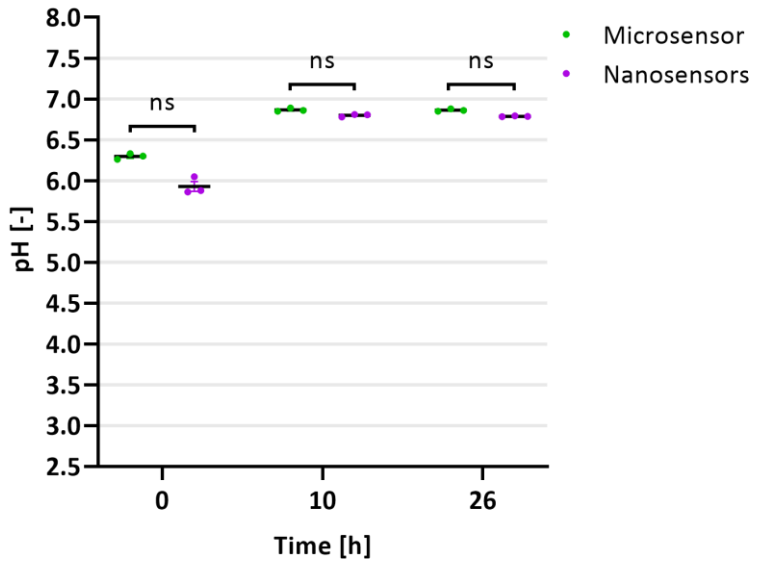


Figure 4.1: Microsensors and nanosensors determine the same pH of a liquid sample over time. Falcon tubes were used to incubate 5 mL of M9G at 37°C and 200 rpm in triplicates with positively charged polyacrylamide nanosensors at a concentration of 1 mg mL^{-1}. After 0 h, 10 h and 26 h, 200 µL of each tube were transferred into a black 96-well plate and the pH was measured using a microsensor (PreSens) before the fluorescence intensity of the nanosensors was measured using a Tecan plate reader (both at room temperature). pH calibration of the nanosensors was performed using pH buffers in a 96-well plate at room temperature. n = 3, with ns = not significant (non-parametric Mann-Whitney test).

The first pH measurement at the beginning of the experiment was slightly different between the nanosensors (pH 5.9) and the microsensor (pH 6.3). However, this was not statistically significant using a non-parametric Mann-Whitney test. No differences were detected after 10 h (pH 6.8 and 6.9) and 26 h (pH 6.8 and 6.9).

To confirm the responsiveness of the nanosensors to their pH environment, biofilms of PAO1-N were grown statically with positively charged nanosensors (2.18.1) and treated with 100 µL of 3% (v/v) acetic acid, pH ~2.4. The biofilms were imaged before and after the treatment to identify pH changes caused by the acetic acid at room temperature (Figure 4.2). The nanosensors calibration was performed under the same conditions at room temperature.

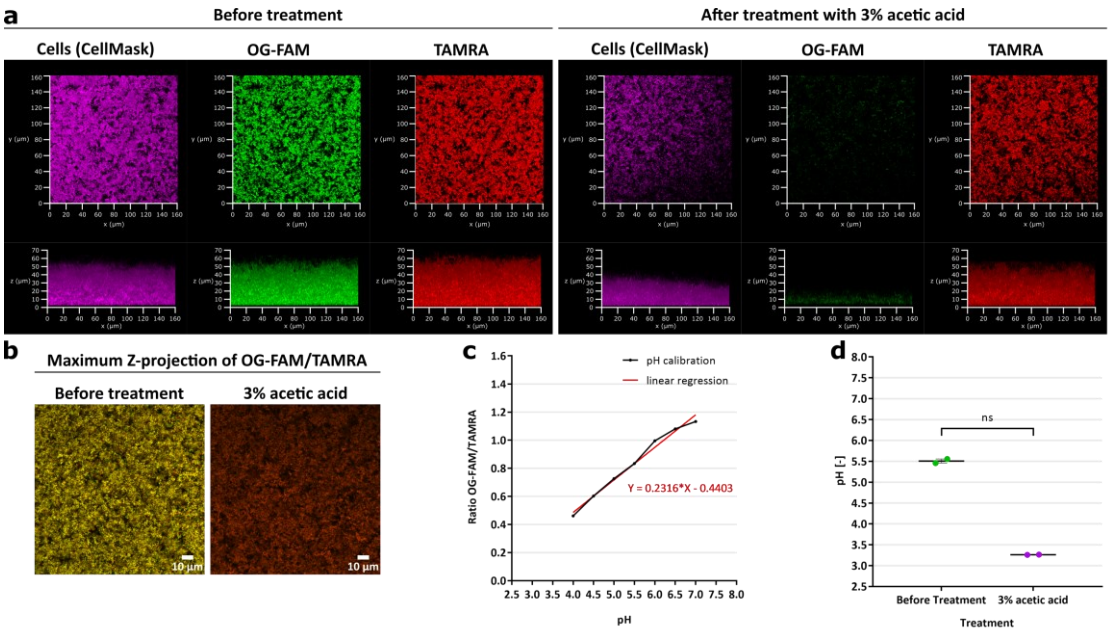


Figure 4.2: pH-sensitive fluorescent polyacrylamide nanosensor respond to induced pH changes within their environment. PAO1-N was inoculated into an 8-well glass bottom chamber at an OD_{600} of 0.05 in M9G containing 1 mg mL^{-1} positive nanosensors. The cells were incubated at 37°C under static conditions for 48 h. **(a)** Cells were stained with CellMask™ (magenta) and nanosensor channels are presented for OG-FAM (green, pH-sensitive) and TAMRA (red, reference). Z-stack images were taken with a Zeiss CLSM using a 40x objective before the treatment (left) and 30 min after the treatment with 3% (v/v) acetic acid (right). Top images represent 3D top view, bottom images 3D side view of biofilms. **(b)** Maximum Z-projection of OG-FAM/TAMRA overlay before the treatment (left) and after the treatment (right). **(c)** Calibration curve of nanosensors using pH buffers. The linear part (pH 4.0 to 7.0) was taken to calculate the linear regression (red) for the pH determination of the biofilm. **(d)** Calculated pH of the biofilms before and after the treatment with 3% (v/v) acetic acid. Error bars represent standard error measured for different biofilm images, where n = 2, with ns = not significant (non-parametric Mann-Whitney test). Imaging and calibration of nanosensors was performed at room temperature.

The biofilms showed a pH of 5.5 before the treatment with 3% (v/v) acetic acid, which lowered the pH down to 3.3 after 30 min (Figure 4.2d). Although the difference was not statistically significant based on a non-parametric Mann-Whitney test (likely because of the low number of replicates for this measurement), the trend was apparent. This pH-drop was also observed in the images, where the fluorescence intensity of the pH-sensitive dyes OG and FAM decreased massively after the addition of the acid, indicating a pH reduction (Figure 4.2a). Because the fluorescence intensity of the red dye (TAMRA) is constant at any pH whereas the fluorescence intensity of the green dyes (OG and FAM) decreases with pH, overlay images appear red, yellow

or green depending on the pH. Almost no green fluorescence was detected after 30 min, resulting in a red coloured maximum Z-projection of the overlay channels as opposed to a yellow colour before the addition (Figure 4.2b).

4.2.2 The addition of glucose reduces the pH of the growth medium when added to planktonic PAO1-N

After testing of different carbon sources for the growth of PAO1-N, glucose and succinate were used for a growth measurement together with a pH determination over 18 h using positively charged polyacrylamide nanosensors (Figure 4.3). The growth and the pH were determined using a Tecan plate reader (2.16.10 and 2.16.11). Both carbon sources showed a reasonable growth in preliminary experiments. Additionally, M9S medium has a lower initial pH (~5.5) compared to M9G (~6.5) making the two carbon sources ideal for a pH comparison. For the pH determination, pH buffers ranging from pH 2.5 to pH 8.0 were used to perform the calibration of the nanosensors for each individual time point.

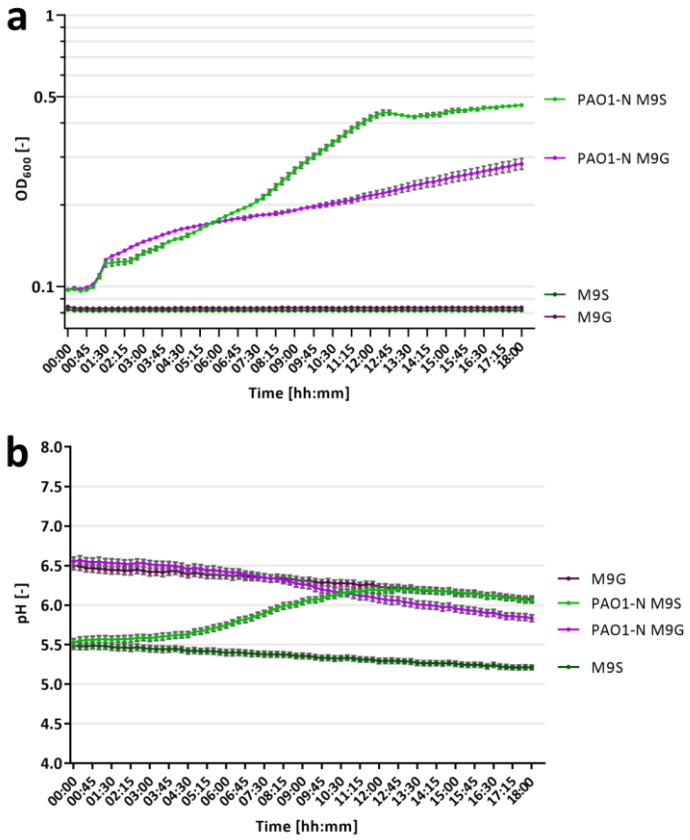


Figure 4.3: The pH of M9S during planktonic growth of PAO1-N increases over time whereas the pH of M9G slightly decreases. PAO1-N was inoculated into a black 96-well plate at an OD_{600} of 0.05 in M9G or M9S containing 1 mg mL^{-1} positive nanosensors. The OD_{600} and fluorescence intensity was measured automatically every 15 min at 37°C. Nanosensor calibration was performed using a range of pH buffers. No path length correction was applied. Error bars represent standard error, where n = 3x4. **(a)** OD_{600} is shown on a log scale against time. **(b)** pH is shown against time.

The growth of PAO1-N in M9S and M9G was comparable at the beginning but was enhanced for M9S after 6 h. The final OD_{600} was higher for bacteria grown in M9S than in M9G.

The calculated pH of the succinate samples with and without bacteria at the beginning of the measurement was around pH 5.5 and was therefore much lower than the pH from the glucose samples, which was around pH 6.5. The pH of the M9G with PAO1-N showed a slight decrease over time, reaching pH 5.7 after 18 h. However, the control with M9G medium alone also showed a slight decrease in the pH over time. In contrast, the pH of M9S containing PAO1-N increased over the first 12 h from pH 5.5 to 6.3, whereas the control without bacteria shows a slight decrease from pH 5.5 to 5.2.

Next, the response of starved planktonic *P. aeruginosa* to the introduction of a fermentable carbon source (glucose) versus a non-fermentable carbon source (lactose) was analysed, with the aim of detecting any pH changes in the medium as an indirect measurement of the fermentation of a carbon source (Figure 4.4). The carbon sources were added to planktonic PAO1-N cells and the pH was observed over 30 min using a fluorescence microscope (2.16.12). For the pH determination, pH buffers ranging from pH 2.5 to pH 8.0 were used to perform the calibration of the nanosensors.

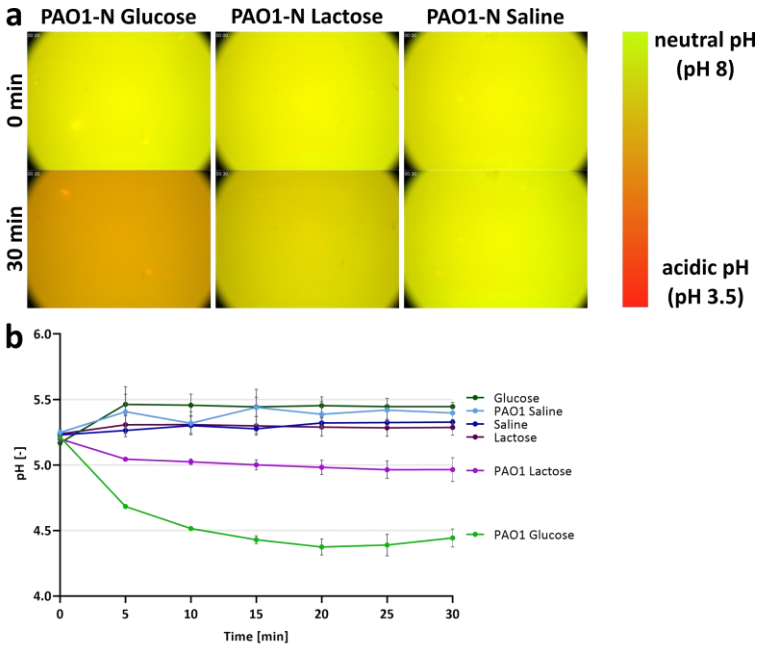


Figure 4.4: Fermentation of glucose but not lactose or saline by PAO1-N visualised with pH-sensitive nanosensors. Positively charged pH-sensitive nanosensors at a concentration of 1 mg mL^{-1} were added to planktonic PAO1-N grown overnight and normalized to an OD_{600} of 1. Time-lapse images were taken with a Nikon widefield fluorescent microscope every 5 min at room temperature. **(a)** Representative fluorescence images of cells in saline before the addition of either glucose, lactose, or saline to a final concentration of 1% (v/v) (top panel) or after 30 minutes (bottom panel). An overlay image of the fluorescence channels for green (OG-FAM) and red (TAMRA) is shown. **(b)** The pH of each condition at the indicated time points was calculated and plotted against the time of addition. Controls without cells are included. Error bars represent standard error measured for different images, where n = 2.

Fluorescence microscopy revealed that the control with saline remained unchanged throughout the experiment. This was also the case following the introduction of the non-fermentable lactose, which resulted in a very slight decrease of the pH during the first 5 min before being

constant during the following 25 min period. In contrast, during the same period, the addition of glucose to the starved cells led to a reduction in pH from pH 5.2 to ~pH 4.4.

4.2.3 pH changes can be observed during biofilm formation in a flow-cell system at a microcolony level using polyacrylamide nanosensors and time-lapse imaging

Time-lapse imaging together with the nanosensor technology was used to investigate pH changes during biofilm formation of PAO1-N over time in a BioFlux flow-cell system. Images were taken every 15 min for 16 h using a Nikon widefield (2.18.2). A red region of interest indicates a low pH, due to diminishing signal from OG and FAM under acidic conditions, whereas green to orange indicate relatively higher pH values, due to an increase in fluorescence from OG and FAM (Figure 4.5).

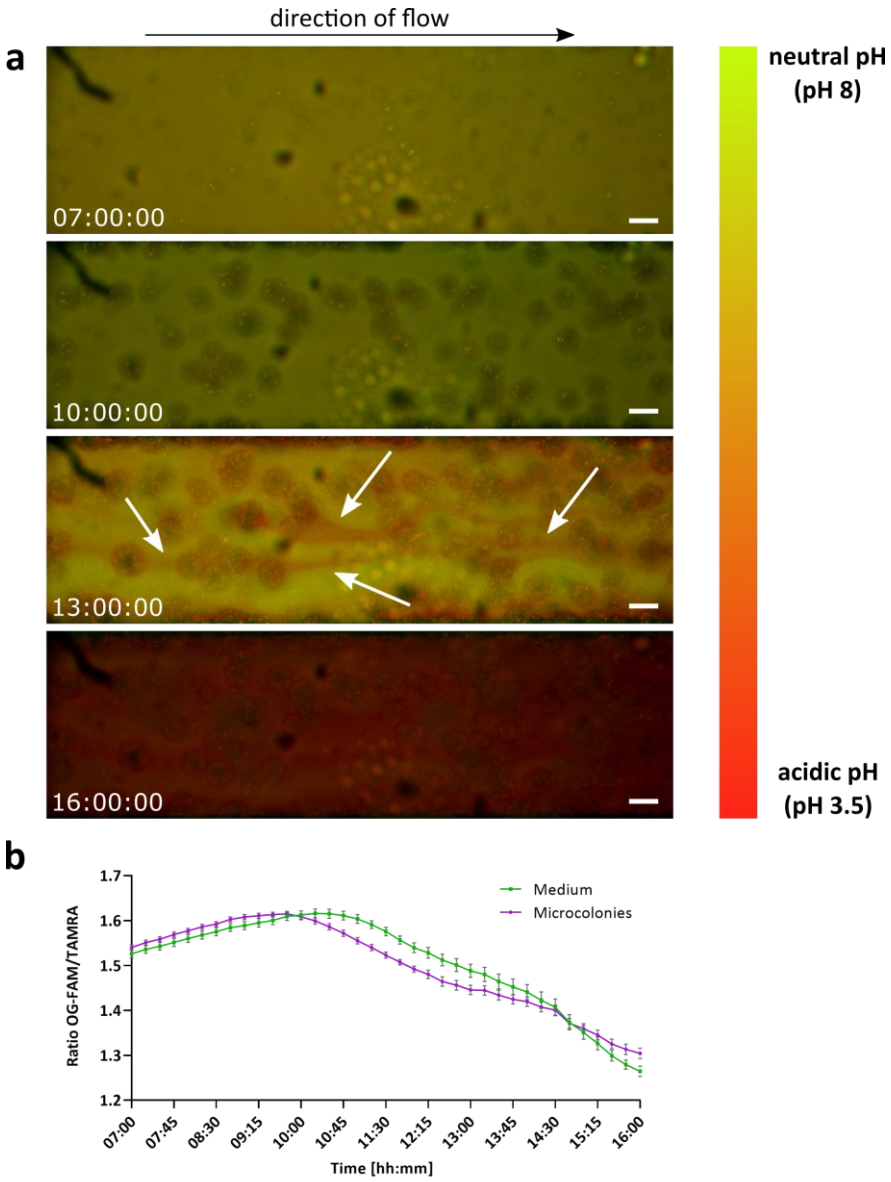


Figure 4.5: A streamer of acidic pH is evident in the downstream flow of PAO1-N biofilm microcolonies. PAO1-N was inoculated into a 48-well BioFlux flow-cell plate at an OD_{600} of 0.05 in M9S containing 5 mg mL^{-1} positively charged polyacrylamide nanosensors. The cells were incubated at 37°C under flow conditions (0.2 dyn cm^{-2}) for 16 h. **(a)** Time-lapse imaging of a PAO1-N biofilm grown in a BioFlux flow-cell after 7 h (start of microcolony formation), 10 h, 13 h and 16 h. Images were taken using a fluorescence Nikon widefield microscope. Red streaks being released downstream by the microcolonies into the medium after 13 h of growth are indicated by the white arrows. Scale bars represent 50 µm. **(b)** Fluorescence intensity of OG-FAM and TAMRA was measured using widefield images in ImageJ and the ratio is plotted against the time of incubation starting after 7 h when microcolony formation occurred. Error bars represent standard error measured for different areas of the images, where n = 6.

During the first couple of hours as microcolony formation starts, the pH increased slightly as observed by a colour shift from a more orange colour (lower pH) towards a more greenish colour

(higher pH) (Figure 4.5a). Once the microcolonies started to form after 10 h, the colour around the microcolonies changed to red indicating an acidification during the microcolony formation. Red streaks could be observed after 13 h coming from the microcolonies and being taken away by the flow. Subsequently, the colour continued changing towards red until the whole biofilm was acidified. This observation was confirmed by analysing the fluorescence intensity of the green channel (pH-sensitive dyes) and red channel (reference dye) within specific regions using ImageJ (Figure 4.5b). Over the first hours when microcolonies started to form, the fluorescence intensity ratio of OG-FAM and TAMRA increased slightly from 1.5 to 1.6, indicating a pH increase. The fluorescence intensity around the microcolonies starts to decrease after 10 h before the intensity of the medium declines. After 16 h of biofilm growth, the fluorescence intensity ratio around the microcolonies as well as within the medium reaches 1.25, indicating an acidification of the whole biofilm.

In addition to time-lapse imaging, CLSM was used to look at the pH variation of single microcolonies of a PAO1-N biofilm grown within a BioFlux flow-cell after an incubation time of 14 h. The biofilm was imaged in 1 µm steps up to 25 µm (Figure 4.6).

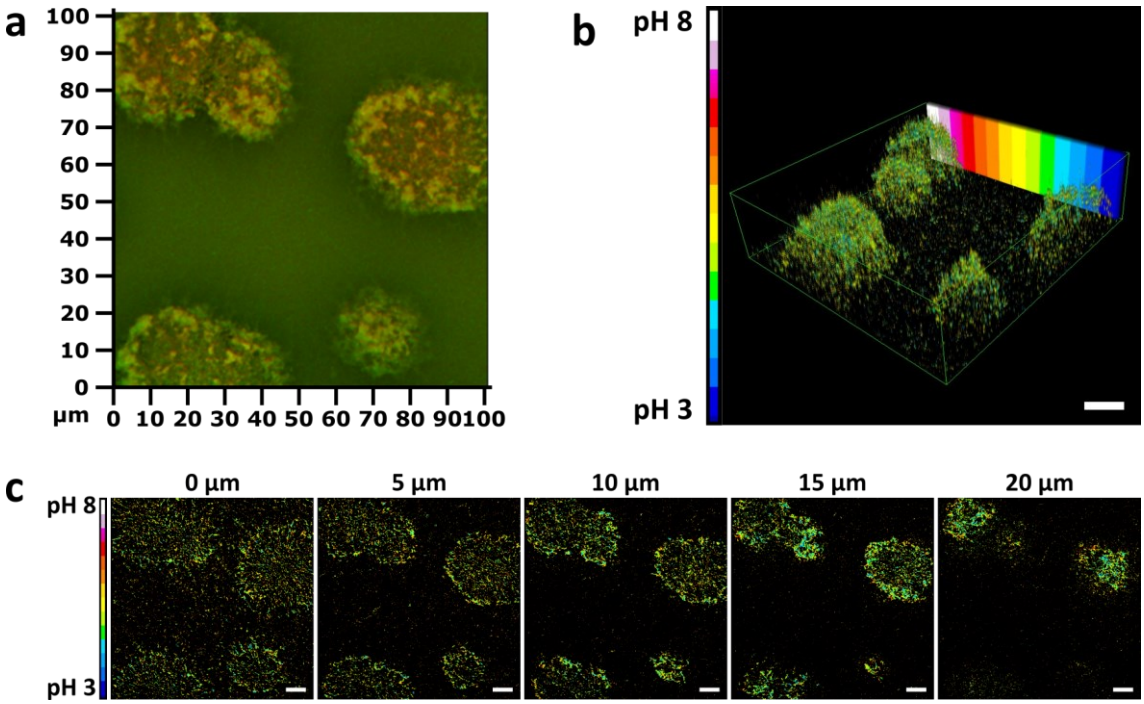


Figure 4.6: PAO1-N microcolonies in flow biofilms have an acidic centre. PAO1-N was inoculated into a 48-well BioFlux flow-cell plate at an OD_{600} of 0.05 in M9S containing 5 mg mL^{-1} positively charged polyacrylamide nanosensors. The cells were incubated at 37°C under flow conditions (0.2 dyn cm^{-2}) for 14 h. **(a)** Confocal 3D Z-stack image (top view) of a single microcolony. **(b)** and **(c)** MatLab analysis of confocal images shows a lower pH of 3.5 – 4.5 within the core of microcolonies and a higher pH of 6.0 – 7.0 at the outer parts. Images represent 3D rendering of the biofilm Z-stack **(b)** and individual pH maps at the bottom of the biofilm (0 µm) and 5 µm, 10 µm, 15 µm and 20 µm from the bottom into the biofilm **(c)**. Scale bars represent 10 µm. pH measurement and calibration was performed at room temperature.

The 3D Z-stack shows a colour change from orange within the core of the microcolonies towards yellow at the outer parts (Figure 4.6a). After calibration of the nanosensors using pH buffers ranging from pH 3 to 8, pH maps and a 3D rendering of the Z-stack of the biofilm were generated using the software MatLab (Figure 4.6b and c). The values of the pH maps correlate with the observations from the 3D Z-stack showing a low pH within the microcolonies (~pH 3.5 – 4.5) and a more neutral pH towards the outside (~pH 6.0 – 7.0).

4.2.4 Examination of the pH independent dye rhodamine B as alternative to TAMRA

The pH-independent dye TAMRA used with our nanosensors showed a slight decrease in fluorescence intensity over time in some cases. Therefore, Rhodamine Red™-X (Rho, Thermo

Fisher Scientific), another pH-independent red fluorescence dye was investigated as an alternative to TAMRA. Nanosensors consisting of OG-FAM and Rho were prepared according to the protocol (2.5) and characterised as presented in Table 4.1.

Table 4.1: Size, PDI and ζ-potential of polyacrylamide nanosensors using Rhodamine Red™-X. PDI polydispersity index

Polyacrylamide nanosensors	Size (nm)	PDI	ζ-potential (mV)
positive OG-FAM and Rho	66.9	0.216	12.86

The size of the Rho nanosensors (66.9 nm) was slightly larger compared to the TAMRA nanosensors (~40 nm), whereas the ζ-potential was slightly lower with 12.86 mV compared to ~18 mV.

Subsequently, both kinds of nanosensors (TAMRA and Rho) were used to measure the fluorescence intensity over time in a range of pH buffers with a Tecan plate reader (Figure 4.7).

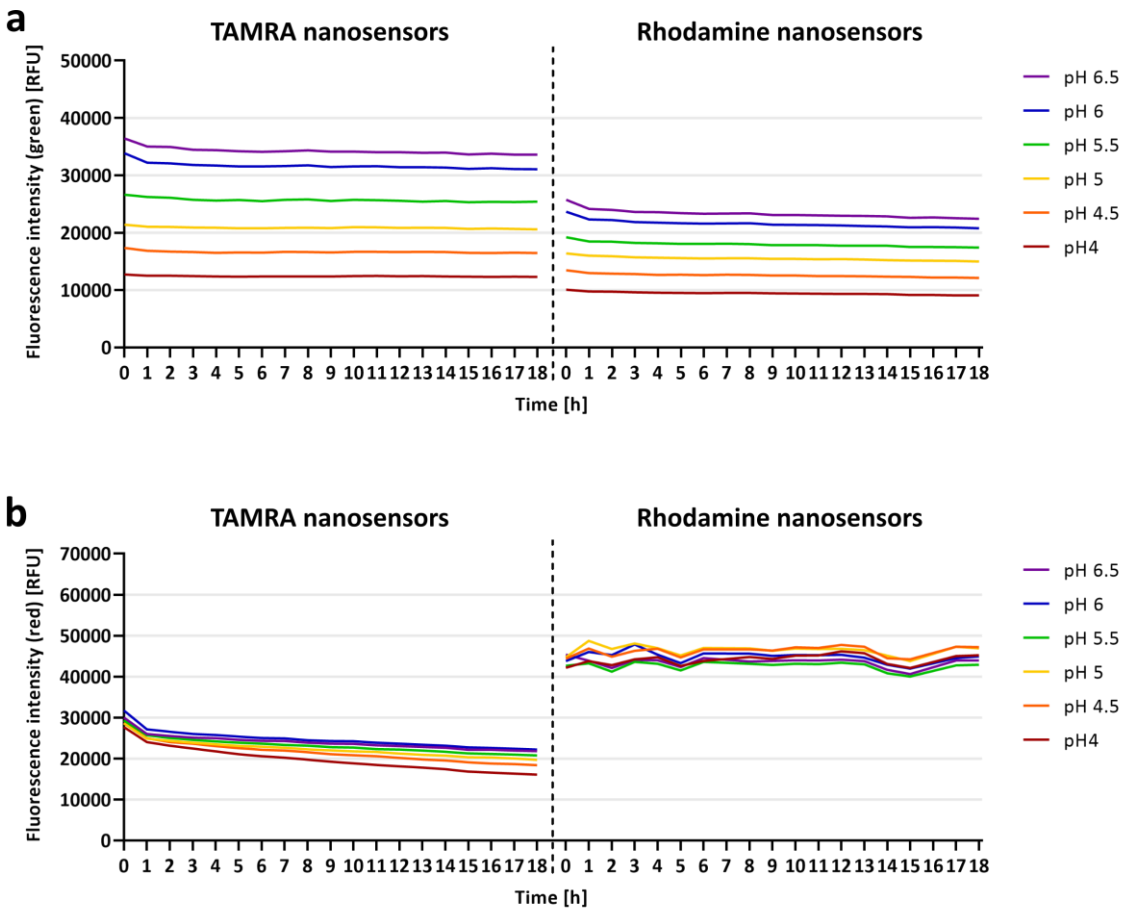


Figure 4.7: Fluorescence intensity of Rhodamine Red™-X stays constant over time when present in a range of pH buffers. OG-FAM with TAMRA nanosensors (left) or OG-FAM with Rho (right) were suspended in pH buffers ranging from pH 4 to pH 6.5 at a concentration of 1 mg mL^{-1}. A black 96-well plate was used with 200 µL of each buffer condition to measure the fluorescence intensity of OG-FAM and TAMRA/rhodamine every 15 min for 18 h at 37°C. **(a)** Fluorescence intensity of OG-FAM (488 nm/520 nm, green) shown against time. **(b)** Fluorescence intensity of TAMRA (540 nm/580 nm) and rhodamine (560 nm/580 nm, red) shown against time.

The fluorescence intensity of OG-FAM was constant over the whole period for both nanosensors, with a slightly lower overall intenstiy of the Rho nanosensors. The TAMRA fluorescence intensity decreased slightly over time from 30000 RFU at the beginning to ~20000 RFU after 18 h. In contrast, the fluorescence intensity of Rho was unaltered over the whole period with some small fluctuations between time points.

4.3 Discussion

This chapter has shown that pH-sensitive polyacrylamide nanosensors report on pH modulation during planktonic growth of the chosen model bacterium, *P. aeruginosa*. Furthermore, once nanosensors have been integrated into biofilms, they are capable of real-time pH quantification in static model systems at high temporal, spatial and measurement resolution. This chapter also includes time-lapse imaging that reveals acidification downstream of microcolonies as well as an acidic core in a flow biofilm model of *P. aeruginosa.*

4.3.1 Polyacrylamide nanosensors are pH responsive in planktonic and biofilm studies

pH-sensitive microsensors (PreSens) were used to investigate the comparability of our nanosensors with commercially available products. The pH of liquid medium was measured at three different time points using both methods (Figure 4.1). At the beginning (0 h), a slight discrepancy was observed between microsensor (pH 6.3) and nanosensors (pH 5.9). However, after the first measurement, the pH of the samples increased for both measurement types to pH 6.8 (microsensor) and 6.9 (nanosensors), respectively, where it stayed constant. The differences between both methods at the first time point as well as the pH increase could be a result of the temperature rise from room temperature at the beginning to 37°C during the rest of the experiment. Overall, it was shown that the nanosensors deliver a pH measurement that is equivalent to that of devices on the market. The nanosensors could even be considered superior; for example, due to their pH-sensitivity within the whole physiological range (pH 3.5-8.0) compared to the microsensors, that are only responsive between pH 5.5 and 8.5. Another advantage is the applicability of the nanosensors for real time experiments over time, as they can easily be added to the planktonic cells or biofilms enabling pH measurements without disrupting the experiment.

The pH responsiveness of the nanosensors within matured biofilms was confirmed by CLSM. Biofilms of *P. aeruginosa* with nanosensors incorporated were imaged before and after treatment with 3% (v/v) acetic acid (Figure 4.2). Fluorescence measurements showed rapid response of the nanosensors to the addition of the acid, detectable by a drop in fluorescence intensity of OG and FAM (Figure 4.2). Using pH buffers, the nanosensors were calibrated and the pH was calculated, showing a drop from pH 5.5 before the treatment to pH 3.3 after 30 min, confirming the suitability of the nanosensors to measure pH changes within biofilms.

Furthermore, by utilising the biological system of *P. aeruginosa*, where carbohydrate supplementation can induce a pH response, the effectiveness of the pH-sensitive polyacrylamide nanosensors as a real-time tool to accurately determine pH changes in extracellular media was illustrated. Firstly, the effect of different carbon sources on the pH during the growth was examined using the pH-sensitive polyacrylamide nanosensors in planktonic cultures of PAO1-N (Figure 4.3). Glucose and succinate were chosen as carbon sources for this experiment as both carbon sources are well-established as growth supplements for bacterial culture (Miller and Ku, 1978; Kirner *et al.*, 1996; Frimmersdorf *et al.*, 2010). A preferred growth with succinate compared to glucose was observed in this study and has been described previously (Tiwari and Campbell, 1869; Ng and Dawes, 1973; Frimmersdorf *et al.*, 2010). Glucose is a less preferred carbon source of *P. aeruginosa* because the Entner-Doudoroff pathway is less efficient than the tricarboxylic acid (TCA) cycle, and is controlled by catabolite repression (Entner and Doudoroff, 1952; Suh *et al.*, 2002; Silo-Suh *et al.*, 2005). Catabolite repression facilitates catabolism of substrates in an ordered way, where short-chain fatty acids, amino acids, polyamines, and C_4-dicarboxylates such as succinate are amongst the preferred carbon und nitrogen sources (Stanier *et al.*, 1966; Lessie and Neidhardt, 1967; Tricot *et al.*, 1994; Valentini and Lapouge, 2013). Although less preferred, sugars such as glucose can also be efficiently metabolised and are commonly found in the environment. Furthermore, succinate is known to alkalinise the medium during growth what makes it a suitable carbon source for this pH assay (Terpe *et al.*,

1999). The results presented in this study confirm those findings. After an initial pH of 5.5 for M9S, the pH increased up to 6.3. Metabolome analysis could be used to determine whether the pH increases due to the uptake and consumption of the succinic acid during the TCA cycle or because of the subsequent production of alkaline metabolites that are released to the medium. For some bacteria, acidification of the medium during growth has been reported using glucose as sole carbon source (Marty-Teysset *et al.*, 1996). This behaviour was also observed in this study for M9G but only with a slight pH decrease instead of a rapid acidification described by Marty-Teysset *et al.* However, Sánchez-Clemente *et al.* did not observe any pH changes during growth experiments of *Pseudomonas putida* when glucose was used as sole carbon source (Sánchez-Clemente *et al.*, 2018).

In a following experiment, starved PAO1-N cells were used to investigate pH changes over a short time period (30 min) as a result of fermentation of different carbon sources (Figure 4.4). With the addition of the simple monosaccharide glucose, a rapid reduction in the pH was observed, as *Pseudomonas* is capable of metabolising glucose via three different pathways to produce 6-phosphogluconate (6PG, Figure 4.8): After glucose has entered the periplasm via outer membrane porins, (i) the glucose can be transported to the cytoplasm, where it is phosphorylated via a glucokinase before the resulting glucose-6-phosphate is converted to 6PG; or the glucose can be oxidised to gluconate within the periplasm, which (ii) can be transported into the cytoplasm where it gets phosphorylated to 6PG; or (iii) oxidised to 2-ketogluconate, which is subsequently transported to the cytoplasm and reduced to 6PG (Whiting *et al.*, 1976; del Castillo and Ramos, 2007; del Castillo *et al.*, 2007; del Castillo *et al.*, 2008; Daddaoua *et al.*, 2009). The 6PG is subsequently fed into the Entner-Doudoroff pathway and metabolised into glyceraldehyde 3-phosphate and pyruvate (Entner and Doudoroff, 1952; Fuhrer *et al.*, 2005). Glyceraldehyde 3-phosphate is further metabolised, while pyruvate is either decarboxylated to acetyl-CoA and enters the TCA cycle, where it eventually gets metabolised into succinate, or is converted into organic acids such as lactate or formate (Daddaoua *et al.*, 2009). The

fermentation of pyruvate gets especially important for *P. aeruginosa* under oxygen limiting conditions, where it can achieve anaerobic growth by substrate-level phosphorylation, for example during lung infections in cystic fibrosis patients, where the diffusion of oxygen is limited by thick layers of mucus.

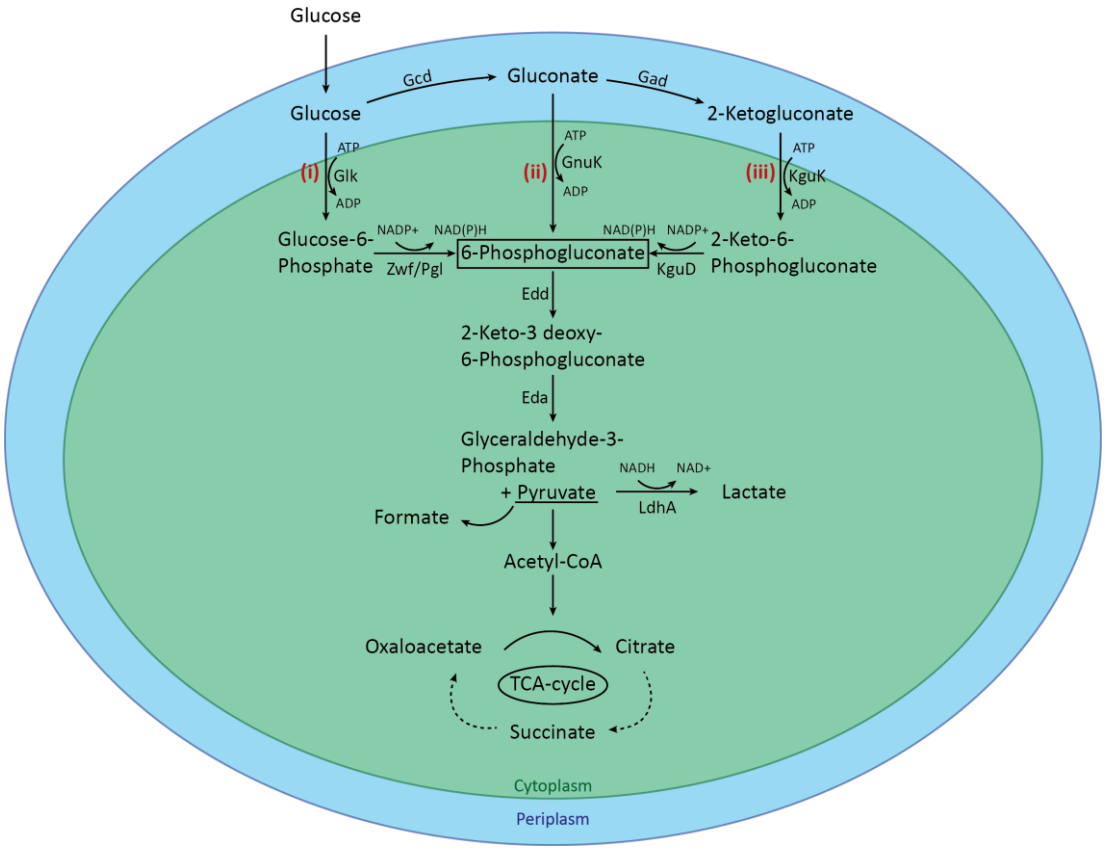


Figure 4.8: Glucose and succinate metabolism pathways in *P. aeruginosa*. Glk = glucokinase, Zwf = glucose-6-phosphate dehydrogenase, Pgl = 6-phosphogluconolactonase, Edd = 6-phosphogluconate dehydratase, Gcd = glucose dehydrogenase, Gad = gluconate oxidase, KguK = 2-ketogluconate kinase, KguD = 2-ketogluconate-6-phosphate dehydrogenase, GnuK = gluconate kinase, TCA = Tricarboxylic Acid Cycle.

The activation of the glycolysis due to the glucose addition could result in enhanced production of gluconate and 2-ketogluconate within the periplasm (pathways (i) and (ii)), which could in turn lead to the secretion of excess acid and subsequent acidification of the extracellular medium. Another possibility is the increased production of organic acids as result of enhanced glucose metabolism. Solé *et al*. reported a rapid extracellular acidification of starved *Serratia marcescens* cells induced by glucose addition (Solé *et al.*, 2000). The feeding of the cells with

glucose led to the production of lactic, acetic, citric, and pyruvic acid, which could also have occurred in this study. However, Solé *et al.* reported no increased concentrations of organic acids or a pH drop using *P. aeruginosa* under shaking conditions.

In contrast, with the addition of lactose, the external pH was unchanged throughout the experiment with only a very slight drop during the first 5 min. This was a result of lactose being non-fermentative by *P. aeruginosa* due to the lack of β-galactosidase activity (Drahos *et al.*, 1986; Iglewski, 1996). Genetic modifications would be needed to introduce *lacY* and *lacZ* from *E. coli*, which encode β-galactosidase and lactose permease, to produce a strain that can grow in M9 lactose (Drahos *et al.*, 1986; Koch *et al.*, 1988).

In addition to planktonic pH changes, this study has shown for the first time that pH-sensitive polyacrylamide nanosensors can be used to visualise pH changes over time during biofilm formation of PAO1-N within a BioFlux flow-cell system at a microcolony level (Figure 4.5). At the beginning of the biofilm formation, the pH increased very slightly while the bacteria start to adapt to the environment, as previously reported. After 10 h, acidification of the biofilm was observed during microcolony formation and subsequently while the biofilm continued to form. The acidic streaks that were released by the microcolonies could be exoproducts from the bacteria, produced during metabolism (Hidalgo *et al.*, 2009). Another possibility is that acidic molecules are released by the cells to help form the biofilms. These molecules could for example be eDNA or exopolysaccharides (Wilton *et al.*, 2016). Furthermore, the EPS could serve as an energy reserve, where enzymatic degradation of glucans and fructans take place to release monosaccharides that could in turn lead to the production of acidic by-products (Costa Oliveira *et al.*, 2017). The importance of the EPS for the acidification of biofilms was shown by using EPS-degrading dextranase, which led to neutralisation of the biofilms (Hwang *et al.*, 2016). It could also be that the cells are actively lowering the pH when biofilm formation is initiated, to facilitate the process, for example to enable better attachment or to increase the pH-dependent turn-over and release of QS molecules like AHLs (Yates *et al.*, 2002). Furthermore, it was shown that

acidic pH promotes the *P. aeruginosa* antibiotic resistance phenotype and can be attained by the accumulation of eDNA in biofilms (Wilton *et al.*, 2016). Therefore, acidification of the biofilm can act as a protection of the bacteria against antibiotic treatment, suggesting that neutralisation of the environmental pH could help to combat biofilm related infections.

Following the pH changes observed over time within the whole biofilm, pH variation was also detected within single microcolonies, showing a more acidic environment within the core of the microcolonies (pH 3.5 - 4.5) and a more neutral pH at the outside edge of the colonies (pH 6.0 - 7.0) (Figure 4.6). Similar observations have been reported for biofilms of *P. fluorescens* and *E. coli* with pH gradients ranging from pH 5 to 7 (Hidalgo *et al.*, 2009; Fulaz *et al.*, 2019). However, these biofilms were grown under static conditions as opposed to flow-cell systems. The acidic cores could result from the production and release of acidic metabolites during growth and biofilm formation. These acidic metabolites are likely to accumulate within the EPS of the biofilm due to reduced diffusion rates. Furthermore, oxygen will likely be depleted within the core and no fresh oxygen would reach the inner part of the microcolonies resulting in fermentation processes of the cells, which would then lead to the production of acidic products, reducing the pH (Allan *et al.*, 1999; Hidalgo *et al.*, 2009).

4.3.2 Alternative pH-independent dyes to replace TAMRA

During long-term experiments, a slight decrease in fluorescence intensity was observed for the pH-insensitive fluorophore TAMRA (Figure 4.7). Rhodamine dyes are among the most photostable fluorescence reagents that are currently available (Thermo Fisher Scientific, 2010a). Furthermore, most of these rhodamine dyes are insensitive to pH changes between pH 4 and 10 as opposed to fluoresceins that are used for many biological applications. Tetramethylrhodamine (TMR) dyes such as the carboxylic acid of TMR, carboxytetramethylrhodamine (TAMRA), are relatively hydrophobic compared to their fluorescein counterparts carboxyfluorescein (FAM) and fluorescein isothiocyanate (FITC) (Thermo Fisher Scientific, 2010a). Consequently, these dyes tend to aggregate in aqueous

solutions when the labelling density is sufficient to permit dye-dye interactions. These interactions can subsequently lead to self-quenching, reducing the fluorescence output of the conjugate, which could explain the slight decrease of TAMRA fluorescence intensity observed in some experiments. Rhodamine Red™-X was chosen as alternative to TAMRA, where the X refers to the fluorophore's extra julolidine ring, which prevents rotation about the nitrogen atoms, resulting in a shifting in the fluorophore's spectra to longer wavelength and usually an increase in its fluorescence quantum yield (Thermo Fisher Scientific, 2010a). Therefore, conjugates of Rhodamine Red™-X are generally more fluorescent than those of Lissamine™ Rhodamine B and the succinimidyl ester is more stable in water. Nanosensors consisting of rhodamine instead of TAMRA were slightly larger (66.9 nm compared to 40 nm) and showed a slightly lower ζ-potential (12.86 mV compared to 18 mV), but the differences were considered negligible. Preliminary experiments comparing both nanosensors showed no loss in fluorescence signal for rhodamine over the whole period of the experiment independent on the pH of the buffers, confirming rhodamine as appropriate alternative to TAMRA (Figure 4.7). Other options include the Alexa Fluor® dyes, that show less dye-dye interactions and self-quenching than TAMRA and are more polar and water-soluble (Thermo Fisher Scientific, 2010a). Other nanosensors that have been used in recent research furthermore include trisodium 8-hydroxypyrene-1,3,6-trisulfonate (HPTS), rhodamine B isothiocyanate (RITC), or Cy5 as reference dyes.

4.4 Conclusion

The nanosensors were shown to provide flexibility as a screening tool to measure pH changes in high throughput fluorescence assays. Additionally, the nanosensors can be used as a more focused tool, to track changes in the pH microenvironment of established biofilms over time, and to map 3D pH microenvironments as highlighted by the flow-cell analysis.

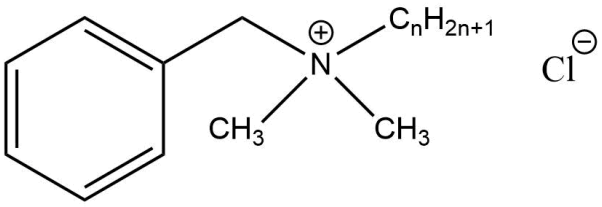
Future work will further explore the molecular mechanisms underpinning the detected acidification of the biofilms and microcolony centres. For example, different fluorophores could be used to stain eDNA or EPS components (see Chapter 3) to investigate whether either correlates with the acidic streaks observed. Furthermore, adding or changing dyes in the nanosensors could enable more powerful tools to be developed for monitoring broader environmental microniche changes within biofilms in real-time and at high resolution. In addition to pH, the nanosensors could be altered to measure oxygen, redox potential, or ion concentrations such as Ca^{2+} and Mg^{2+} at the same time.

Chapter 5 Isolation and characterisation of bacteria from washing machines with a focus on *P. aeruginosa*

5.1 Introduction

5.1.1 Background

Recent studies about biofilm formation within washing machines indicated that an increase in infection rates is associated with less effective laundry processes, such as using lower temperatures, less bleach, or using communal laundry, which enables pathogen transfer (Bloomfield *et al.*, 2011). It has been reported that bacteria isolated from WMs show a higher tolerance to chemical detergents and antimicrobials in comparison to control strains (Gattlen *et al.*, 2010; Gattlen *et al.*, 2011). One example is the elevated frequency of β-lactamase genes present in WM isolates that pose a potential risk for cross-contamination and horizontal gene transfer of genes encoding resistance against clinically important β-lactam antibiotics (Rehberg *et al.*, 2017). Additionally, the constant challenge of microorganisms by a gradient of biocide concentration at a subinhibitory level in domestic, health-care, and industrial growth environments can lead to enhanced biocide tolerance (Mc Cay *et al.*, 2010). The biocide benzalkonium chloride (BKC) was detected across diverse environments at concentrations of 1.9 µg L^{-1} in surface water, 170 µg L^{-1} in wastewater influent and up to 6.03 mg L^{-1} in hospital water (Kim *et al.*, 2018). BKC is a widely used cationic surfactant in disinfectants including cleaning products and belongs to the quaternary ammonium compounds (QACs) used as bactericide (Bajpai and Tyagi, 2007; Bridier *et al.*, 2011b). The chemical structure of BKC can be found in Figure 5.1.



n = 8, 10, 12, 14, 16, 18

Figure 5.1: Chemical structure of BKC.

Disinfectants have a broad spectrum of antimicrobial activity and act on several targets as opposed to most antibiotics (Bridier *et al.*, 2011a). BKC is a membrane-active compound and is therefore considered to be less effective against Gram-negative bacteria due to the presence of the outer membrane that can limit the uptake of antibacterial agents (Murtough *et al.*, 2001; Bridier *et al.*, 2011a). The biocidal activity of BKC against microbial, algal, fungal, and viral organisms is based on the following five modes of action collated by Kim *et al.* (2018): (i) adsorption and penetration of the BKC into the cell wall, (ii) interaction with the cytoplasmic membrane (lipid or protein) followed by membrane disorganisation, (iii) leakage of intracellular low-molecular-weight material, (iv) degradation of proteins and nucleic acids, and (v) cell wall lysis by activity of autolytic enzymes (Salton, 1968; McDonnell and Russell, 1999; Kim *et al.*, 2018). Increased concern has emerged that BKC released into the environment via laundry products can lead to antimicrobial resistance and hence increased infection risks (Russell, 1998; Price *et al.*, 2002; Russell, 2002; Langsrud *et al.*, 2003; Karatzas *et al.*, 2007; McMahon *et al.*, 2007; Mc Cay *et al.*, 2010; Kim *et al.*, 2018). Strains exhibiting an increased tolerance to BKC were also identified showing a co-resistance to other QACs, including the membrane-active disinfectants cetylpyridinium chloride and cetrimide as well as the antibiotics chloramphenicol and polymyxin B (Adair *et al.*, 1969; Loughlin *et al.*, 2002; Kim *et al.*, 2018). Further studies confirm the hypothesis of decreased susceptibilities to selected antibiotics as a result of exposure to biocides (Moken *et al.*, 1997; Akimitsu *et al.*, 1999; Price *et al.*, 2002; Karatzas *et al.*, 2007; McMahon *et al.*, 2007).

5.1.2 Aims of this chapter

The aim of this chapter was to isolate, identify, and characterise bacteria from household WMs. Phenotypic analysis and whole genome sequencing of selected strains was used to answer the following questions:

- Can bacteria be isolated from household WMs and is *P. aeruginosa* amongst them?
- How do the phenotypes of WM isolates differ from the lab strain PAO1-N?
- Are WM isolates different in their susceptibility to antimicrobials?
- Do WM isolates show altered biofilm formation compared to PAO1-N?
- Can differences in the pH microenvironments of biofilms be detected?
- Can differences be identified between the genomes of the isolated strains compared to the lab strain?

5.2 Results

In this chapter, the bacterial colonisation of 19 different domestic WMs was investigated with a focus on the model organism *P. aeruginosa* and close relatives. Isolates were phenotypically analysed using diverse microbiological assays. Special attention was paid to attachment abilities and biofilm formation of the strains as well as the tolerance to the biocide BKC. In addition, whole genome sequencing was performed on selected strains to examine genotypic differences that can help to explain the observed phenotypic differences.

5.2.1 Various bacterial species were isolated and identified from different sections of household washing machines

Throughout the whole study, 19 different household WMs were sampled to investigate the presence of bacteria and to specifically identify *P. aeruginosa* species. Three of the WMs were resampled again after six weeks, leading to a total of 22 samplings (subsequently referred to as 22 WMs, which includes the three resampled WMs). For each WM, samples were taken from three different sites that all came into contact with water: the detergent drawer, the rubber seal and the metal drum. The swabbing was performed using sterile plastic loops and samples were directly streaked onto LB agar plates for initial cultivation without selection. Bacterial growth was observed for all WMs and all three sites with the exception that not all WMs had growth for the drum and most bacteria were grown from the drawer. In total, 413 single colonies of different morphology were picked and subcultured onto *Pseudomonas* Isolation Agar (PIA) to preliminary screen for *Pseudomonas* species, covering all WMs and all sites where possible. Most bacteria could be isolated from the drawer (45.28%, 187 colonies), followed by the seal (31.72%, 131 colonies) and the drum (23.00%, 95). From all 413 colonies, 265 colonies were able to grow on PIA under aerobic conditions and at 37°C, which is 64.16% of the selected isolated colonies, still covering all three sites and all WMs, with most isolates coming from the drawer (53.21%) (Figure 5.2).

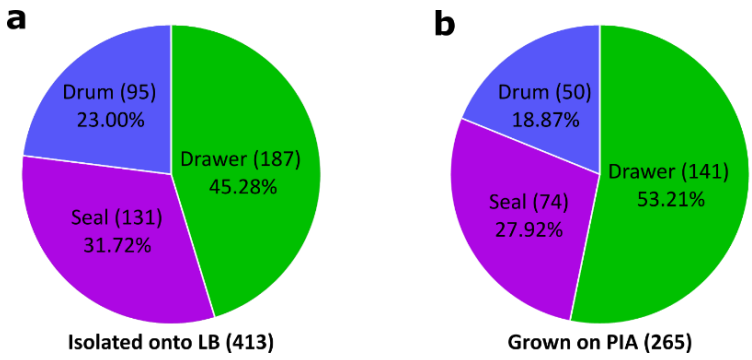


Figure 5.2: Distribution of bacterial samples isolated from different sites of 22 household washing machines. Drawer = green, Seal = purple, Drum = blue. **(a)** Initial sampling from WMs onto LB agar, where a total of 413 colonies were picked from all three sites and grown on LB agar. **(b)** 413 selected single colonies were subcultured onto PIA, resulting in 265 colonies from all three sites to grow.

To further narrow down the number of potential *P. aeruginosa* isolates, oxidase, catalase, and Gram-staining was performed on 115 selected strains (Figure 5.3). The strains were selected to cover all WMs and sites and colonies with different morphologies were included.

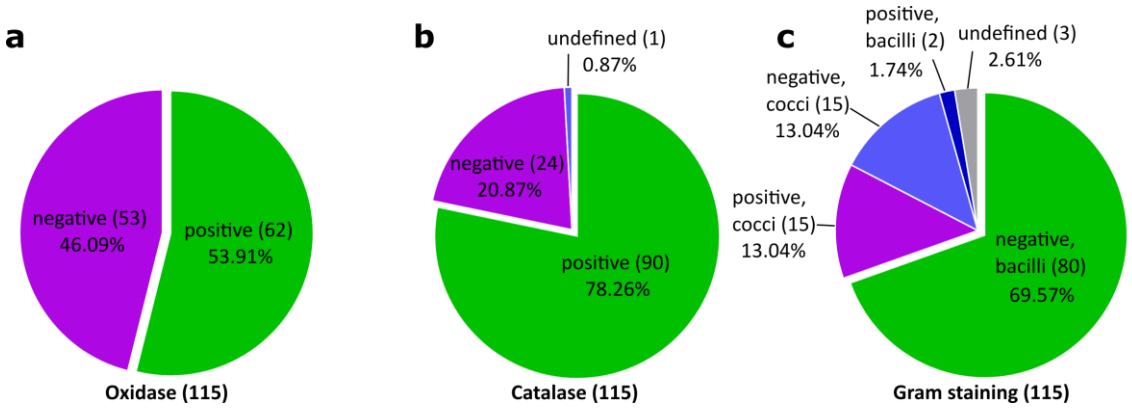


Figure 5.3: Phenotypic distribution of strains used for *P. aeruginosa* identification by three assays. **(a)** Oxidase assay showing the number of oxidase positive (green) or negative (purple) strains. **(b)** Catalase assay showing the number of catalase positive (green), negative (purple) or undefined (blue) strains. **(c)** Gram-staining, showing the number of Gram-negative bacilli (green), Gram-positive cocci (purple), Gram-negative cocci (light blue), Gram-positive bacilli (dark blue) or undefined (grey) strains.

Again, all three sites and all sampled WMs were included, where 62 strains were oxidase positive (53.91%), 90 strains were catalase positive (78.26%) and 80 strains were Gram-negative (69.57%). The Gram-staining revealed some diversity including Gram-positive cocci (15, 13.04%),

but also Gram-negative coccibacilli (15, 13.04%) and Gram-positive bacilli (2, 1.74%). Three strains could not be identified.

Overall, 43 Gram-negative bacilli strains from 15 different WMs (including all three reswabbed WMs) showed both oxidase and catalase activity, which matches the phenotype of *P. aeruginosa*. These 43 strains were taken forward for a conclusive identification (Figure 5.4).

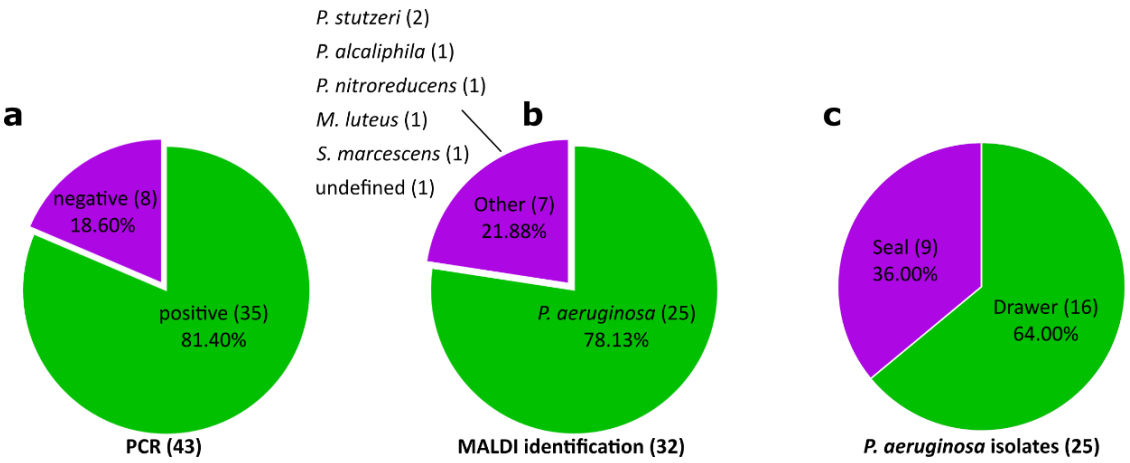


Figure 5.4: Distribution of *P. aeruginosa* strains isolated from different washing machines and sites. **(a)** Number of strains showing a positive (green) or negative (purple) result for 16S rRNA PCR using *P. aeruginosa* specific primer. **(b)** Distribution of strains identified by MALDI-TOF MS including *P. aeruginosa* (green) and 7 other strains (purple). **(c)** Final distribution of WM sites from which confirmed *P. aeruginosa* were isolated.

Genomic DNA extraction was preformed to enable strain identification by PCR. DNA amplification was conducted using 16S rRNA primers specific for *P. aeruginosa* (see Table 2.6), which was positive for 35 of the strains (81.40%). To confirm correct identification, 32 strains were sent for matrix-assisted laser desorption/ionization (MALDI) coupled with time of flight mass spectrometry (TOF MS). During the MALDI-TOF MS process, intact cells can be used to identify the strain type based on their peptide mass fingerprint (PMF), mainly represented by ribosomal proteins and a few housekeeping proteins. However, identification can only be successful if the database already contains the peptide mass fingerprint of the specific strain. Out of the 32 strains, 25 were confirmed as *P. aeruginosa* (78.13%) and 5 as other species, including *Pseudomonas stutzeri* (2), *Pseudomonas alcaliphila* (1), *Pseudomonas nitroreducens*

(1), *Micrococcus luteus* (1), and *Se. marcescens* (1). Only one strain could not be identified. The 25 confirmed *P. aeruginosa* strains were collected from 11 different WMs including all three WMs that were resampled. In one of them, *P. aeruginosa* was collected within the reswab but not within the initial sampling. In the end, 16 of the confirmed strains were isolated from the drawers (64%), 9 were picked up in the seals (36%) and none came from the drum. A summary about the steps including an overview about the number of strains, WMs and sites at each time point is presented in Figure 5.5.

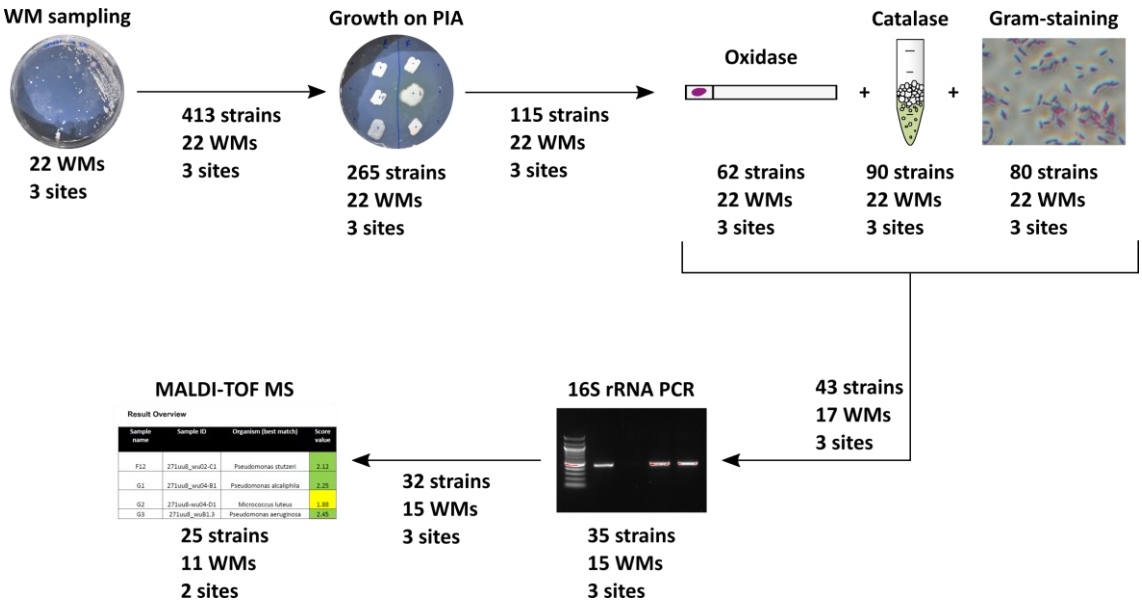


Figure 5.5: Overview about the selection process from the washing machine sampling-up until the strain identification using MALDI-TOF MS. For each step, the number of strains that showed a positive result for the specific *P. aeruginosa* phenotype is given together with the quantity of different WMs and sites that are still involved. The numbers given between the experiments highlight the number of strains (and the corresponding number of WMs and sites) that were picked for the following assay.

5.2.2 Phenotypes such as growth, attachment, and antimicrobial resistance differ between washing machine isolates and the lab strain PAO1-N

After twenty-five strains were identified as *P. aeruginosa*, isolated from eleven different WMs, nine strains were chosen for further phenotypic analysis, covering five different WMs and two sites: (i) Drawer: WMB1.3, WM01D1, WM05D1, WM05D1R, WM07C1, and WM07D1. (ii) Seal:

WM02F1, WM05F1, and WM05F1R. Two of the strains, WM05D1R and WM05F1R, were isolated from the same WM as WM05D1 and WM05F1 when it was resampled again after six weeks.

Firstly, the planktonic growth in LB medium was assessed and compared to the lab strain PAO1-N using a Tecan plate reader with 96-well plates (2.16.10). Two separate graphs were prepared as the experiments were performed under slightly different conditions, where the lid of the 96-well plate was removed for the experiment with WMB1.3 but not for the other strains, resulting in slight path differences of the readings (Figure 5.6).

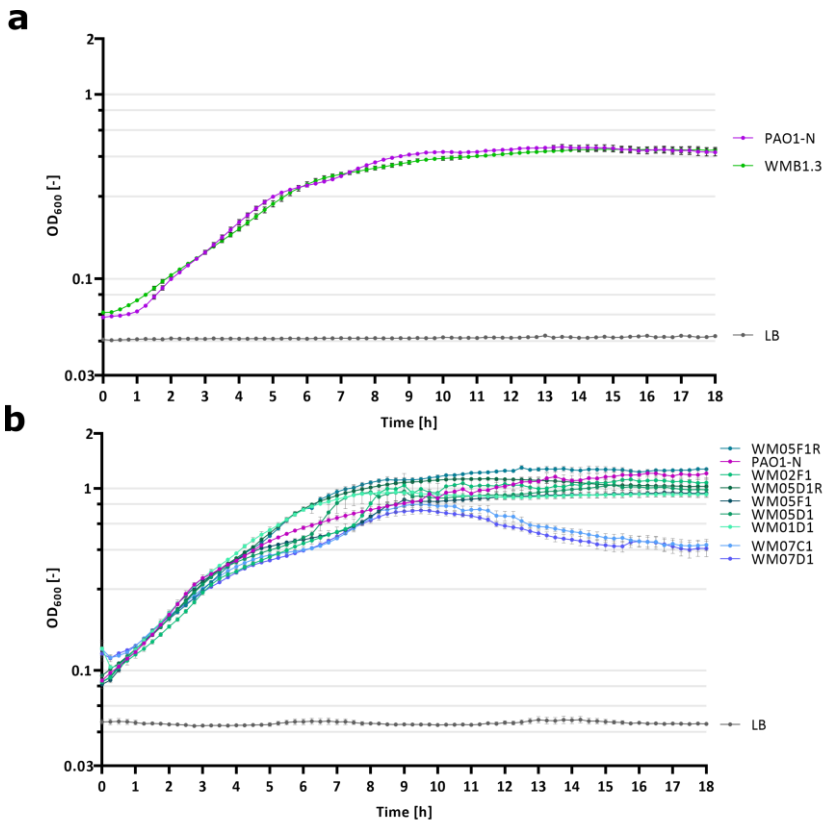


Figure 5.6: Two washing machine isolates show reduced growth compared to PAO1-N, whereas all other isolates only show minor reduction or equal growth. PAO1-N and nine WM isolates were inoculated into a 96-well plate at an OD_{600} of 0.05 in LB medium. The OD_{600} was measured automatically every 15 min at 37°C and is shown on a log scale against time. No path length correction was applied. Error bars represent standard error. **(a)** PAO1-N and WMB1.3, where n = 3x4. **(b)** PAO1-N, WM01D1, WM02F1, WM05D1, WM05D1R, WM05F1, WM05F1R, WM07C1, and WM07D1, where n = 2x4.

All strains were culturable in LB liquid medium showing no differences in growth over the first 4 h. At the end of the experiment, five strains (WM01D1, WM05D1, WM05F1, WM07C1, and

WM07D1) showed reduced growth compared to PAO1-N, although only the diminished growth of WM07C1 and WM07D1 was considered biologically significant. All four other strains (WMB1.3, WM02F1, WM05D1R, and WM05F1R) did not show altered growth.

Subsequently, the motility and protease production of all strains was assessed and compared to PAO1-N. The motility of bacteria plays an important role in colonisation and can contribute to the virulence of pathogenic bacteria. Furthermore, protease is an important virulence factor that can cause damage to host cells. Representative images for all three assays are shown for PAO1-N and the WM isolate WM01D1 in Figure 5.7.

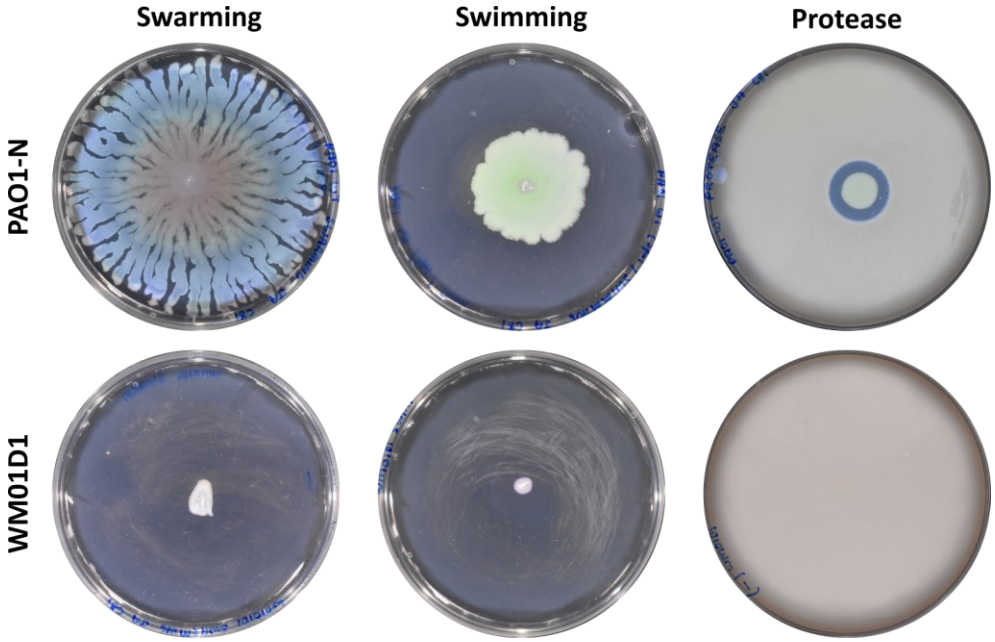


Figure 5.7: Representative images show swarming, swimming, and protease production for PAO1-N, whereas WM01D1 shows negative results for all three assays. Overnight cultures of PAO1-N and WM01D1 were normalised to an OD_{600} of 1. Swarming and swimming motility were assessed by adding 3 µL or 1 µL of cells, respectively, to the middle of a swarming agar plate (left) or swimming agar plate (middle). Motility was determined after 24 h incubation at 37°C by eye. Protease production was measured by adding 10 µL cells to skimmed milk agar plates (right), where the zone of clearance was assessed after 24 h incubation at 37°C.

PAO1-N showed both swarming motility and swimming motility indicated by extensive movement of the cells on the plates. In addition, protease production was observed resulting in a zone of clearance around the cells where the milk was degraded by the protease. All three

phenotypes are characteristic for *P. aeruginosa*. In contrast, the WM isolate WM01D1 showed negative results for all three assays. An overview of all nine WM strains is presented in Table 5.1.

Table 5.1 Overview of swarming motility, swimming motility, and protease production of PAO1-N and nine washing machine isolates. Positive results (observed motility and protease production) are indicated with a green "Yes", whereas negative results are specified with a purple "No".

Sample ID	Swarming	Swimming	Protease
PAO1-N	Yes	Yes	Yes
WMB1.3	Yes	Yes	No
WM01D1	No	No	No
WM02F1	No	No	Yes
WM05D1	Yes	Yes	Yes
WM05D1R	Yes	No	Yes
WM05F1	Yes	Yes	Yes
WM05F1R	Yes	No	Yes
WM07C1	Yes	No	Yes
WM07D1	Yes	No	Yes

Overall, all WM isolates but WM01D1 and WM02F1 showed swarming motility, whereas only three isolates were able to swim (WMB1.3, WM05D1, and WM05F1). Protease production was observed for seven strains, with only WMB1.3 and WM01D1 not producing any protease. Two strains, WM05D1 and WM05F1, were positive for all three assays and one strain, WM01D1, showed entirely negative results.

To investigate the potential of the strains to form biofilms, a crystal violet (CV) attachment assay was performed (2.16.7). The amount of attachment can indicate how easy bacteria can form biofilms on surfaces (Figure 5.8).

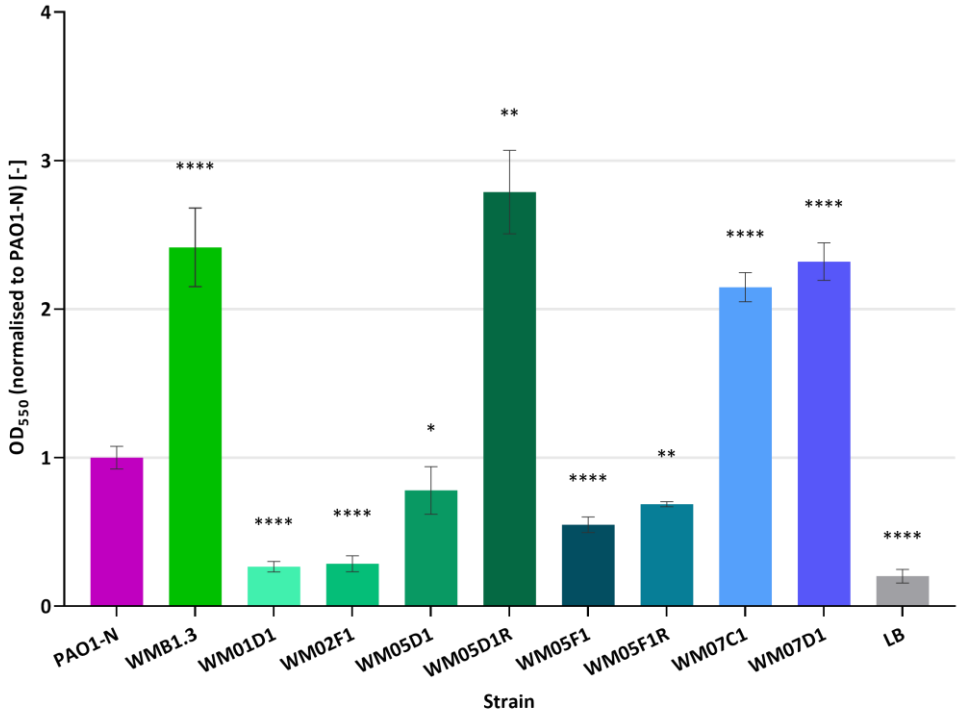


Figure 5.8: Selected washing machine isolates show enhanced attachment abilities in 96-well plates. PAO1-N and nine WM isolates were inoculated into a 96-well plate at an OD_{600} of 0.05 in LB medium and incubated for 24 h at 37°C in a static incubator. Planktonic cells were removed and attached cells were stained using crystal violet. Acetic acid was used to release the bound crystal violet before the OD_{550} was measured and normalised to the reference strain PAO1-N. Error bars represent standard error, where n = 3x3 for WMB1.3, n = 4 for WM05D1R and WM05F1R, n = 3x4 for all other strains, with $p<0.05$ = *, $p<0.01$ = **, $p<0.0001$ = ****, ns = not significant (non-parametric Mann-Whitney test).

The CV staining revealed four strains with statistically significant elevated attachment abilities ($p<0.0001$ and $p<0.001$) compared to PAO1-N, including WMB1.3, WM05D1R, WM07C1, and WM07D1. The attachment of the other five strains (WM91D1, WM02F1, WM05D1, WM05F1, WM05F1R with $p<0.05$, $p<0.01$ and $p<0.0001$), with WM01D1 and WM02F1 showing attachment at the same level as the negative control without cells (LB).

Furthermore, the susceptibility of the strains to the biocide BKC was analysed (2.16.9). BKC is commonly used in cleaning products and was therefore chosen for this study (Figure 5.9).

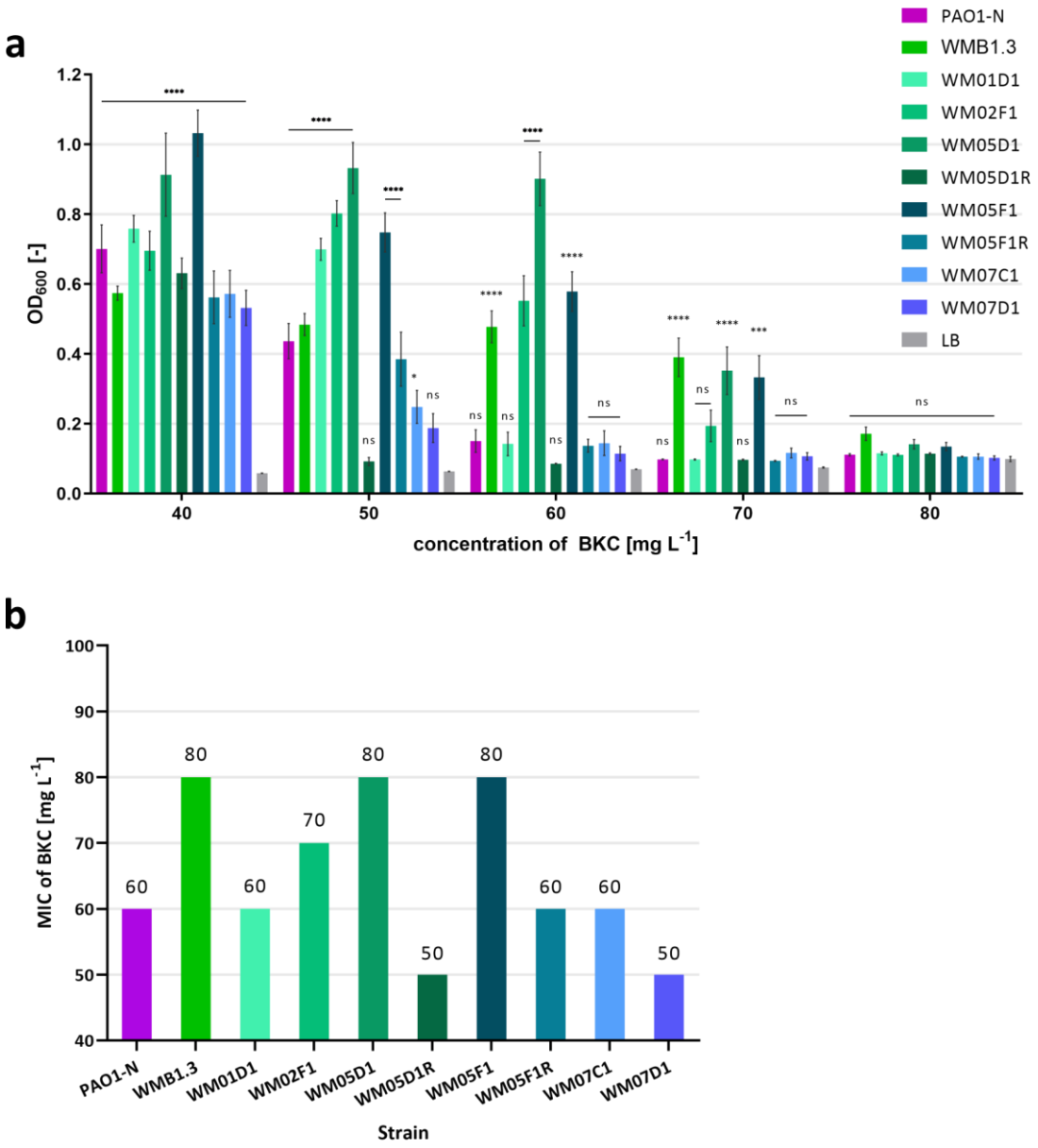


Figure 5.9: Selected strains isolated from washing machines show reduced susceptibility against BKC. PAO1-N and nine WM isolates were inoculated into a 96-well plate at an OD_{600} of 0.05 in MH medium containing BKC ranging from 40 mg L^{-1} to 80 mg L^{-1} in 10 mg L^{-1} steps. The plate was incubated for 24 h at 37°C in a static incubator before the OD_{600} was measured. **(a)** The OD_{600} is shown against the concentration of BKC. Error bars represent standard error, where n = 3x3, with $p<0.05$ = *, $p<0.001$ = ***, $p<0.0001$ = ****, ns = not significant (two-way ANOVA test). Statistical significance was calculated between the strains and the LB control representing no bacterial growth. **(b)** Minimal inhibitory concentration against BKC for each of the strains.

The minimal inhibitory concentration against BKC of the lab strain PAO1-N was 60 mg mL^{-1}, which was also the case for the WM isolates WM01D1, WM05F1R, and WM07C1. The two

isolates WM05F1R and WM07D1 were less tolerant to BKC with an MIC of 50 mg mL^{-1}. In contrast, the remaining four isolates were less susceptible to BKC, with an MIC of 70 mg mL^{-1} for WM02F1 and 80 mg mL^{-1} for WMB1.3, WM05D1, and WM05F1. An overview of all examined strains and their individual phenotypes is presented in Table 5.2.

Table 5.2 PAO1-N and nine washing machine isolates show phenotypic variation. Information on sample ID, isolation site within the WM, growth, swarming and swimming motility, protease production, crystal violet (CV) attachment, and minimal inhibitory concentration (MIC) against BKC is presented. A green "Yes" indicates positive results, whereas a purple "No" specifies negative results. The green "+" means enhanced phenotype, purple "-" reduced phenotype and yellow "=" same phenotype compared to PAO1-N.

Sample ID	Location	Planktonic growth	Swarming	Swimming	Protease	CV attachment	MIC BKC
PAO1-N	/	/	Yes	Yes	Yes	/	/
WMB1.3	Drawer	=	Yes	Yes	No	+	+
WM01D1	Drawer	=	No	No	No	-	=
WM02F1	Seal	=	No	No	Yes	-	+
WM05D1	Drawer	=	Yes	Yes	Yes	-	+
WM05D1R	Drawer	=	Yes	No	Yes	+	-
WM05F1	Seal	=	Yes	Yes	Yes	-	+
WM05F1R	Seal	=	Yes	No	Yes	-	=
WM07C1	Drawer	-	Yes	No	Yes	+	=
WM07D1	Drawer	-	Yes	No	Yes	+	-

5.2.3 Washing machine isolate WMB1.3 shows elevated pyocyanin production and biofilm formation

The WM isolate WMB1.3 showed enhanced attachment abilities as well as increased resistance against the biocide BKC compared to the lab strain PAO1-N and was therefore selected for

further analysis. As enhanced pigment production was observed for WMB1.3 in previous experiments resulting in a dark blue colour of the culture medium, the pyocyanin production was investigated (2.16.8, Figure 5.10). Pyocyanin is a blue/green phenazine toxic metabolite produced in large quantities by *P. aeruginosa* (Lau *et al.*, 2004a; Blankenfeldt and Parsons, 2014).

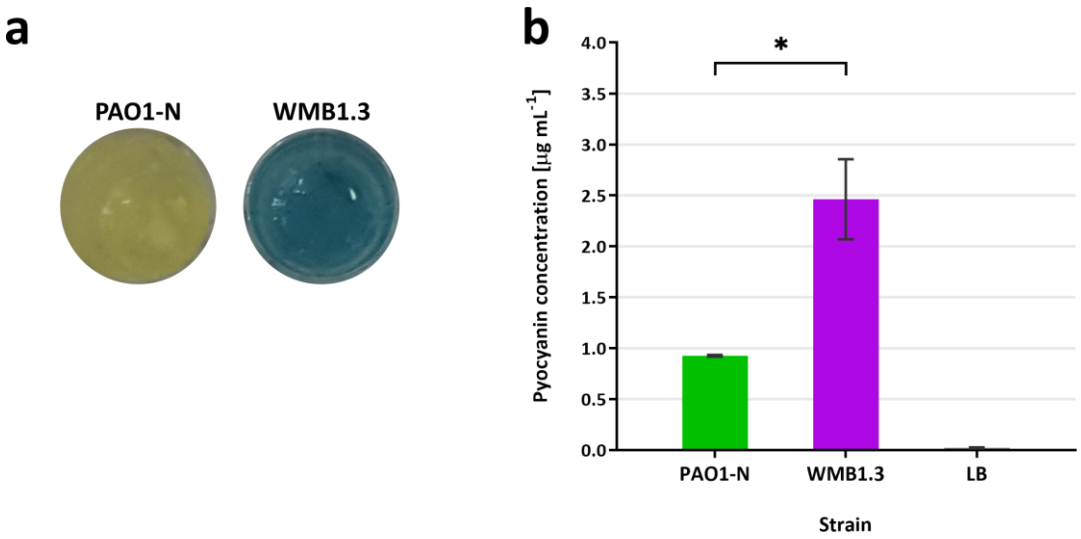


Figure 5.10: The washing machine isolate WMB1.3 shows increased production of the toxic substance pyocyanin. (a) Representative images of PAO1-N (left) and WMB1.3 (right) liquid cultures in MH medium after 24 h growth at 37°C in a 96-well plate. **(b)** PAO1-N and WMB1.3 were inoculated into a 100 mL round bottom flask at an OD_{600} of 0.05 in LB medium. The flasks were incubated for 24 h at 37°C in a static incubator before pyocyanin was extracted and quantified. The pyocyanin concentration is shown against the strains. Error bars represent standard error, where n = 2x2, with $p<0.05$ = * (non-parametric Mann-Whitney test).

Enhanced pyocyanin production was confirmed for the WM isolate WMB1.3 with 2.5 µg mL^{-1} of pyocyanin compared to PAO1-N that only produced 1 µg mL^{-1}.

After having observed increased attachment of WMB1.3 (see Figure 5.8), the biofilm formation of the isolate was analysed. In a first experiment, the thickness and structure of a statically grown biofilm was compared to PAO1-N (2.18.1, Figure 5.11).

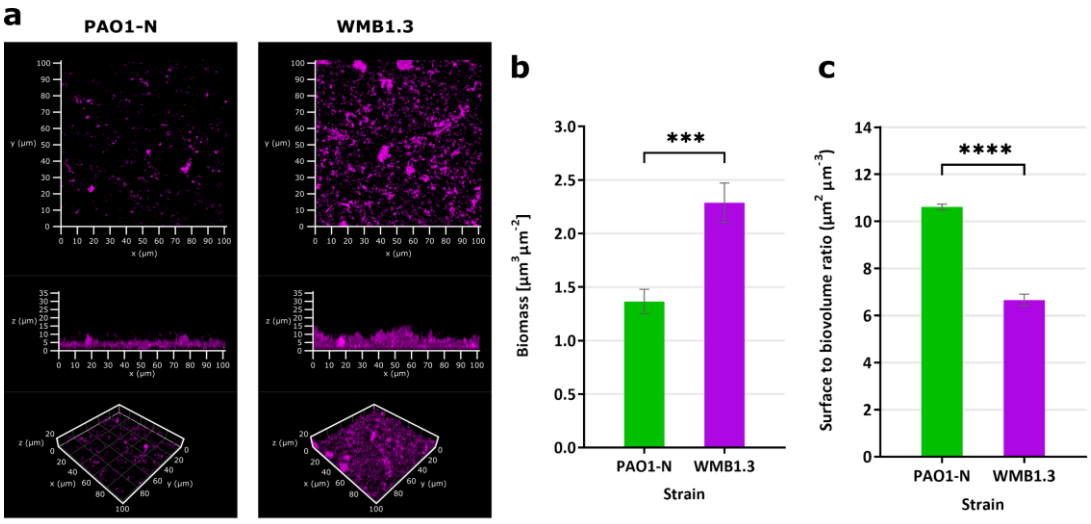


Figure 5.11: The washing machine isolate WMB1.3 grows thicker biofilms under static conditions than the lab strain PAO1-N. PAO1-N and WMB1.3 were inoculated into an 8-well glass bottom chamber at an OD_{600} of 0.05 in M9S. The cells were incubated at 37°C under static conditions for 48 h and stained with CellMask™. Z-stack images were taken with a Zeiss CLSM using a 63x objective. **(a)** Representative images of PAO1-N (left) and WMB1.3 (right). The top row shows a 3D view from the top of the biofilm, the middle row shows a 3D view from the front of the biofilm and the bottom row an angled 3D view from the top. Quantitative Comstat analysis of the biofilm images was performed using ImageJ. Graphs represent **(b)** biomass and **(c)** surface to biovolume ratio. Error bars represent standard error measured for different biofilm images, where n = 20, with $p<0.001$ = *** and $p<0.0001$ = **** (non-parametric Mann-Whitney test).

Biofilms of WMB1.3 were approximately 1.6 times thicker than biofilms of PAO1-N, with a biomass of 1.4 $\mu m^3\ \mu m^{-2}$ compared to 2.3 $\mu m^3\ \mu m^{-2}$. The structure was also different with biofilms of WMB1.3 showing a dense structure resulting in a smaller surface to biovolume ratio (6.5 $\mu m^2\ \mu m^{-3}$ compared to 10.5 $\mu m^2\ \mu m^{-3}$).

Furthermore, the influence of the positive polyacrylamide nanosensors on the biofilm formation of WMB1.3 was investigated as the positive charge was shown to alter biofilm formation of PAO1-N (Chapter 3). At the same time, the pH distribution within static biofilms was analysed with the help of the nanosensors (Figure 5.12).

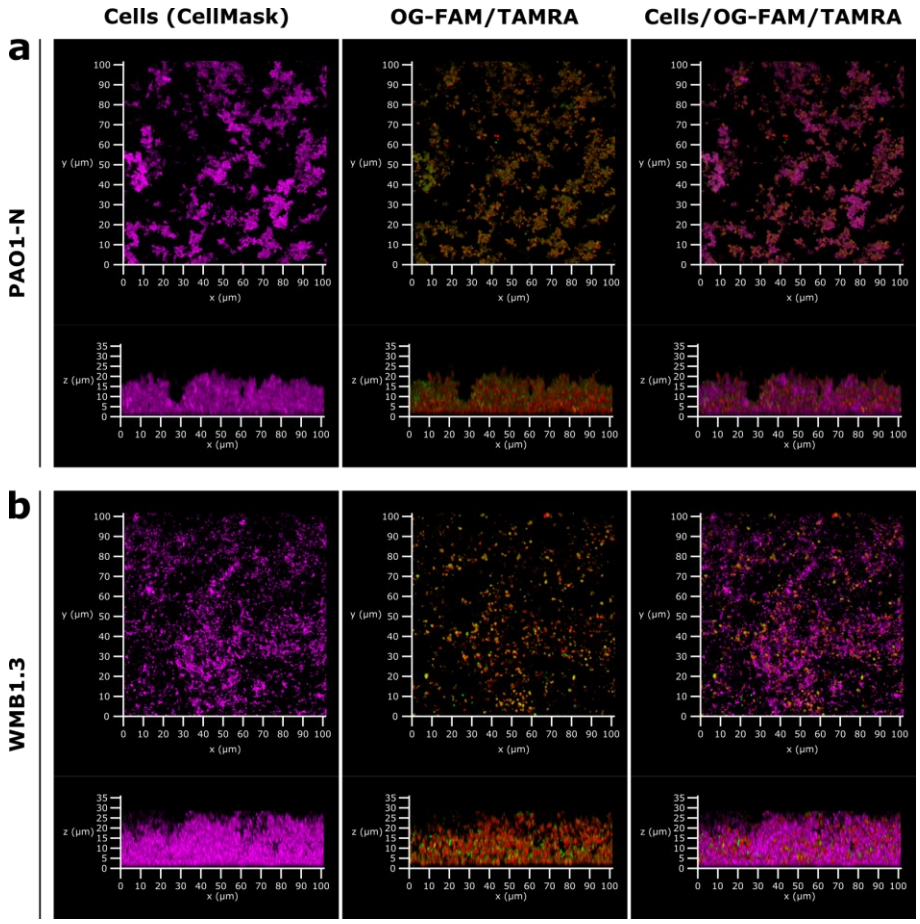


Figure 5.12: The presence of positive nanosensors does not influence the density of biofilms grown by WMB1.3. PAO1-N and WMB1.3 were inoculated into an 8-well glass bottom chamber at an OD_{600} of 0.05 in M9S containing 1 mg mL^{-1} positive nanosensors. The cells were incubated at 37°C under static conditions for 48 h and stained with CellMask™. Z-stack images were taken with a Zeiss CLSM using a 63x objective. Representative images of **(a)** PAO1 and **(b)** WMB1.3 show cells (magenta) and OG-FAM/TAMRA overlay fluorescence of nanosensors (green and red). The top row shows a 3D view from the top of the biofilm and the bottom row shows a 3D view from the front of the biofilm.

Unlike with the lab strain PAO1-N, the presence of the positive nanosensors does not seem to alter the biofilm structure of WMB1.3. Biofilms of WMB1.3 grew slightly thicker, which has already been shown for biofilms grown without nanosensors. No pH difference between strains was detected when grown under static conditions. The investigation of pH variation within biofilms of WMB1.3 grown under flow conditions can be found in Figure 5.13 (2.18.2).

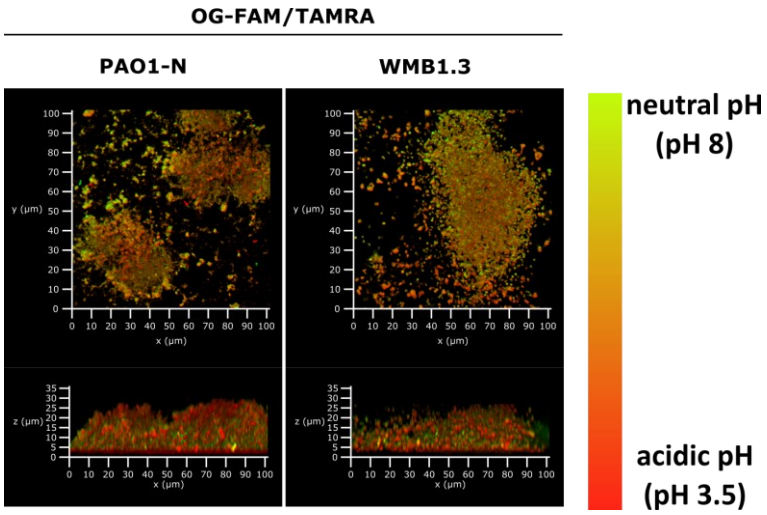


Figure 5.13: pH maps of biofilms grown under flow conditions show similarities between the two different *P. aeruginosa* strains, PAO1-N and WMB1.3. PAO1-N (left) and WMB1.3 (right) were inoculated into a 48-well BioFlux flow-cell plate at an OD_{600} of 0.05 in M9S containing 5 mg mL^{-1} positive nanosensors. The cells were incubated at 37°C under flow conditions (0.2 dyn cm^{-2}). Z-stack images were taken with a Zeiss CLSM using a 63x objective. Representative images show OG-FAM/TAMRA overlay fluorescence of nanosensors (green and red). The top row shows a 3D view from the top of the biofilm and the bottom row shows a 3D view from the front of the biofilm.

In Chapter 4, pH variation within single microcolonies of PAO1-N biofilms grown within the BioFlux flow-cell system was reported. This variation was also observed for WMB1.3, with a slightly more acidic core of the microcolonies represented by a darker orange colour as opposed to a more yellow colour at the edges of the microcolonies. No differences were detected between the two strains.

5.2.4 Whole genome sequencing reveals genotypic differences between strains

The genomes of nine WM isolates that were used for the phenotypic analysis were sequenced alongside the reference strain PAO1-N, which was used throughout this study. Genome analysis including assembly and annotation was performed using the online platform PATRIC, with good quality of all genomes based on the annotation statistics and comparison to other genomes within the same species in PATRIC. All strains were confirmed to belong to the species group *Pseudomonas aeruginosa*. Information on the genome length, GC content, number of contigs,

coding sequences (CDS), and single nucleotide polymorphisms (SNPs) can be found in Table 5.3. Each SNP represents a difference in a single nucleotide of the DNA compared to the reference PAO1-N, for example a cytosine instead of a thymine at a specific position.

Table 5.3: Genome analysis information for all ten sequenced genomes. Strain ID, genome length, GC content of genome, number of contigs, number of coding sequences (CDS), and number of single nucleotide polymorphisms (SNPs) are presented.

Strain	Genome Length [bp]	GC Content [%]	# Contigs	# CDS	# SNPs
PAO1-N	6,183,409	66.56	75	5869	-
WMB1.3	7,360,329	65.43	219	7357	28293
WM01D1	6,556758	66.3	146	6273	52369
WM02F1	7,209,158	65.6	104	7091	22794
WM05D1	7,186,925	65.69	236	7199	51277
WM05D1R	7,400,566	65.46	182	7380	51737
WM05F1	7,537,775	65.22	178	7648	51434
WM05F1R	6,810,583	66.02	120	6587	59181
WM07C1	7,440,876	65.49	153	7448	26546
WM07D1	7,437,979	65.49	154	7446	26561

The total genome length for all strains was between 6,183,409 bp (PAO1-N) and 7,537,775 bp (WM05F1), showing that the lab strains PAO1-N has the smallest genome compared to the WM isolates. The GC content was very similar between all ten strains, ranging between 65.22% and 66.56%. The number of CDS lies between 5869 (PAO1-N) and 7380 (WM05F1), showing a correlation between the genome length and the number of CDS. The quantity of SNPs between the reference PAO1-N and the individual WM isolates ranges between 22794 (WM02F1) and 59181 (WM05F1R), giving a first indication about the similarity between the isolates and the lab strain. Additionally, a phylogenetic tree was constructed using PATRIC to illustrate the family relationship (Figure 5.14). Besides the ten sequenced genomes, the two cystic fibrosis Liverpool

epidemic strains LESB65 and LESB58 (Jeukens *et al.*, 2014), as well as the highly virulent clinical strain PA14 (Lee *et al.*, 2006) and the published reference strain for PAO1 (Stover *et al.*, 2000) were included. LESB58 is a hypervirulent human CF lung isolate and known to be a biofilm hyperproducer (Winstanley *et al.*, 2009).

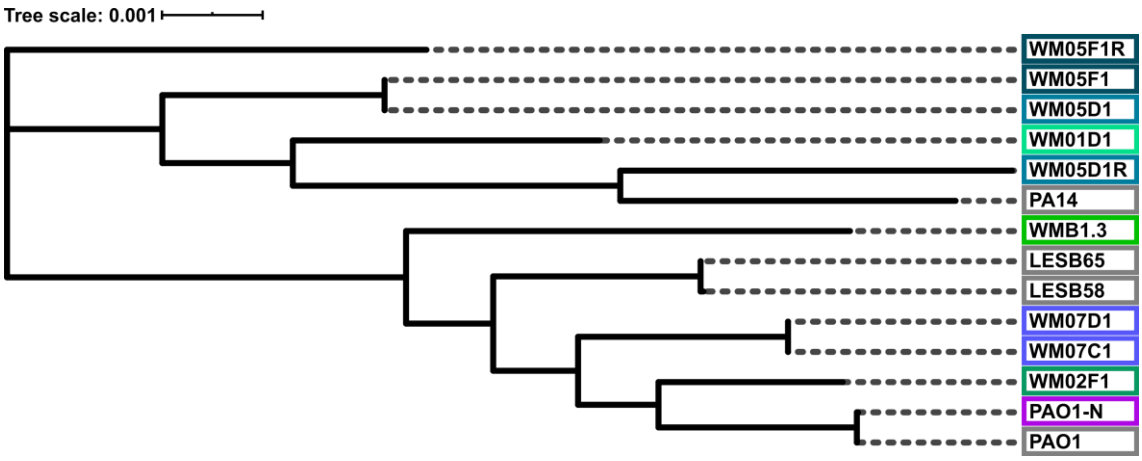


Figure 5.14: Phylogenetic tree showing the relationship between nine washing machine isolates, the lab strain PAO1-N, the reference genome PAO1, PA14, LESB65, and LESB58. Green/blue colours indicate the WM, of which the strain was isolated, purple highlights the lab strain PAO1-N and grey the three strains taken from the reference database.

As expected, the reference sequence for PAO1 and the lab strain PAO1-N are clustered, with WM02F1 being the closest relative. Both LESB strains are clustered, as well as WM07C1 with WM07D1 and WM05F1 with WM05D1. Overall, the strains isolated from WM05 and WM01 are more related to the clinical strain PA14, whereas isolates from WM07, WM02 and WMB1.3 are closer related to PAO1. PA7, another reference strain that forms a separate clade to PA14 and PAO1, was originally included but showed no close relationship to any of the WM isolates and was therefore excluded from the figure.

Furthermore, PATRIC was used to analyse and compare the proteome of all strains as well as to identify SNPs between WM isolates and the reference strains PAO1-N and PAO1. If SNPs occur within the coding sequence of genes, it can cause amino acid changes during the translation, which in turn can lead to the loss of functionality, for example if a stop codon is introduced or essential amino acids within the catalytic regions are exchanged. Even if SNPs are found between

genes within the untranslated region, it can lead to the disruption of promotor binding sites and other positions essential for the functionality and regulation of transcription. Therefore, SNPs as well as differences in the overall proteomes could explain phenotypic differences between the isolates and give indications on virulence potential or biofilm formation. An overview of the proteome comparison can be found in Figure 5.15.

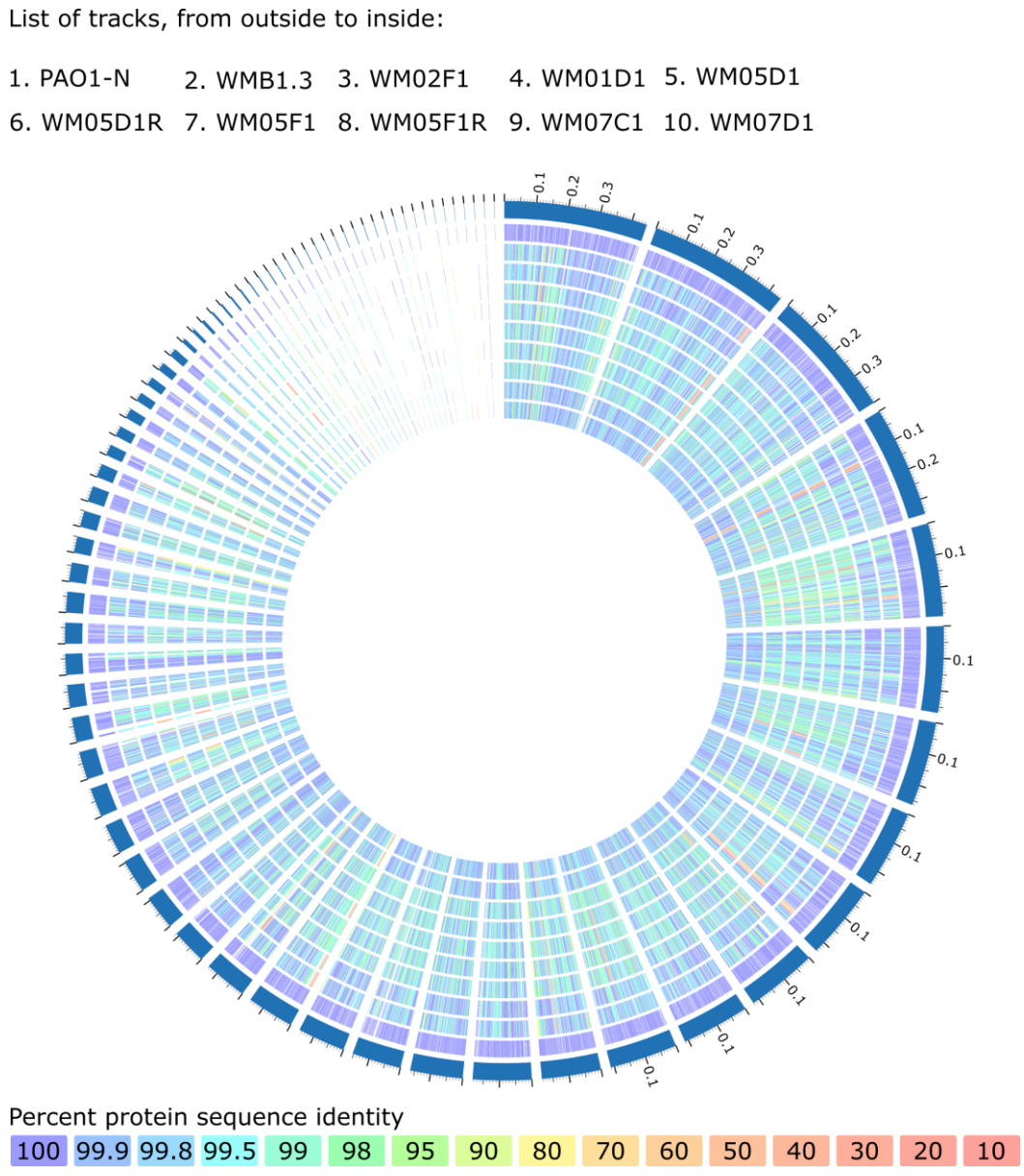


Figure 5.15: Proteome comparison of PAO1-N, WMB1.3, WM02F1, WM01D1, WM05D1, WM05D1R, WM05F1, WM05F1R, WM07C1 and WM07D1. Regions in dark blue indicate high similarity, regions in red show high discrepancies up to complete absence of the protein families. The numbers show the location of the proteins on their contigs, based on the size, starting with the largest contig.

Based on the proteome comparison, regions with very low protein sequence identity were observed between WM isolates and PAO1-N. Overall, 17 protein families were found in PAO1-N that are missing in all 9 WM isolates, whereas 46 protein families are present in all WM isolates but not in PAO1-N. In both cases, most of these proteins are hypothetical proteins with unknown function to date. Additionally, from the total of 370,192 SNPs found in all 9 WM isolates, 246,552 SNPs were present in more than one isolate, leading to 123,640 singular SNPs. SNPs with a low fraction (<0.95, indicating the fraction of the variant read depth among all the reads that cover this region) and low variant coverage (<30, indicating the average read depth of the variant) were removed, resulting in 97,730 SNPs. Predictions showed that most of these SNPs only have low or moderate effects; and only SNPs with a predicted high effect were further analysed in this study. A quantitative overview about the proteome analysis and SNPs can be found in Figure 5.16

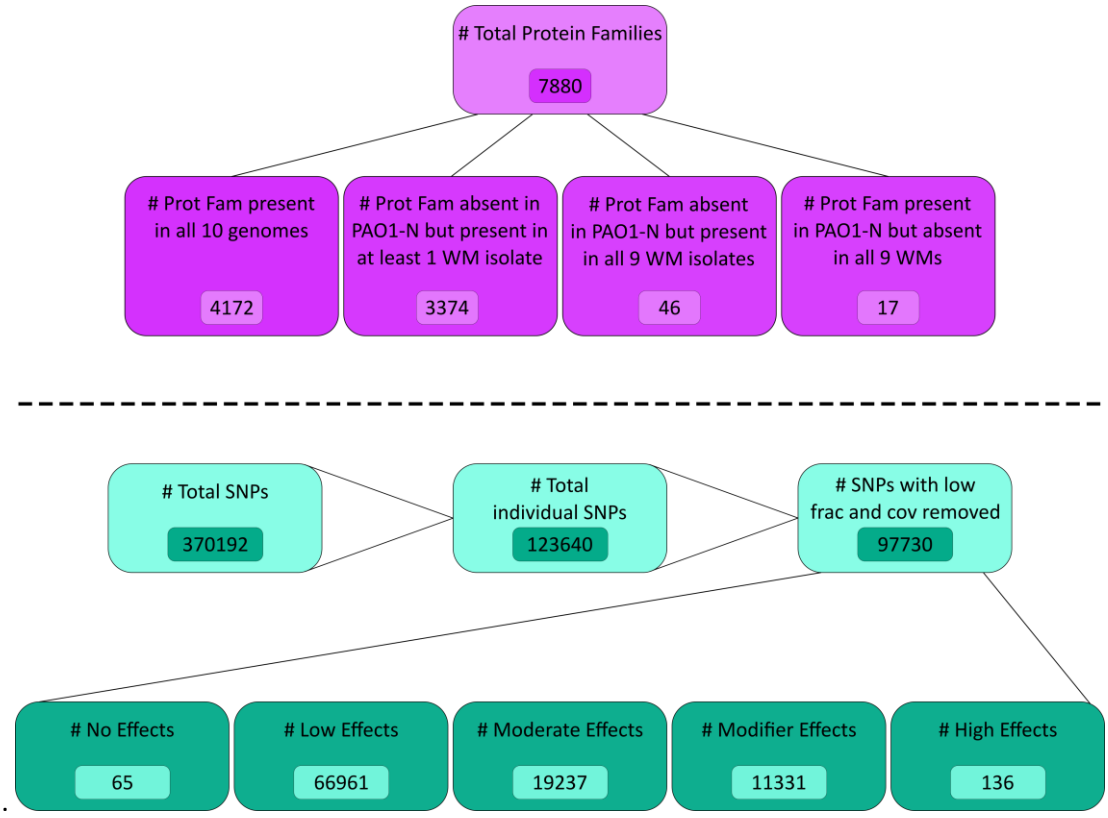


Figure 5.16: Overview about protein families and SNPs found in the sequences of PAO1-N and nine washing machine isolates. Top: Number of protein families. Bottom: Number of SNPs.

For a more targeted approach towards the goal of this study - associate the genomics with phenotypes such as virulence, motility, and biofilm formation - mutations were extracted within genes annotated as virulence factors or involved in motility, antibiotic resistance, and biofilm formation. With the availability of the PAO1 genome sequence on the World Wide Web, sequences of the PAO1 proteins found in the *Pseudomonas* genome database (www.pseudomonas.com) were compared with sequences from WM isolates and PAO1-N.

Pilin and flagellin are the two major adhesins identified in *P. aeruginosa* and are associated with surface attachment, motility, biofilm formation, and virulence (Leid *et al.*, 2009; Burrows, 2012; Okuda *et al.*, 2013; Persat *et al.*, 2015). Mutations in the gene clusters of *pil* genes, required for the assembly of type IV pili, as well as *morA*, *fli* and *flg* gene clusters involved in flagella assembly, were identified, and the protein sequence identity was quantified using the PATRIC BLAST service (Figure 5.17). Some of the mutations are SNPs, resulting in only slight sequence changes, whereas other genes/proteins are not present at all (highlighted in dark red).

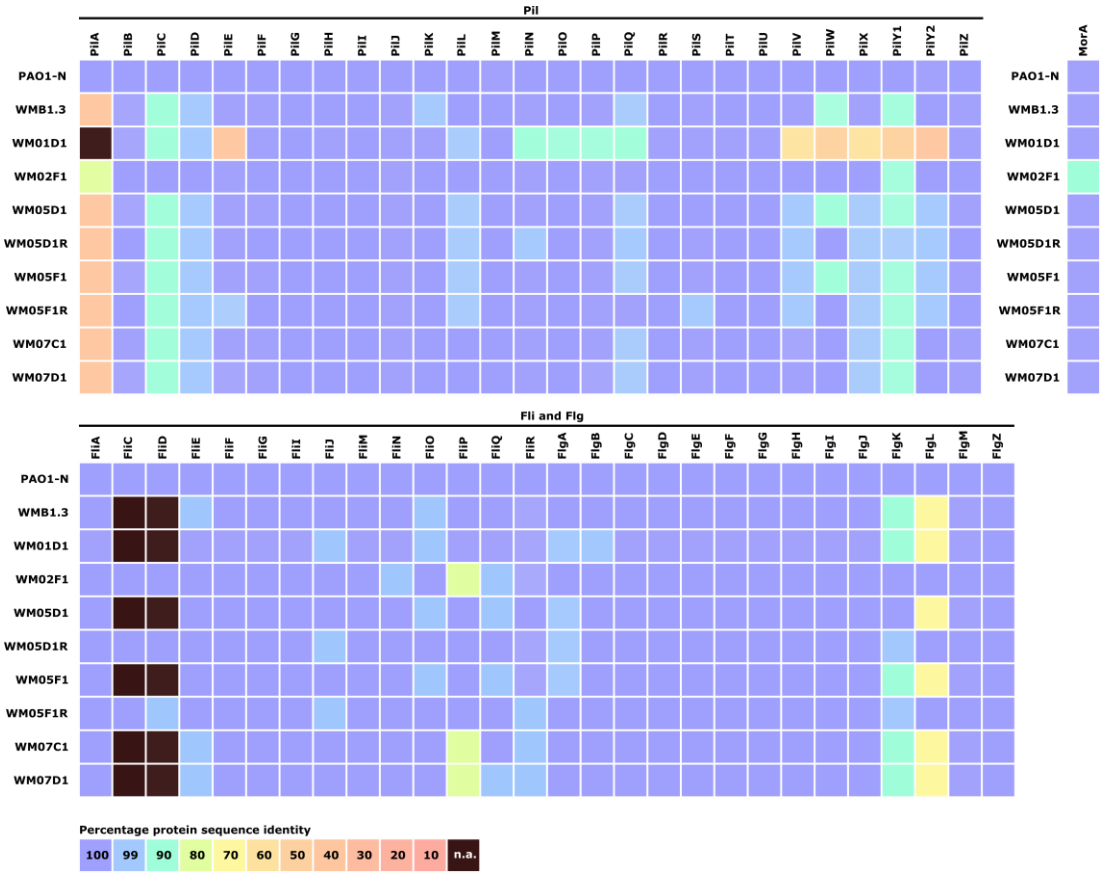


Figure 5.17: Protein heat maps of Pil, MorA and Fli/Flg show sequence differences between strains. The percentage of protein sequence identity is highlighted by colour, ranging from blue (100% identity) to dark red (not available).

All nine WM strains are lacking large parts of the *pilA* gene. WM01D1 furthermore shows low sequence identity within multiple other genes of the *pil* cluster, including *pilCENOPQVWXY1Y2*. In contrast, WM02F1 only demonstrates low sequence diversity for most of the genes. WM02F1 lacks the end of the MorA protein (amino acids 1327-1418) that is a membrane-localised regulator controlling the timing of flagella development and affects motility, chemotaxis, and biofilm formation (Choy *et al.*, 2004). Looking at the proteins of Fli and Flg, it is striking that WMB1.3, WM01D1, WM05D1, WM05F1, WM07C1, and WM07D1 are all lacking FliC and FliD as well as a large proportion of FlgK and FlgL. Additionally, WM02F1, WM07C1, and WM07D1 only show 80% percentage protein sequence identity for FliP. By generating multiple sequence alignments (MSA) of proteins with moderate/low identity or genes with SNPs, it was possible to

investigate whether the changes are likely to have an effect on the function of the protein or not. A representative MSA is presented in Figure 5.18for the protein sequence of FliP.

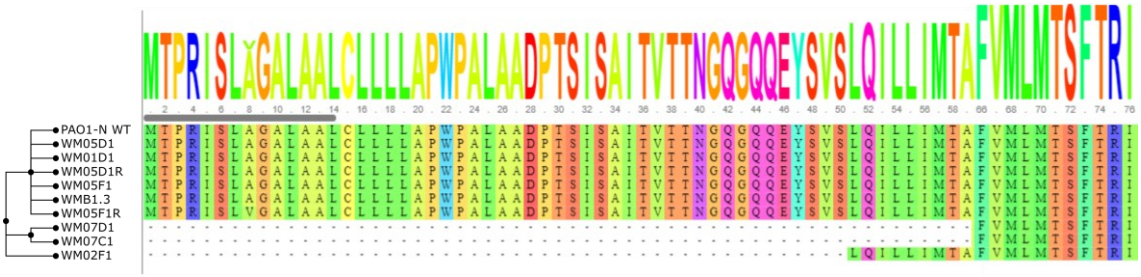


Figure 5.18: Multiple sequence alignment of FliP shows missing start of the protein in WM02F1, WM07C1 and WM07D1. The alignment represents the first 76 amino acids and was generated using the PATRIC BLAST service.

Within all three strains, WM02F1, WM07C1, and WM07D1, the start of the protein FliP is missing, whereas the rest of the protein sequence is complete and identical with the reference strain PAO1-N.

Furthermore, three genes associated with biofilm formation were identified showing changes between strains (see Figure 5.19). BfmR and BmfS (biofilm maturation factor R and S) are two proteins belonging to a two-component system that becomes phosphorylated during biofilm formation and is required for the development and maintenance of biofilm architecture (Petrova and Sauer, 2009). BfmSR is also associated with virulence of *P. aeruginosa* during chronic infection in CF lungs (Cao *et al.*, 2014). The *arr* gene (aminoglycoside response regulator) encodes a phosphodiesterase that is essential for the induction of biofilm formation following exposure to subinhibitory concentrations of aminoglycoside antibiotics and leads to subsequent biofilm specific aminoglycoside resistance (Hoffman *et al.*, 2005).

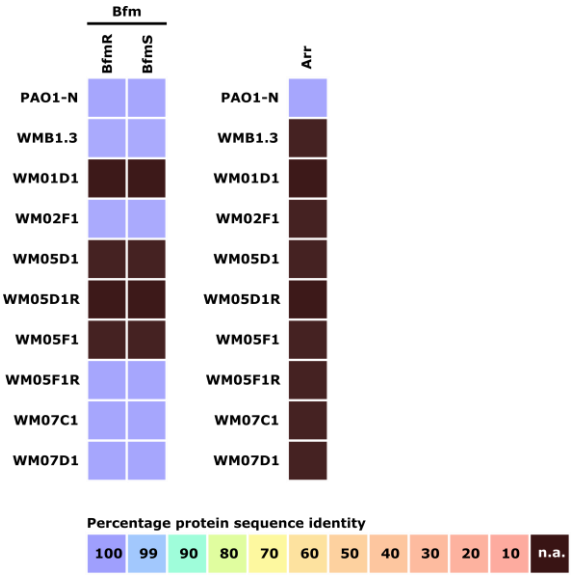


Figure 5.19: Protein heat maps of Bfm and Arr show sequence differences between strains. The percentage of protein sequence identity is highlighted by colour, ranging from blue (100% identity) to dark red (not available).

Both genes encoding for BfmSR are missing in WM01D1, WM05D1, WM05D1R and WM05F1. Furthermore, none of the WM isolates possesses the *arr* gene.

More sequence differences were identified in the phenazine cluster as shown in Figure 5.20. The two phenazine operons *phzA1B1C1D1E1F1G1* and *phzA2B2C2D2E2F2G2* are homologous and each one is sufficient for the production of phenazine-1-carboxylic acid (PCA), the precursor of the toxic substance pyocyanin (Mavrodi *et al.*, 2001). The conversion of PCA to pyocyanin is mediated by PhzM and PhzS, a putative phenazine-specific methyltransferase and a flavin-containing monooxygenase, respectively.

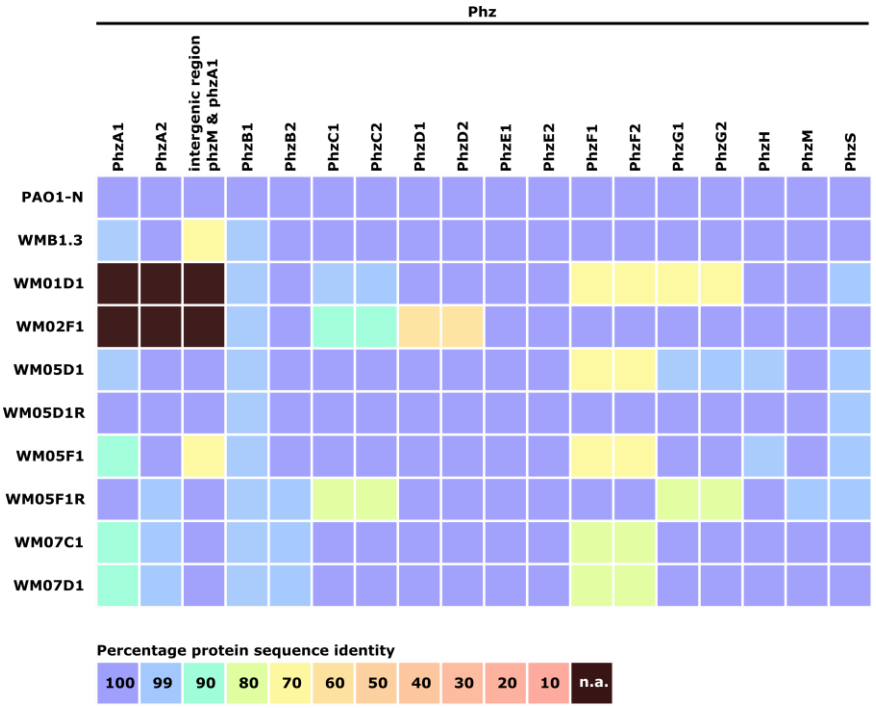


Figure 5.20: Protein heat map of Phz cluster shows sequence differences between strains. The percentage of protein sequence identity is highlighted by colour, ranging from blue (100% identity) to dark red (not available).

WM01D1 and WM02F1 are lacking both PhzA proteins as well as the intergenic region between *phzM* and *phzA1*, containing the promoter regions and multiple binding sites including a LasR and RsaL binding site. WM05F1, WM07C1, and WM07D1 only show 90% sequence identity for PhzA1. PhzF1, PhzF2, PhzG1, and PhzG2 all show low sequence identity for multiple strains, and further differences and SNPs were found in some of the other proteins, including PhzM and PhzS.

Amongst the many virulence factors identified in *P. aeruginosa* are LPS. *P. aeruginosa* can express two forms of LPS, A-band and B-band LPS (Burrows *et al.*, 1996). Genes of the *wbp* gene cluster, which are involved in the synthesis of the B-band O antigen are known to be differently expressed in various *P. aeruginosa* serotypes (Burrows *et al.*, 1996; Rocchetta *et al.*, 1999). This was confirmed for the strains in this study, as the genome sequencing revealed that some of the WM isolates show very low sequence identity with the whole gene cluster of PAO1-N as shown in Figure 5.21.

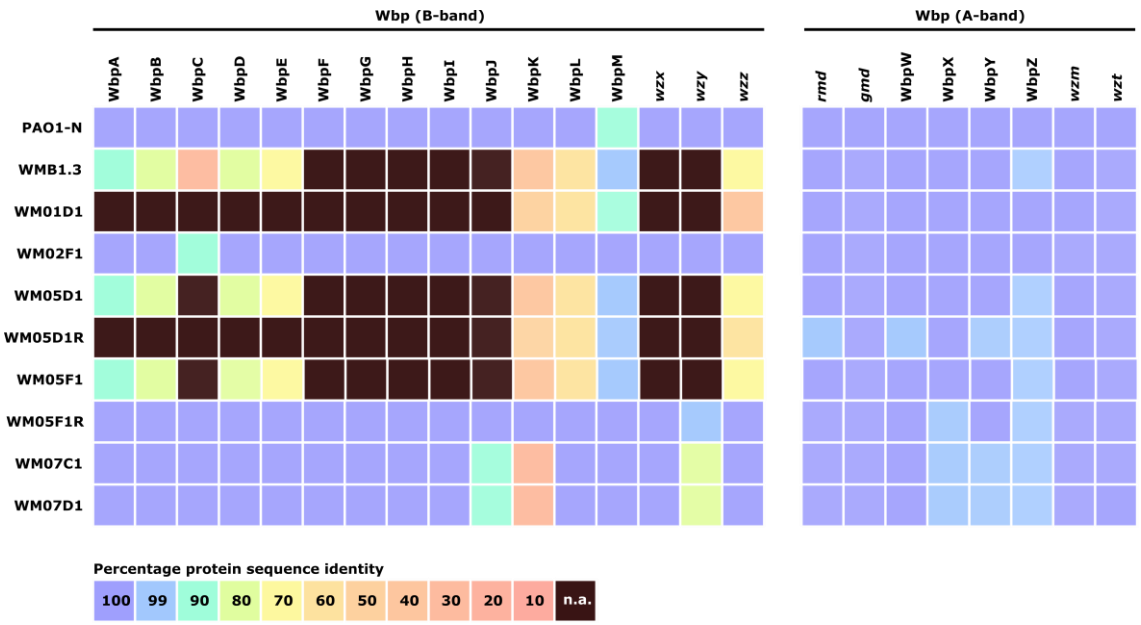


Figure 5.21: Protein heat map of Wbp cluster shows sequence differences between strains. The percentage of protein sequence identity is highlighted by colour, ranging from blue (100% identity) to dark red (not available).

WMB1.3, WM01D1, WM05D1, WM05D1R, and WM05F1 lack most of the Wbp proteins from PAO1-N involved in B-band O antigen regulation, whereas WM07C1 and WM07D1 only have mutations within three proteins. WbpM is known to be conserved throughout most *P. aeruginosa* serotypes and is the only protein that has a high sequence identity for all WM strains. Interestingly, PAO1-N also shows some sequence variation within WbpM compared to the reference strain PAO1. In contrast, within the A-band proteins, only some SNPs were observed, with all sequences showing at least 99% identity with PAO1.

Two protein clusters that are involved in antibiotic resistance (mainly β-lactam and polymyxin B resistance) were identified with changes between strains (Figure 5.22). Mex proteins regulate the T3SS in *P. aeruginosa* and are involved in multidrug resistance (Köhler *et al.*, 1997; Jin *et al.*, 2011). PmrAB is a two component system that regulates resistance to polymyxin B and cationic antimicrobials (McPhee *et al.*, 2003).

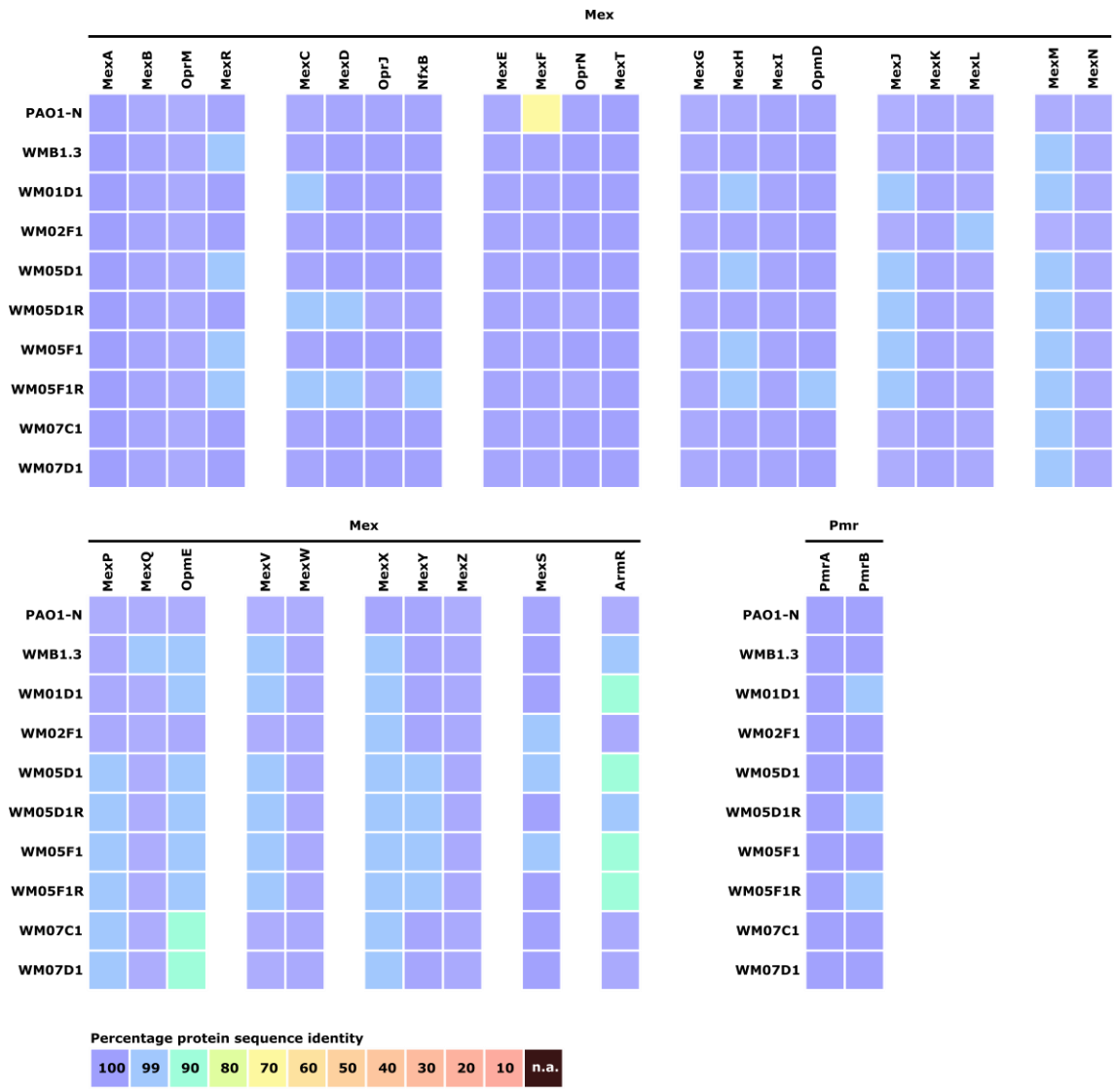


Figure 5.22: Protein heat maps of Mex and Pmr clusters show sequence differences between strains. The percentage of protein sequence identity is highlighted by colour, ranging from blue (100% identity) to dark red (not available).

Both clusters contain multiple SNPs in all the WM isolates. However, only the SNPs in MexF and ArmR were predicted to have a high impact on the protein structure/function. PAO1-N lacks the first 344 amino acids of the MexF protein. ArmR is an anti-repressor for MexR, which negatively regulates the efflux operon *mexAB-oprM* and shows increased sequence differences within strains WM01D1, WM05D1, WM05F1, and WM05F1R (Daigle *et al.*, 2007).

5.3 Discussion

The phenotypic diversity of bacteria and especially *P. aeruginosa* in household WMs was explored in this study by taking samples from 19 different WMs. The age of WMs and treatment of the WMs was not considered for this study. It was shown that household WMs are colonised by a variety of different bacteria, including *P. aeruginosa* species, and that these strains exhibit different phenotypes such as lower susceptibility against BKC or increased biofilm formation. Following phenotypic characterisation with a focus on phenotypes traditionally associated with pathogenicity, whole genome analysis was performed to compare virulence associated regions between strains. Although no mutations were observed in regions that could clearly explain the various phenotypes, some mutations provided guidance for further analysis that could help to identify key differences, for example by looking at transcriptome data. It became apparent that the use of WM isolates instead of lab strains to characterise and improve current washing products especially with respect to antimicrobial resistance is important and that it is crucial to find out more about WM strains to help eliminate biofilm formation in WMs.

5.3.1 A variety of bacteria was successfully isolated from three different sites of domestic washing machines

Previous studies have shown that domestic WMs act as a reservoir of microorganisms, including non-pathogenic and pathogenic bacteria such as *S. aureus, Acinetobacter spp.* and *P. aeruginosa* (Davis and Ainsworth, 1989; Gattlen *et al.*, 2010; Callewaert *et al.*, 2015; Nix *et al.*, 2015). In this study, 19 WMs were investigated, of which three were resampled after six weeks. All WM revealed bacterial contamination showing a variety of bacteria that were isolated from all three tested sites: the detergent drawer, the rubber seal, and the metal drum (Figure 5.2). The site showing the highest number of isolates was the detergent drawer, followed by the rubber seal and the metal drum, confirming reports that biofilms can be found abundant at places within the WM that come into contact with water, with increased biofilm formation on the plastic filter and rubber tubes (Gattlen *et al.*, 2010). In contrast to this study, Gattlen *et al.* was not able to

isolate any strains from the metal drum, but highlighted the surprisingly high occurrence of bacteria within the detergent drawer, where the extremely concentrated detergent is added (Gattlen *et al.*, 2010). However, it has been suggested that a lower water temperature at the rubber seal within the door and the detergent drawer could result in reduced thermal disinfection and therefore lead to the elevated biofilm infestation (Kim *et al.*, 2018).

From the 115 strains that were taken forward for identification of possible *Pseudomonas* species, 69.57% were Gram-negative bacilli and 13.04% Gram-negative cocci, making a total of 82.61% Gram-negative bacteria (Figure 5.3). Studies by Nix *et al.* identified 90% of their WM isolates as Gram-negative, confirming these findings (Nix *et al.*, 2015). However, it should be noted that only strains that grew on PIA were taken forward for this study, which biased the outcome of the test. Furthermore, a cultivation-based approach was chosen to assess the bacterial growth within WMs, which neglects the vast majority of micro-organisms that cannot be easily cultivated and that can thus only be detected by molecular methods (Xu *et al.*, 1982; Rappé and Giovannoni, 2003). For this study, a cultivation-based method was used as it was crucial to verify growth for future use of the WM isolates in culture-based assays. Based on basic identification tests such as oxidase, catalase, and Gram-staining, isolated strains in this study could include *Staphylococcus* spp. such as *S. aureus* or *S. epidermidis*, *Micrococcus* spp. such as *M. luteus*, or *Acinetobacter* spp. such as *A. baumannii*, most of which have been isolated from WMs in various studies (Callewaert *et al.*, 2015; Nix *et al.*, 2015; Jacksch *et al.*, 2019). *S. aureus, S. epidermidis,* and *A. baumannii* all belong to the human skin microbiota and could therefore be introduced to the WMs through dirty laundry. *M. luteus* is a ubiquitous bacterium that can often be found in dust and the soil surface, making it easy to settle on clothes. Detailed strain identification would be needed to draw any further conclusions, which was not proceeded any further as only strains showing phenotypes characteristic for *P. aeruginosa* were selected. In this respect, 43 of the strains were oxidase and catalase positive as well as Gram-negative, highlighting them as potential *P. aeruginosa* strains, with 35 strains being positive for 16S rRNA

PCR using *P. aeruginosa* specific primers (Figure 5.4). In a final identification step, MALDI-TOF MS was used to confirm the isolated species, which has been used in previous studies (Nix *et al.*, 2015; Rehberg *et al.*, 2017; Schmithausen *et al.*, 2019). The process is rapid, sensitive, cost-effective, and does not require much preparation of the bacteria as identification can be performed directly from single colonies grown on agar plates. However, identification of the organism is only possible when the database already contains information about the strain specific peptide mass fingerprint (Singhal *et al.*, 2015).

Out of the 32 strains sent for MALDI-TO MS identification, 25 strains were correctly identified as *P. aeruginosa*. From these strains, 16 were isolated from the detergent drawer and 9 from the rubber seal, all collected from 11 different WMs including one that has been resampled. The other seven strains included *P. stutzeri* (2x), *P. alcaliphila* (1x), *P. nitroreducens* (1x), *M. luteus* (1x), and *Se. marcescens* (1x). One strain could not be identified. *P. stutzeri* and *P. nitroreducens* were also isolated from WMs in a study by Rehberg *et al.*, who investigated eleven WMs and four dishwashers (Rehberg *et al.*, 2017). *P. stutzeri* is an opportunistic human pathogen that is widely distributed in the environment, whereas *P. nitroreducens* is a ubiquitously distributed soil bacterium known for its denitrifying capabilities and is closely related to *P. aeruginosa* (Lalucat *et al.*, 2006; Iyer *et al.*, 2017). In contrast, *P. alcaliphila* is an alkaliphilic bacterium first isolated from sea water in Japan in 2001 (Yumoto *et al.*, 2001). Interestingly, both species, *P. nitroreducens* as well as *P. alcaliphila*, are cold-loving extremophiles, with *P. nitroreducens* being a psychrotroph and *P. alcaliphila* being a psychrophile (Yumoto *et al.*, 2001; Iyer *et al.*, 2017). Psychrotrophic bacteria are cold-tolerant with the ability to grow at low temperatures, but having an optimal growth temperature between 15°C and 20°C, whereas psychrophilic bacteria have an optimal growth temperature at temperatures around 15°C or lower and cannot grow at higher temperatures above 20°C (Witter, 1961; Morita, 1975; Moyer and Morita, 2007). Both species are often found in cold regions such as the poles or the deep sea (Moyer and Morita, 2007). Therefore, colonisation of

WMs by these species was unexpected, as temperatures within the WM should exceed 20°C even during a normal 30°C or 40°C wash cycle. However, cultivation of both strains at 37°C was successful, suggesting that the MALDI-TOF identification was incorrect and should be repeated. It could be that these strains are new species closely related to the ones identified but able to grow at higher temperatures.

Another identified species was *Se. marcescens*, a Gram-negative bacterium, that can widely be found in food and is known to be an important cause of nosocomial infection (Hejazi and Falkiner, 1997). As opposed to the afore mentioned species, *M. luteus* is a Gram-positive bacterium that can be isolated from skin, soil, and water. *M. luteus* can enter a dormant state that permits the bacterium to survive for extended periods when reasonable growth conditions are not available, which could be the case when found in WMs (Mukamolova *et al.*, 2002).

5.3.2 Selected *P. aeruginosa* strains exhibit different phenotypes such as production of virulence factors and antimicrobial resistance

For further characterisation, nine *P. aeruginosa* strains were chosen from five different WMs, including seven strains isolated from the drawer (WMB1.3, WM01D1, WM05D1, WM05D1R, WM05F1, WM07C1, and WM07D1) and three from the seal (WM02F1, WM05F1, and WM05F1R). Strains WM05D1R and WM05F1R were isolated from the same WM and site as WM05D1 and WM05F1, respectively, when the WM was resampled after six weeks.

To exclude that potential differences in phenotypes result from different growth behaviours, the growth of all strains including the control strain PAO1-N was analysed (Figure 5.6). Only two strains isolated from the same WM, WM07C1 and WM07D1, showed diminished growth after 18 h. However, both strains were culturable and only showed reduced growth after 9 h, when the OD_{600} started to slightly decrease over time instead of being constant during the stationary phase. Following, phenotypes such as motility, protease production, attachment, and BKC susceptibility were analysed.

5.3.2.1 Motility

A subsequent investigation of different virulence factors for the selected strains included swarming and swimming motility (Figure 5.7). Motility is an important factor enabling biofilm formation, as it allows bacteria to move on surfaces to find suitable spots to start biofilm formation. Swimming is termed as the movement in liquid medium, whereas swarming occurs on the top of surfaces, often associated with an increase in the number of flagella per cell (Kearns, 2010). *P. aeruginosa* is able to both swim and to swarm using flagella and pili. During swarming, *P. aeruginosa* retains its polar flagellum, but may produce additional flagella and synthesises an alternative motor required to propel movement on viscous surfaces (Köhler *et al.*, 2000; Rashid and Kornberg, 2000; Doyle *et al.*, 2004; Toutain *et al.*, 2005). In this study, only three of the nine WM isolates showed swimming motility (Table 5.1). In contrast, all but two strains were able to swarm, where both strains without swarming motility also lacked swimming motility. Although both modes of movement involve flagella under normal conditions, it was shown that swarming can still occur using type IV pili when flagella are lost, suggesting that strains showing swarming but no swimming primary use type IV pili instead of flagella, as flagella seem to be absent based on the observed phenotypes (Rashid and Kornberg, 2000; Kaiser, 2007).

Flagellar biogenesis is complex and involves the expression of more than 40 different genes (Choy *et al.*, 2004). The analysis of the whole genome sequencing revealed high protein sequence identity for most of the proteins of the Fli and Flg clusters except FliC, FliD, FliP, FlgK, and FlgL for strains WMB1.3, WM01D1, WM02F2, WM05D1, WM05F1, WM07C1, and WM07D1. Particular striking were proteins FliC and FliD, that showed very low identity for six of the nine WM isolates compared to PAO1 (Figure 5.17). FliC is the flagellin protein which polymerises and forms the filaments of the flagella, whereas FliD is required for the elongation of the flagellar filament and furthermore forms a capping structure that prevents the leakage of flagellin subunits (Yokoseki *et al.*, 1995; Brimer and Montie, 1998; Dasgupta *et al.*, 2004). Furthermore,

FliD is essential for motility and responsible for adhesion to mucin (Arora *et al.*, 1998). A schematic representation of the flagellar apparatus including the three main components, the filament, the hook, and the basal body, can be found in Figure 5.23.

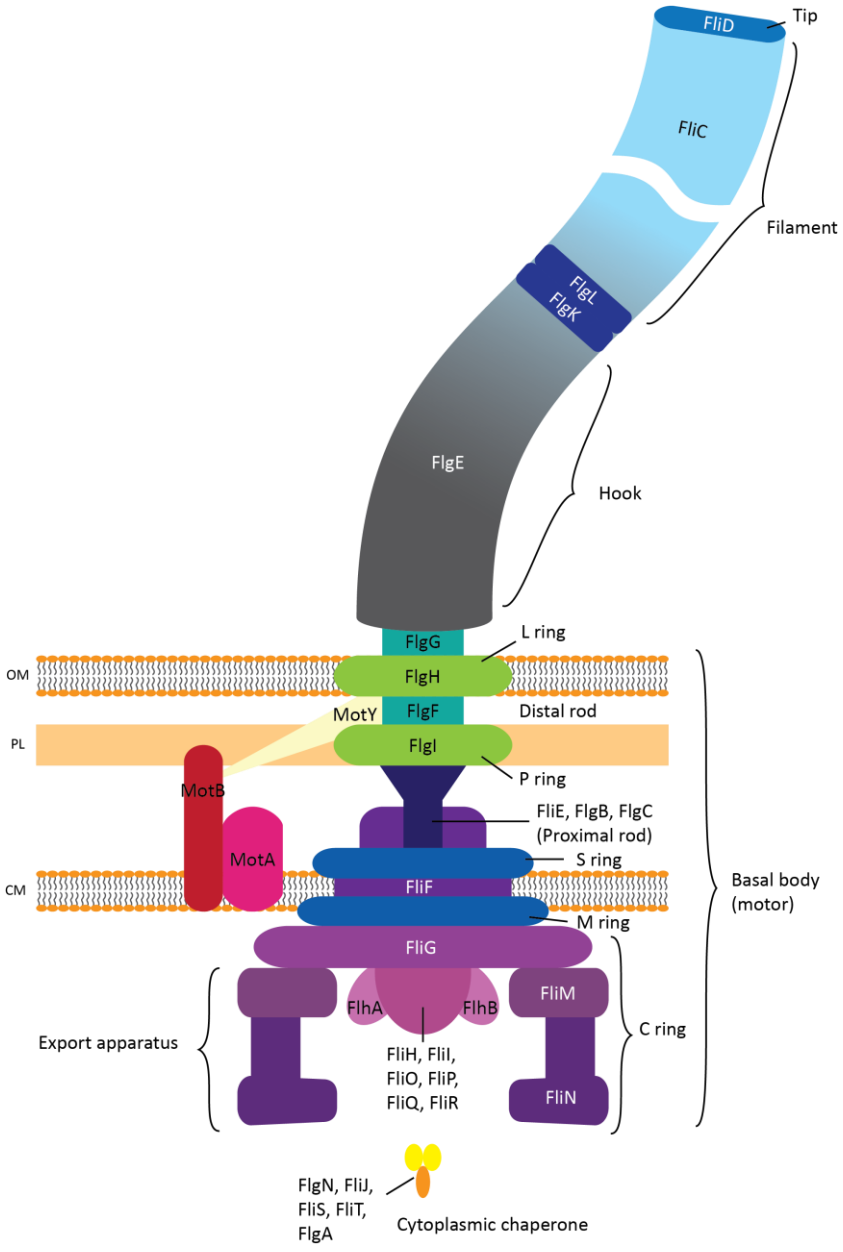


Figure 5.23: Flagellar apparatus consisting of its three main components (i) filament, (ii) hook, and (iii) basal flagellar motor. CM = cytoplasmic membrane, OM = outer membrane, PL = Peptidoglycan layer. Adapted from (Kanehisa and Goto, 2000; Kanehisa, 2019; Kanehisa *et al.*, 2019) https://www.genome.jp/kegg/pathway/eco/eco02040.html

FliC and FliD can both be divided into two subgroups within *P. aeruginosa* strains, type a (PAO1 reference) and b (PAK reference) (Lányi, 1970; Arora *et al.*, 2000). As PAO1 was used as reference strain for the protein comparison, all WM isolates were compared with type a FliC and FliD. Based on the very low protein identity of FliC and FliD for some of the strains, the genomes were also blasted against type b proteins, resulting in 99-100% sequence identity for all six strains, confirming that these strains possess type b proteins. It has been suggested that the expression of different types of flagellar cap proteins (FliD) enables *P. aeruginosa* to escape immune recognition by presenting different variants of a surface epitope (Arora *et al.*, 2000). Thus, it would be interesting to investigate whether the WM isolates of this study, which possess type b proteins, differ in their adhesion, pathogenesis, and ability of host invasion compared to the strains that express type a proteins. Although none of the other Fli and Flg proteins are grouped into different types of proteins, studies have shown low sequence similarity between different isolates of *P. aeruginosa* for multiple other proteins, including FlgK and FlgL (Dasgupta *et al.*, 2004; Subedi *et al.*, 2018). The FlgK protein of PAK only shows 88% protein identity compared to PAO1, and FlgL 69%, which is equivalent to sequence identities for the same proteins in WMB1.3, WM01D1, WM05D1, WM05F1, WM07C1, and WM07D1 (Dasgupta *et al.*, 2004). Detailed analysis of FliP, a protein showing only 80% sequence identity for WM02F1, WM07C1, and WM07D1, showed that the start of the protein sequence is missing for all three strains whereas the sequence was identical after the first 66 amino acids (Figure 5.18), suggesting that this protein might not be functional in these strains. FliP plays a role in the flagellum-specific transport system, but it is not clear if the protein is essential for flagellar assembly. Although it could be shown that all WM isolates possess genes potentially enabling flagellar assembly, seven of the nine strains were negative for swimming motility, with two of these strains also being negative for swarming, suggesting that these phenotypes may only be explained by altered transcription or post-transcriptional and post-translational regulation rather than by genomic variations.

One of the regulators affecting flagellar development and biofilm formation in *Pseudomonas* species is MorA, a protein showing mutations in WM02F1, which are predicated to have a high impact (Figure 5.17). MorA is a membrane-localised negative regulator of flagellar formation, with *morA* mutants of *P. putida* showing a constitutive expression of flagella (Choy *et al.*, 2004). Although no effects on motility were observed in mutants of *P. aeruginosa*, biofilm formation was reduced and secretion of LasB protease through the T2SS was increased (Choy *et al.*, 2004; Ravichandran *et al.*, 2015). From the total of 1415 amino acids of MorA, WM02F1 is missing the last 92. WM02F1 was non-motile, but positive for protease production/secretion and showed reduced attachment in CV assays, which could be a result of the loss of MorA function.

In addition to variations within genes involved in flagellar biosynthesis, genome sequencing also revealed deletions and SNPs within proteins of the Pil cluster (Figure 5.17). Pil proteins are required for the assembly of type IV pili that are essential for twitching motility and are furthermore involved in swarming motility, bacterial adherence, DNA uptake, and invasion of cells (Doig *et al.*, 1988; O'Toole and Kolter, 1998; Whitchurch *et al.*, 2005; Burrows, 2012; Okuda *et al.*, 2013; Persat *et al.*, 2015). Type IV pili can be divided into two subgroups, type IVa and type IVb, based on differences between major and minor pilin subunits (Burrows, 2012). In this study, many sequence differences were observed between Pil proteins of PAO1 and the WM isolates, especially within the PilA protein (Figure 5.17). PilA is a 15-kDa protein and the major unit of the pilus that is located on the surface of the bacteria. The pilus can be visualised as a thin filament composed of thousands of PilA subunits that are processed by PilD prior to assembly (Giltner *et al.*, 2011; Burrows, 2012). In addition to PilA, the minor pilin proteins FimU and PilVWXE are incorporated into the pilus fibre after PilD processing, although the exact functions are not yet clear (Giltner *et al.*, 2010; Giltner *et al.*, 2011). Over 40 genes are involved in the assembly and regulation of the type IV pili system, and a schematic representation of the structures of the type IV pili assembly subcomplex components are shown in Figure 5.24.

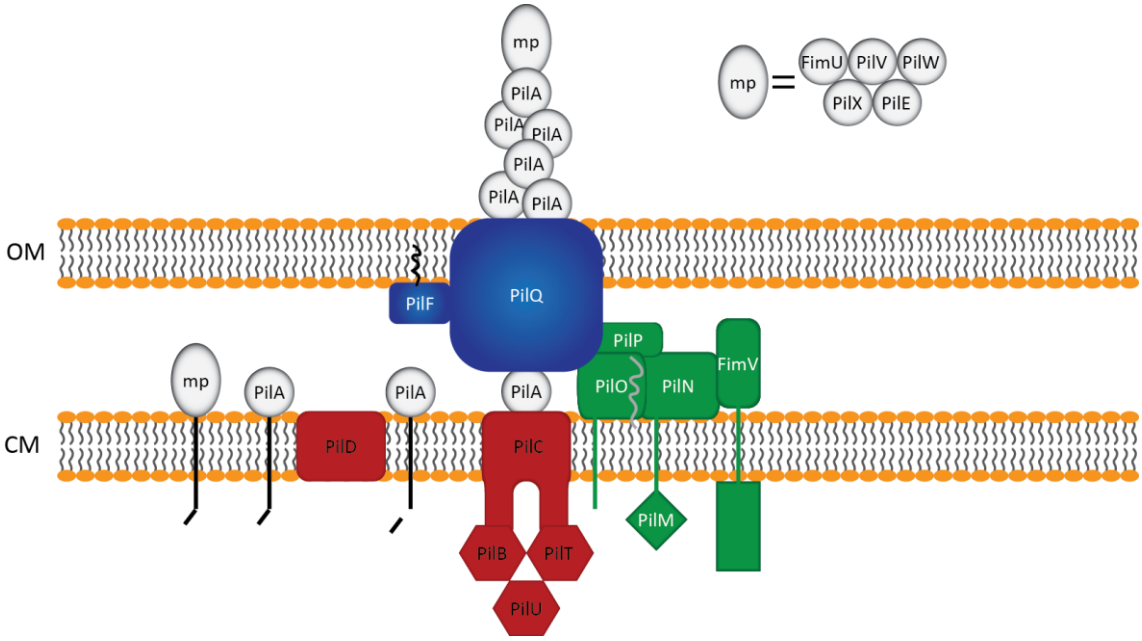


Figure 5.24: Schematic representation of type IV pili. The assembly system consists of four subcomplexes: (i) outer membrane subcomplex (PilF and PilQ, highlighted in blue), (ii) inner membrane motor subcomplex (PilB, PilC, PilD, PilT, and PilU, highlighted in red), (iii) alignment subcomplex (PilM, PilN, PilO, PilP, and FimV, highlighted in green), and (iv) pilus subcomplex (minor pilins (mp) FimU, PilV, PilW, PilX, PilE and PilA, highlighted in white). OM = outer membrane, CM = cytoplasmic membrane. Adapted from (Burrows, 2012).

With more than five different groups of PilA existent in *P. aeruginosa* strains, variations within the type IV pilin *pil* locus are very common in *P. aeruginosa*, likely because of random mutations within a strain or by recombination with other strains and species (Paranchych *et al.*, 1997; Kus *et al.*, 2004; Winstanley *et al.*, 2009). Therefore, sequence differences to the reference genome of PAO1 within Pil proteins do not necessarily indicate changes or loss of function. PAO1 expresses a group II pilin, that is similar to WM02F1. In contrast, sequence analysis revealed that WM05D1, WM05D1R, and WM05F1 all possess PilA similar to LESB58, with more than 80% sequence identity, whereas PilA of WM01D1 is 99% identical with PilA from PA14. It is therefore likely that all WM isolates possess PilA of one of the groups, although it does not seem to be the same as for PAO1, except for WM02F1. Apart from WM01D1, all WM isolates show high protein sequence identity of 90-100% for all other proteins of the Pil cluster. However, as mentioned previously, a single SNP could already result in the loss of function of the protein, although none

of these SNPs were predicted to have a high effect. Comparison of WM01D1 with other *P. aeruginosa pil* sequences revealed high sequence identity of several proteins with strain PA14, as already observed for PilA. Twitching motility was not assessed in this study, and microscopy was not used to confirm the assembly of pili on the bacterial surface. However, as swarming but no swimming motility was observed for some of the WM isolates, it can be suggested that type IV pili are expressed and functional despite the observed sequence differences. However, further experiments should be carried out to verify these findings.

Overall, the observation of WM isolates being able to swarm but not swim is very interesting, as, unlike swimming motility, where the movement takes place as individual cells, swarming motility occurs in multicellular groups (Kearns, 2010). Therefore, swarming requires not only an increase in flagella biosynthesis or type IV pili formation, but also cell-cell interactions and the presence of a surfactant. *P. aeruginosa* uses rhamnolipids as surfactant, which is commonly regulated by QS (Ochsner and Reiser, 1995; Köhler *et al.*, 2000; Kearns, 2010). Therefore, QS could be used by the bacteria to ensure surfactant production and hence swarming is only active when sufficient bacteria are present. Although genome analysis did not reveal any discernible changes between strains looking at QS genes, changes in QS regulation could be present.

In addition, flagella can initiate inflammatory responses of host cells, whereas non-flagellated mutants seem to have selection advantage during chronic infections (Luzar *et al.*, 1985; Feldman *et al.*, 1998). As swarming was widespread between the isolates, but flagella seemed to be absent, these strains could be primed for infection. However, flagella and type IV pili are also involved in attachment, biofilm formation, and microcolony formation, and loss of flagella and pili could indicate reduced biofilm formation of these strains (O'Toole and Kolter, 1998). Looking at the biofilm formation of WMB1.3, the only strain that was assessed for biofilm formation, no differences in microcolony formation was observed, and biofilm formation was enhanced, suggesting that type IV pili biosynthesis in this strain is intact and functional regardless the type differences (see 5.3.2.3).

5.3.2.2 Protease production

Seven of the nine WM isolates showed protease production (Table 5.1). *P. aeruginosa* is known to produce at least five different proteases that are involved in virulence and can cause bleeding and tissue necrosis in respiratory infections, although one of the proteases, Lon, is not secreted (see 1.1.1). The secretion of proteases from most of the isolates under the tested conditions underpin the potential pronounced virulence of the strains. The genome analysis of the two isolates not showing protease production did not reveal any changes in genes directly involved in the synthesis of proteases, but regulators could be affected by SNPs that were not detected. Furthermore, protease production can be upregulated by QS systems, but as already mentioned, no discernible differences within QS systems were observed based on the whole genome analysis (Jaffar-Bandjee *et al.*, 1995; Lee and Zhang, 2015).

5.3.2.3 Attachment and biofilm formation

After growth for 24 h in 96-well plates, CV staining revealed enhanced attachment for four of the nine WM isolates, whereas the remaining five strains showed diminished attachment compared to the reference (Figure 5.8). This finding confirms the results of a study by Gattlen *et al.*, who found that nine of their fifteen WM isolates showed enhanced CV staining after 24 h of growth (Gattlen *et al.*, 2010). Interestingly, the two isolates that were unable to swarm or swim also showed reduced CV attachment, confirming a link between the absence of flagella/pili and attachment. Additionally, an increased attachment was observed for both strains showing a significantly reduced growth (WM07C1 and WM07D1), suggesting that growth alone is not an evidence for biofilm formation. Although CV staining is not a direct indication for the formation of biofilms, an increased attachment can still point towards improved biofilm formation. For example, CLSM of static biofilms of WMB1.3 revealed slightly increased biofilm formation compared to PAO1-N with a biomass of 2.3 $\mu m^3\,\mu m^{-2}$ compared to 1.4 $\mu m^3\,\mu m^{-2}$, which could be a consequence of the enhanced attachment observed for the CV staining (Figure 5.11). That means this WM isolate seems to be well adapted to a biofilm forming lifestyle, allowing the

bacteria to protect themselves against biocidal effects of laundry products within the WMs. In future studies, CLSM of biofilm formation should be investigated for all isolates. That way, the composition of the biofilms could also be analysed by looking at matrix components such as eDNA and EPS, as Gattlen *et al.* observed enhanced EPS production for some of their WM isolates (Gattlen *et al.*, 2010).

Looking at the genome analysis, two clusters were identified, which are involved in biofilm formation and showed changes between strains (Figure 5.19). The BfmSR two-component system is one of three systems involved in biofilm formation following transition to the surface attached lifestyle (Petrova and Sauer, 2009). BfmSR is an OmpR-like system that becomes phosphorylated during biofilm formation. Inactivation of the response regulator BfmR leads to arrested biofilm formation, and discontinuation of *bfmR* expression in already established biofilms result in the collapse of biofilms (Petrova and Sauer, 2009). Furthermore, deletion of *bfmS* was shown to lead to the activation of BfmR, which directly binds to the promoter of the *rhlR* gene, encoding the QS regulator RhlR. Binding of the promoter in turn results in decreased expression of *rhlR*, causing inhibition of the whole *rhl* QS system (Cao *et al.*, 2014). Additionally, BfmS is involved in the expression of 202 other genes, and deletion of *bfmS* leads to reduced virulence, but enhanced invasion (Cao *et al.*, 2014). Specific SNPs in BfmS can already be sufficient to result in activation or repression of BfmR and can subsequently cause inhibition of the *rhl* QS system (Cao *et al.*, 2004). Four WM isolates, WM01D1, WM05D1, WM05D1R, and WM05F1, lack both proteins, BfmR and BfmS, suggesting that the *rhl* QS system is not repressed, and production of the QS signal molecule *N*-butanoyl-L-homoserine lactone would be enhanced. Unless these strains possess a homologous two-component system, that can replace the BfmSR function, alterations in virulence factor production between these four strains and the remaining six strains would be expected as a result of increased QS activation and should be investigated in future studies, for example by looking at the transcriptome or the production of QS molecules.

Another protein involved in biofilm formation is Arr, that is missing in all WM isolates (Figure 5.19). It was shown that Arr in *P. aeruginosa* is essential for the induction of biofilm formation after exposure of the bacteria to subinhibitory concentrations of aminoglycoside antibiotics. Additionally, Arr contributes to biofilm-specific aminoglycoside resistance (Hoffman *et al.*, 2005). *Arr* encodes an inner-membrane phosphodiesterase with c-di-GMP as its substrate, and *arr* mutants showed diminished c-di-GMP phosphodiesterase activity and reduced tobramycin resistance within biofilms (Hoffman *et al.*, 2005). Although in many cases, induction and overproduction of phosphodiesterases result in reduction of c-di-GMP concentration and subsequently suppression of biofilm formation, it was shown that the activity of Arr is linked to tobramycin-inducible biofilm formation, suggesting that the effects of c-di-GMP might be dependent on which phosphodiesterase or diguanylate cyclase is affected (Gotoh *et al.*, 2008). Future experiments could investigate if the WM isolates show altered biofilm formation under exposure to subinhibitory concentrations of aminoglycoside antibiotics as a result of the missing *arr* gene.

5.3.2.4 Antimicrobial resistance

In addition to enhanced biofilm formation, previous studies found that WM isolates were generally more resistant to the laundering process compared to lab strains, even when the lab strains were carrying antibiotic resistance genes (Rehberg *et al.*, 2017). Rehberg *et al*. isolated fifteen strains from different WMs and dishwashers carrying genes for β-lactamase production (Rehberg *et al.*, 2017). Furthermore, studies demonstrated resistance and adaptation towards sanitisers like active chlorine compounds or quaternary ammonium bases, such as BKC (Sundheim *et al.*, 1998; Yildiz and Schoolnik, 1999; Langsrud *et al.*, 2003; Russell, 2004). In this study, the tolerance of the WM isolates and the lab strain PAO1-N against BKC was investigated. The MIC of PAO1-N was 60 mg L^{-1}, which was similar to the three WM isolates WM01D1, WM05F1R, and WM07C1 (Figure 5.9). Two isolates were less tolerant against BKC with an MIC of 50 mg L^{-1} (WM05D1R and WM07D1), while the remaining four strains showed enhanced

resistance with 70 mg L^{-1} (WM02F1) and 80 mg L^{-1} (WMB1.3, WM05D1, and WM05F1), respectively. These results are consistent with other studies, showing an average MIC between 50-70 mg L^{-1} for *Pseudomonas* test strains, and much higher concentrations for some isolated strains (MIC up to 200 mg L^{-1}) (Langsrud and Sundheim, 1997). Some studies showed that *Pseudomonas* strains can even be adapted to a BKC concentration of over 240 mg L^{-1} or 350 mg L^{-1}, respectively, when being continuously exposed to BKC (Mc Cay *et al.*, 2010; Kim *et al.*, 2018). *P. aeruginosa* ATCC 15442, a strain used as organism in the European standard method for testing bactericidal activity of chemical disinfectants, also showed an MIC of 60 mg L^{-1} against BKC (Langsrud *et al.*, 2003). It has been suggested that efflux pumps are amongst the major contributors to an enhanced tolerance against biocides and specifically BKC (Mc Cay *et al.*, 2010). One of the systems involved in decreased susceptibility of *P. aeruginosa* strains against BKC is the multiple efflux (Mex) pump system (Mc Cay *et al.*, 2010; Kim *et al.*, 2018). It was shown that the susceptibility of isolates against BKC increased enormously in the presence of an efflux pump inhibitor from an MIC >350 mg L^{-1} BKC to 50 mg L^{-1}. Furthermore, the expression of *mex* genes was increased in BKC-adapted *P. aeruginosa* isolates (Mc Cay *et al.*, 2010; Kim *et al.*, 2018).

Mex pumps belong to the resistance-nodulation-cell division (RND) superfamily of transporters (Li and Plésiat, 2016). The RND family in *P. aeruginosa* consists of 17 systems, with 12 RND efflux pumps being well characterised, including two divalent metal cation transporters, nine Mex efflux pumps and one triclosan pump (Stover *et al.*, 2000; Lister *et al.*, 2009; Li and Plésiat, 2016). RND pumps are typically composed of three systems that form a channel throughout the entire membrane enabling drug transport from the periplasmic space and cytoplasm to the extracellular environment: (i) A periplasmic membrane fusion protein (MFP), (ii) an outer membrane factor (OMF), and (iii) a cytoplasmic membrane (RND) transporter (Lister *et al.*, 2009). Substrates of the pumps include antibiotics, biocides, dyes, detergents, and homoserine lactones and differ from system to system. An extensive overview about the different RND

pumps, their function, regulation, and substrates can for example be found in reviews by Lister *et al.* and Li and Plésiat (Lister *et al.*, 2009; Li and Plésiat, 2016). The nine Mex systems are named MexAB-OprM, MexCD-OprJ, MexEF-OprN, MexXY, MexGHI-OpmD, MexVW, MexPQ-OpmE, and MexMN. Genes encoding the pumps are organised into operons composed of at least two genes coding for the MFP and RND transporter, with six operons additionally possessing an OMF gene. Furthermore, some of the Mex systems contain a gene that encodes a regulator (activator or repressor) for the specific pump, for example MexR of the MexAB-OprM system or NfxB of the MexCD-OprJ pump. In this study, SNPs were discovered in many of the Mex proteins of the various systems, including MexS and ArmR, two proteins involved in regulatory roles of the MexEF-OprN pump and the MexAB-OprM pump, respectively. Mutations within any of the pump components can increase the susceptibility of the bacteria against diverse antimicrobial agents, whereas overproduction of the systems contributes to multidrug resistance and was observed in clinical isolates, where mutations in repressor proteins occurred (Li and Plésiat, 2016). However, most of the mutations that were detected in this study were predicted to have no, low or moderate effects, and only the mutations within MexF and ArmR were further analysed.

The RND transporter MexF in the lab strain PAO1-N is missing the first 344 amino acids, suggesting that the protein and thus the whole MexEF-OprN system is not functional in this strain (Figure 5.22). Substrates of the MexEF-OprN include fluoroquinolones, chloramphenicol, trimethoprim, biocides, and aromatic hydrocarbons (Lister *et al.*, 2009). However, none of these substrates are specific to only MexEF-OprN and can also be transported via at least one of the other RND efflux pumps. In addition, it was found that the MexEF-OprN pump is not well expressed in wild type cells of *P. aeruginosa*, leading to only small or no changes in antimicrobial susceptibility after inactivation (Köhler *et al.*, 1997; Li and Plésiat, 2016). MIC experiments in this study using the biocide BKC also showed no reduced susceptibility of PAO1-N compared to published MICs of other wild type strains, suggesting that the absence of a functional MexEF-

OprN pump in PAO1-N has no phenotypic effects. Other possible reasons include a missing start site, which was not picked up by the sequence analysis or a sequencing error. However, another view at the region of interest could not support this hypothesis.

ArmR is the anti-repressor of MexR, whereby MexR is a repressor of the *mexAB-OprM* transcription. Thus, expression of *mexAB-OprM* is positively regulated by ArmR, and disruption of ArmR is associated with enhanced MexR activity and subsequent reduced MexAB-OprM expression, which compromises multidrug resistance (Cao *et al.*, 2004; Daigle *et al.*, 2007; Wilke *et al.*, 2008). Under normal conditions, MexAB-OprM is constitutively expressed in wild type strains and therefore significantly contributes to intrinsic drug resistance, where inactivation of any component of the system makes the wild type strain hypersusceptible (Li and Plésiat, 2016). Interestingly, all four strains that showed SNPs within ArmR were either less susceptible to BKC or equal with the wild type strain, suggesting that these SNPs have no negative impact on the function of ArmR.

Furthermore, in a study by Kim *et al.*, mutations within the QS regulator gene *lasR,* which regulates various efflux pump genes, led to a loss of BKC resistance (Kim *et al.*, 2018). However, in this study, no mutations within *lasR* were observed for mutants showing increased BKC susceptibility. The use of efflux pump inhibitors as well as transcriptome analysis could be used in future studies to confirm a role of efflux systems in the tolerance of the WM isolates of this study against BKC.

Another system involved in resistance of *P. aeruginosa* to polymyxin and other cationic antimicrobials is the two-component system PmrAB (McPhee *et al.*, 2003). PmrAB is involved in the regulation of the *arnBCADTEF-pmrE* operon, that encodes enzymes required for lipid A modification of LPS that are associated with polymyxin resistance and reduction of negative surface charge (Moskowitz *et al.*, 2012). In response to antimicrobial exposure, the sensor kinase PmrB activates the transcriptional regulator PmrA, resulting in elevated *arnBCADTEF-pmrE* transcription. It was shown in multiple studies that gain-of-function mutations of PmrB can lead

to enhanced activation of PmrA and subsequent elevated polymyxin resistance (Abraham and Kwon, 2009; Barrow and Kwon, 2009; Schurek *et al.*, 2009). In all three studies, the substitution of single amino acids within PmrB were shown to be the cause for the observed phenotype. Another study by Kim *et al.* also identified PmrB mutations as consequence of exposure to BKC, whereby BKC is a membrane-disrupting agent, similar to polymyxin (Kim *et al.*, 2018). However, mutations in different parts of PmrB can also lead to the loss of BKC resistance, making the correct interpretation of the genome data difficult (Kim *et al.*, 2018). In this study, four amino acid substitutions within PmrB were observed in WM01D1 and WM05D1R, and three changes in WM05F1R (Figure 5.22). WM01D1 and WM05F1R both showed the same MIC against BKC than PAO1-N, whereas the MIC of WM05D1R was lower. However, no amino acid changes were detected in strain WM07D1, which also showed reduced BKC resistance. These results indicate that a change in PmrB activity is possible but cannot be linked with the observed phenotype of BKC resistance using the present data.

Another reason for developed BKC resistance can be the dealkylation of BKC to benzyl dimethylamine (BDMA), as BDMA is 500 times less toxic than BKC (Tezel *et al.*, 2012; Oh *et al.*, 2014). The amount of BDMA produced by the WM isolates could be measured to determine if the dealkylation of BKC could be a reason for the enhanced BKC resistance in some of the strains. Furthermore, the surface charge, cell surface roughness, cell surface hydrophobicity, and fatty acid components on the cell surface can influence the membrane permeability and hence BKC resistance and should be further analysed (Nagai *et al.*, 2003; Tezel and Pavlostathis, 2015; Kim *et al.*, 2018). The finding in this study, that almost 50% of the WM isolates were more tolerant against BKC than lab strains used for the testing of detergents highlights the demand to use environmental strains to test detergent efficiency, as the use of lab strains can easily overestimate the effectiveness compared to real conditions in WMs.

5.3.2.5 Pyocyanin production

One isolate that was able to swarm and swim and showed enhanced CV attachment and tolerance against BKC was WMB1.3. This isolate was one of the first isolates and especially noticeable because of enhanced pigment production during cultivation resulting in a dark blue/green culture medium (Figure 5.10). One of the most prominent blue pigments produced by *P. aeruginosa* is pyocyanin, a phenazine toxic metabolite. Phenazine compounds are metabolites produced by *Pseudomonas* species and are involved in microbial competitiveness and virulence (Winstanley *et al.*, 2009). More than 90% of all *P. aeruginosa* isolates produce the redox-active phenazine compound pyocyanin, with high concentrations of pyocyanin leading to tissue damage in chronic lung infections (Wilson *et al.*, 1988a; Mavrodi *et al.*, 2001). The toxic effects of pyocyanin against eukaryotic cells are widespread as it acts in a range of ways, including inhibition of cell respiration and epidermal cell growth, inactivation of catalases, induction of apoptosis in neutrophils, and inactivation of α_1 protease inhibitors and therefore contributing to the imbalance of protease-antiprotease activity in CF lungs (Wilson *et al.*, 1988b; Sorensen and Joseph, 1993; Britigan *et al.*, 1999; Usher *et al.*, 2002; O'Malley *et al.*, 2003; Lau *et al.*, 2004b)

Measurement of the pyocyanin concentration produced by the WM isolate WMB1.3 compared to the lab strain PAO1-N confirmed an elevated production for WMB1.3 (2.5 µg mL^{-1} compared to 1 µg mL^{-1}). An increased pyocyanin production could therefore indicate enhanced infection potential of the WM isolate. Genome analysis revealed that, as for many *P. aeruginosa* genomes, all WM isolates contain two clusters of genes (*phzA1B1C1D1E1F1G1* and *phzA2B2C2D2E2F2G2*) encoding proteins of the phenazine biosynthesis pathway responsible for the synthesis of phenazine-1,6 dicarboxylate (PDC) or PCA, with some isolates missing sets of genes or showing mutations (Figure 5.20). Three additional genes, *phzM, phzS,* and *phzH*, encode enzymes that are involved in the conversion of PCA to pyocyanin, 1-hydroxyphenazine

(1OH-PHZ) or phenazine-1-carboxamide (PCN) (Mavrodi *et al.*, 2001). The phenazine biosynthesis pathway is illustrated in Figure 5.25.

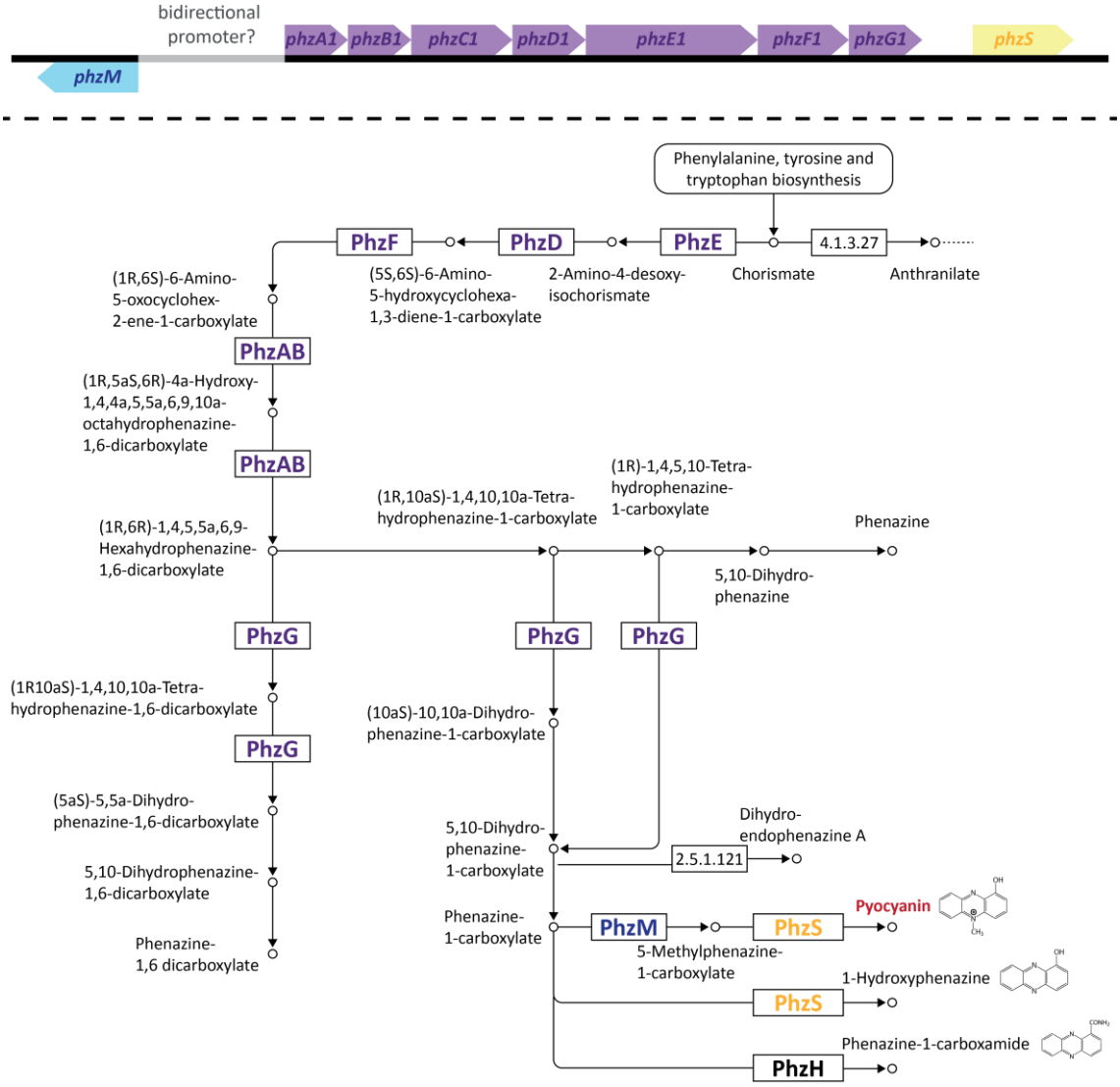


Figure 5.25: Phenazine biosynthesis pathway in *P. aeruginosa* PAO1. Top: Phenazine operon *phzA1B1C1D1E1F1G1* located between *phzM* and *phzS*. Bottom: Mechanism for the synthesis of phenazine-1,6 dicarboxylate, pyocyanin, 1-hydroxyphenazine and phenazine-1-carboxamide.

WM01D1 and WM02F1 both lack PhzA1, PhzA2, and the intergenic region between *phzM* and *phzA1*. Additionally, sequence identities of 90% and lower were found within different phenazine proteins of WM01D1, WM02D1, WM05D1, WM05F1, WM05F1R, WM07C1, and WM07D1. Interestingly, in most cases, both homologous proteins were affected, which means that if PhzF1 showed reduced sequence identity, its homologue PhzF2 also showed low sequence identity. It is therefore unlikely that the loss of function of one of the proteins could

be compensated by the homolog. Based on the relatively low protein sequence identity of at least two genes in WM01D1, WM02F1, WM05D1, WM05F1, WM05F1R, WM07C1, and WM07D1, is can be suggested that the phenazine production is altered in these strains compared to PAO1-N. However, WMB1.3 was the only strain that was examined for pyocyanin production. WMB1.3 showed sequence variation within the intergenic region of *phzM* and *phzA1*, where promoter regions as well as a LasR binding site is predicted. In the pyocyanin production assay, elevated pyocyanin production was observed, suggesting that the changes within the promoter region might lead to enhanced transcription of the phenazine genes. Furthermore, changes within the LasR binding site could have a positive impact on the efficiency of LasR, which is a transcriptional activator of *P. aeruginosa* virulence genes including the *phzA1B1C1D1E1F1G1* operon (Whiteley *et al.*, 1999; Kiratisin *et al.*, 2002). Measurement of pyocyanin as well as PCA, PCN, PDC and 1OH-PHZ concentrations for all isolates could give a first indication of which proteins are functional and how the mutations affect their functionality. Transcriptome analysis could furthermore confirm if the differences within the intergenic region of WMB1.3 leads to enhanced transcription.

5.3.2.6 Lipopolysaccharides

One of the major components of Gram-negative bacteria are LPS, that can be divided into three main parts: (i) The hydrophobic lipid A component that ensures that the molecules stay within the outer membrane, (ii) a central core oligosaccharide region that links the lipid A region to the O antigen, and (iii) the O antigen region of repeating polysaccharides (Rocchetta *et al.*, 1999). If attachment of the O antigen to the core-lipid A occurs, LPS is often described as smooth, whereas rough LPS describes the lack of O antigen. LPS is relevant for the initial bacterial attachment to surfaces, evasion of host immune systems, and the establishment of infection, where it was shown that smooth LPS is more effective compared to rough LPS, suggesting that intact O antigen is important for virulence of *P. aeruginosa* (Rocchetta *et al.*, 1999). Two different forms of O antigen are produced by *P. aeruginosa*: (i) A-band O antigen, composed of

D-rhamnose homopolymers and (ii) B-band O antigen, containing heteropolymers (di- to pentasaccharide repeating units of various monosaccharides) (Rocchetta *et al.*, 1999; Lam *et al.*, 2011). The exact B-band composition varies between serotypes of *P. aeruginosa* and 20 different O serotypes were identified to date, with PAO1 belonging to the O5 O antigen serotype. A schematic representation of O5 LPS is shown in Figure 5.26.

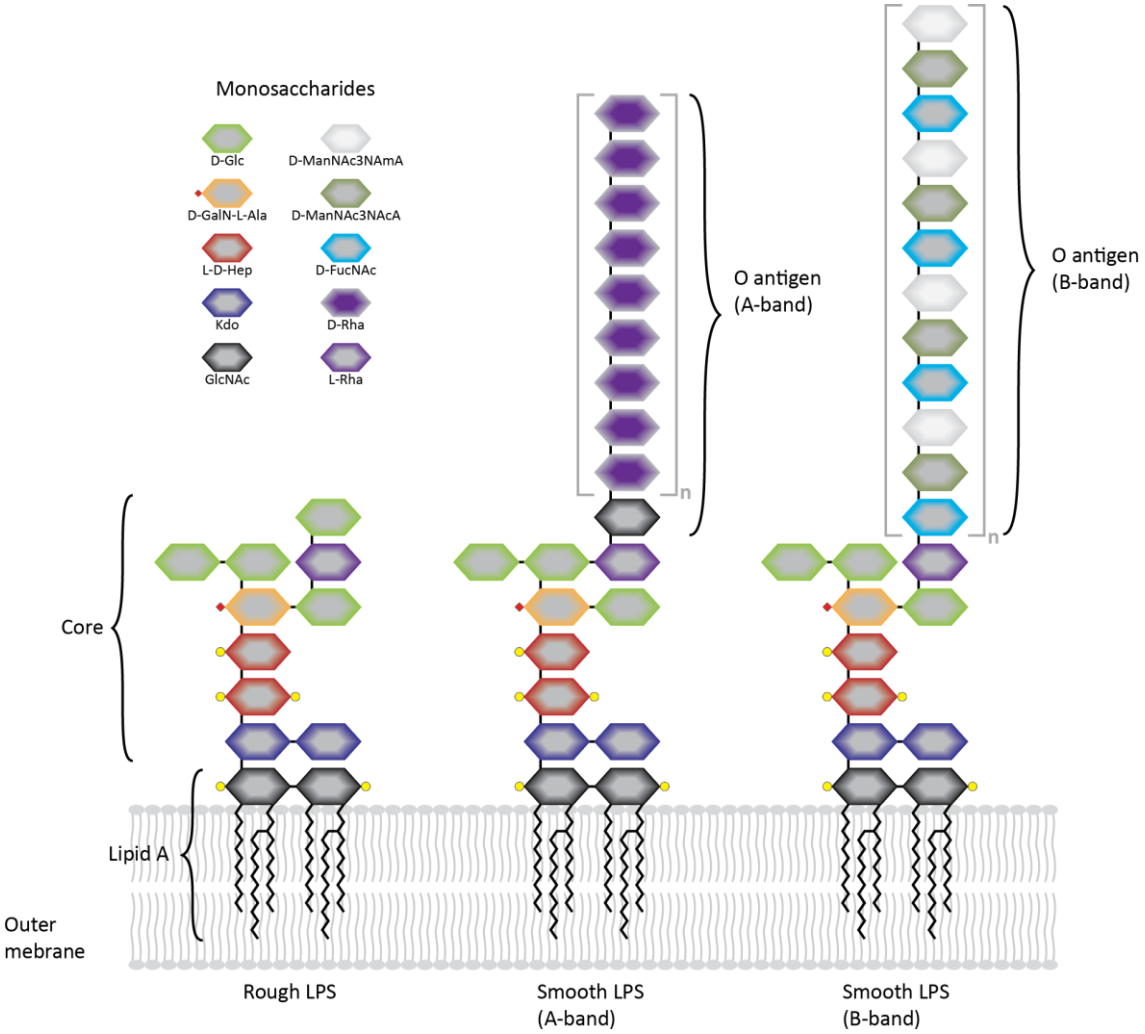


Figure 5.26: Schematic representation of rough and smooth LPS, with the B-band O antigen of the O5 serotype of *P. aeruginosa*. The length of A-band and B-band O antigen can differ depending on serotype, mutations, and environmental influences. Yellow circles represent phosphate groups. n = variable number of repeats. D-Glc = D-Glucose, D-GalN-L-Ala = D-Galactosamine-L-Alanine, L-D-Hep = L-D-Heptose, Kdo = Ketodeoxyoctonic acid, GlcNAc = 2-acetamido-2-deoxy-D-glucopyranose, D-ManNAc3NAmA = 2-acetamido-3-acetamidino-2,3-dideoxy-d-mannuronic acid, D-FucNAc = 2-acetamido-2,6-dideoxy-D-galactopyranose, D-Rha = D-Rhamnose, L-Rha = L-Rhamnose. Adapted from Lam *et al.* (2011).

Interestingly, studies have shown that chronic *P. aeruginosa* isolates from CF patients often completely lack B-band O antigen, while only producing A-band O antigen (Penketh *et al.*, 1982; Hancock *et al.*, 1983; Fomsgaard *et al.*, 1988; Lam *et al.*, 1988; Rocchetta *et al.*, 1999). Furthermore, it was found that the loss of B-band O antigen indicates resistance to aminoglycosides (Bryan *et al.*, 1984; Kadurugamuwa *et al.*, 1993).

In this study, all strains showed very high protein sequence identity (>99%) for all proteins of the Wbp A-band cluster, which was expected as the gene cluster for A-band O antigen is highly conserved in *P. aeruginosa* (Figure 5.21). In contrast, high sequence diversity was observed for proteins of the Wbp B-band for WMB1.3, WM01D1, WM05D1, WM05D1R, and WM05F1 in almost all proteins except WbpM. WM07C1 and WM07D1 showed sequence variations within three proteins, whereas WM02F1 and WM05F1R proteins were almost identical to PAO1, suggesting that these four strains belong to the same O5 serotype as PAO1. As WM07C1 and WM07D1 show very low sequence identity for WbpK, and WbpK is necessary for B-band synthesis, it should be investigated if these two strains are still able to successfully synthesise B-band O antigen. For WMB1.3, WM01D1, WM05D1, WM05D1R, and WM05F1, it is very likely that these isolates belong to a different O serotype than PAO1 and thus produce B-band antigen that differs from PAO1. However, further identification of serotypes was not part of this study and should be investigated in the future. Interestingly, Makin and Beveridge reported complete loss of B-band O antigen when PAO1 was grown at high temperature around 45°C (Makin and Beveridge, 1996b). It is likely that the WM isolates were exposed to high temperatures while growing in WMs, suggesting that they could have completely lost B-band production as a result.

Additionally, B-band O antigen are highly anionic and influence the cell surface charge of bacteria (Makin and Beveridge, 1996a). If no B-band O antigen is produced, the surface charge is increased, which could influence antibiotic resistance and interaction with other cationic particles, such as the cationic nanosensors used in this study as well as the cationic biocide BKC. Thus, one possible explanation for altered surface charge could be the observed changes within the LPS gene cluster and should be further investigated.

5.3.2.7 pH variation within biofilms

The pH microenvironments of WMB1.3 and PAO1-N were analysed using pH-sensitive polyacrylamide nanosensors and both models, static and flow-cell, with no differences being observed between strains (Figure 5.12 and Figure 5.13). As for PAO1-N, microcolonies of

WMB1.3 formed in a flow-cell show a more acidic core and a more neutral pH towards the edges (also see Chapter 4). The presence of the positively charged pH-sensitive nanosensors during static biofilm growth also led to the formation of a thicker biofilm, as previously seen for PAO1-N (Chapter 3). However, the WMB1.3 cells are less aggregated, suggesting that the effect of the positive charge of the nanosensors is reduced. One possible reason could be that the surface charge of WMB1.3 cells is less negative, which would underpin the previous hypothesis that changes in the surface charge could be a reason for enhanced BKC resistance, for example as a result of altered LPS.

5.3.3 Genome analysis reveals that different *P. aeruginosa* strains co-develop within the same washing machine

Comparison of the whole genome sequencing enabled insights into the relationship between different WM isolates and well-characterised *P. aeruginosa* strains, including PAO1 and PA14 (Figure 5.14). It was apparent that strains isolated from WM05 and WM01 are more related to PA14, whereas isolates from WMB1.3, WM07, and WM02 are closer related to PAO1. Although the two isolates from WM07, WM07C1 and WM07D1, are directly linked with each other, this is not the case for all four isolated strains from WM05. WM05D1 and WM05F1 were isolated at the same time from the same WM but from different locations (drawer and seal, respectively) and are located within one branch. In contrast, WM05D1R and WM05F1R, both isolated six weeks after the first sampling, do not cluster together and are furthermore not directly linked with the strains WM05D1 and WM05F1. Although in general, all isolates are somehow clustered, none of the strains from different WMs are identical. This was confirmed by looking at the general genome analysis information, where most of the strains varied in genome length, number of contigs, number of CDS, and number of SNPs (Table 5.3). Only WM07C1 and WM07D1 were very similar, suggesting that one single strain from WM07 was isolated twice. This observation confirmed previous findings, where both strains showed the same phenotypes for almost all assays (Table 5.2).

Proteome comparison revealed that some protein clusters are missing completely in WM isolates, whereas some proteins exist in the WM strains but are missing in PAO1-N (Figure 5.15 and Figure 5.16). However, most of these proteins are hypothetical proteins with unknown function. The same was observed for most of the SNPs found with a predicted high effect on the gene transcription or protein translation and function. Nevertheless, some mutations in genes and proteins were identified that could impact motility, biofilm formation or virulence and were discussed above to potentially link observed phenotypes with genome features. Furthermore, analyses of genes typically associated with phenotypes such as biofilm formation and virulence were conducted, for example by looking at QS genes. However, if no anomalies were observed, these results were not described in more detail.

5.4 Conclusion

The isolation of a variety of bacteria from household WMs, including *P. aeruginosa*, emphasises the need for improved washing products and a change in WM design to reduce infection risks and malodour. Although the identification of the entire spectrum of bacterial species grown in WMs was not a purpose of this study, it was demonstrated that many pathogenic bacteria can be found in WMs, which exhibit phenotypes such as increased antibiotic resistance, biofilm formation, and virulence factor production. The finding of this study points out the importance to use environmental strains instead of lab strains to develop and test the efficiently of new antimicrobial agents and biocides in washing products.

Furthermore, whole genome sequencing revealed that different *P. aeruginosa* strains coexist in the same WMs, with no direct ancestry to each other based on phylogenetic analysis and genome comparison. Overall, it was difficult to link the identified mutations with the phenotypic diversity of the strains, suggesting that adaptations have occurred at a different level, such as cell physiology, transcriptional/translational regulation, or post-transcriptional/translational regulation. Therefore, transcriptome analysis should be conducted in future studies in order to identify mechanisms for adaptation to WM environments. However, multiple differences between genomes with respect to LPS modifications were identified that could promote changes in surface charge, biofilm formation, and antimicrobial resistance and should be investigated in more detail.

Chapter 6 Laundry formulations and ingredients including the antimicrobial BKC differ in their ability to inhibit growth and viability of *P. aeruginosa*

6.1 Introduction

6.1.1 Background

A number of potential approaches exist to reduce bacterial colonisation of WMs; two of those are focussed in this chapter: (i) Altering laundry products to be more effective at killing bacteria at the new low temperature profiles and (ii) changing WM surfaces to prevent bacterial adherence. Reduction of bacterial colonisation can be achieved by using active oxygen bleaching agents and optimising rinsing to deliver a higher dilution of bacteria (Munk *et al.*, 2001; Bloomfield *et al.*, 2013). However, conventional bleaching systems are not applicable to liquid washing agents (Munk *et al.*, 2001). Nevertheless, sale numbers for washing powders that may consist of bleaching agents have decreased over time. In 1999, powder detergents accounted for 44% of the U.S. market and in 2019, sale numbers for washing powder only reached 11% in the U.S. (Teng, 2000; Munk *et al.*, 2001; IRI, 2020). Thus, development of new laundry products is required, which are effective in reducing biofilm formation at lower temperatures at the same time as being environmentally friendly and mild to fabrics.

As already discussed in Chapter 5, one biocide that is widely used in various hygiene products is BKC (Kim *et al.*, 2018). BKC is one of the only non-bleach biocides allowed in laundry products as listed in Annex 1 of the Biocidal Products Regulation BPR, No.528/2012 (European Union, 2012). Due to its chemical properties, BKC cannot be incorporated readily into non-ionic surfactant based detergent products. It is significantly less effective in the presence of anionic surfactants, which are required for high performing stain and particulate soil cleaning, and

account for almost all mainstream laundry detergent products (both powders and liquids). Hence, methods are being under investigation to enable the stable incorporation of BKC to laundry products by preventing complexation of the cationic biocide with anionic surfactants, which generally results in precipitation and loss of activity. A specific approach that can be considered is to compartmentalise the BKC though encapsulation. However, as mentioned in Chapter 5, increased concern has risen that BKC released into the environment can lead to antimicrobial resistance and therefore increased infection risks (Russell *et al.*, 1998; Price *et al.*, 2002; Russell, 2002; Langsrud *et al.*, 2003; Karatzas *et al.*, 2007; McMahon *et al.*, 2007; Mc Cay *et al.*, 2010; Kim *et al.*, 2018). Consequently, alternatives to biocides are being investigated to prevent bacterial attachment and biofilm formation in WMs.

One option is the use of surface treatments and coatings that prevent the initial attachment of bacteria or reduce the strength of microbial attachment rendering them easier to remove. Coating of biomedical devices has already proven to be very successful (Danese, 2002; Li *et al.*, 2010; Hook *et al.*, 2012; Hook *et al.*, 2013; Wang *et al.*, 2014; Junter *et al.*, 2016; Magennis *et al.*, 2016; Zaltsman *et al.*, 2017). The potential coating of WMs has the advantage over biomedical devices that specific properties of the antibacterial material need not be considered, such as sustained cell adhesion of permanent implants when devices are integrated into the foreign body (Junter *et al.*, 2016). Currently used materials include chitosan and derivates, although microbial polysaccharides and antimicrobial peptides might become more focussed in the future (Junter *et al.*, 2016). In this study, four different materials were used for the coating of glass disks to investigate anti-attachment properties against *P.* aeruginosa: Poly(2-ethyl-2-oxazoline) 500 (PEOX 500), triblock poly(ethylene oxide) 18-poly(propylene oxide) 62-poly(ethylene oxide) 18 copolymer (Pluronic P-123), poly(ethylene glycol methacrylate 350)-PEG500) 29:1 copolymer (P19), and polydimethylsiloxane (PDMS). All materials have previously been used for other biofilm related studies within the Unilever group. Amongst other things, peg lids were coated with the materials to investigate biofilm formation and oxygen

concentration over time. It was shown that PEOX 500 and P-123 significantly reduced oxygen consumption ($p<0.001$), whereas PDMS significantly increased oxygen consumption over time ($p<0.005$) (Perkins, unpublished).

6.1.2 Aims of this chapter

This chapter aimed to analyse effects of laundry products and formulations on biofilm formation and eradication by addressing the following questions:

- Can the addition of laundry ingredients and full formulations prevent planktonic cell growth and biofilm formation, and can the addition of the ingredients or products to an established biofilm kill the cells?
- Is there a difference between the addition of free BKC compared to silica encapsulated BKC with regards to planktonic cell growth, biofilm formation, and biofilm eradication?
- Can the combination of encapsulated BKC with liquid detergent improve killing effects on biofilms?
- Can we identify materials that can effectively prevent biofilm formation on surfaces to be used as alternative to biocides?

6.2 Results

In this chapter, testing of currently used household laundry products was performed to provide insight into the effectiveness of these products to reduce biofilm formation in WMs and identify areas for future improvement. A liquid detergent, a powder detergent, and a fabric conditioner, provided by Unilever, were tested. Their effects on growth, biofilm formation, and killing of *P. aeruginosa* were assessed using PAO1-N and the WM isolate WMB1.3. The latter has been characterised in Chapter 5 and was chosen for this study to investigate if a WM isolate that was already in contact with washing formulations is better adapted to laundry products compared to the lab strain. The "free" (unencapsulated) biocide BKC was included in this study alongside encapsulated BKC (eBKC) samples provided by Unilever. The samples consist of a silica-based coating to shield the incorporated BKC from the detergent during product manufacture and storage as well as in use during the main wash stage (pre-rinse). In addition, some samples contain a zein protein layer which can be degraded by microbial enzymes to give another protective barrier preventing the BKC from being leaked. The encapsulates are designed to become entrapped in biofilm structures during the wash cycle and be retained after the detergent product has been drained during the water rinse step, which would remove the interfering detergent. Subsequently, the zein protein layer of selected samples would be degraded by microbial enzymes if bacteria or biofilm formation is present, so that the BKC would slowly diffuse out of capsule. As the interfering anionic detergent had been removed by the rinse, the BKC would be available to give optimum antibacterial performance. The samples were supplied as dried powders and the composition of nine different samples of eBKC is shown in Table 6.1.

Table 6.1: Composition of encapsulated BKC samples. The material amount of span 80, glycerol, BKC, 6-amino-fluorescein, zein protein, silica, epoxy-silica, and glutaraldehyde is given in % for each of the eBKC sample A-I.

Material	A	B	C	D	E	F	G	H	I
Span 80 [%]	10.43	9.64	9.63	9.62	10.43	9.64	9.63	9.62	9.62
Glycerol [%]	19.56	18.08	18.06	18.04	19.55	18.07	18.05	18.03	54.09
BKC [%]	39.13	36.15	36.12	36.08	39.11	36.13	36.1	36.06	0
6-amino-fluorescein [%]	0.02	0.02	0.02	0.02	0.02	0.02	0.02	0.02	0.02
Zein protein [%]	0	0	0.1	0.2	0	0	0.1	0.2	0.2
Silica [%]	30.85	28.5	28.48	28.45	30.84	28.49	28.46	28.43	28.43
Epoxy-Silica [%]	0	7.61	7.6	7.59	0	7.6	7.6	7.59	7.59
Glutaraldehyde [%]	0	0	0	0	0.05	0.05	0.05	0.05	0.05
Total [%]	100	100	100	100	100	100	100	100	100

Span 80 is used as emulsification surfactant for the encapsulation synthesis, glycerol is needed as BKC carrier, 6-amino-fluorescein functions as fluorescent tag to allow fluorescence microscopy characterisation of the capsules such as aggregation and rate of leakage, the zein protein serves as a protease responsive capsule, epoxy-silica is a silica capsule precursor, and glutaraldehyde is used as protein cross-linking agent. The main differences lie in the composition of the outer coating: The presence of zein protein, the provision of epoxy-silica, and the availability of glutaraldehyde. eBKC I does not contain any BKC and was included as a negative control to investigate side effects of the capsules.

Under normal conditions, the silica shell is porous and the water soluble BKC will therefore diffuse out of the capsule following dispersion in water. Selected capsules were therefore coated with a low solubility protein (zein) layer to slow BKC leakage into the surrounding medium. The zein was optionally cross-linked with glutaraldehyde to further reduce the water solubility of the

coating. Extracellular biofilm protease enzymes would then degrade the protein coating, providing triggered release of the encapsulated biocide. Critically, this approach would segregate the cationic BKC biocide, protecting it from interaction with and deactivation by anionic surfactants. The protein coating would prevent premature leakage of the biocide during the main wash process (while the detergent was present) and the protease triggered release mechanism would subsequently allow the biocide to be released directly on or within the biofilm allowing optimum efficacy. A schematic overview showing a capsule including the zein protein coating is shown in Figure 6.1.

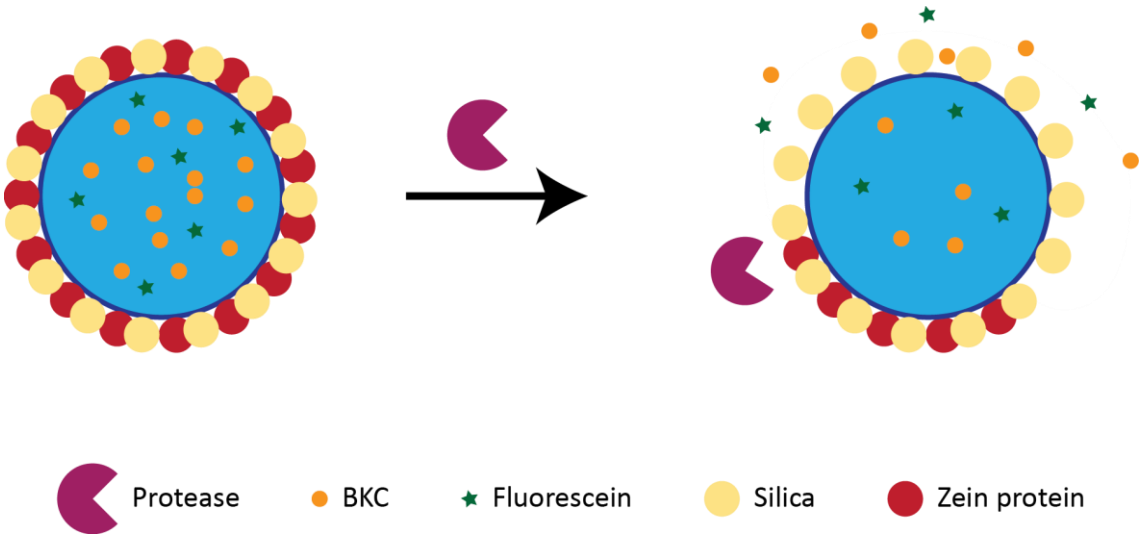


Figure 6.1: Schematic representation of eBKC containing zein protein. Left part: Intact particle, where BKC and fluorescein is encapsulated in a silica-zein matrix. Right part: BKC and fluorescein gets released when the particles come in contact with proteases released by bacteria, which degrade the zein protein.

The eBKC samples were included in the study to explore (i) if BKC can be delivered more efficiently allowing improved performance from low BKC inclusion levels (for fabric conditioners) while minimising environmental loadings, and (ii) if BKC can be allowed to be delivered from anionic based laundry detergent products. Since chemical treatment of bacteria can lead to resistance and non-biocidal approaches to hygiene are of interest as a route to reduce the environmental biocide loading, four different polymers that can be used for surface coating were analysed to investigate whether they could reduce initial attachment of *P. aeruginosa*.

6.2.1 The planktonic growth of *P. aeruginosa* is inhibited by the addition of powder detergent

Firstly, the effects of household laundry products on the planktonic growth of the *P. aeruginosa* lab strain PAO1-N and the WM isolate WMB1.3 was assessed (Figure 6.2). The base formulations of the products can be found in Appendix A. A growth measurement over 18 h in 96-well plates was performed to detect growth effects on PA01-N and WMB1.3 caused by a liquid detergent (LD, UK Persil Non-Bio, 2.9 mg mL-^{1}), a powder detergent (PD, UK Persil Non-Bio, 1 mg mL^{-1}), or a fabric conditioner (FC, UK Comfort, 2.9 mg mL^{-1}) in liquid culture (M9S, 2.16.10). The given concentrations were chosen in collaboration with Unilever, and the concentrations reflect the typical product dosages under EU conditions and resulting “in wash” product concentrations for conventional UK front loader WMs. If not otherwise stated, the same concentrations were used throughout the whole study.

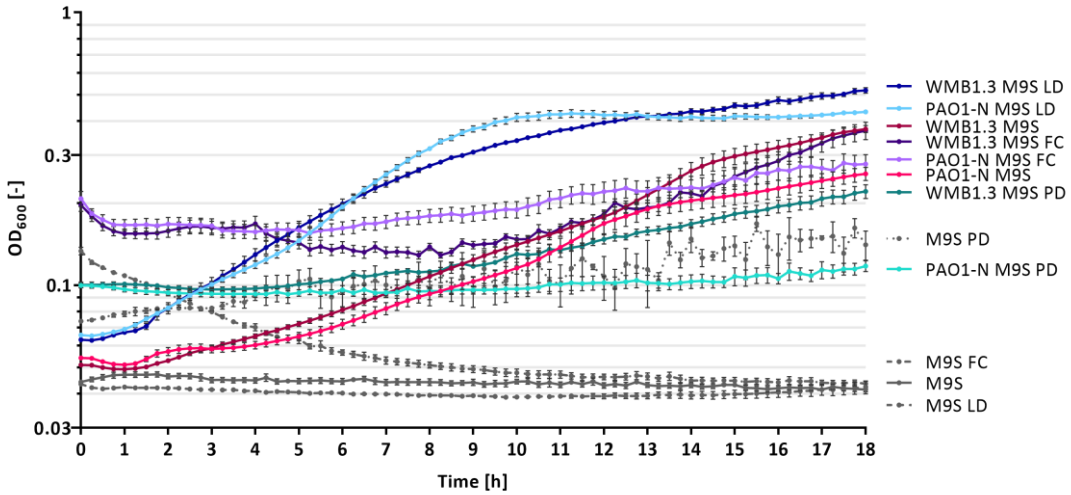


Figure 6.2: The addition of powder detergent reduces the growth of PAO1-N and WMB1.3 in M9S whereas liquid detergent and fabric conditioner only have minimal effects. PAO1-N and WMB1.3 were inoculated into a 96-well plate at an OD_{600} of 0.05 in M9S containing liquid detergent (LD, 2.9 mg mL^{-1}), powder detergent (PD, 1 mg mL^{-1}) or fabric conditioner (FC, 2.9 mg mL^{-1}). The OD_{600} was measured automatically every 15 min at 37°C and is shown on a log scale against time. No path length correction was applied. Error bars represent standard error, where n = 3x6.

Comparing the growth between the two strains, differences were observed for all conditions after 18 h, with a slightly elevated growth for samples grown in M9S LD. However, these changes are not considered biologically relevant and the differences may be a reflection of the high number of replicates. Additionally, samples with the addition of laundry products had a higher starting OD_{600} that is likely to be attributed to the background solution turbidity due to the formulation than bacterial growth. The OD_{600} of the fabric conditioner-containing sample reduced over time in the control without bacteria, culminating in a clear medium after ~11 h. M9S FC samples inoculated with bacteria showed growth starting after ~9 h; growth before that time point was presumably masked by the high starting OD_{600}. For PAO1-N, no growth was observed in M9S PD over the whole period, whereas WMB1.3 still showed slight growth at the end when powder detergent was added. However, due to the changes in OD as a consequence of product additions, interpretation of the growth data was difficult.

6.2.2 The addition of powder and liquid detergent to cells of *P. aeruginosa* can reduce biofilm formation, both in a static and a flow-cell model

Microorganisms located in a biofilm exhibit higher metabolic functional diversity and metabolic cooperation than those living in planktonic form (Tribedi *et al.*, 2015). Furthermore, the extracellular matrix of the biofilm provides an increased tolerance against antibiotics and a protection against disruptive forces. Therefore, it is crucial that biocidal effects shown for planktonic cells are also assessed in biofilm models. To do so, static biofilms of PAO1-N and WMB1.3 were grown in 8-well glass bottom chambers for 48 h at 37°C with the addition of laundry products to analyse effects on biofilm formation (2.18.1). After incubation, the cells were stained with SYTO 9 and propidium iodide (PI) using the LIVE/DEAD™ BacLight™ Bacterial Viability Kit (Thermo Fisher Scientific). The green dye, SYTO 9, is membrane permeable and stains all cells, living and dead, whereas the red dye, PI, can only pass through damaged membranes where it subsequently displaces SYTO 9 due to its higher affinity to DNA (Stocks, 2004). Hence, live bacteria, or bacteria with intact membranes, fluoresce green whereas bacteria with permeable membranes fluoresce red and are considered dead. All biofilms were imaged using CLSM. Quantification of the images was performed using ImageJ to count the live and dead cells of each sample (Figure 6.3).

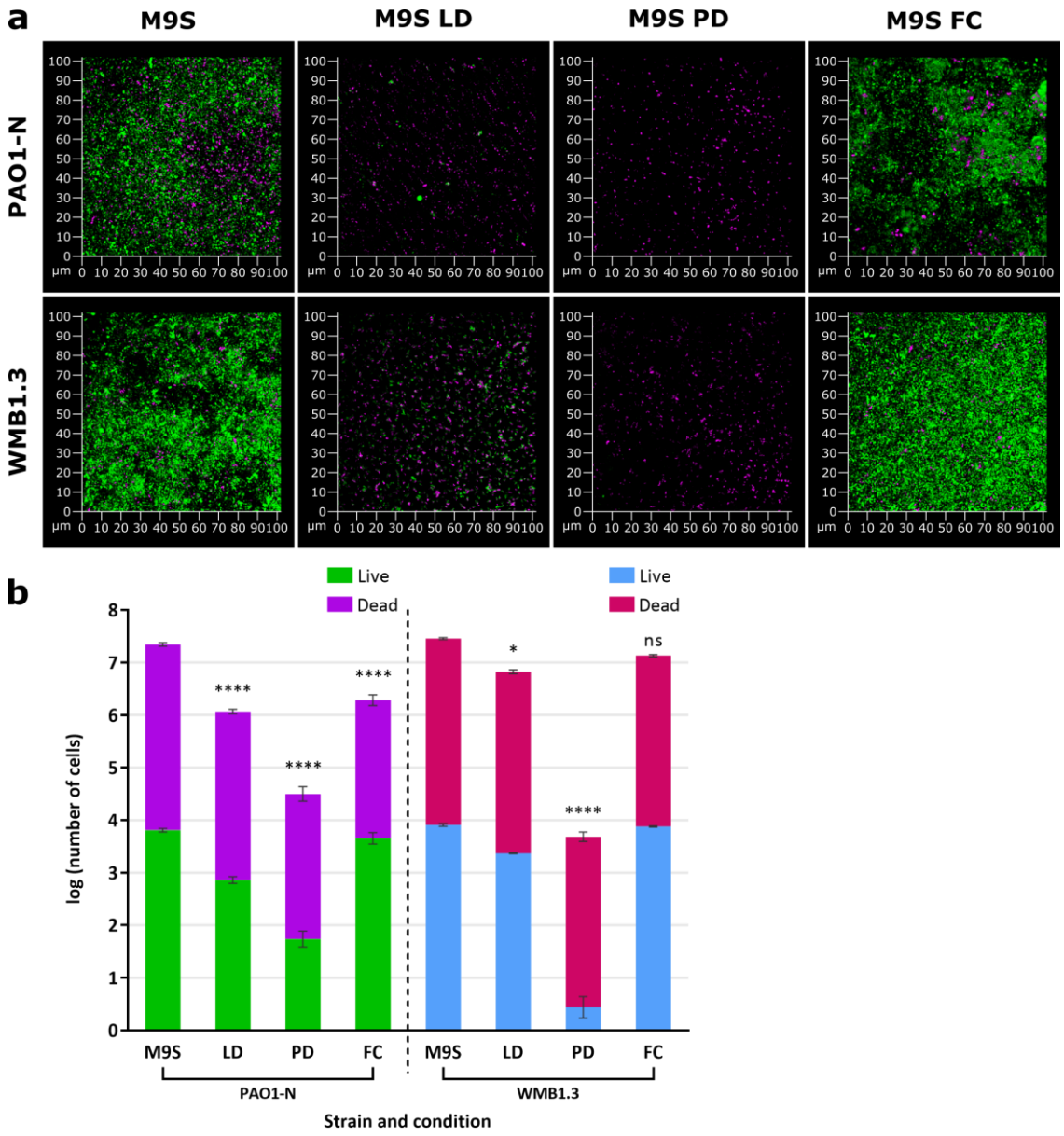


Figure 6.3: Representative images of PAO1-N and WMB1.3 show reduced biofilm formation when grown statically in M9S LD or PD, whereas no difference is apparent for the addition of FC. (a) PAO1-N (top panel) and WMB1.3 (bottom panel) were inoculated into an 8-well glass bottom chamber at an OD_{600} of 0.05 in M9S containing no supplement, liquid detergent (LD, 2.9 mg mL^{-1}), powder detergent (PD, 2 mg mL^{-1}), or fabric conditioner (FC, 2.9 mg mL^{-1}). The cells were incubated at 37°C under static conditions for 48 h. Live cells were stained with SYTO 9 (green) and dead cells with PI (magenta). Z-stack images were taken with a Zeiss CLSM using a 63x objective and 3D top view images are presented. **(b)** Biofilm images were quantified by counting live (lower bars, PAO1-N green, WMB1.3 blue) and dead (upper bars, PAO1-N purple, WMB1.3 pink) cells of the individual channels (SYTO 9 and PI) using ImageJ. The logarithm of the number of cells is shown against the bacterial strains grown in M9S containing liquid detergent (LD), powder detergent (PD) or fabric conditioner (FC). Error bars represent standard error measured for different biofilm images, where n = 6. Statistical difference was calculated using the total cell numbers, with $p<0.5$ = *, $p<0.0001$ = ****, ns = not significant (ordinary one-way ANOVA test).

The total number of cells and hence biofilm formation was reduced when liquid or powder detergent was present in the growth medium for both strains, PAO1-N and WMB1.3, with powder detergent being more effective than liquid detergent. Furthermore, the effect of the powder detergent appeared to be more pronounced for the WM isolate WMB1.3 compared to the lab strain PAO1-N. In addition, the proportion of live cells differs between samples and strains, with 65% and 70% for M9S, 31% and 45% for M9S LD, 10% and 0.2% for M9S PD, and 90% and 81% for M9S FC for PAO1-N and WMB1.3 respectively. This is interesting as for the addition of fabric conditioner to PAO1-N, the number of total cells was significantly reduced ($p<0.0001$, ordinary one-way ANOVA test), while the proportion of live cells was simultaneously higher compared to medium alone.

To verify the results obtained using CLSM and image quantification, colony forming unit (CFU) experiments were undertaken (2.18.4). The biofilms were grown under the same conditions as before with the exception that 24-well cell culture treated plates (Thermo Fisher Scientific, Nunc™ Cell-Culture Treated) were used to increase the number of replicates in one experiment. After 48 h of incubation, the cells were resuspended in PBS, diluted, and plated onto LB agar plates. The number of colonies grown after 24 h at 37°C was counted and the CFUs per mL were calculated (Figure 6.4).

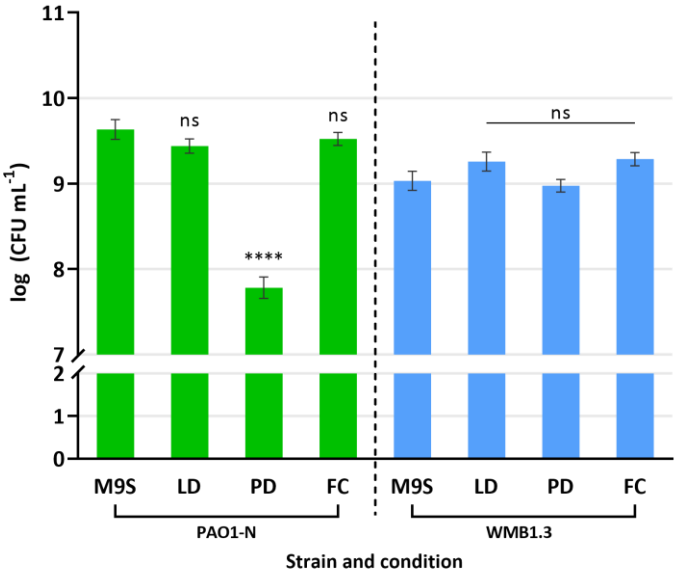


Figure 6.4: CFUs of PAO1-N and WMB1.3 biofilms show a reduction in viable cells for PAO1-N biofilms grown in M9S powder detergent under static conditions. PAO1-N (green) and WMB1.3 (blue) were inoculated into a 24-well plate at an OD_{600} of 0.05 in M9S containing liquid detergent (LD, 2.9 mg mL^{-1}), powder detergent (PD, 2 mg mL^{-1}), or fabric conditioner (FC, 2.9 mg mL^{-1}). After 48 h of static incubation at 37°C, cells were resuspended and dilutions plated onto LB plates. The number of CFUs was counted after 24 h and is shown against bacterial strains and conditions. Error bars represent standard error, where n = 3x6, with p<0.0001 = ****, ns = not significant (non-parametric Mann-Whitney test).

A significant reduction in CFUs was observed for PAO1-N treated with powder detergent ($p<0.0001$, non-parametric Mann-Whitney test). All other conditions contained comparable numbers of viable cells, with strain WMB1.3 CFUs being generally lower than those of PAO1-N.

In addition to the static biofilm model, the BioFlux flow-cell system was used to analyse biofilm formation since this would mimic conditions in a WM more closely (2.18.2). After seeding of the bacteria, a constant flow of media with LIVE/DEAD staining and different laundry products was applied for 24 h before the biofilms were imaged using CLSM and quantified using ImageJ (Figure 6.5).

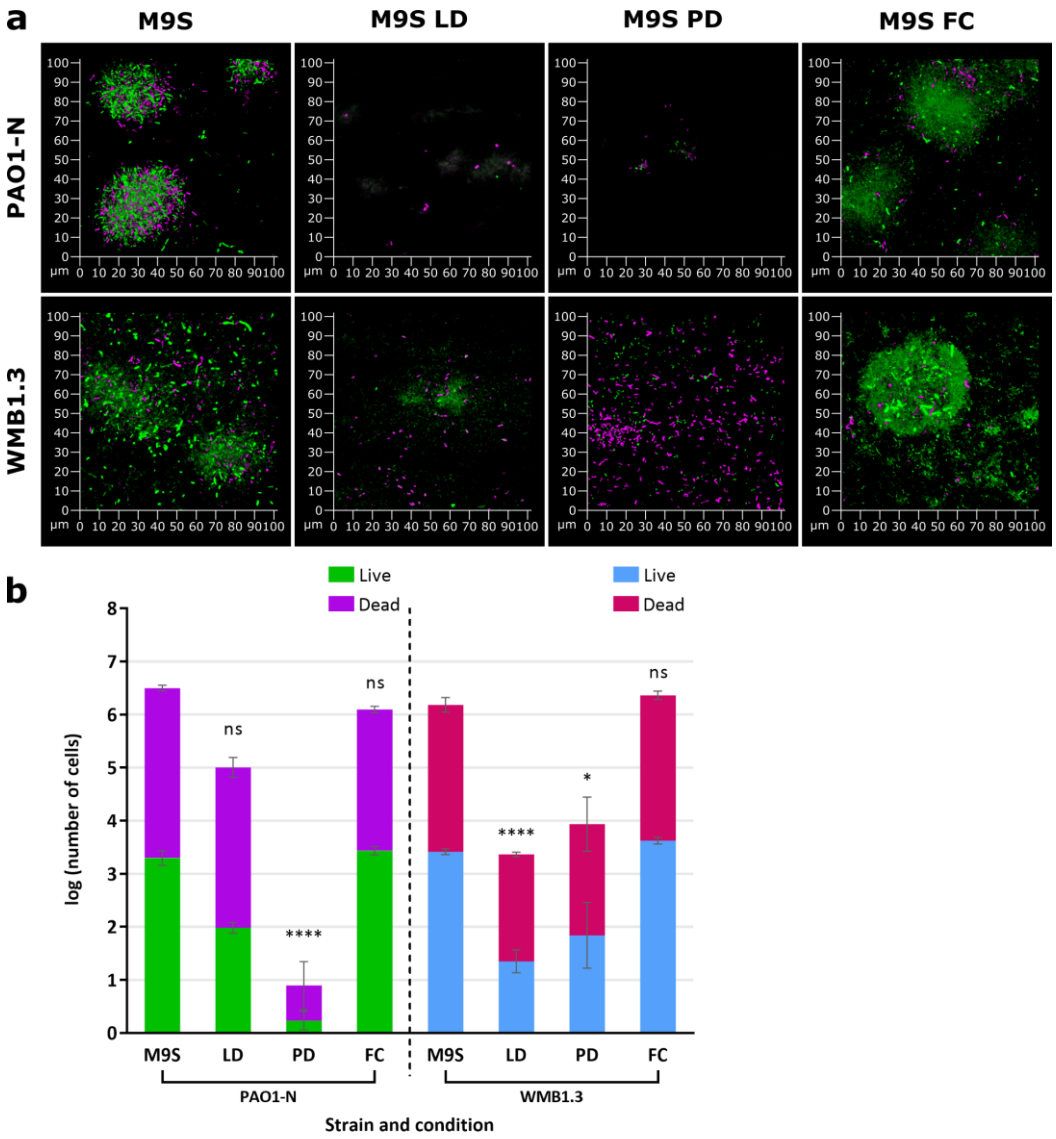
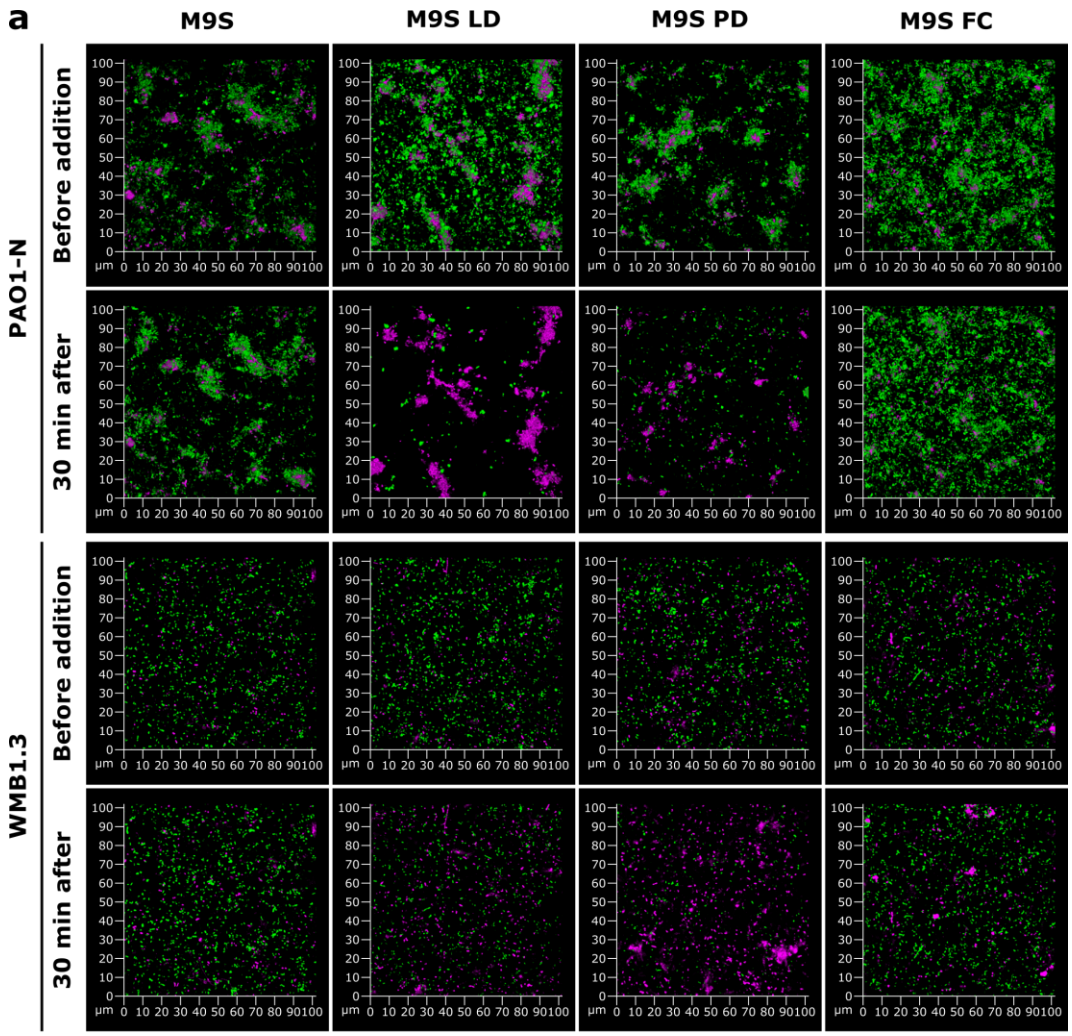


Figure 6.5: Representative images of PAO1-N and WMB1.3 show reduced biofilm formation when grown in M9S with liquid or powder detergent in a flow-cell system whereas no reduction is shown for the addition of fabric conditioner. (a) PAO1-N (top panel) and WMB1.3 (bottom panel) were inoculated into a 48-well BioFlux flow-cell plate at an OD_{600} of 0.05 in M9S containing no supplement, liquid detergent (2.9 mg mL^{-1}), powder detergent (2 mg mL^{-1}), or fabric conditioner (2.9 mg mL^{-1}). The cells were incubated at 37°C under static flow of 0.25 dyn cm^{-2} for 24 h. Live cells were stained with SYTO 9 (green) and dead cells with PI (magenta). Z-stack images were taken with a Zeiss CLSM using a 63x objective and 3D top view images are presented. **(b)** Biofilm images were quantified by counting live (lower bars, PAO1-N green, WMB1.3 blue) and dead (upper bars, PAO1-N purple, WMB1.3 pink) cells of the individual channels (SYTO 9 and PI) using ImageJ. The logarithm of the number of cells is shown against the bacterial strains grown in M9S containing liquid detergent (LD), powder detergent (PD), or fabric conditioner (FC). Error bars represent standard error measured for different biofilm images, where n = 6. Statistical difference was calculated using the total cell numbers, with $p<0.05$ = *, $p<0.0001$ = ****, ns = not significant (ordinary one-way ANOVA test).

A clear reduction in biofilm formation in the presence of liquid and powder detergent was observed, with the reduction being most pronounced for PAO1-N with the powder detergent. No biofilm reduction was observed with the fabric conditioner for any of the two strains. Comparing both strains with each other, WMB1.3 was less affected by the powder detergent, resulting in more cells overall, both live and dead, compared to PAO1-N under the same conditions. Furthermore, as already described for the static model, the proportion of live cells for PAO1-N grown in M9S FC (85%) was higher than for the control grown in M9S (55%). No CFU counting could be performed because of technical barriers using the BioFlux flow-cell system.

6.2.3 Addition of powder and liquid detergent to an established biofilm affects cells of *P. aeruginosa*

To investigate if laundry products have effects on already established biofilms, biofilms were grown in plain M9S for 48 h under static conditions before liquid detergent, powder detergent, or fabric conditioner was added to the biofilms. The biofilms were stained with LIVE/DEAD staining and imaged before the addition as well as every 5 minutes after the addition of the laundry products for 30 min using CLSM. For the quantification, the percentage of live cells in each condition and each replicate was taken and normalised to the value before the addition of that specific sample. That way, each sample starts with a value of 1 for live cells before the addition of laundry products. This is to reduce variation that exists between individual biofilms (Figure 6.6).


a
M9S
M9S LD
M9S PD
M9S FC
PAO1-N
WMB1.3
Before addition
30 min after
μm 0 10 20 30 40 50 60 70 80 90100

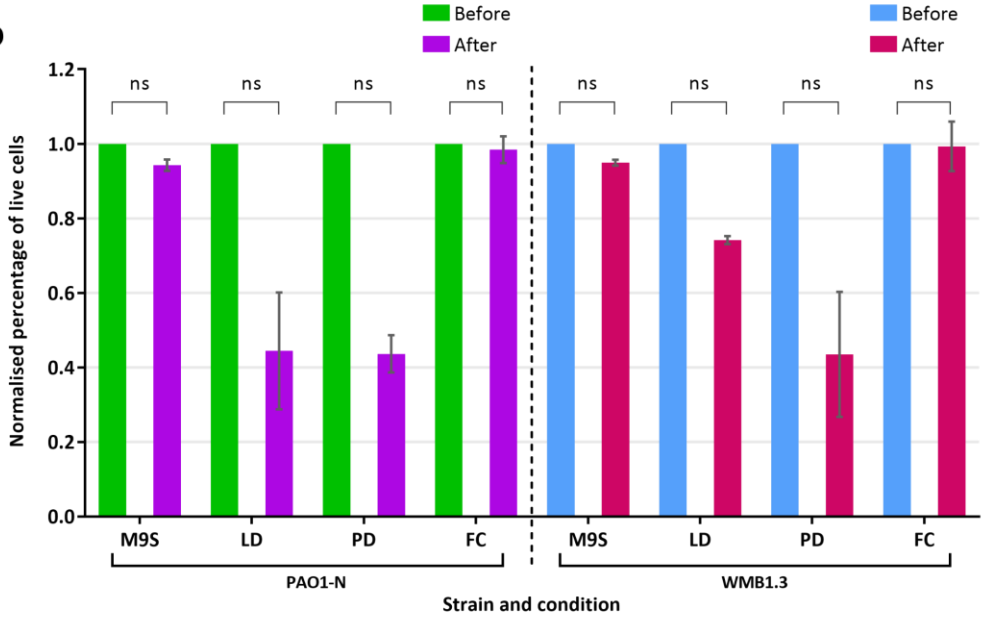

b
Before
After
Before
After
ns
Normalised percentage of live cells
0.0
0.2
0.4
0.6
0.8
1.0
1.2
M9S
LD
PD
FC
PAO1-N
WMB1.3
Strain and condition

Figure 6.6: Representative images of PAO1-N and WMB1.3 show liquid or powder detergent added to established biofilms kill bacteria, whereas fabric conditioner does not. (a) PAO1-N (top panel) and WMB1.3 (bottom panel) were inoculated into an 8-well glass bottom chamber at an OD_{600} of 0.05 in M9S. The cells were incubated at 37°C under static conditions for 48 h. Live cells were stained with SYTO 9 (green) and dead cells with PI (magenta). Images presented were taken before the addition (top) and 30 min after the addition (bottom) of M9S containing no supplement, liquid detergent, powder detergent, or fabric conditioner to the established biofilms to give a final concentration of 2.9 mg mL^{-1} (LD and FC) or 2 mg mL^{-1} (PD). Z-stack images were taken with a Zeiss CLSM using a 63x objective and 3D top view images are presented. **(b)** Biofilm images of PAO1-N and WMB1.3 were quantified by counting live and dead cells of the individual channels (SYTO 9 and PI) using ImageJ before (PAO1-N green, WMB1.3 blue) and after (PAO1-N purple, WMB1.3 pink) the addition of M9S with liquid (LD), powder (PD), or fabric conditioner (FC). The normalised percentage of live cells before and after the addition is shown against the conditions. Error bars represent standard error measured for different biofilm images, where n = 2, with ns = not significant (non-parametric Mann-Whitney test).

No detectable change was observed for either strain PAO1-N or WMB1.3 when M9S or fabric conditioner was added to established biofilms. In contrast, looking at PAO1-N, the addition of M9S LD and M9S PD both resulted in a reduction of the proportion of live cells after 30 min up to a 0.4-fold change. This change was also observed for the addition of M9S PD to biofilms of WMB1.3. However, no killing activity was detected for WMB1.3 with the addition of M9S LD. All changes were not statistically significant based on a non-parametric Mann-Whitney test, likely because of the low number of replicates (n=2).

CFU experiments were performed to confirm the results obtained using CLSM. The experimental set up was the same as before, where biofilms of both strains were grown for 48 h before M9S containing laundry products was added to the biofilms. After 30 min, the cells were suspended in PBS, diluted, and spotted onto LB plates. After 24 h of incubation, the colonies were counted and the CFUs per mL were calculated (Figure 6.7).

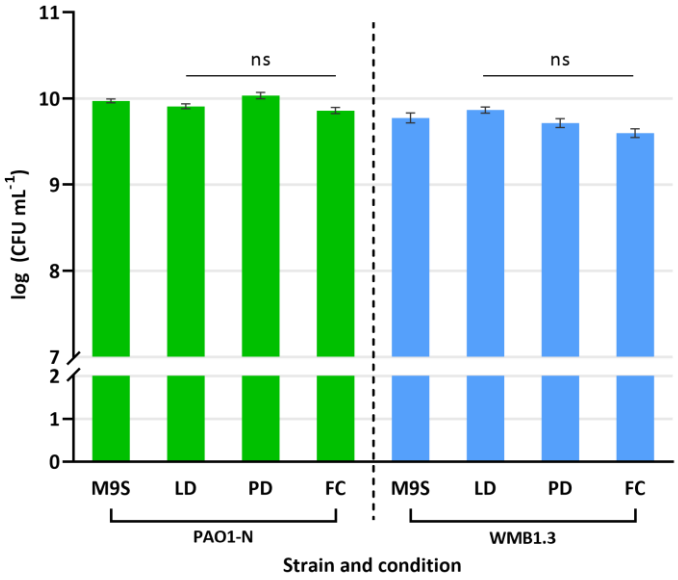


Figure 6.7: CFUs of PAO1-N and WMB1.3 biofilms reveal that bacterial viability in established biofilms is not altered by the addition of laundry supplements. PAO1-N (green) and WMB1.3 (blue) were inoculated into a 24-well plate at an OD_{600} of 0.05 in M9S. After 48 h of static incubation at 37°C, cells were treated with liquid detergent, powder detergent, or fabric conditioner for 30 min to give a final concentration of 2.9 mg mL^{-1} (LD and FC) or 2 mg mL^{-1} (PD). Subsequently, cells were resuspended and dilutions plated onto LB plates. The number of CFUs was counted after 24 h and is shown against bacterial strains and conditions. Error bars represent standard error, where n = 3x6, with ns = not significant (non-parametric Mann-Whitney test).

In contrast to the observations using CLSM, no significant difference in CFUs was detected between the addition of medium compared to the laundry products to established biofilms of PAO1-N or WMB1.3.

After the analysis of the data sets, discrepancies existed between both chosen methods, CLSM and CFUs, to investigate the viability of the cells under the given conditions. Therefore, the BacTiter-Glo™ Microbial Cell Viability Assay (Promega, 2019) was performed on an overnight culture of PAO1-N to further explore if the addition of laundry products to cells can impede the viability of the bacteria (2.17). After normalising the OD_{600} to 1, the laundry products were added to the planktonic cells for 30 min. Following the incubation, the cell viability assay kit was used to measure the adenosine triphosphate (ATP) present by looking at the luminescence. ATP is used as an indicator for metabolically active cells. The luminescence signal is proportional to the

ATP present and hence proportional to the number of viable cells in culture. Therefore, less luminescence signal means less ATP, and therefore less viable cells within the sample (Figure 6.8).

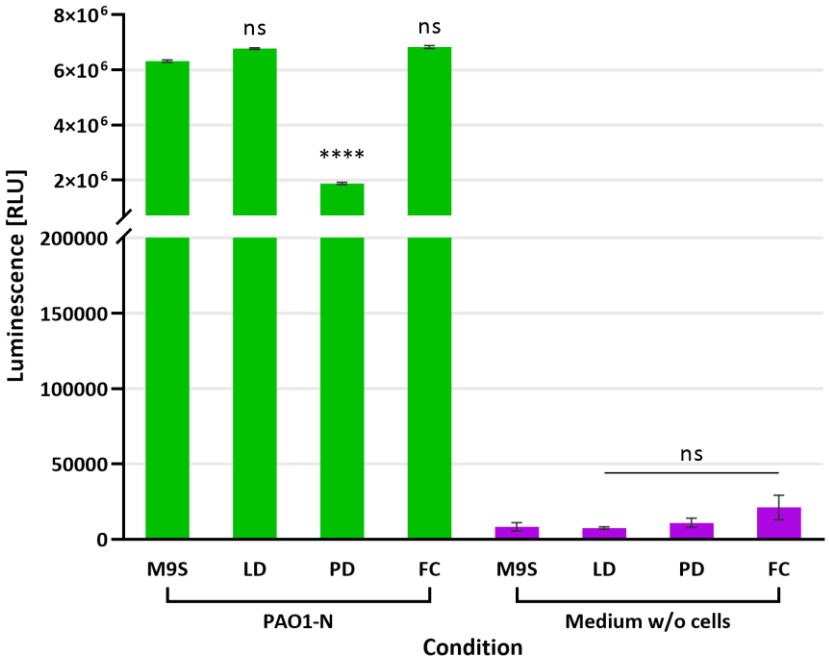


Figure 6.8: Fewer viable planktonic PAO1-N cells detected following exposure to powder detergent. PAO1-N was inoculated into a 1 mL centrifuge tube at an OD_{600} of 1 in M9S containing no supplement, liquid detergent (LD, 2.9 mg mL^{-1}), powder detergent (PD, 2 mg mL^{-1}), or fabric conditioner (FC, 2.9 mg mL^{-1}). After 30 min of static incubation at room temperature, 100 µL of cells were used for the viability assay in a 96-well plate and luminescence was recorded using a Tecan plate reader. The luminescence intensity is shown against conditions. Error bars represent standard error, where n = 6 for PAO1-N and n = 3 for medium without cells, with $p<0.0001$ = ****, ns = not significant (ordinary one-way ANOVA test).

The luminescence intensity was significantly lower ($p<0.0001$, ordinary one-way ANOVA test) for the sample where M9S powder detergent was added compared to the control sample with M9S, indicating less viable cells after 30 min. For both other conditions, the addition of M9S LD and M9S FC, no significant reduction in metabolic activity of cells could be observed. Controls consisting of the different media without cells confirmed minimal background luminescence in this assay. Overall, these results showed fewer effects than observed by CLSM, where both liquid and powder detergent showed effects after 30 min, but more effects than noted by CFU

experiments, where no differences were observed for any of the additions. Hence, further investigation was needed to find out why the LIVE/DEAD staining showed a bigger effect of the laundry products on biofilm formation compared to other methods. To exclude the possibility of a direct interaction between the dyes used for staining (SYTO 9 and PI) with the laundry products, medium was prepared without dyes, with single dyes, and with both dyes and was mixed with liquid detergent, powder detergent, or fabric conditioner. Subsequently, the green (SYTO 9) and red (PI) fluorescence intensity was measured for each sample (Figure 6.9).

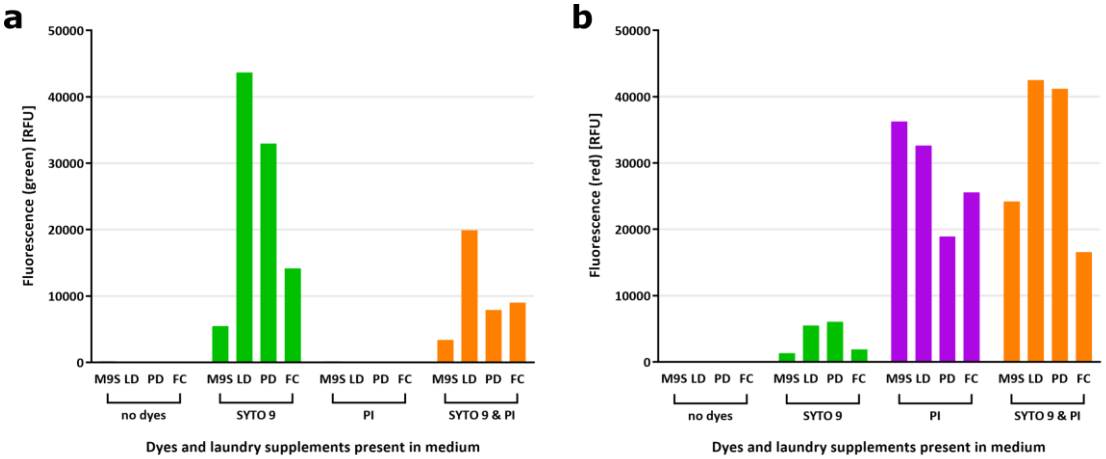


Figure 6.9: Fluorescence intensity measurement shows SYTO 9 and PI fluorescence for medium with and without laundry supplements. Medium containing no supplement, liquid detergent (LD, 2.9 mg mL^{-1}), powder detergent (PD, 2 mg mL^{-1}), or fabric conditioner (FC, 2.9 mg mL^{-1}) was supplemented with SYTO 9 (green), PI (purple), or both dyes simultaneously (orange) and 200 µL were used to measure fluorescence intensity using a Tecan plate reader at room temperature. The fluorescence intensity is shown against conditions. **(a)** Fluorescence intensity of SYTO 9 (green fluorescence, 480 nm/515 nm). **(b)** Fluorescence intensity of PI (red fluorescence, 490 nm/635 nm).

When no dyes were present in the medium, neither green nor red fluorescence was detected for any of the conditions, excluding the possibility of background fluorescence from the laundry products. With SYTO 9 present, green as well as some red fluorescence was measured, but the red fluorescence intensity was very low. The green fluorescence was much higher for the medium containing liquid detergent or powder detergent and slightly increased for M9S FC compared to the control with just M9S. No green fluorescence was detected in any of the media where only PI was present, as expected, whereas red fluorescence was measured in all four

samples. When both dyes were added to the medium, both green and red fluorescence was detected. The overall signal intensity for the green fluorescence was higher when only SYTO 9 was present compared to both dyes. This was not the case for the red fluorescence intensity.

Additionally, a detailed analysis of the images taken after addition of the liquid and powder detergent to the established biofilm of PAO1-N was performed to investigate which cells are stained with SYTO 9 (green), PI (magenta), or not stained at all over time. Images taken before the addition and every 10 min after the addition were chosen and the staining of the cells was investigated including the brightfield channel to have an overview about the total cells present. Representative images using liquid detergent are shown in Figure 6.10.

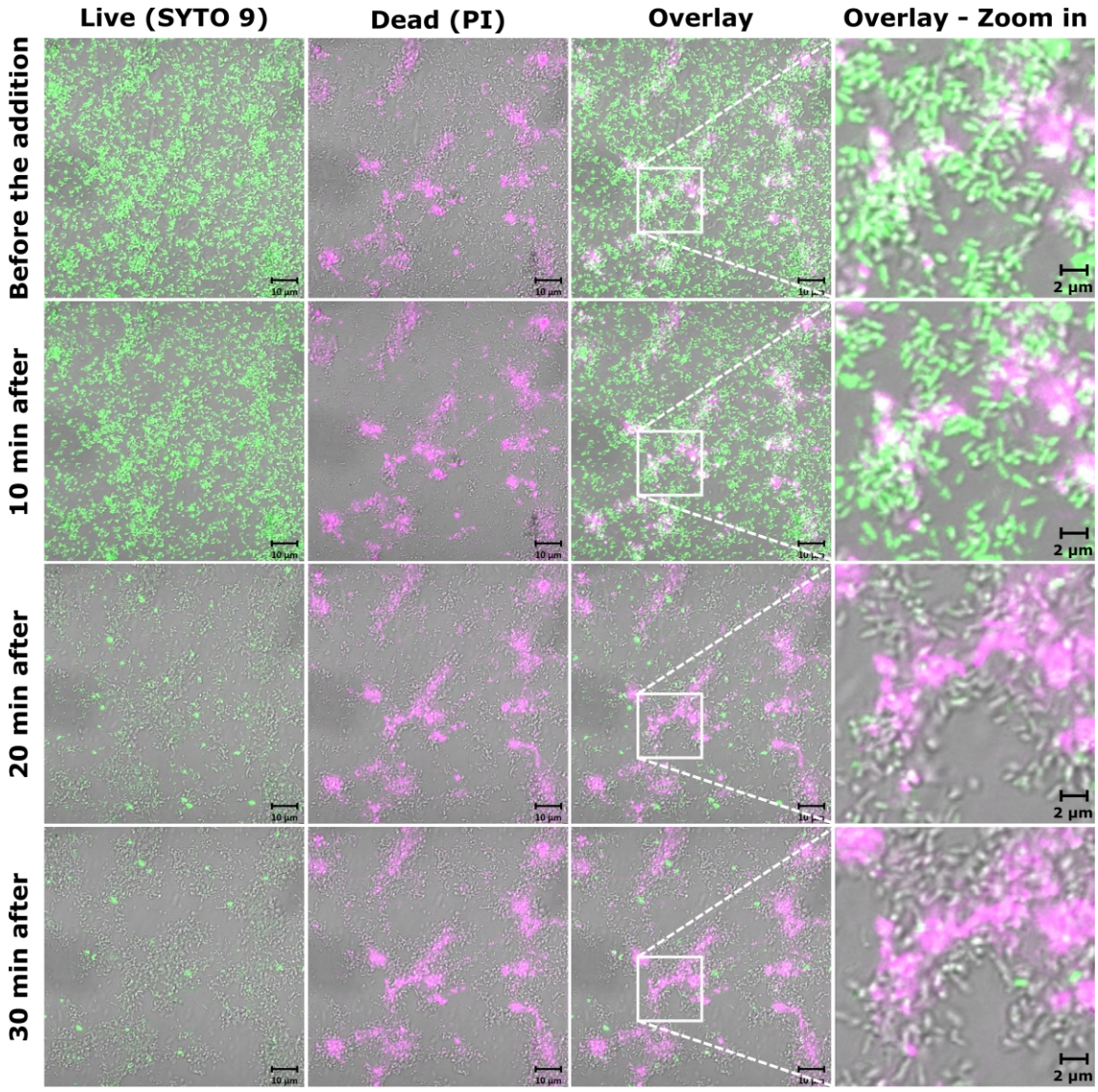


Figure 6.10: Representative images of PAO1-N cells stained with SYTO 9 show loss of fluorescence signal over time when liquid detergent is added to the cells. PAO1-N was inoculated into an 8-well glass bottom chamber at an OD_{600} of 0.05 in M9S. The cells were incubated at 37°C under static conditions for 48 h. Live cells were stained with SYTO 9 (green) and dead cells with PI (magenta) and images were taken with a Zeiss CLSM and a 63x objective. M9S containing liquid detergent was added to the established biofilm to give a final concentration of 2.9 mg mL^{-1} and imaged every 5 min over a period of 30 min. Representative 2D images before the addition as well as 10 min, 20 min, and 30 min after the addition are presented. Right panel shows a zoom-in view of the square indicated in the overlay images.

Before the addition of liquid detergent, most cells were stained with SYTO 9 (green, live) and some cells, mostly clustered, were stained with PI (magenta, dead). Looking at the zoom-in, no cells could be detected that are not stained. The same could be seen 10 min after the addition of the liquid detergent to the biofilm. However, at the later time points, the same cells as before

were stained with PI, but fewer cells were stained with SYTO 9. Instead, a lot of cells were not stained at all as seen in the zoom-in images. That means that the overall number of cells stained with PI stayed the same, but the number of cells stained with SYTO 9 decreased markedly over time. These cells were not stained with PI instead but stayed unstained. The same was observed for the addition of powder detergent but less pronounced (Appendix A).

In summary, the addition of both powder and liquid detergent to established biofilms can reduce the number of live cells, with WMB1.3 showing slightly increased. However, observations differ between methods, with LIVE/DEAD staining revealing more effects than CFU counting. Further examination of these discrepancies between methods showed effects of the laundry products on the staining ability of the dyes, which needs more extensive investigation.

6.2.4 Free BKC prevents biofilm formation of *P. aeruginosa* more than encapsulated BKC

BKC is one of the biocides commonly used in hygiene products, mainly in hard surface cleaning products. However, it cannot be easily incorporated into laundry detergents due to charge interactions with anionic surfactants that reduces its biocidal action. Furthermore, there are concerns that the release of BKC into the environment can result in antimicrobial resistant bacteria (Russell, 1998; Russell, 2002; Langsrud *et al.*, 2003; McMahon *et al.*, 2007; Mc Cay *et al.*, 2010). Chapter 5 also revealed increased BKC resistance of some *P. aeruginosa* strains isolated from WMs compared to PAO1-N. In this chapter, BKC was compared to different versions of encapsulated BKC to assess their relative abilities to prevent planktonic growth and biofilm formation or kill bacteria in an already established biofilm. The concentration of the eBKC samples were adjusted so that the BKC concentration was the same as the free BKC (0.2 mg mL^{-1}). The chosen BKC concentration was based on previous studies investigating the minimal concentration to remove already established biofilms of *P. aeruginosa* performed by Unilever and was therefore much higher than the MIC observed in Chapter 5 (60 mg L^{-1}). In addition to the usual control without addition (M9S), a control for the eBKC samples was added,

which consisted of the empty capsule without BKC incorporated (eBKC I). Due to the low availability of eBKC samples, the experiments were only performed using strain PAO1-N.

To look at effects on planktonic growth, cells were grown in 96-well plates and the OD_{600} was measured every 15 min for 22 h using a Tecan plate reader (Figure 6.11). Two separate graphs were prepared as the experiments were performed under slightly different conditions, where the lid of the 96-well plate was removed for the experiment with unencapsulated BKC but not for the eBKC, resulting in slight path differences of the readings.

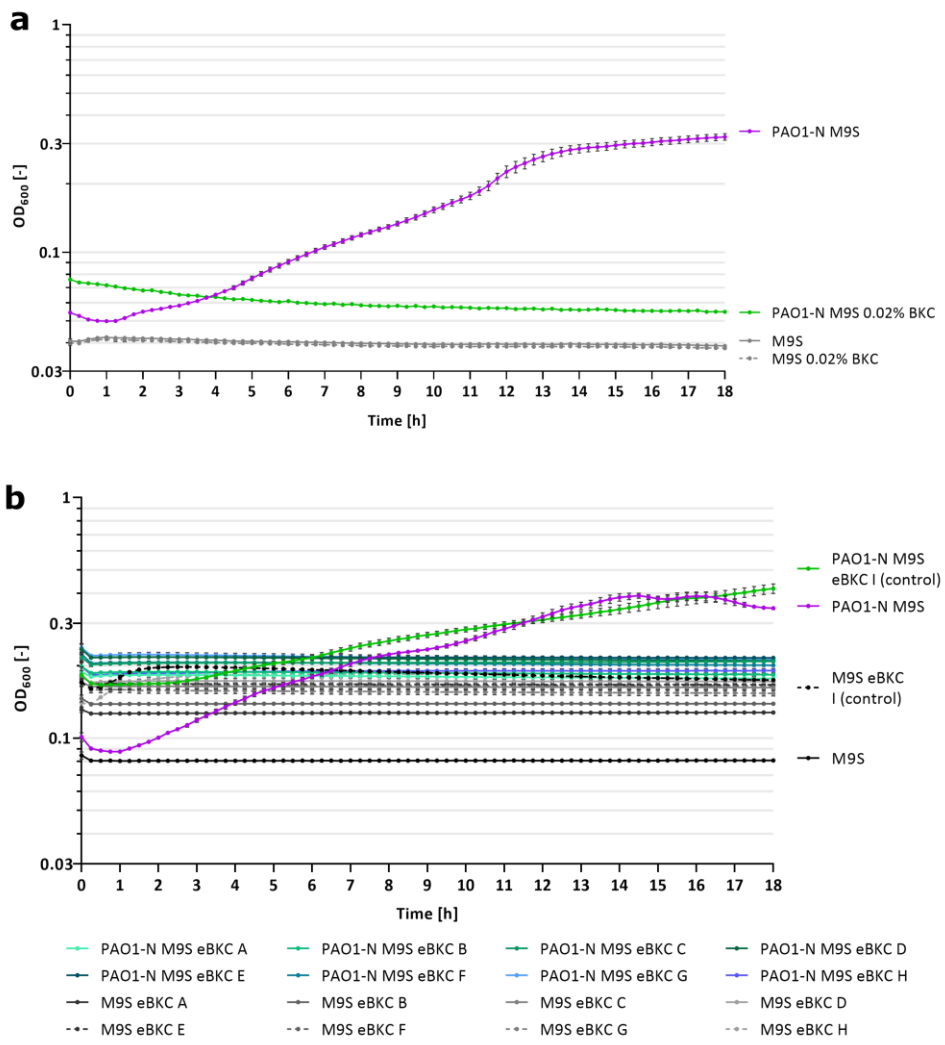


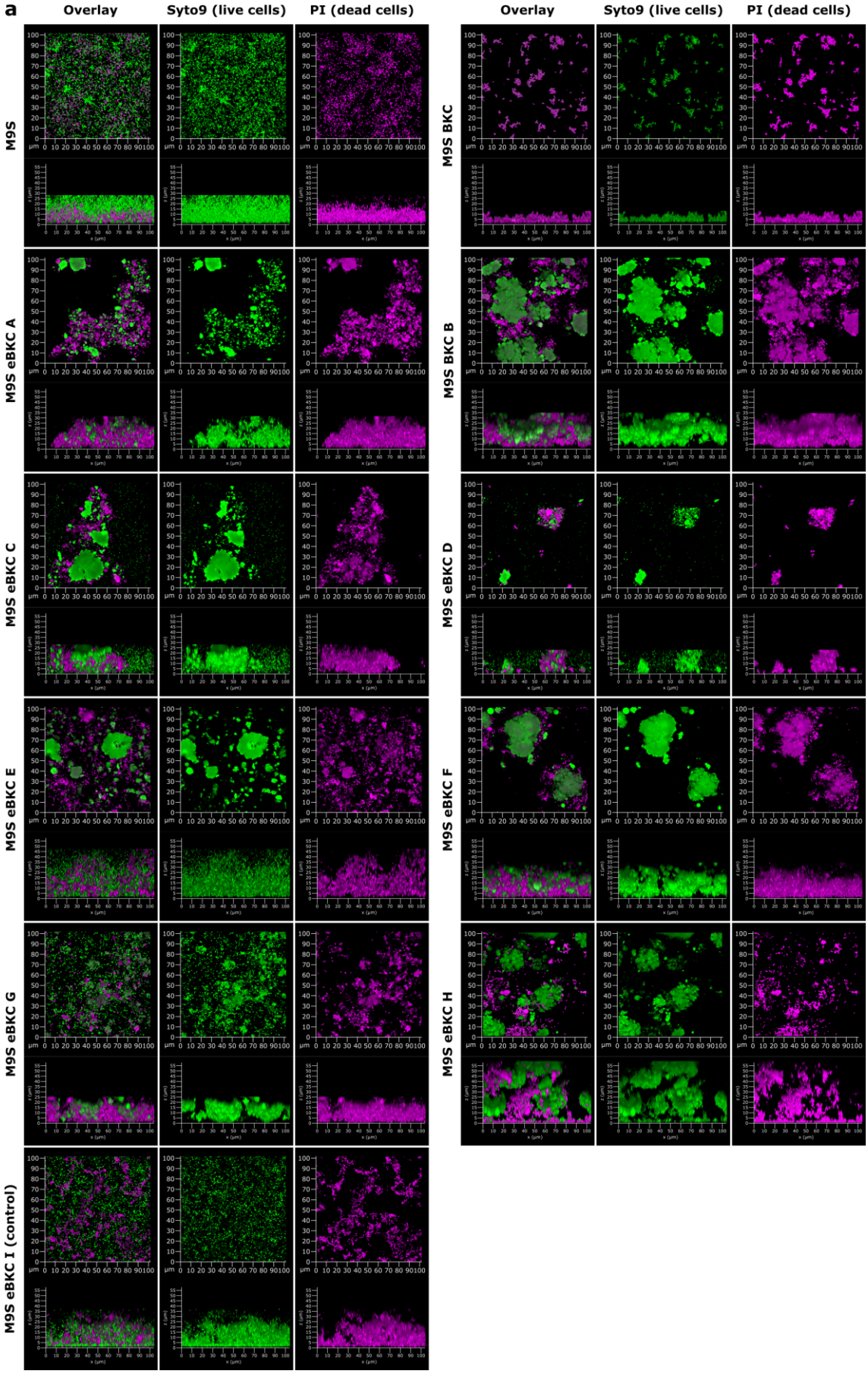
Figure 6.11: Addition of free BKC or eBKC A-H prevents the growth of PAO1-N in M9S, whereas the addition of eBKC I (control without BKC) shows normal growth. PAO1-N was inoculated into a 96-well plate at an OD_{600} of 0.05 in M9S containing free BKC or different samples of eBKC. The OD_{600} was measured automatically every 15 min at 37°C and is shown on a log scale against time. No path length correction was applied. Error bars represent standard error, where n = 3x7 for free BKC and n = 3x8 for eBKC samples. **(a)** Free BKC (0.2 mg mL^{-1}). **(b)** eBKC (0.51 mg mL^{-1} for A and E, 0.55 mg mL^{-1} for B-D and F-I).

The addition of free BKC as well as all eBKC samples led to complete inhibition of cell growth over the whole time period with the exception of eBKC I, the negative control, which grew normally. The overall OD_{600} for controls with eBKC and no cells was slightly higher than the M9S alone, likely because of the formulations of the eBKC.

As presented in Table 6.1, all eBKC samples contain 0.02% 6-amino-fluorescein, which fluoresces in green (490 nm/525 nm). Therefore, any interference with the LIVE/DEAD staining was

excluded before conducting further imaging experiments. To do this, biofilms were grown with selected samples of eBKC for 48 h and bacteria were stained with PI. Using CLSM, no green fluorescence was observed, indicating that the fluorescein dye cannot be detected in the sample (Appendix D). Hence, LIVE/DEAD staining including the green dye SYTO 9 to stain live cells could be used for experiments containing eBKC.

To compare the effects between different eBKC samples and free BKC on biofilm formation, PAO1-N biofilms were grown statically with the addition of free BKC or eBKC for 48 h, stained with SYTO 9 and PI and imaged using CLSM. Overlay images with SYTO 9 and PI as well as the individual images were chosen to highlight differences between samples. Representative images and the quantification can be found in Figure 6.12.


a
Overlay
Syto9 (live cells)
PI (dead cells)
M9S
M9S BKC
M9S eBKC A
M9S BKC B
M9S eBKC C
M9S eBKC D
M9S eBKC E
M9S eBKC F
M9S eBKC G
M9S eBKC H
M9S eBKC I (control)

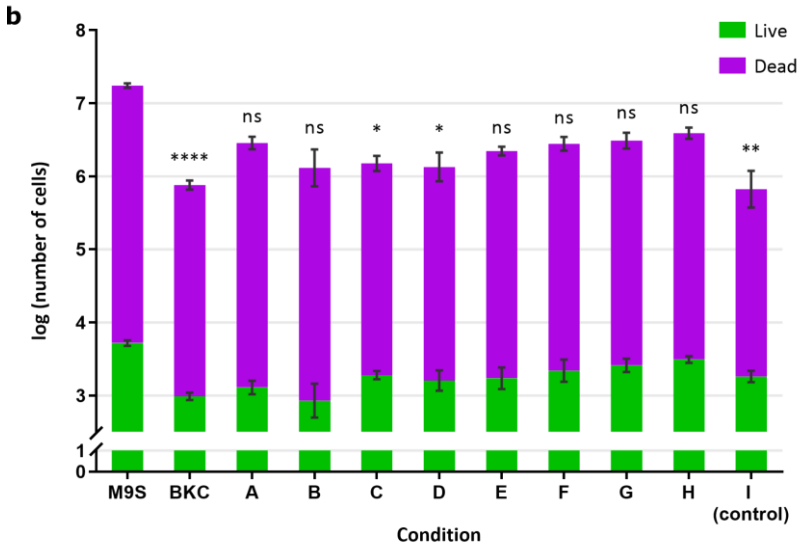


Figure 6.12: Representative images of PAO1-N show altered biofilm formation when grown statically in M9S with the addition of free BKC or different eBKC samples. (a) PAO1-N was inoculated into an 8-well glass bottom chamber at an OD_{600} of 0.05 in M9S containing no supplement, free BKC (0.2 mg mL^{-1}), or eBKC A-I (0.51 mg mL^{-1} for A and E, 0.55 mg mL^{-1} for B-D and F-I). The cells were incubated at 37°C under static conditions for 48 h. Live cells were stained with SYTO 9 (green) and dead cells with PI (magenta). Z-stack images were taken with a Zeiss CLSM using a 63x objective. Top images represent 3D top view, bottom images 3D side view of biofilms. **(b)** Biofilm images were quantified by counting live (lower bars, green) and dead (upper bars, purple) cells of the individual channels (SYTO 9 and PI) using ImageJ. The logarithm of the number of cells is shown against the strain grown in M9S containing free BKC or eBKC A-I. Error bars represent standard error measured for different biofilm images, where n = 8 for M9S and M9S eBKC I, n = 6 for M9S BKC, n = 4 for M9S eBKC A-H. Statistical difference was calculated using the total cell numbers compared to the control M9S, with $p<0.05$ = *, $p<0.01$ = **, $p<0.0001$ = ****, ns = not significant (non-parametric Kruskal-Wallis test).

The addition of unencapsulated BKC to the growth medium led to highly reduced biofilm formation of PAO1-N, where only one layer of cells was formed at the bottom of the chamber. Interestingly, when looking at the individual channels, it seemed that the cells were stained with both SYTO 9 and PI at the same time. The majority of the eBKC samples (eBKC A, B, C, D, E, F, and H) resulted in a structural change of the biofilm formation with lots of clumps being formed. Sample G looked like the WT control although some clumps could still be detected, especially in the green channel. The negative control, eBKC I, formed a non-homogenous biofilm with some parts comparable to the WT, whereas other parts showed less cells and some clumping. The

clumps in all samples were mostly pronounced in the green channel and as already described for free BKC, there seemed to be regions that were stained with both dyes at the same time. Overall, less cells were detected for the samples containing BKC although some biofilms were thicker due to the clumping. The quantification mostly confirmed the results seen in the images, although the clumping complicated the quantification. As already indicated, the addition of free BKC as well as all eBKC samples to the growth medium at the beginning of the biofilm formation resulted in less live cells compared to the control. However, the reduction of total cells with the addition of eBKC A, B, E, F, G, and H was not significant, likely due to the low number of replicates. It should be noted that the negative control, eBKC I, that does not contain any BKC led to a significant reduction of biofilm formation ($p<0.01$, non-parametric Kruskal-Wallis test). In addition to CLSM, CFU experiments were performed as previously described (Figure 6.13).

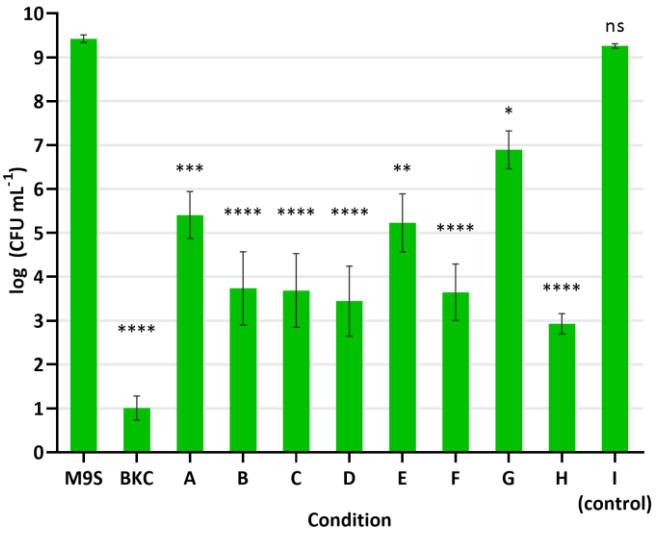
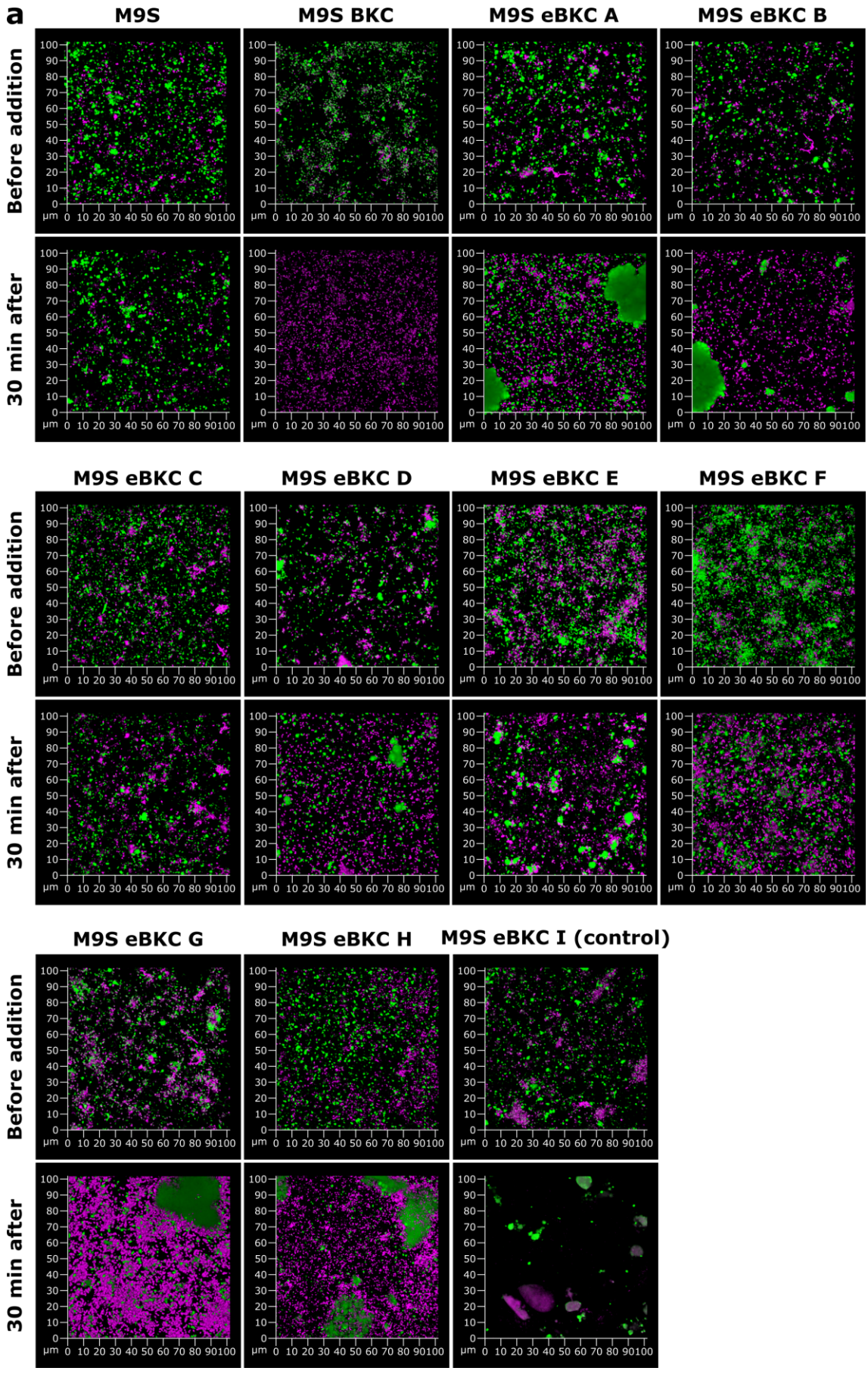


Figure 6.13: CFUs of PAO1-N biofilms show reduced number of viable cells for all biofilms grown with the addition of free BKC or eBKC apart from eBKC I (control) under static conditions. PAO1-N was inoculated into a 24-well plate at an OD_{600} of 0.05 in M9S containing no supplement, free BKC (0.2 mg mL^{-1}), or eBKC A-I (0.51 mg mL^{-1} for A and E, 0.55 mg mL^{-1} for B-D and F-I). After 48 h of static incubation at 37°C, cells were resuspended and dilutions plated onto LB plates. The number of CFUs was counted after 24 h and is shown against conditions. Error bars represent standard error, where n = 3x6, with $p<0.5$ = *, $p<0.01$ = **, $p<0.001$ = ***, $p<0.0001$ = ****, ns = not significant (non-parametric Kruskal-Wallis test).

The CFU counting confirms the results obtained with CLSM with all eBKC samples leading to significantly reduced biofilm formation (non-parametric Kruskal-Wallis test) apart from eBKC I that showed no significant difference, which is in contrast to the CLSM results where the control led to reduced biofilm formation and clumping of the cells. Free BKC showed the biggest effect whereas eBKC G had the smallest reduction in viable cells.

To analyse the killing ability of the different samples, free BKC or eBKC was added to established biofilms of PAO1-N grown for 48 h and stained with SYTO 9 and PI. Images were taken before the addition and subsequently every 5 min during a period of 30 min using CLSM. Representative images and quantification can be seen in Figure 6.14.


a
M9S
M9S BKC
M9S eBKC A
M9S eBKC B
Before addition
30 min after
M9S eBKC C
M9S eBKC D
M9S eBKC E
M9S eBKC F
Before addition
30 min after
M9S eBKC G
M9S eBKC H
M9S eBKC I (control)
Before addition
30 min after
µm 0 10 20 30 40 50 60 70 80 90100

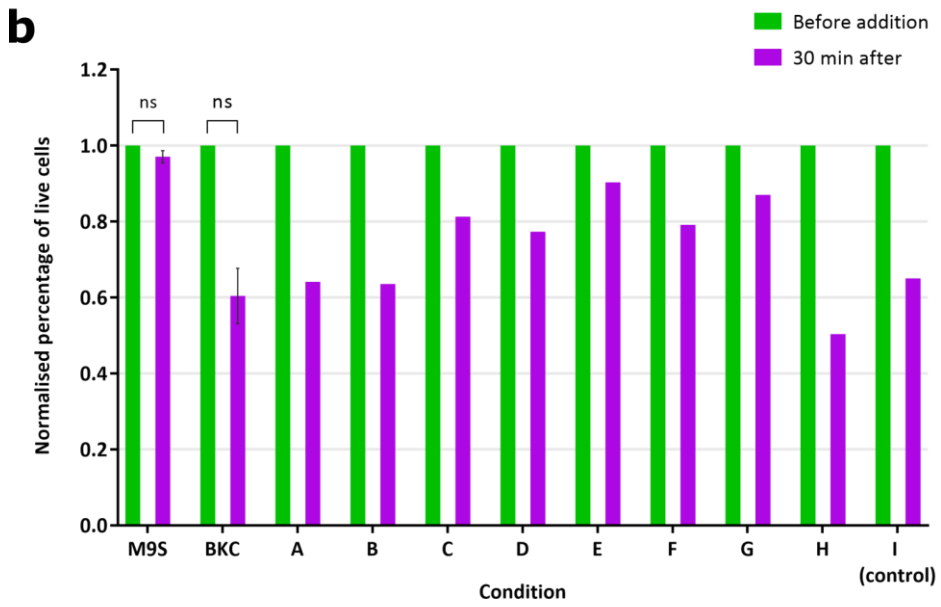


Figure 6.14: Representative images of PAO1-N show killing effects at different intensities when free BKC or eBKC was added to established biofilms for 30 min. (a) PAO1-N was inoculated into an 8-well glass bottom chamber at an OD_{600} of 0.05 in M9S. The cells were incubated at 37°C under static conditions for 48 h. Live cells were stained with SYTO 9 (green) and dead cells with PI (magenta). Images presented were taken before the addition (top) and 30 min after the addition (bottom) of M9S containing no supplement, free BKC, or eBKC A-I to the established biofilms to give a final concentration of 0.2 mg mL^{-1} (free BKC), 0.51 mg mL^{-1} (A and E) and 0.55 mg mL^{-1} (B-D and F-I). Z-stack images were taken with a Zeiss CLSM using a 63x objective and 3D top view images are presented. **(b)** Biofilm images were quantified by counting live and dead cells of the individual channels (SYTO 9 and PI) using ImageJ. The normalised percentage of live cells before (green) and after (purple) the addition of M9S, free BKC, or eBKC A-I is shown against the conditions. Error bars represent standard error measured for different biofilm images, where n = 6 for M9S, n = 2 for M9S BKC and n = 1 for eBKC A-I, ns = not significant (non-parametric Mann-Whitney test).

As already seen previously, the addition of M9S to the biofilm did not lead to any changes of the biofilm. However, when the negative control eBKC I was added, a lot of the biofilm got disrupted and clumping occurred. The addition of eBKC A, B, G, and H also led to clumping including an increase in dead cells especially for eBKC B, G, and H. When free BKC or eBKC C, D, E, or F were added, some killing of cells was observed but not much clumping. Based on the images, free BKC as well as eBKC B, G, and H showed the highest effects on biofilm eradication. Looking at the quantification, all BKC samples, including the negative control eBKC I, showed a reduction in the percentage of live cells within the biofilm after 30 min. It should be noted that, due to limited

sample availability and high expenditure of time, this experiment was only performed once for each eBKC sample. Free BKC was the only sample apart from the control with M9S where two replicates were performed, but the reduction of live cells was found not significant based on a non-parametric Mann-Whitney test. CFU experiments were performed as described before and the results are shown in Figure 6.15.

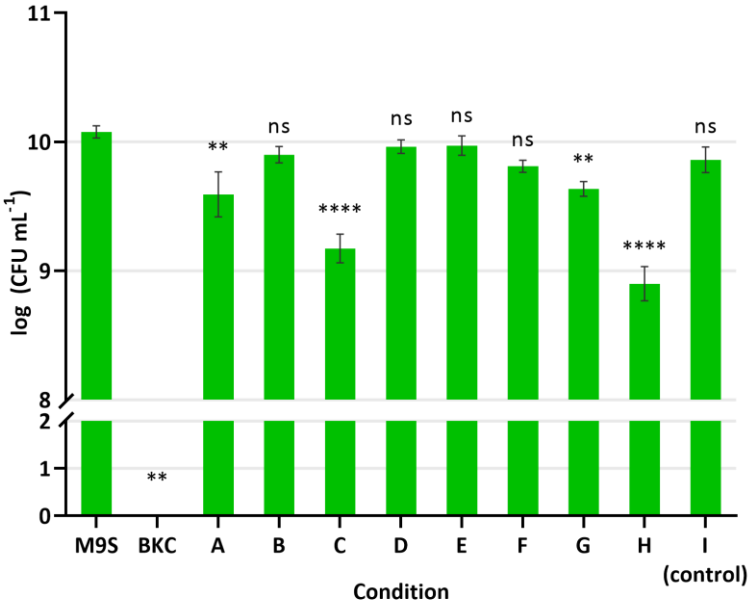
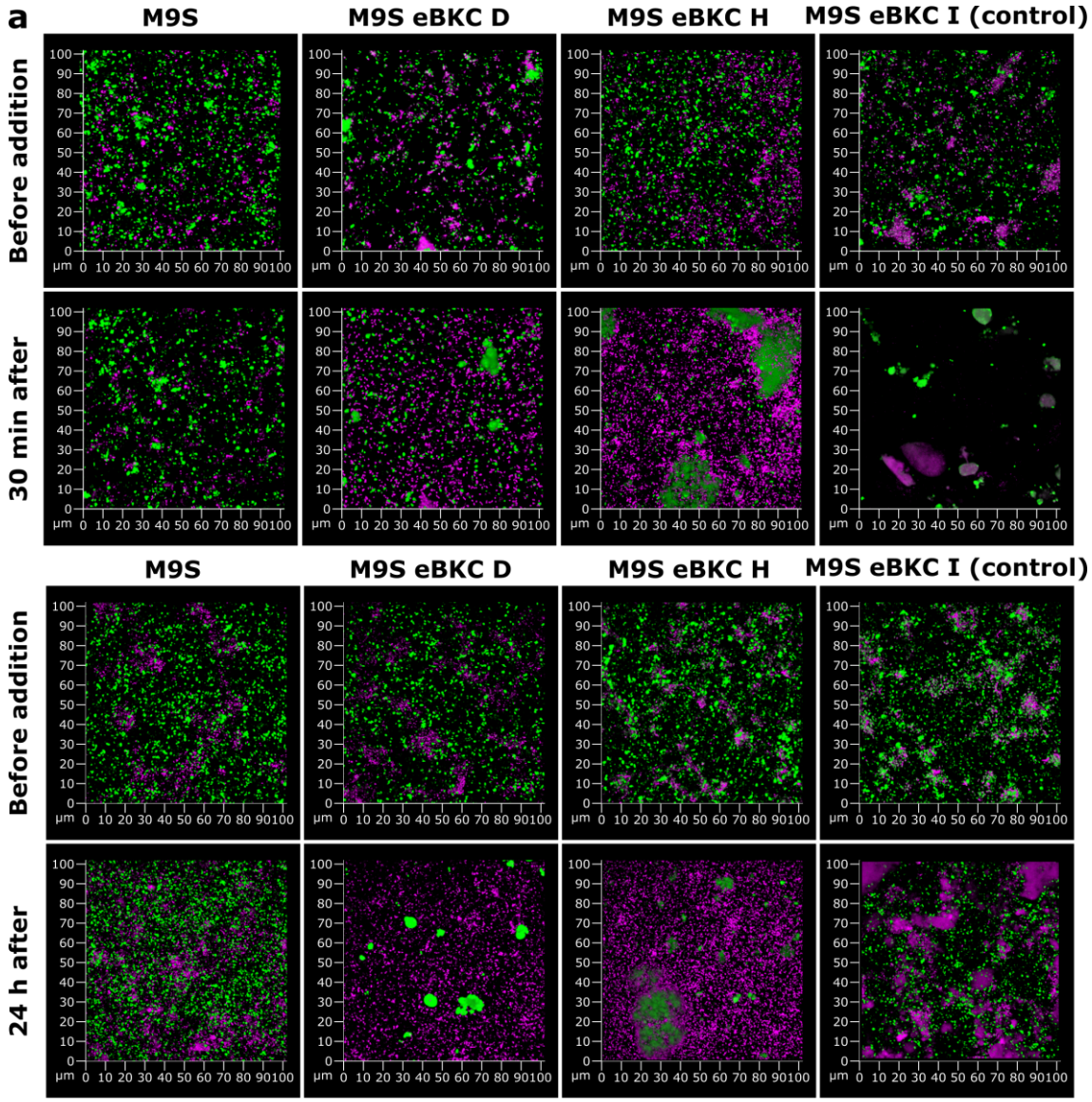


Figure 6.15: CFUs of PAO1-N biofilms show killing activity when free BKC or eBKC A, C, G, or H was added to established biofilms for 30 min. PAO1-N was inoculated into a 24-well plate at an OD_{600} of 0.05 in M9S. After 48 h of static incubation at 37°C, cells were treated with free BKC or eBKC A-I for 30 min to give a final concentration of 0.2 mg mL^{-1} (free BKC), 0.51 mg mL^{-1} (A and E), and 0.55 mg mL^{-1} (B-D and F-I). Subsequently, cells were resuspended and dilutions plated onto LB plates. The number of CFUs was counted after 24 h and is shown against conditions. Error bars represent standard error, where n = 6, with $p<0.01$ = **, $p<0.0001$ = ****, ns = not significant (non-parametric Mann-Whitney test for BKC, rest ordinary one-way ANOVA test).

No significant differences in CFU counts were observed for eBKC B, D, E, F, and I compared to the control M9S. The addition of free BKC or eBKC A, C, G, and H led to a significant reduction in CFUs, where free BKC, eBKC C, and eBKC H showed the biggest effect. The addition of unencapsulated BKC was especially striking as no colonies at all were formed following the 30 min addition for none of the six replicates.

In the previous experiment, the eBKC samples were added for 30 min to look for any effects on the already established biofilm. However, the eBKC samples might need more time to deploy their whole killing capability due to the BKC being incorporated inside the capsules. Therefore, three samples were chosen for further experiments where the eBKC was added to the biofilms for an elongated time of 24 h, before the biofilms were imaged again. During the additional 24 h, the biofilms were incubated at 37°C in a static incubator. After prior consultation with Unilever, eBKC D, H, and I were chosen for the further experiments. Representative images and quantification can be found in Figure 6.16, where Figure 6.16a represents the previous images showing the addition for 30 min as well as the results for the 24 h addition. It should be noted that for the 24 h addition, the images were not taken at the same spot as the image before the addition as this was technically not possible.


a
M9S
M9S eBKC D
M9S eBKC H
M9S eBKC I (control)
Before addition
30 min after
M9S
M9S eBKC D
M9S eBKC H
M9S eBKC I (control)
Before addition
24 h after
µm 0 10 20 30 40 50 60 70 80 90100

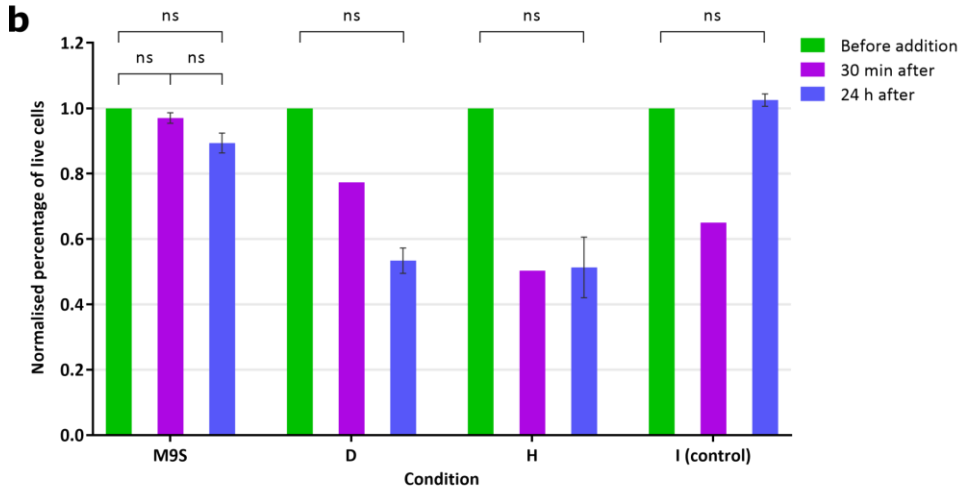

b
ns
Before addition
30 min after
24 h after
Normalised percentage of live cells
1.2
1.0
0.8
0.6
0.4
0.2
0.0
M9S
D
H
I (control)
Condition

Figure 6.16: Representative images of PAO1-N biofilms show increased killing effects of selected eBKC samples when added to established biofilms for 24 h. (a) PAO1-N was inoculated into an 8-well glass bottom chamber at an OD_{600} of 0.05 in M9S. The cells were incubated at 37°C under static conditions for 48 h. Live cells were stained with SYTO 9 (green) and dead cells with PI (magenta). Images were taken before M9S containing no supplement or eBKC D, H, or I was added to the established biofilms to give a final concentration of 0.55 mg mL^{-1}. Subsequently, cells were incubated for another 24 h at 37°C and imaged again (bottom panel). For comparison, addition of supplements for 30 min taken from previous experiments is also shown (top panel). Z-stack images were taken with a Zeiss CLSM using a 63x objective and 3D top view images are presented. **(b)** Biofilm images were quantified by counting live and dead cells of the individual channels (SYTO 9 and PI) using ImageJ. The normalised percentage of live cells before (green) and after (30 min purple, 24 h pink) the addition of M9S or eBKC E, H, or I is shown against the conditions. Error bars represent standard error measured for different biofilm images, where n = 6 for M9S 30 min, n = 1 for M9S eBKC D, H and I 30 min, n = 2 for all conditions 24 h, with ns = not significant (non-parametric Mann-Whitney test).

No significant changes were observed for M9S after 30 min and 24 h. The negative control eBKC I also showed no significant difference in the percentage of live cells after 24 h as opposed to 30 min, where a decrease was observed. An increased killing effect was seen for eBKC D for both time points, with an increase in killing between 30 min and 24 h. No difference was detected between 30 min and 24 h for the addition of eBKC H. However, there was still a decrease in the percentage of live cells for both time points overall. However, due to the low number of replicates, no statistical significance could be determined. It should also be noted that clumping was observed for the addition of eBKC D and H, with only a few clumps detected for eBKC I. Results for the performed CFU experiments can be found in Figure 6.17.

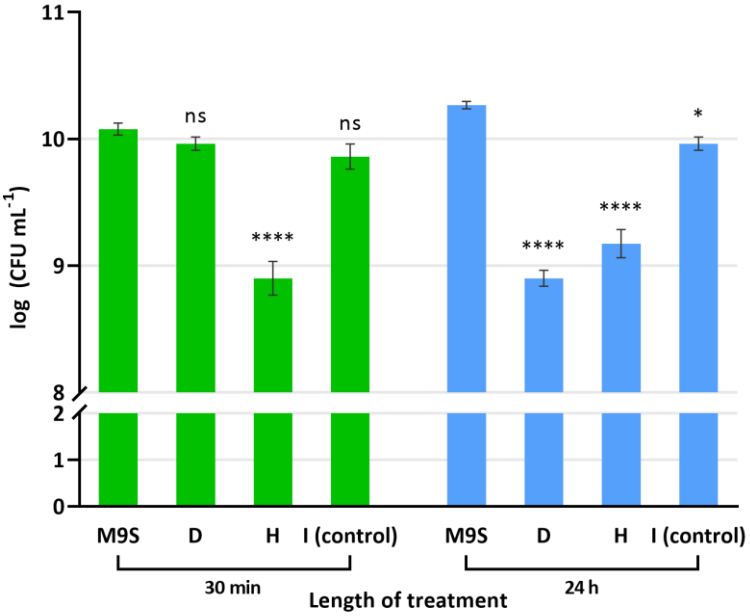


Figure 6.17: CFUs of PAO1-N biofilms show increased killing activity when eBKC D was added to established biofilms for 24 h. PAO1-N was inoculated into a 24-well plate at an OD_{600} of 0.05 in M9S. After 48 h of static incubation at 37°C, eBKC D, H, or I was added to the biofilms to give a final concentration of 0.55 mg mL^{-1} and incubated for another 24 h. Cells were resuspended and dilutions plated onto LB plates. The number of CFUs was counted after 24 h (blue) and is shown against conditions. Results obtained for 30 min (green) of treatment from previous experiments are shown for comparison. Error bars represent standard error, where n = 6, with $p<0.05$ = *, $p<0.0001$ = ****, ns = not significant (two-way ANOVA test).

After 24 h of treatment, all samples resulted in a significant decrease of CFUs compared to the control with M9S. The decrease was bigger for eBKC D and H than for eBKC I. Comparing the length of the treatments, eBKC D was only effective when added for 24 h whereas eBKC H showed killing effects for both time points, 30 min and 24 h. The addition of eBKC I only had a slight effect following the longer treatment of 24 h.

In a meeting with our industrial partner Unilever, the treatment of biofilms with a combination of eBKC together with liquid detergent was discussed. Due to the anionic properties of BKC, free BKC cannot be combined with liquid detergent. The idea is that the encapsulation of the eBKC would protect the BKC in such a way as to enable it to be stably incorporated to laundry detergents. To test the effectiveness, the previously selected samples eBKC D, H, and I were combined with liquid detergent and added to an already established PAO1-N biofilm. The cells

were stained with SYTO 9 and PI and imaged before and after the addition for 30 min using CLSM (Figure 6.18).

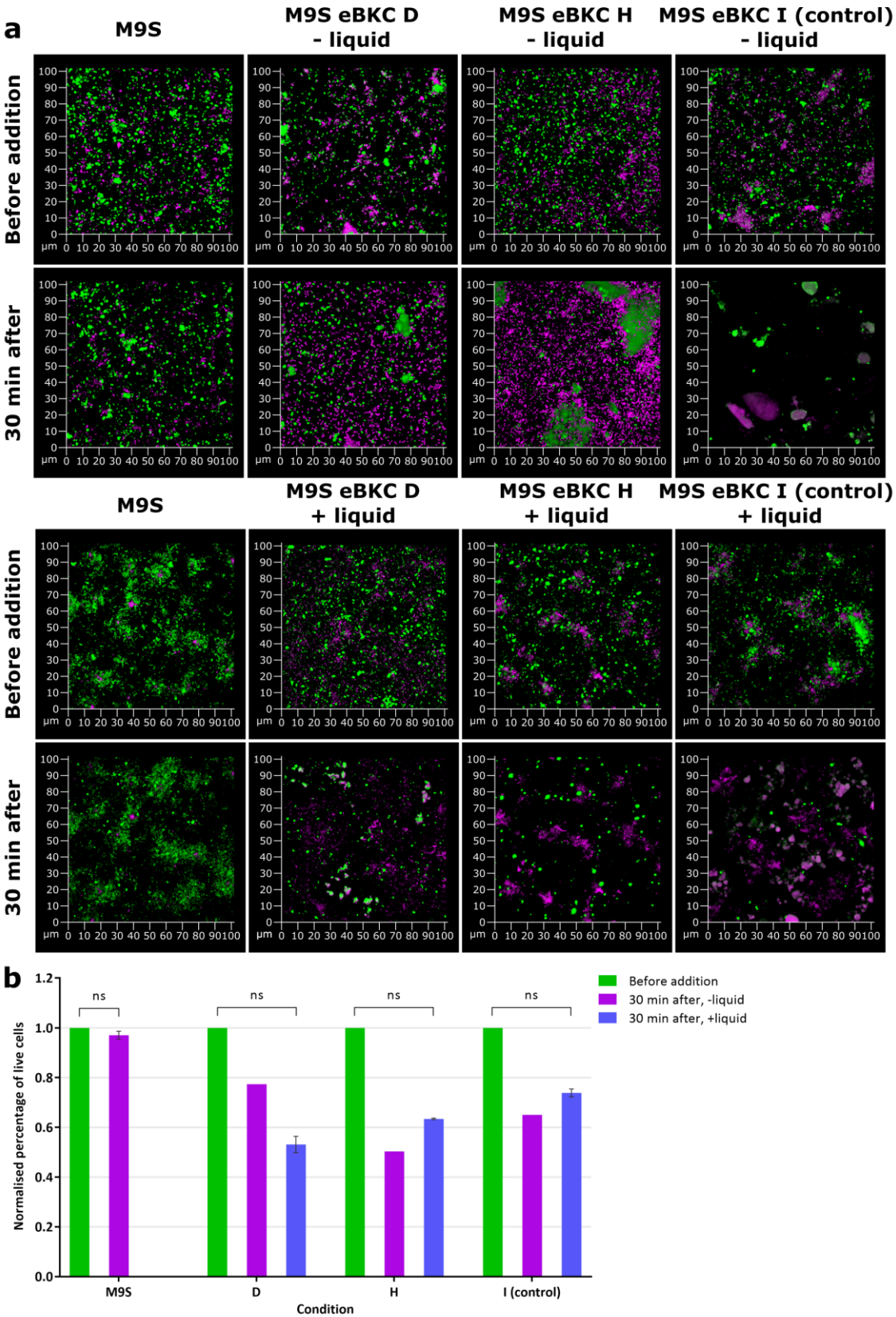


Figure 6.18: Representative images of PAO1-N show no increased killing effects of selected eBKC samples when added together with liquid detergent to established biofilms for 30 min. (a) PAO1-N was inoculated into an 8-well glass bottom chamber at an OD_{600} of 0.05 in M9S. The cells were incubated at 37°C under static conditions for 48 h. Live cells were stained with SYTO 9 (green) and dead cells with PI (magenta). M9S containing no supplement or eBKC D, H, or I together with liquid detergent was added to the established biofilms to give a final concentration of 0.55 mg mL^{-1} (eBKC) and 2.9 mg mL^{-1} (liquid detergent) (top panel). Biofilms were imaged before the addition and after 30 min. For comparison, addition of supplements without liquid detergent from previous experiments is also shown (top panel). Z-stack images were taken with a Zeiss CLSM using a 63x objective and 3D top view images are presented. **(b)** Biofilm images were quantified by counting live and dead cells of the individual channels (SYTO 9 and PI) using ImageJ. The fold change of the percentage of live cells before (green) and after (30 min purple, 24 h pink) the addition of M9S or eBKC D, H, or I with or without liquid detergent is shown against the conditions. The results were normalised to the percentage of live cells before the addition for each condition. Error bars represent standard error measured for different biofilm images, where n = 6 for M9S, n = 1 for eBKC without liquid detergent, n = 2 for eBKC with liquid detergent, with ns = not significant (non-parametric Mann-Whitney test).

As previously seen, the addition of M9S did not lead to any changes, whereas the combination of eBKC D, H, and I with liquid detergent resulted in a reduction of live cells. However, as described in 6.2.3, this could be due to the cells losing the SYTO 9 staining rather than a killing effect. The decrease in percentage of live cells for the addition of eBKC D with liquid detergent was increased compared to no liquid detergent. However, for eBKC H, the killing effect was reduced when liquid detergent was present. No difference was observed for the addition of eBKC I with or without liquid detergent, but a killing activity was still detected for both conditions. Due to the low number of replicates, observed differences were not statistically significant. No clumps were observed for any of the samples containing liquid detergent. The results for CFU experiments are shown in Figure 6.19.

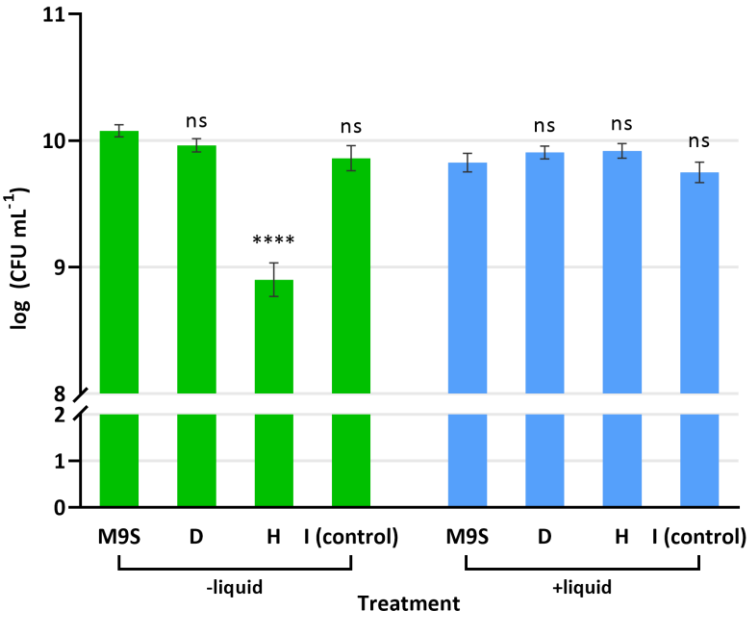


Figure 6.19: CFUs of PAO1-N biofilms show no killing activity when eBKC was added to the biofilms together with liquid detergent for 30 min. PAO1-N was inoculated into a 24-well plate at an OD_{600} of 0.05 in M9S. After 48 h of static incubation at 37°C, eBKC D, H, or I was added to the biofilms together with liquid detergent to give a final concentration of 0.55 mg mL^{-1} (eBKC) and 2 mg mL^{-1} (liquid detergent). After 30 min, cells were resuspended and dilutions plated onto LB plates. The number of CFUs was counted after 24 h and is shown against conditions (blue). Results obtained without liquid detergent are shown for comparison (green). Error bars represent standard error, where n = 6, with $p<0.0001$ = ****, ns = not significant (two-way ANOVA test).

Looking at the CFU counts, no significant changes were observed compared to M9S for any of the three eBKC samples when liquid detergent was present. This is in contrast to the results obtained without liquid detergent, where the addition of eBKC H to the biofilm for 30 min resulted in a significant reduction of CFUs.

6.2.5 Different materials used for the coating of glass disks can reduce initial attachment of PAO1-N

Instead of using biocides that could cause bacterial resistance and are associated with environmental concerns, material coating was investigated as an alternative to prevent biofilm formation. The ability of PAO1-N to form biofilms on differently coated glass disks was analysed using scanning electron microscopy (SEM). The disks were coated by Unilever using four

different materials: PEOX 500, P-123, P19, and PDMS. For this experiment, PAO1-N was grown on coated glass disks for 3 h before being fixed and imaged using SEM (2.20). For each sample, three images were taken at a magnification of 2,000x and the number of attached cells was counted. A control disk without coating was included in the experiment. Representative images at 2,000x and 20,000x magnification and quantification are shown in Figure 6.20.

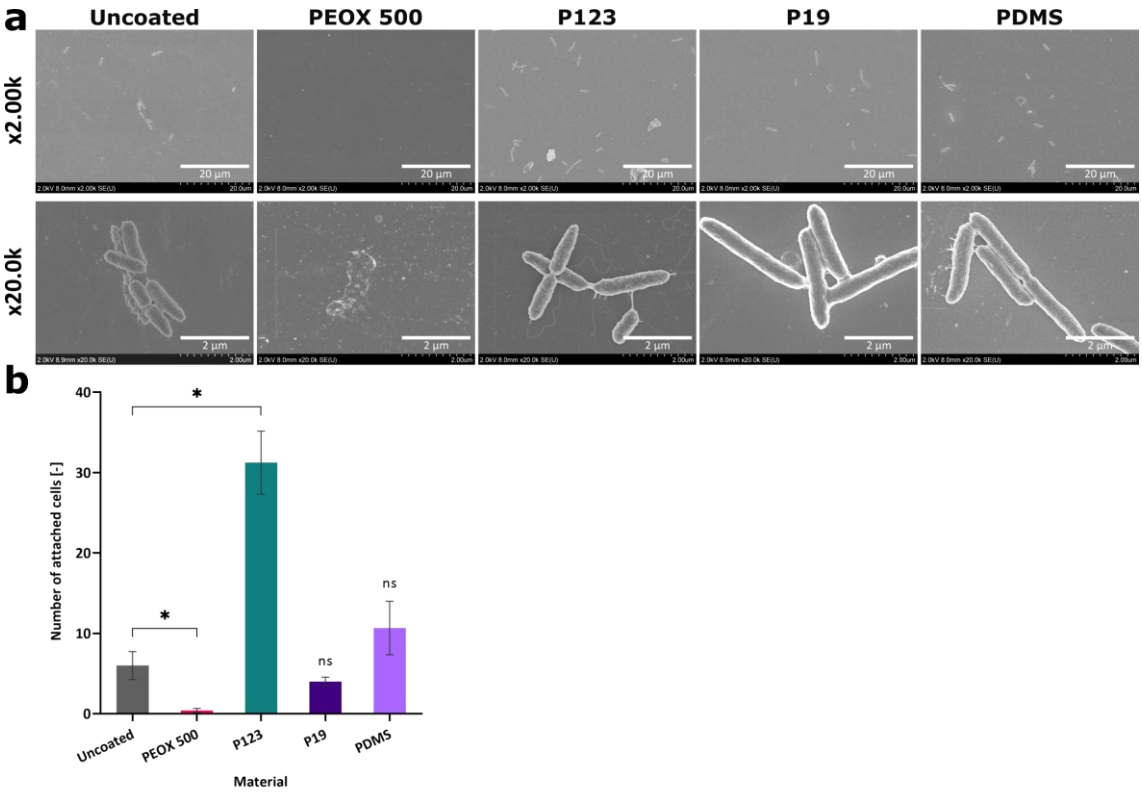


Figure 6.20: Representative SEM images show different attachment of PAO1-N to various coatings. PAO1-N was inoculated into a 12-well plate consisting of glass disks (uncoated or coated with PEOX500, PL123, P19, or PDMS) at an OD_{600} of 0.05 in TSB medium. After 3 h of static incubation at 37°C, cells were fixated and disks were prepared for SEM. **(a)** Images were taken with a Hitachi S-4800 SEM at magnification of 2000x (top) and 20,000x (bottom). **(b)** Image quantification by counting attached cells of 2000x magnification. The number of cells is shown against the coating material. Error bars represent standard error measured for different biofilm images, where n = 3 for uncoated and PDMS, n = 4 for P123 and n = 5 for PEOX500 and P19, with $p<0.05$ = *, ns = not significant (non-parametric Mann-Whitney test).

Looking at the images taken with 2000x magnification, cells were observed for all conditions except PEOX 500, where only very few cells or no cells were detected. In contrast, more cells were detected for the disk coated with P-123. Furthermore, a closer look with the 20,000x

magnification revealed differences in the cell shapes. Bacteria grown on P19 looked elongated compared to the control grown on uncoated glass. A lot of flagella were observed for cells grown on P-123, whereas dead cells were detected on the PEOX 500 coated surface. The quantification show that the attachment of bacteria was significantly reduced ($p<0.05$, non-parametric Mann-Whitney test) when the disk was coated with PEOX 500 whereas the attachment was significantly increased ($p<0.05$, non-parametric Mann-Whitney test) for coating with P-123. No significant difference was detected for P19 and PDMS. However, this experiment was only performed once, and biological replicates are required for a more secured analysis.

6.3 Discussion

This chapter aimed to investigate the impact of different laundry products on the growth and biofilm formation of two *P. aeruginosa* strains, the lab strain PAO1-N and the WM isolate WMB1.3. Furthermore, the practicality and effectiveness of using encapsulated BKC instead of free BKC in laundry detergents was investigated. A secondary aim was the investigation of materials that can be used for surface coating to prevent bacterial attachment and biofilm formation as an alternative to the treatment using biocides potentially harmful to the environment.

6.3.1 Various laundry products have different effects on growth, biofilm formation and biofilm killing of *P. aeruginosa*

Previous research has indicated that different laundry products have various effects on the hygiene of laundry. Because of the presence of active bleaching agents in powder detergents, these were found to be more effective in reducing bacterial colonisation of WMs compared to liquid detergent (Munk *et al.*, 2001). Furthermore, the use of fabric conditioners was proposed as alternative for washes at lower temperatures due to its bacteriostatic properties (Davis and Ainsworth, 1989). Previous studies have also found evidence that the use of biocides in laundry products can lead to bacterial resistance (International Scientific Forum on Home Hygiene, 2018). Therefore, the WM isolate *P. aeruginosa* WMB1.3 that was characterised in Chapter 5 was included in this study to compare the effects of the laundry products on this strain with the lab strain PAO1-N.

The analysis of three different laundry products - a liquid detergent, a powder detergent, and a fabric conditioner, all provided by Unilever - revealed differences between the products but also between the two strains. Growth experiments carried out in minimal medium with the addition of the laundry products at defined concentrations showed no initial growth for both strains when powder detergent was present (Figure 6.2). After 17 h, WMB1.3 started to grow very

slightly, possibly because the WM isolate is slightly more resistant to the powder detergent due to previous exposure within the WM. Overall, as the powder detergent contains bleaching agents, the presence was likely to reduce the growth of bacteria (Munk *et al.*, 2001). This is not the case for the liquid detergent or fabric conditioner that are rather used to leach out stains and soil and to soften the clothes than to kill bacteria. Therefore, the addition of liquid detergent or fabric conditioner showed no reduced growth; instead, the growth was even slightly enhanced with the addition of liquid detergent for both strains. However, this increase was considered not to be biologically relevant and more due to the high number of replicates.

Besides the analysis of planktonic growth, biofilm formation and killing abilities of the laundry products were assessed. For this study, CLSM of LIVE/DEAD staining and CFU experiments were chosen to investigate the effects of the laundry products on biofilm formation and biofilm eradication. The LIVE/DEAD™ BacLight™ Bacterial Viability was used in this study for microscopic quantification of the biofilms to look for general biofilm formation on the one hand but also to investigate viability of these biofilms under various growth conditions.

In a first approach, the laundry products were added to the growth medium of PAO1-N and WMB1.3 before cells were incubated for 48 h at 37° under static conditions or for 24 h with a constant flow of medium (Figure 6.3 and Figure 6.5). Imaging of the biofilms revealed reduced biofilm formation for both strains PAO1-N and WMB1.3 when powder detergent was present in the growth medium under static as well as flow condition. As already discussed for the planktonic growth, this effect can be explained by the presence of active bleach agents in the powder detergent. Interestingly, the presence of liquid detergent in the growth medium also resulted in reduced biofilm formation for both strains and both biofilm models. This was unexpected as normal growth was observed in the growth assay. One possible explanation is that the presence of the liquid detergent in the medium leads to reduced attachment ability of the bacteria. In this case, the flow of the BioFlux system would remove all unattached bacteria and no biofilm formation can occur. However, under static conditions, no wash step was

included before the imaging because the biofilms became very viscous when cells were grown statically in medium containing either liquid or powder detergent. A wash step prior to imaging would have disrupted and removed most of the biofilm. Therefore, decreased attachment abilities of the cells due to the liquid detergent cannot explain the reduced biofilm formation seen here. Looking at the different procedures between growth measurement and biofilm formation, the incubation time of the bacteria within medium containing the detergents is double the time for the static biofilm formation than for the growth experiment. A longer exposure to the detergent could hence lead to cell death and subsequently reduced biofilm formation after 48 h. Furthermore, no shaking was applied in the static biofilm model whereas the cells during the growth experiment were shaken every 15 min to ensure even cell dispersion within the wells. Without shaking, the liquid detergent is likely to settle down at the bottom of the wells over time, resulting in increased concentrations on the surface. This increased concentration could lead to enhanced toxicity and cell death at the same time as reducing nutrient availability essential for cell growth and biofilm formation.

Although LIVE/DEAD staining is a valid method to investigate biofilm formation and viability, there is a need to compare the results to classical microbiological techniques. Therefore, the most traditional way to quantify bacteria was chosen: CFU experiments (Doll *et al.*, 2016). Unfortunately, due to technical limitations, it was not possible to perform these experiments for the flow-cell model. For statically grown biofilms, the only significant change in CFUs was observed for the presence of powder detergent in growth medium of PAO1-N, as presented in Figure 6.4. No reduced biofilm viability was shown for WMB1.3 under the same conditions and none of the other products (liquid detergent and fabric conditioner) led to changes in CFUs. This is in contrast to the results obtained using CLSM, where the addition of powder as well as liquid detergent led to reduced biofilm formation for both strains. One reason for these discrepancies could be that the powder detergent in the medium does not completely kill the WMB1.3 cells but instead the bacteria can recover under non-selecting conditions. The same could be true for

the effect of the liquid detergent on both strains. As previously described, the two dyes used for the staining differ in their ability to cross intact membranes, where cells with an intact membrane are considered viable. Thus, if powder or liquid detergent influence the membrane permeability, PI could enter the cells where it would displace the SYTO 9 due to its stronger affinity for nucleic acids (Stocks, 2004). Subsequently, this could lead to overestimation of dead cell as viable cells in this experiment could be incorrectly detected as dead although still culturable as seen in the CFU counting. Previous studies have shown that the addition of ethylenediaminetetraacetic acid (EDTA) to cells of Gram-negative bacteria destabilises the outer membrane by chelating divalent cations responsible for the cross-linking of the lipopolysaccharide layer (Leive, 1965). Therefore, EDTA can be used to facilitate translocation of macromolecules into Gram-negative bacteria without the loss of viability (Hitchener and Egan, 1976; Marvin *et al.*, 1989). EDTA is not biodegradable and cannot be used for laundry products in Europe due to environmental concerns, but other chelators can be used in both liquid and powder laundry products designed to work in hard water, which could potentially enhance membrane integrity when detergents are present and could explain the observed results (Hinton Jr and Ingram, 2012).

Overall, lower CFUs were recorded for WMB1.3 after 24 h growth in M9S compared to the control for PAO1-N. In previous studies, it was shown that WMB1.3 forms a thicker biofilm under control conditions compared to PAO1-N (Figure 5.11). One possible explanation for reduced CFUs could be that although WMB1.3 forms thicker biofilms, more cells are dead compared to biofilms of PAO1-N. These dead cells would not be detected in the CFU experiments; yet would be visible by membrane staining. However, LIVE/DEAD staining of both strains did not support this hypothesis; instead, biofilms of WMB1.3 even appeared more viable showing more green cells. A more likely explanation for the reduced WMB1.3 CFUs is the stronger attachment ability that was shown for the WM isolate compared to PAO1-N by performing CV attachment assays (Figure 5.8). CFU experiments rely on the detachment and separation of all individual cells of the

biofilm while maintaining their viability. In this study, these steps included a short sonication followed by a manual scratching of the cells using blue pipette tips and subsequent resuspension by pipetting up and down. The frequency and time of the treatment is crucial as a short treatment with high frequency cannot provide enough separation of cells, whereas long exposure to ultrasound affects cell viability (Qian *et al.*, 1997; Joyce *et al.*, 2003; Kobayashi *et al.*, 2007; Doll *et al.*, 2016). Due to the increased attachment properties of WMB1.3, change of sonication length or frequency as well as treatment of the biofilms with enzymes to promote detachment should be considered for future experiments. Comparing LIVE/DEAD staining and CFUs, it should also be highlighted that CFUs cannot be directly linked to the number of viable cells. One bacterial colony can be generated from more than a single cell, which is especially notable for genera like staphylococci and streptococci that grow in clusters and chains (Doll *et al.*, 2016). Hence, the total cell number can easily be underestimated in CFU experiments, which could be the case for WMB1.3.

In addition to analyse how laundry products affect the formation of biofilms, the ability of these products to disrupt and kill an already established biofilm was assessed using CLSM and CFUs (Figure 6.6 and Figure 6.7). Laundry products were added to already established biofilms of PAO1-N or WMB1.3 for 30 min, where the biofilms were imaged every 5 min to look for changes in the LIVE/DEAD staining. For both detergents, liquid and powder, a reduction in live cells was observed after 30 min, suggesting that these products can kill a good proportion of bacteria of an established biofilm within minutes. However, when comparing these results with the performed CFU experiments, the bactericidal properties could not be confirmed. No differences in CFUs were observed for any of the strains and conditions after 30 min of treatment. Again, this discrepancy could be explained by the detergents not completely killing the cells, as illustrated above. It was discussed that the environment, stress, and physiological state of the cell affect the membrane permeability leading to overestimation of the number of dead cells because bacteria with compromised membranes could still be capable of recovering and

reproducing. If the addition of the powder or liquid detergents to the cells results in changes in membrane integrity but not viability, LIVE/DEAD imaging could show less vital cells whereas CFU counting would still detect these cells as viable resulting in differences between both methods.

Another possibility in this case is bleaching of the SYTO 9, as biofilms were imaged before treatments, and subsequently an additional six times every 5 min. Bleaching of SYTO 9 has been reported in previous studies, where cells stained with SYTO 9 were imaged every 5 minutes. The loss of signal intensity accounted for 4-8% every five minutes depending on the physiological state of the cell and cell number (Stiefel *et al.*, 2015). However, if bleaching of SYTO 9 was the reason for the results obtained, this would have been expected to occur for all samples including the control, which was not the case. Yet it is possible that liquid and/or powder detergent enhances the bleaching properties of SYTO 9 so that only these samples show a reduced number of live cells after 30 min. Nevertheless, these results were rather unexpected and further investigation was undertaken.

As described above, various methods are available to investigate viability of cells and the effectiveness of treatments, such as new antimicrobials. In addition to LIVE/DEAD staining and CFU counting, the BacTiter-Glo™ assay (BacTiter-Glo™ Microbial Cell Viability Assay, Promega, Mannheim, Germany) was used to investigate the effects of laundry products on the viability of PAO1-N cells (Promega, 2019) (Figure 6.8). A significant reduction in viable cells was observed for the treatment with powder detergent ($p>0.0001$) after 30 min but not for the other conditions, confirming results that the powder detergent influences PAO1-N cell viability, which could not be revealed by looking at CFUs. However, no effect was seen for the addition of liquid detergent. It should be noted that this method is based on the quantification of ATP within cells, which is only produced within phases of metabolic activity, is not stored inside cells, and is rapidly degraded after cell death (Doll *et al.*, 2016; Promega, 2019). That means, that only effects on the metabolic activity of the cells will be detected but no other physiological aspects like membrane permeability. Therefore, it could be that the liquid detergent has indeed an effect on

the cells as observed by CLSM that cannot be picked up by this method. It must also be pointed out that, due to practicability and time, this method was only applied to planktonic cells and not to 48 h matured biofilms, which could lead to different results and should therefore also be investigated in the future. Moreover, instead of analysing whole cells, the supernatant of the cultures could be examined to gain insights into the effects of the laundry products on membrane integrity. If the membrane becomes porous, ATP could leak out of the cells and would be picked up with the assay, whereas no ATP would be measured when cell membranes are intact.

Another possible explanation for the reduced green fluorescence that was detected in CLSM experiments could be a direct interaction between SYTO 9 and the liquid or powder detergent that inhibits the fluorescence capability of the dyes. To further examine this hypothesis, samples were prepared consisting of M9S with or without laundry products and either SYTO 9, PI, or both dyes. A fluorescence measurement using a Tecan plate reader revealed no background fluorescence for any of the conditions when looking at the intensity of both dyes, green and red (Figure 6.9). Green fluorescence was detected for all samples when SYTO 9 was present alone as well as when both dyes were available in the medium. The same was observed for red fluorescence when PI alone or both dyes were added. The green fluorescence intensity was even increased when liquid or powder detergent was present in the medium, disproving the hypothesis that the laundry products alone reduce the fluorescence of SYTO 9. Interestingly, the overall fluorescence intensity for SYTO 9 was reduced when both dyes were present as opposed to when only SYTO 9 was available. This lower emission could be a result of the PI absorbing parts of the SYTO 9 emission due to an overlapping emission spectrum of SYTO 9 with the excitation spectrum of PI resulting in resonance energy transfer and quenching (FRET) (Stocks, 2004). Furthermore, some fluorescence signal was detected for the red channel when only SYTO 9 was present in the medium but no PI. Again, this can be explained by the overlapping excitation and emission spectra of both dyes. It was previously shown that SYTO 9 has a much

stronger emission intensity than PI (Stocks, 2004). Exciting SYTO 9 at a higher wavelength that is usually chosen for PI (490 nm instead of 480 nm) can therefore still result in notable emission of SYTO 9 without PI being present, which has also been reported before (Stiefel *et al.*, 2015). To exclude that cross-talk of the dyes led to false assumptions, biofilms grown with or without the addition of laundry products were single-dye stained and imaged using CLSM as suggested by Stiefel *et al.* (Stiefel et al., 2015). However, no difference could be observed compared to the biofilms simultaneously stained with both dyes, suggesting that cross-talk does not play a big role in this study (Appendix C).

As investigating the interaction of the dyes with the laundry detergents did not lead to any new evidence, time-lapse images taken after the addition of liquid detergent to the matured biofilms were analysed again in detail with regards to the single cell staining (Figure 6.10). It was noted that almost all cells were stained at the beginning of the experiment, either with SYTO 9 (green) or PI (magenta). Already 20 min after the addition of liquid detergent to the biofilm, the majority of cells that were previously stained in green no longer show fluorescence signal. After 30 min, only very few cells were fluorescing in green, leading to the assumption that the cells were killed by the liquid detergent. However, when looking at the magenta channel, the number of cells stained with PI remained constant instead of increasing, which would be expected when the cells die. One of the earlier hypotheses was that liquid and powder detergent can increase the membrane permeability of the cells leading to a displacement of the SYTO 9 dye by PI. This seems to be questionable because although the cells lose SYTO 9 signal, it is not the result of PI displacing the SYTO 9. Instead, the SYTO 9 dye seems to exit the cells leaving behind intact cells without staining. Interestingly, is has been reported that ethidium bromide (EB), another nucleic acid stain, can cross intact cell membranes like SYTO 9 but is actively pumped out of the cell via non-specific proton antiport transport systems in healthy cells (Midgley, 1987; Hewitt and Nebe-Von-Caron, 2004). Stiefel *et al.* also described the active export of SYTO 9 from the bacterial cytoplasm as a possible explanation for the absent staining of intact Gram-negative bacteria

(Stiefel *et al.*, 2015). Hence, in this case, the addition of liquid and powder detergent could result in enhanced activity of transport systems within the intact cells leading to the export of SYTO 9, leaving behind unstained, viable cells that cannot be detected by LIVE/DEAD staining but through CFU counting.

6.3.2 Encapsulated BKC as alternative to free BKC does not show enhanced biocidal effects

Biofilm formation in WMs is a rising concern, therefore new approaches are needed to tackle this issue. This section focusses on the improvement of existing laundry products to prevent biofilm formation in its early stages. BKC is one of the commonly used biocides in hygiene products (Kim *et al.*, 2018). The idea was to facilitate the addition of BKC into liquid and powder laundry detergents by encapsulating the BKC, as addition is not possible with free BKC. Different capsule compositions were tested to find out the most effective formulation. All eBKC samples were compared to the treatment of biofilms with free BKC, where the concentration of the capsules was set to equalise the concentration of free BKC (0.2 mg mL^{-1} for all conditions). The concentration for BKC was chosen based on previous studies by Unilever showing a minimal biofilm eradication concentration between 0.2 mg mL^{-1} and 0.3 mg mL^{-1} of BKC for biocidal activity against biofilm formation of PAO1 (unpublished).

Firstly, the effects of eBKC on planktonic PAO1-N growth were assessed and compared to free BKC (Figure 6.11). It was shown that all samples led to the inhibition of growth, except eBKC I, which is the negative control without BKC incorporated. This was as expected because BKC at the chosen concentration should kill planktonic cells as already shown and discussed in Chapter 5. The eBKC samples were able to release the incorporated BKC to prevent bacterial growth, whereas the capsules alone without biocide (eBKC I) did not influence planktonic growth.

Secondly, the ability of PAO1-N to form biofilms when grown in medium consisting of free BKC or eBKC was investigated using LIVE/DEAD staining with CLSM and CFU counting, as previously

discussed (6.3.1). Although all eBKC samples contain 0.02% fluorescein, a green fluorescent dye, CLSM imaging has shown that the fluorescence was not detectable when biofilms were grown in medium with eBKC present (Appendix D). Consequently, LIVE/DEAD staining could be used in this approach. Both methods, CLSM and CFU, led to similar trends with reduced viable cells for all samples and reduced number of total cells for most of the eBKC samples after 48 h of incubation (Figure 6.12 and Figure 6.13). The main exception was the negative control eBKC I that showed reduced biofilm formation and live cells for the LIVE/DEAD staining but no difference in viable counts for the CFU experiment. If the negative control eBKC I has an effect on the biofilm formation, it must be considered that all effects seen for the other samples could be a consequence of the capsules itself being toxic to the cells rather than the incorporated BKC. However, as no growth defect was observed neither for the planktonic growth nor for the CFU experiment, it is more likely that the results obtained from eBKC I for the LIVE/DEAD staining are explainable by the negative charge of the control particles (see Appendix E) and artifacts like simultaneous staining of live and dead cells. A negative charge of nanoparticles could negatively influence biofilm formation as a result of repulsion between the particles and the anionic nature of the biofilm matrix (see Chapter 3). Overall, the results indicate that the eBKC is working as the presence within the growth medium inhibits biofilm formation for most of the samples and leads to a reduced number of viable cells. However, the effect is lower than for free BKC although the concentration of BKC present is the same. One possible explanation is the time that it takes for the capsules to release the BKC to the medium. The free BKC can work and inhibit biofilm formation right from the beginning of the experiment, whereas for samples with eBKC, cells can start biofilm formation before the BKC is being released. Hence, some microcolonies can already exist that are subsequently protected against the BKC because of the biofilm structure and matrix (Tribedi *et al.*, 2015). Even though the BKC can subsequently inhibit further growth and extended biofilm formation, more viable cells would be detected after 48 h compared to the treatment with free BKC. Interestingly, these results are in contrast to the planktonic growth experiment showing no growth at all for all samples underlaying the

difference between planktonic growth and biofilm growth as well as the importance of experiments investigating both aspects.

Looking at the images taken of the matured biofilms it was striking that almost all eBKC samples resulted in clumping of the cells, which was not seen for the free BKC. This is likely to be a side effect from the capsules, that are relatively large with a size of 11-18 µm (Appendix E). In Chapter 3, the addition of cationic amidine beads with a size of 1.56 µm also resulted in clumping of the cells during biofilm formation, which was suggested to be a result of the size. It was not possible to determine whether the clumps consisted only of cells or also of other artefacts like components of the capsules that were unintentionally stained with the LIVE/DEAD kit and should be further investigated. Either way, the clumping led to difficulties in determining the exact cell numbers for live and dead cells as a large clump usually only gets counted as one cell. Therefore, underestimation for both the live and the dead numbers of cells can occur.

It should also be noted that simultaneous colouring was observed for live and dead staining at the same time when comparing the two individual channels. This was especially true for the biofilms grown in medium with free BKC and for the regions with accumulated clumping. Thus, determination between live and dead cells was difficult and could have led to overestimation of live or dead cells, respectively. Simultaneous staining of cells using the LIVE/DEAD™ BacLight™ Bacterial Viability Kit has been reported in the literature (Stocks, 2004; Müsken *et al.*, 2010; Stiefel *et al.*, 2015). One possible explanation is that SYTO 9 is not completely displaced by PI in dead cells; hence these cells are still fluorescing in green at the same time as in red (Müsken *et al.*, 2010). Stiefel *et al.* even reported an 18-fold stronger SYTO 9 fluorescence intensity for dead *P. aeruginosa* cells than for live cells, which was still the case after counterstaining with PI (Stiefel *et al.*, 2015). This effect of stronger SYTO 9 staining of dead cells was also shown for other Gram-negative bacteria, such as *E. coli*, but not for Gram-positive species (Stiefel *et al.*, 2015). Although it is widely known and one of the advantages of both dyes that the fluorescent signal is strongly enhanced when bound to nucleic acid, up to 100-fold for SYTO 9 and 20 to 30-fold for PI, this

does not explain the enhanced SYTO 9 signal for dead cells compared to live cells (Stocks, 2004; Stiefel *et al.*, 2015). Instead, Stocks *et al.* assumes that the reason for the dual staining arise from the equal fluorescence intensity of SYTO 9 and PI at 600 nm emission when bound to DNA. It seems to be important to provide PI in excess to DNA to stain all nucleic acid present whereas the concentration of SYTO 9 is less important and can be adjusted to optimise fluorescence intensity (Stocks, 2004). In this work, the recommended ratio and amount of dye was used following the manufacturer's advice. For future experiments, an increased concentration of PI should be considered to secure an excess of the dye and thus reduce simultaneous staining with both dyes. Additionally, alternative dyes to stain DNA, such as SYBR green, should also be taken into account. SYBR green shows similar properties like SYTO 9 with regards to fluorescence enhancement upon binging and membrane permeability, but problems with stronger staining of dead cells in Gram-negative bacteria was also reported (Barbesti *et al.*, 2000; Berney *et al.*, 2007). Other dyes are often less suitable, for example due to high background fluorescence signal. Instead of staining live cells, genetic engineering could be used to label cells with the green fluorescence protein (GFP) or other derivates. One advantage is that only viable cells would be detected, whereas dead cells could still be stained using PI. However, it can take some time for GFP to be degraded again, even when using the half-life version, which could again lead to green and red fluorescence at the same time. Cross-talk between GFP fluorescence and autofluorescence of PAO1 could also impede the analysis. In addition, labelling strains with GFP involves genetic modification, which is not always appropriate especially for environmental strains. Furthermore, the production of a large molecule like GFP might alter the cell metabolism and could therefore influence the outcome of the experiment.

In a third approach, BKC was added to established biofilms for 30 min to investigate killing effects (Figure 6.14 and Figure 6.15). Again, LIVE/DEAD staining and CFU counting showed the same trends indicating that free BKC as well as some eBKC samples have a negative effect on cell viability after 30 min. CLSM demonstrated killing ability for free BKC as well as for all eBKC

samples (although not statistically significant due to low number of replicates), whereas CFU counting resulted in significantly reduced viability of cells when unencapsulated BKC and eBKC A, C, G, or H was added. As already discussed, LIVE/DEAD staining and CFUs cannot directly be linked to each other. Nevertheless, both experiments show a partial functionality of the eBKC samples to combat biofilm formation, although free BKC is more effective than encapsulated BKC. Equally to the previous experiment, the addition of some eBKC samples (namely A, B, G, H, and to some extent I) led to clumping that was observed with CLSM, likely because of their size. Again, it was not clear whether the clumps consist of mostly cells or other fragments and quantification as well as interpretation was difficult. Looking at Table 6.2, it seems that the clumping is independent of the different components of the capsules.

Table 6.2: Overview about the presence or absence of zein protein, epoxy-silica and glutaraldehyde used for the outer coating of the eBKC samples. n = no, not present (highlighted in purple), y = yes, present (highlighted in green), yy = yes, present with double the amount (highlighted in yellow)

Sample	Zein	Epoxy-Silica	Glutaraldehyde	Description
A	n	n	n	no outer coating
B	n	y	n	Epoxy-Silica only
C	y	y	n	Zein and Epoxy-Silica
D	yy	y	n	Zein (2x) and Epoxy-Silica
E	n	n	y	Glutaraldehyde only
F	n	y	y	Epoxy-Silica and Glutaraldehyde
G	y	y	y	Zein, Epoxy-Silica and Glutaraldehyde
H	yy	y	y	Zein (2x), Epoxy-Silica and Glutaraldehyde
I	yy	y	y	Zein (2x), Epoxy-Silica and Glutaraldehyde (no BKC)

Sample A has no additional outer coating but still led to clumping when added to the biofilm. In contrast, G, H, and I all contain zein, epoxy-silica and glutaraldehyde and still resulted in cell clumping as well as sample B, which only consists of epoxy-silica. Furthermore, no obvious relation can be found between the composition and the effectiveness of the different samples.

Another possible factor that could influence the interaction of the capsules with the biofilm is the charge of the eBKC. All eBKC samples that consist of BKC are positively charged, whereas the control without BKC, eBKC I, contains a negative surface charge (Appendix E). In Chapter 3 it was shown that the surface charge of the particles can influence the biofilm structure when added to an established biofilm, with positively charged particles being more disturbing. However, as clumping was observed for both positively and negatively charged samples, it is unlikely that the charge alone is responsible for the observed side effects in this study.

Overall, it was shown that free BKC has a stronger negative effect on biofilm formation and viable cells compared to the eBKC samples, even though eBKC also seems to work to an extent. Especially notable was the CFU result for free BKC, which showed no cell recovery at all after 30 min of treatment, indicating entire killing of the cells. That means that under the tested conditions, a concentration of 0.2 mg mL^{-1} unencapsulated BKC is enough to enable biofilm eradication. This result was not as evident in the CLSM; however as mentioned above, this could be a result of simultaneous staining of SYTO 9 and PI leading to overestimation of live cells. One influencing factor that has been discussed before is time. The treatment of the biofilms with BKC was performed for 30 min, which might not be long enough for the eBKC to fully display its whole effect. To investigate if a longer treatment with encapsulated BKC would lead to the same complete eradication of biofilms as seen for unencapsulated BKC, three samples were chosen for further experiments: eBKC D, H, and I, the negative control. The samples were selected in consultation with Unilever and based on the results discussed so far.

Using LIVE/DEAD staining, it was shown that a longer treatment with eBKC D for 24 h instead of 30 min resulted in increased killing represented by a reduced percentage of live cells (Figure

6.16). In contrast, treatment with eBKC H did not lead to higher biofilm eradication after 24 h. The negative control eBKC I showed no difference in viability after 24 h of treatment compared to before the addition of the sample, although some clumping was still observed. This supports the hypothesis that the previous results showing an effect of eBKC I on the viability are not trustworthy but rather an experimental artefact. Results for the CFU counting support these studies showing an increased effect for eBKC D and an unchanged impact of eBKC H (Figure 6.17). However, even after a 24 h treatment, viable cells were still detected and cells were able to reproduce, validating the observation that free BKC is more effective than eBKC.

As already mentioned, recent data shows that consumers buy more liquid products than powder detergent, which can lead to reduced hygienic effects due to the absence of bleaching agents in liquid products. However, unencapsulated BKC cannot be included in liquid or powder products. Therefore, liquid detergent was combined with selected samples of eBKC to investigate the possibility of incorporating BKC into liquid products. The same three eBKC samples were selected as before (eBKC D, H and I), mixed with liquid detergent and added to established biofilms for 30 min. Interestingly, the CFU experiments show a diminished effect of the treatment compared to the eBKC alone, with no reduction in viable cells for any of the samples (Figure 6.19). In contrast, data for the LIVE/DEAD staining still show a reduction in live cells after 30 min, with an increased lowering in viable cells for eBKC D when liquid detergent was included (Figure 6.18). However, it is very likely that these observations are a result of the cells losing the SYTO 9 signal due to the addition of liquid detergent rather than a real effect of the combined treatment. One possibility is that the chemical properties of the liquid detergent are preventing the BKC from being released, although this is rather unlikely. More likely, it can be speculated that the liquid detergent still mitigates the biocidal effect of encapsulated BKC because of charge neutralisation as result of the interaction between the cationic BKC with anionic surfactants. This problem could be overcome by including a wash step to remove the liquid detergent after a certain time, so that only the eBKC stays within the biofilm sample while the BKC gets released.

However, due to the viscosity of the biofilm samples when liquid detergent was present, no wash step could be conducted as the whole biofilm would have been disrupted. A possible work-around would be the use of a flow-cell system such as the BioFlux. However, the rather big size of the eBKC samples would have led to congestion of the BioFlux channels and was therefore not performed. Instead, the use of other more suitable flow-cell systems should be considered for future experiments involving the eBKC samples.

6.3.3 Surface coating with anti-attachment materials could be a valid alternative to biocides to prevent biofilm formation in washing machines

Recent research pointed out that BKC and other biocides that are released into the environment via cleaning products can lead to antimicrobial resistance and therefore increased infection risks (Russell *et al.*, 1998; Price *et al.*, 2002; Russell, 2002; Langsrud *et al.*, 2003; Karatzas *et al.*, 2007; McMahon *et al.*, 2007; Mc Cay *et al.*, 2010; Kim *et al.*, 2018). Moreover, the accumulation of released biocides is harmful for the environment and should ideally be suspended. One of the currently favoured options over the application of biocides is the use of surface materials that prevent the initial attachment of bacteria.

To investigate the anti-biofouling properties of the four investigated materials in this study, attachment of PAO1-N was assessed using scanning electron microscopy (SEM) after 3 h of static incubation (Figure 6.20). Quantification of the images revealed significantly reduced attachment for the coating with PEOX, whereas P-123 led to significantly increased attachment of PAO1-N. Both other materials, P19 and PDMS, did not result in significant changes compared to the uncoated glass disk. The lower attachment of bacteria on the glass disk coated with PEOX 500 was not surprising as anti-attachment properties of PEOX, also known as PEtOX, has already been outlined in multiple publications, for example by Tauhardt *et al.*, who observed a clear reduction of bioadhesion by up to 66% compared to uncoated glass (Tauhardt *et al.*, 2014). Antifouling benefits and reduced protein contamination of surfaces that have been coated with

PEOX was also shown by Wang *et al* (Wang *et al.*, 2011). PEOX is found to be a suitable material for biomedical application due to its biocompatibility, stealth behaviour, low critical solution temperature in water, and little immunogenicity (Lin *et al.*, 1988; Woddle *et al.*, 1994; Zalipsky *et al.*, 1995; Mero *et al.*, 2008; Hoogenboom, 2009; Moreadith *et al.*, 2017; Salmanpour *et al.*, 2017). Because of these properties, PEOX is investigated as an alternative coating material to PEG, which is a widely used polymer for biopassive and repellent coatings, but undergoes degradation by auto-oxidation that reduces its long term application (Amiji and Park, 1993; Bearinger *et al.*, 2003; Banerjee *et al.*, 2011; Tauhardt *et al.*, 2014). Furthermore, the preparation of PEOX yields well-defined polymers with controlled molar masses and low polydisperity index values whilst at the same time being less labour intensive than the preparation of PEG (Tauhardt *et al.*, 2014).

In contrast, the coating with P-123 led to inverse effects of increased attachment of bacteria. P-123 is another biocompatible polymer that has been studied mostly for its use in drug delivery systems (Zhang *et al.*, 2011; Wang *et al.*, 2013). P-123 is a hydrophobic block polymer and was found to be extremely non-toxic to human cells whilst being active against promastigotes and amastigotes of the parasite *Leishmania amazonensis* (Amin and Dannenfelser, 2006; Oyama *et al.*, 2019). Zoom-in images showed enhanced flagella production for the cells grown on P-123 coated glass, which could improve the attachment of cells and subsequently increase biofouling. Further investigation is needed to work out if this observation was a false negative result due to the lack of replicates or if not, why flagella production and attachment of PAO1-N was enhanced.

Both other materials, P19 and PDMS, did not show any significant anti-attachment properties, which was as expected for PDMS. PDMS is a very hydrophobic polymer that has been widely used in biomedical applications such as catheters, contact lenses, disease diagnostics, and drug delivery (Abbasi *et al.*, 2001; Abbasi *et al.*, 2006; Pirmoradi *et al.*, 2011; Zhang *et al.*, 2011). The material is biocompatible, shows a low toxicity, is gas permeable, and low in manufacturing costs, making it an attractive target (Zhang *et al.*, 2011). However, due to its high hydrophobicity,

PDMS-based devices are affected by low wettability and biofouling problems caused by nonspecific protein adsorption and bacterial adhesion leading to acute and chronic healthcare-associated infections (Zhang *et al.*, 2011; Magennis *et al.*, 2016). In contrast, P19 is a Unilever developmental material that has not been used in other studies published to date.

Overall, good anti-attachment properties were observed for the coating of glass disks with PEOX 500, which should be further investigated. However, this study only provides preliminary data with only one replicate for each material being analysed, making it difficult to draw any secure statements.

6.4 Conclusion

Various methods were used to demonstrate that different laundry products have diverse effects on planktonic cell growth and biofilm formation of *P. aeruginosa*. Both techniques that were used, LIVE/DEAD staining combined with CLSM as well as CFU counting, are valid methods to investigate cell viability. Although LIVE/DEAD staining exhibited some challenges, microscopy was proven to be crucial to detect structural changes under the various conditions that would get lost otherwise, such as the clumping of the cells during the presence of eBKC samples. Powder detergent was shown to be the most effective product out of the three laundry products to prevent bacterial growth and biofouling. Although literature suggested fabric conditioner as alternative to improve hygiene in WM, this could not be validated. Furthermore, the WM isolate WMB1.3 showed partially increased resistance to the laundry products, as expected. LIVE/DEAD staining of biofilms was shown to be affected by the presence of liquid and powder detergent, hypothesising that efflux pump activity might be enhanced, which needs further investigation, for example by using efflux pump mutants. All experiments were conducted at 37°C, which lies within the temperature mostly used for laundry in European countries (30°C-40°C). However, the experiments should also be investigated under different temperature profiles.

Encapsulated BKC as alternative to free BKC was shown to reduce biofilm formation of PAO1-N; however, unencapsulated BKC was more effective independent on the length of the treatment. Furthermore, a functional combination of eBKC with liquid detergent could not be shown under the tested conditions. In addition, the controlled release of the BKC turned out to be difficult because of the leakage of the capsules, that could not retain the water soluble BKC inside the capsules (Unilever, unpublished), so that no advantages of the eBKC over unencapsulated BKC could be demonstrated. Moreover, preliminary data on material coating confirmed studies showing that the polymer PEOX 500 could be a suitable alternative to biocides by effectively preventing initial bacterial attachment in coated WMs.

Chapter 7 Final Conclusion and Future Aspects

7.1 Summary

A major goal of this study was the investigation of pH microniches within biofilms of *P. aeruginosa* using novel pH-sensitive optical nanosensors. In addition, special attention was given to biofilm formation within WMs, which has become a growing concern because of the spread of opportunistic human pathogens like *P. aeruginosa* in domestic environments. The main questions of this work were as follows and could successfully be answered throughout this study:

- Can optical pH-sensitive polyacrylamide nanosensors be produced and used within planktonic as well as static and flow-cell biofilm models of *P. aeruginosa*?
- How does the pH change over time within planktonic cells as well as biofilms and can those changes and gradients be measured and visualised using the pH-sensitive nanosensors?
- How do bacteria isolated from household washing machines differ in their phenotypes and genotypes and are those strains better adapted to their environment within washing machines compared to lab strains?
- What effects do commercially available laundry products have on biofilm formation of *P. aeruginosa* and can encapsulated biocides improve the hygienic effect?

Chapter 3 describes the successful production, characterisation, and examination of different types of nanosensors used in two different *in vitro P. aeruginosa* biofilm models. pH-sensitive nanosensors were fabricated using three fluorophores, the two pH-sensitive fluorophores OG and FAM and the pH-insensitive fluorophore TAMRA, that were incorporated into an inert polyacrylamide matrix to enable fluorescence signal detection corresponding to the surrounding pH. The size of the nanoparticles ranged between 38 nm and 47 nm, with batches of

nanosensors prepared containing a neutral charge (~-2.17 mV) or a positive charge (13 mV-18 mV). The nanosensors were responsive to changes in their pH environment, which was analysed using different pH buffer solutions ranging between pH 2.5 and pH 8. The fluorescence response of the reference dye TAMRA remained stable independent of the pH, whereas the fluorescence signal of OG and FAM decreased with declining pH, as expected (Chauhan *et al.*, 2013).

It was shown that both neutral and positively charged polyacrylamide nanosensors at concentrations below 25 µg mL^{-1} had no effect on planktonic growth and could thus be used to analyse the pH microenvironments. Furthermore, SIM was used to confirm that the nanosensors did not get internalised by the cells, meaning that any future pH measurements represented the environment outside of the cells rather than within the bacteria. Optical characterisation using CLSM was performed revealing that both types of nanosensors were able to penetrate biofilms of *P. aeruginosa* while being well distributed throughout the whole structure. However, a positive charge of the nanosensors was shown to influence static biofilm formation by enhancing biomass and making the biofilm more robust, probably because of interactions between the positive charge of the nanosensors and the negative charge of the cells and matrix components such as eDNA or polysaccharides. This thickness promoting effect was not observed in flow-cell biofilm models, suggesting that a continuous flow of medium prevents a stronger interaction between the nanosensors and the biofilm components. The interaction between positively charged nanosensors and the biofilm components was investigated in more detail using mutant strains, selectively binding dyes, and single-coloured nanoparticles, exhibiting the same characteristics as the pH-sensitive nanosensors. Initially, no direct interaction was observed between positive particles and the two exopolysaccharides Psl (neutral charge) and Pel (positive charge). However, staining of the specific polysaccharides was found to be challenging so that an interaction could not be excluded. In contrast, co-localisation of eDNA and nanoparticles was observed suggesting a direct interaction between both components. Additionally, SIM revealed

coating of the negative surface of bacteria with positively charged nanosensors. It is therefore likely that the nanosensors interacted with multiple components of the biofilm, probably neutral or negatively charged.

Chapter 4 investigated the pH responsiveness of the nanosensors during planktonic and biofilm growth of *P. aeruginosa* and revealed pH gradients inside biofilm microcolonies. The pH of planktonic cell cultures was measured over time and compared using the pH-sensitive nanosensors and commercially available microsensors (PreSens). It was shown that both systems delivered equivalent pH measurements, with the nanosensors being a more suitable tool for biofilm analysis as they can be incorporated within planktonic cultures and biofilms. Responsiveness of the nanosensors to pH changes within matured biofilms was also assessed, with a sharp drop in pH after the addition of acetic acid to the biofilm, as expected, and served as a proof of concept. During growth measurements of *P. aeruginosa* cell cultures, pH changes using nanosensors were observed, which were dependent on the two different carbon sources used: glucose and succinate. While the consumption of succinate over time led to an obvious increase of pH possibly as a result of acid uptake, the metabolisation of glucose only resulted in a small pH drop. However, when starved cells were fed with glucose, a rapid reduction in the pH was observed because of enhanced glucose metabolism.

For the first time, a release of acidic products was shown during biofilm formation under flow conditions using time-lapse imaging. After 10 h of biofilm development, a red streak was observed coming from the microcolonies that was taken away by the flow, indicated by a colour change of the nanosensors. The visualised acidic streaks could consist of eDNA or exopolysaccharides that are released by the cells to help biofilm formation. Other possible explanations include the active lowering of the pH by the cells to initiate biofilm formation, for example to increase the pH-dependent turn-over of QS signalling pathways. In addition to pH changes observed between microcolonies, pH variation was also detected within single microcolonies using CLSM, showing a more acidic core with a neutral pH at the outside. These

findings were in accordance with observations by Hidalgo *et al.* and Fulaz *et al.* and are likely a result of oxygen depletion within the core of microcolonies as well as accumulation of acidic metabolites due to reduced diffusion rates (Hidalgo *et al.*, 2009; Fulaz *et al.*, 2019).

A schematic overview about the influence of the charge of the nanosensors on biofilm formation in static biofilm models and the pH heterogeneity is given in Figure 7.1.

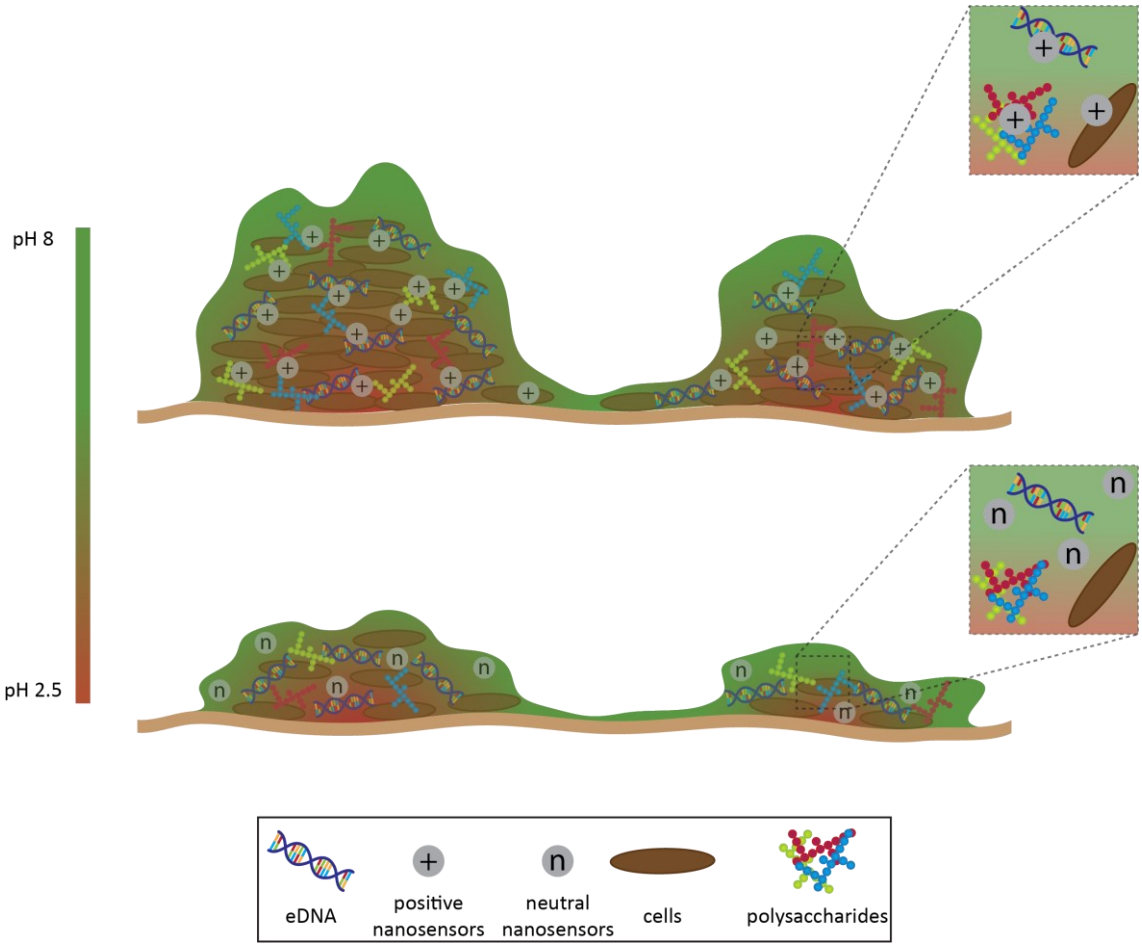


Figure 7.1: Schematic model of static biofilm formation of *P. aeruginosa* with positive (top) or neutral (bottom) pH-sensitive nanosensors. A positive charge of the nanosensors leads to enhanced biofilm thickness, with nanosensors interacting with eDNA, cells, and possibly polysaccharides, whereas a neutral charge has no effect on biofilm thickness, suggesting that no direct interaction between nanosensors and biofilm components occurs.

In addition to TAMRA as reference dye, Rhodamine Red™-X was tested after a slight decrease of TAMRA fluorescence signal was observed in long-term experiments, possibly due to self-quenching as consequence of aggregation within aqueous solutions. Rhodamine Red™-X has

similar excitation and emission wavelength as TAMRA, and nanosensors fabricated using this dye showed comparable characteristics. Preliminary experiments confirmed the usability of Rhodamine Red™-X as alternative to TAMRA, with no reduction in fluorescence intensity over time.

Chapter 5 focussed on the isolation, identification, and characterisation of bacteria from biofilms grown in household WMs. Biofilm formation in WMs by bacteria such as *P. aeruginosa* are a cause of malodour and pose potential infection risks, especially to immunocompromised patients in their household environment. Investigation of environmental strains and their comparison with lab strains should help to identify weak points that can be used to prevent biofilm formation in WMs. Various bacteria were successfully isolated from three different sites of 22 household WMs, including three WMs that were resampled after six weeks. Isolation was performed using swabs and conventional microbiology methods, meaning that a large number of bacteria could not be picked up, for example because they are not culturable. However, as this study focused on the isolation of *P. aeruginosa*, this downside was not of relevance. Most bacteria were isolated from the drawer, followed by the seal and the drum. To reduce the number of samples for further characterisation, phenotypic assays were performed to specifically screen for *P. aeruginosa* strains, including Gram-staining, oxidase and catalase assays, 16S rRNA PCR, and MALDI identification. Although the culturing was biased towards *P. aeruginosa* strains, a variety of bacteria was identified, such as *P. stutzeri, P. alcaliphila, P. nitroreducens, M. luteus, Se. marcescens,* and *P. aeruginosa*. Some of these strains were likely introduced to the WMs through dirty laundry that came into contact with skin, whereas other species might have entered through the water. Nine *P. aeruginosa* strains were picked for analysis of virulence factor production, including swimming and swarming motility, protease production, surface attachment, and susceptibility against BKC, a biocide used in cleaning products. The results were broad with a mix of phenotypes. Most strains were able to swarm but not to swim, which could be an indication that these strains have increased cell-cell

communication, because swarming as opposed to swimming occurs in multicellular groups. Furthermore, four strains showed reduced susceptibility against BKC, suggesting that the exposure of the strains to washing products within the WMs led to resistances. Enhanced biofilm formation as well as elevated pyocyanin production, a toxic substance produced by *P. aeruginosa*, was observed for one of the WM isolates, which could refer to increased infection potential of the WM isolate and enhanced protection against environmental stresses like biocides when forming biofilms. Whole genome sequencing was performed for all nine WM isolates and the reference strain to identify changes between genomes that could explain the observed phenotypes and give indications about the pathogenesis of these strains. A possible reduced surface charge of some WM isolates was suggested based on multiple phenotypic observations, which could be a result of altered LPS production indicated by genome differences and should be followed up in future experiment. Although many more SNPs and mutations were identified between strains that could affect genes and proteins involved in motility, antibiotic resistance, and virulence, no other direct link could be confirmed between genotypes and phenotypes, suggesting that other regulations are involved such as post-transcriptional and translational regulation. However, this study showed that household WMs are colonised by many different bacteria including opportunistic human pathogens that can cause infection risks and malodour, and that all analysed strains have the potential to become virulent, which highlights the need for improved hygienic concepts of WMs.

To address this issue, Chapter 6 describes the use of common laundry products and their effectiveness against bacterial colonisation and eradication. In addition, different formulations were tested to analyse the effectiveness of encapsulated BKC compared to free BKC in laundry products, with the aim to eventually better control the release of BKC into the environment and to improve the hygienic effects of existing products. Different *in vitro* models were used to assess successful biofilm formation, including static and flow-cell biofilm models combined with LIVE/DEAD staining and CLSM as well as CFU counting of suspended biofilms. Overall, it was

found that the powder product reduced biofilm formation more effectively than liquid product or fabric conditioner, but results differed between used models. LIVE/DEAD staining of bacteria that was analysed using CLSM showed reduction in bacterial growth and biofilm development for both powder and liquid detergent, whereas CFU counting did not reveal changes between treatment and control. Further investigations suggested that the addition of laundry detergents to the cells might enhance efflux pumps, leading to the release of molecules including the dyes that were used for staining. It can only be speculated that an enhanced activation of efflux pumps as a result of washing product addition could also lead to the efflux of biocides present in the detergents, which in turn could negate the effect of the biocide.

Furthermore, it was shown that regardless of the formulation or incubation time, free BKC was more effective in biofilm prevention than eBKC, suggesting that alternative formulations or methods need to be investigated to improve current products. One popular idea is to initially prevent biofilm formation instead of treating it, which would reduce the amount of detergents being released to the environment and subsequently lower the number of antimicrobial resistant strains. Some preliminary experiments were conducted to look at materials that could be used for coating of WMs to prevent initial attachment of bacteria. Using SEM to look at early attachment of *P. aeruginosa* on differently coated glass discs, one material, PEOX 500, was successfully identified that significantly reduced bacterial colonisation and should be further investigated.

7.2 Future aspects

Understanding the microenvironments within biofilms is crucial to develop new methods to treat and prevent biofilm infections in healthcare. However, most techniques used so far show limitations that need to be overcome, for example the disruption of biofilms during the measurements. The use of nanosensors can help overcome these limitations and were shown to provide a useful tool to analyse pH microniches in biofilms of *P. aeruginosa*. Although acidification of biofilms and microcolonies was shown in this study, it is not yet clear why

acidification takes place and what the mechanisms are, which should be investigated in the future to find potential weak points that can be approached to prevent biofilm formation. Reporter systems could be used to look at the transcription or translation of specific genes or proteins during acidification, although the combination with the nanosensors might be challenging due to the colour limitation of suitable fluorescence proteins. Future work should also explore the molecular mechanisms underpinning the detected acidification of the biofilms and microcolony centres, for example by looking at the metabolome of specific regions. Potential techniques could involve TOF-SIMS, cryo-OrbiSIMS, or Raman spectroscopy of biofilms (Davies *et al.*, 2017; Barzan *et al.*, 2020; Zhang *et al.*, 2020). In addition, other parameters than pH could be monitored using polyacrylamide nanosensors within the same system by substituting the pH-sensitive fluorophores to alternative compounds that can monitor oxygen, glucose, or enzymes such as proteases by adding the substrate to the surface of the nanosensors, which can be cleaved off when the enzyme is present, releasing fluorescence signals (Welser *et al.*, 2011). Monitoring these additional parameters could provide further insights into the heterogeneity of biofilm microniches. Apart from biofilms, the nanosensors could also be applied to other systems to improve understanding of pH variation, even in *ex vivo* or *in vivo* models. A practical application of our nanosensor system could be envisioned for testing oral hygiene products or sweetener alternatives in soft drink production, in order to determine the impact on pH changes. The nanosensors would provide flexibility as a screening tool to measure pH changes in high throughput fluorescence assays. However, the choice of the nanosensors should be well considered as interaction of the positively charged nanosensors with negatively charged particles of the biofilm was observed. This behaviour should be further analysed, for example to exclude the possibility that positively charged antimicrobials have a stimulating effect on biofilm formation rather than a negative impact. Furthermore, the interaction of the positive nanosensors with other negatively charged molecules of the matrix such as alginate could be analysed in more detail, for example by using various mutants. DNase could be added to biofilm assays to reduce the amount of eDNA, which could confirm

interactions between the cationic nanosensors and the negatively charged eDNA. Detailed information on the impact of the nanosensors on the transcriptome is also missing, although no reduction in growth was observed. However, Li *et al.* showed enhanced QS signal production upon addition of Ag and Go nanoparticles, and examination of transcriptome and proteome data should be considered for the effects of nanosensors used in this study (N. Li *et al.*, 2018). In addition, QS reporters could be used to investigate QS activity and QS regulator expression, and production of QS signalling molecules could be measured.

Another aim of this study was the characterisation of biofilms within WMs, including their colonisation and use of laundry products. This is important because biofilms in WMs pose infection risks and malodour due to changes in washing behaviours and increasing population of antimicrobial resistant bacteria in the environment. Although it was shown that phenotypes and genotypes of bacteria isolated from WMs differ from commonly used lab strains, it is not yet clear how these changes can affect the pathogenesis and virulence of the isolates. Transcriptome analysis would help to identify changes in the regulation systems such as quorum sensing or virulence factor production. Additionally, transcriptome analysis, e.g. RNASeq, would be interesting to perform during exposure of biofilms to laundry products, as enhanced efflux pump activation was suggested and shown by Kim *et al.* during the exposure of bacteria to BKC (Kim *et al.*, 2018). These findings could help to improve current laundry products and make them more effective in treating WM colonisation in the future. The isolation of the environmental isolates provides a broad range of strains that will help to investigate new antimicrobial approaches in the future, as this study confirmed the importance to not only use lab strains, because relevant differences exist such as antimicrobial susceptibility.

The approach to use coatings to prevent biofilm formation in WMs instead of treatment with antimicrobials should be followed up, as first trials were promising and could significantly reduce infection risks, malodour, and environmental pollution by detergents in the future. Examples for the discovery of materials that are resistant to bacterial attachment already exist using non-

biased polymer screenings, and the coating of medical devices such as catheters to reduce biofilm formation in the clinical environment has already been followed up as a promising approach (Danese, 2002; Hook *et al.*, 2012; Hook *et al.*, 2013; Magennis *et al.*, 2016; Mikulskis *et al.*, 2018; Dundas *et al.*, 2019).

References

Abbasi, F., Mirzadeh, H. and Katbab, A.-A. 2001. Modification of polysiloxane polymers for biomedical applications: a review. *Polymer International*, 50, 1279-1287.

Abbasi, F., Mirzadeh, H. and Simjoo, M. 2006. Hydrophilic interpenetrating polymer networks of poly(dimethyl siloxane) (PDMS) as biomaterial for cochlear implants. *J Biomater Sci Polym Ed*, 17, 341-355.

Abbaszadegan, A., Nabavizadeh, M., Gholami, A., Aleyasin, Z. S., Dorostkar, S., Saliminasab, M., Ghasemi, Y., Hemmateenejad, B. and Sharghi, H. 2015. Positively charged imidazolium-based ionic liquid-protected silver nanoparticles: a promising disinfectant in root canal treatment. *Int Endod J*, 48, 790-800.

Abraham, N. and Kwon, D. H. 2009. A single amino acid substitution in PmrB is associated with polymyxin B resistance in clinical isolate of *Pseudomonas aeruginosa*. *FEMS Microbiol Lett*, 298, 249-254.

Abràmoff, M. D., Magalhães, P. J. and Ram, S. J. 2004. Image processing with ImageJ. *Biophotonics International*, 11, 36-42.

Adair, F. W., Geftic, S. G. and Gelzer, J. 1969. Resistance of *Pseudomonas* to quaternary ammonium compounds I. Growth in benzalkonium chloride solution. *Appl Microbiol*, 18, 299-302.

Ahmed, K. and Jones, M. N. 2003. The effect of shear on the desorption of liposomes adsorbed to bacterial biofilms. *J Liposome Res*, 13, 187-197.

Ahmed, N. A. A. M., Petersen, F. C. and Scheie, A. A. 2008. Biofilm formation and autoinducer-2 signaling in *Streptococcus intermedius* - role of thermal and pH factors. *Oral Microbiol Immunol*, 23, 492–497.

Ainsworth, P. and Fletcher, J. 1993. A comparison of the disinfectant action of a powder and liquid detergent during lowtemperature laundering. *J Consumer Stud Home Econ*, 17, 67-73.

Akimitsu, N., Hamamoto, H., Inoue, R. I., Shoji, M., Akamine, A., Takemori, K. I., Hamasaki, N. and Sekimizu, K. 1999. Increase in resistance of methicillin-resistant *Staphylococcus aureus* to beta-lactams caused by mutations conferring resistance to benzalkonium chloride, a disinfectant widely used in hospitals. *Antimicrob Agents Chemother*, 43, 3042–3043.

Al-Wrafy, F., Brzozowska, E., Gorska, S. and Gamian, A. 2017. Pathogenic factors of *Pseudomonas aeruginosa* - the role of biofilm in pathogenicity and as a target for phage therapy. *Postepy Hig Med Dosw (Online)*, 71, 78-91.

Aleraj, B., Kruzić, V. and Borcić, B. 1990. Epidemiology of enteroviral meningitis in Croatia 1958-1988 with special emphasis on the great epidemic of 1988. *Lijec Vjesn*, 112, 305-309.

Alhede, M. and Alhede, M. 2014. The biofilm challenge. *EWMA*, 14, 54-58.

Allan, V. J. M., Macaskie, L. E. and Callow, M. E. 1999. Development of a pH gradient within a biofilm is dependent upon the limiting nutrient. *Biotechnol Lett*, 21, 407–413.

Allesen-Holm, M., Barken, K. B., Yang, L., Klausen, M., Webb, J. S., Kjelleberg, S., Molin, S., Givskov, M. and Tolker-Nielsen, T. 2006. A characterization of DNA release in *Pseudomonas aeruginosa* cultures and biofilms. *Mol Microbiol*, 59, 1114-1128.

Amiel, E., Lovewell, R. R., O'Toole, G. A., Hogan, D. A. and Berwin, B. 2010. *Pseudomonas aeruginosa* evasion of phagocytosis is mediated by loss of swimming motility and is independent of flagellum expression. *Infect Immun*, 78, 2937-2945.

Amiji, M. and Park, K. 1993. Surface modification of polymeric biomaterials with poly(ethylene oxide), albumin, and heparin for reduced thrombogenicity. *J Biomater Sci Polym Ed*, 4, 217-234.

Amin, K. and Dannenfelser, R. M. 2006. *In vitro* hemolysis: guidance for the pharmaceutical scientist. *J Pharm Sci*, 95, 1173-1176.

Arciola, C. R., Alvi, F. I., An, Y. H., Campoccia, D. and Montanaro, L. 2005. Implant infection and infection resistant materials: A mini review. *Int J Artif Organs*, 28, 1119-1125.

Arild, A. H., Brusdal, R., Gunnarsen, J. T. H., Terpstra, P. M. J. and van Kessel, I. A. C. 2003. An investigation of domestic laundry in Europe – Habits, hygiene and functional performance, *European Commission - Consumer policy programme*, National Institut for Consumer Research.

Arora, S. K., Dasgupta, N., Lory, S. and Ramphal, R. 2000. Identification of two distinct types of flagellar cap proteins, FliD, in *Pseudomonas aeruginosa*. *Infect and Immun*, 68, 1474-1479.

Arora, S. K., Ritchings, B. W., Almira, E. C., Lory, S. and Ramphal, R. 1998. The *Pseudomonas aeruginosa* flagellar cap protein, FliD, is responsible for mucin adhesion. *Infect and Immun*, 66, 1000-1007.

Aylott, J. W. 2003. Optical nanosensors - an enabling technology for intracellular measurements. *Analyst*, 128, 309-312.

Bae, S. W., Tan, W. and Hong, J. I. 2012. Fluorescent dye-doped silica nanoparticles: new tools for bioapplications. *Chem Commun (Camb)*, 48, 2270-2282.

Bajpai, D. and Tyagi, V. K. 2007. Laundry detergents: an overview. *J Oleo Sci.*, 56, 327-340.

Balasubramanian, V., Natarajan, K., Hemambika, B., Ramesh, N., Sumathi, C. S., Kottaimuthu, R. and Rajesh Kannan, V. 2010. High-density polyethylene (HDPE)-degrading potential bacteria from marine ecosystem of Gulf of Mannar, India. *Lett Appl Microbiol*, 51, 205-211.

Banerjee, I., Pangule, R. C. and Kane, R. S. 2011. Antifouling coatings: recent developments in the design of surfaces that prevent fouling by proteins, bacteria, and marine organisms. *Adv Mater*, 23, 690-718.

Banin, E., Vasil, M. L. and Greenberg, E. P. 2005. Iron and *Pseudomonas aeruginosa* biofilm formation. *Proc Natl Acad Sci U S A*, 102, 11076-11081.

Bao, W., Gong, R. H., Ding, X., Xue, Y., Li, P. and Fan, W. 2017. Optimizing a laundering program for textiles in a front-loading washing machine and saving energy. *Journal of Cleaner Production*, 148, 415-421.

Barbesti, S., Citterio, S., Labra, M., Baroni, M. D., Neri, M. G. and Sgorbatti, S. 2000. Two and three-color fluorescence flow cytometric analysis of immunoidentified viable bacteria. *Cytometry*, 40, 214-218.

Bardoel, B. W., van der Ent, S., Pel, M. J., Tommassen, J., Pieterse, C. M., van Kessel, K. P. and van Strijp, J. A. 2011. *Pseudomonas* evades immune recognition of flagellin in both mammals and plants. *PLoS Pathog*, 7, e1002206.

Barrie, D., Hoffman, P. N., Wilson, J. A. and Kramer, J. M. 1994. Contamination of hospital linen by *Bacillus cereus*. *Epidemiol Infect*, 113, 297-306.

Barrow, K. and Kwon, D. H. 2009. Alterations in two-component regulatory systems of *phoPQ* and *pmrAB* are associated with polymyxin B resistance in clinical isolates of *Pseudomonas aeruginosa*. *Antimicrob Agents Chemother*, 53, 5150-5154.

Barzan, G., Sacco, A., Mandrile, L., Giovannozzi, A. M., Brown, J., Portesi, C., Alexander, M. R., Williams, P., Hardie, K. R. and Rossi, A. M. 2020. New frontiers against antibiotic resistance: A Raman-based approach for rapid detection of bacterial susceptibility and biocide-induced antibiotic cross-tolerance. *Sensors and Actuators B: Chemical*, 309, 1-8.

Bayer, A. S., Eftekhar, F., Tu, J., Nast, C. C. and Speert, D. P. 1990. Oxygen-sependent up-regulation of mucoid exopolysaccharide (alginate) production in *Pseudomonas aeruginosa*. *Infect Immun*, 58, 1344-1349.

Bearinger, J. P., Terrettaz, S., Michel, R., Tirelli, N., Vogel, H., Textor, M. and Hubbell, J. A. 2003. Chemisorbed poly(propylene sulphide)-based copolymers resist biomolecular interactions. *Nat Mater*, 2, 259-264.

Bellezza, I., Peirce, M. J. and Minelli, A. 2014. Cyclic dipeptides: from bugs to brain. *Trends Mol Med*, 20, 551-558.

Ben Haj Khalifa, A., Moissenet, D., Vu Thien, H. and Khedher, M. 2011. Virulence factors in *Pseudomonas aeruginosa*: mechanisms and modes of regulation. *Ann Biol Clin (Paris)*, 69, 393-403.

Benjaminsen, R. V., Sun, H., Henriksen, J. R., Christensen, N. M., Almdal, K. and Andresen, T. L. 2011. Evaluating nanoparticle sensor design for intracellular pH measurements. *ACS Nano*, 5, 5864–5873.

Benoit, D. S. W. and Koo, H. 2016. Targeted, triggered drug delivery to tumor and biofilm microenvironments. *Nanomedicine*, 11, 873-879.

Benoit, D. S. W., Sims, K. R., Jr. and Fraser, D. 2019. Nanoparticles for oral biofilm treatments. *ACS Nano*, 13, 4869-4875.

Berney, M., Hammes, F., Bosshard, F., Weilenmann, H. U. and Egli, T. 2007. Assessment and interpretation of bacterial viability by using the LIVE/DEAD BacLight Kit in combination with flow cytometry. *Appl Environ Microbiol*, 73, 3283-3290.

Bertani, G. 1951. Studies on lysogenesis I. The mode of phage liberation by lysogenic *Escherichia coli*. *J Bacteriol*, 62, 293-300.

Bielecki, P., Glik, J., Kawecki, M. and Martins dos Santos, V. A. 2008. Towards understanding *Pseudomonas aeruginosa* burn wound infections by profiling gene expression. *Biotechnol Lett*, 30, 777-790.

Bjarnsholt, T. 2013. The role of bacterial biofilms in chronic infections. *APMIS*, 121, 1-51.

Bjarnsholt, T., Alhede, M., Alhede, M., Eickhardt-Sørensen, S. R., Moser, C., Kuhl, M., Jensen, P. O. and Høiby, N. 2013. The *in vivo* biofilm. *Trends Microbiol*, 21, 466-474.

Bjarnsholt, T. and Givskov, M. 2007. The role of quorum sensing in the pathogenicity of the cunning aggressor *Pseudomonas aeruginosa*. *Anal Bioanal Chem*, 387, 409-414.

Blankenfeldt, W. and Parsons, J. F. 2014. The structural biology of phenazine biosynthesis. *Curr Opin Struct Biol*, 29, 26-33.

Bloomfield, S. F., Exner, M., Signorelli, C., Nath, K. J. and Scott, E. A. 2011. The infection risks associated with clothing and household linens in home and everyday life settings, and the role of laundry. Available: https://www.ifh-homehygiene.org/review-best-practice/infection-risks-associated-clothing-and-household-linens-home-and-everyday-life.

Bloomfield, S. F., Exner, M., Signorelli, C. and Scott, E. A. 2013. Effectiveness of laundering processes used in domestic settings. Available: http://www.ifh-homehygiene.org/review/effectiveness-laundering-processes-used-domestic-home-settings-2013.

Bockmühl, D. 2011. Hygiene aspects in domestic laundry. *Hyg Med*, 36, 280–286.

Boratyn, G. M., Camacho, C., Cooper, P. S., Coulouris, G., Fong, A., Ma, N., Madden, T. L., Matten, W. T., McGinnis, S. D., Merezhuk, Y., Raytselis, Y., Sayers, E. W., Tao, T., Ye, J. and Zaretskaya, I. 2013. BLAST: a more efficient report with usability improvements. *Nucleic Acids Res*, 41, W29-33.

Bowen, W. H. and Koo, H. 2011. Biology of *Streptococcus mutans*-derived glucosyltransferases: role in extracellular matrix formation of cariogenic biofilms. *Caries Res*, 45, 69-86.

Bowling, F. L., Jude, E. B. and Boulton, A. J. M. 2009. MRSA and diabetic foot wounds: contaminating or infecting organisms? *Curr Diab Rep*, 9, 440-444.

Brackman, G. and Coenye, T. 2016. *In vitro* and *in vivo* biofilm wound models and their application. *Adv Exp Med Biol*, 897, 15-32.

Brandel, J., Humbert, N., Elhabiri, M., Schalk, I. J., Mislin, G. L. and Albrecht-Gary, A. M. 2012. Pyochelin, a siderophore of *Pseudomonas aeruginosa*: physicochemical characterization of the iron(III), copper(II) and zinc(II) complexes. *Dalton Trans*, 41, 2820-2834.

Breidenstein, E. B., Janot, L., Strehmel, J., Fernandez, L., Taylor, P. K., Kukavica-Ibrulj, I., Gellatly, S. L., Levesque, R. C., Overhage, J. and Hancock, R. E. 2012. The Lon protease is essential for full virulence in *Pseudomonas aeruginosa*. *PLoS One*, 7, e49123.

Bridier, A., Briandet, R., Thomas, V. and Dubois-Brissonnet, F. 2011a. Comparative biocidal activity of peracetic acid, benzalkonium chloride and *ortho*-phthalaldehyde on 77 bacterial strains. *J Hosp Infect*, 78, 208-213.

Bridier, A., Briandet, R., Thomas, V. and Dubois-Brissonnet, F. 2011b. Resistance of bacterial biofilms to disinfectants: a review. *Biofouling*, 27, 1017-1032.

Brimer, C. D. and Montie, T. C. 1998. Cloning and comparison of *fliC* genes and identification of glycosylation in the flagellin of *Pseudomonas aeruginosa* a-type strains. *J Bacteriol*, 180, 3209-3217.

Britigan, B. E., Railsback, M. A. and Cox, C. D. 1999. The *Pseudomonas aeruginosas* secretory product pyocyanin inactivates α_1 protease inhibitor: implications for the pathogenesis of cystic fibrosis lung disease. *Infect and Immun*, 67, 1207–1212.

Brown, J. M., Blunk, B., Williams, P. and Hardie, K. R. 2019. Microfluidic-based growth and imaging of bacterial biofilms. *Bio-Protocol*, 9, 1-8.

Brusdal, R. 2003. Assessment of the consumer laundry habits – a quantitative survey, *SIFO Professional Report No. 1*, European Commission - Consumer policy programme.

Bryan, L. E., O'Hara, K. and Wong, S. 1984. Lipopolysaccharide changes in impermeability-type aminoglycoside resistance in *Pseudomonas aeruginosa*. *Antimicrob Agents Chemother*, 26, 250-255.

Burns, A., Sengupta, P., Zedayko, T., Baird, B. and Wiesner, U. 2006. Core/Shell fluorescent silica nanoparticles for chemical sensing: towards single-particle laboratories. *Small*, 2, 723-726.

Burrows, L. L. 2012. *Pseudomonas aeruginosa* twitching motility: type IV pili in action. *Annu Rev Microbiol*, 66, 493-520.

Burrows, L. L., Charter, D. F. and Lam, J. S. 1996. Molecular characterization of the *Pseudomonas aeruginosa* serotype O5 (PAO1) B-band lipopolysaccharide gene cluster. *Mol Microbiol*, 22, 481-495.

Byrd, M. S., Sadovskaya, I., Vinogradov, E., Lu, H., Sprinkle, A. B., Richardson, S. H., Ma, L., Ralston, B., Parsek, M. R., Anderson, E. M., Lam, J. S. and Wozniak, D. J. 2009. Genetic and biochemical analyses of the *Pseudomonas aeruginosa* Psl exopolysaccharide reveal overlapping roles for polysaccharide synthesis enzymes in Psl and LPS production. *Mol Microbiol*, 73, 622-638.

Cai, S., Li, Y., Wang, K., Cen, Y., Lu, H., Dong, B., Chen, Y. and Kong, J. 2016. Pathogenic effects of biofilm on *Pseudomonas aeruginosa* pulmonary infection and its relationship to cytokines. *Med Sci Monit*, 22, 4869-4874.

Callewaert, C., Van Nevel, S., Kerckhof, F. M., Granitsiotis, M. S. and Boon, N. 2015. Bacterial exchange in household washing machines. *Front Microbiol*, 6, 1381.

Cao, H., Krishnan, G., Goumnerov, B., Tsongalis, J., Tompkins, R. and Rahme, L. G. 2001. A quorum sensing-associated virulence gene of *Pseudomonas aeruginosa* encodes a LysR-like transcription regulator with a unique self-regulatory mechanism. *Proc Natl Acad Sci U S A*, 98, 14613-14618.

Cao, L., Srikumar, R. and Poole, K. 2004. MexAB-OprM hyperexpression in NalC-type multidrug-resistant *Pseudomonas aeruginosa*: identification and characterization of the *nalC* gene encoding a repressor of PA3720-PA3719. *Mol Microbiol*, 53, 1423-1436.

Cao, Q., Wang, Y., Chen, F., Xia, Y., Lou, J., Zhang, X., Yang, N., Sun, X., Zhang, Q., Zhuo, C., Huang, X., Deng, X., Yang, C. G., Ye, Y., Zhao, J., Wu, M. and Lan, L. 2014. A novel signal transduction pathway that modulates *rhl* quorum sensing and bacterial virulence in *Pseudomonas aeruginosa*. *PLoS Pathog*, 10, e1004340.

Cerca, N., Jefferson, K. K., Oliveira, R., Pier, G. B. and Azeredo, J. 2006. Comparative antibody-mediated phagocytosis of *Staphylococcus epidermidis* cells grown in a biofilm or in the planktonic state. *Infect Immun*, 74, 4849-4855.

Chauhan, V. M., Burnett, G. R. and Aylott, J. W. 2011. Dual-fluorophore ratiometric pH nanosensor with tuneable pK_a and extended dynamic range. *Analyst*, 136, 1799-1801.

Chauhan, V. M., Giuntini, F. and Aylott, J. W. 2016. Quadruple labelled dual oxygen and pH-sensitive ratiometric nanosensors. *Sens Biosensing Res*, 8, 36-42.

Chauhan, V. M., Orsi, G., Brown, A., Pritchard, D. I. and Aylott, J. W. 2013. Mapping the pharyngeal and intestinal pH of *Caenorhabditis elegans* and real-time luminal pH oscillations using extended dynamic range pH-sensitive nanosensors. *ACS Nano*, 7, 5577–5587.

Choi, Y., Park, H. Y., Park, S. J., Park, S. J., Kim, S. K., Ha, C., Im, S. J. and Lee, J. H. 2011. Growth phase-differential quorum sensing regulation of anthranilate metabolism in *Pseudomonas aeruginosa*. *Mol Cells*, 32, 57-65.

Choy, W. K., Zhou, L., Syn, C. K., Zhang, L. H. and Swarup, S. 2004. MorA defines a new class of regulators affecting flagellar development and biofilm formation in diverse *Pseudomonas species*. *J Bacteriol*, 186, 7221-7228.

Chua, S. L., Hultqvist, L. D., Yuan, M., Rybtke, M., Nielsen, T. E., Givskov, M., Tolker-Nielsen, T. and Yang, L. 2015. *In vitro* and *in vivo* generation and characterization of *Pseudomonas aeruginosa* biofilm-dispersed cells via c-di-GMP manipulation. *Nat Protoc*, 10, 1165-1180.

Ciccarelli, F. D., Doerks, T., von Mering, C., Creevey, C. J., Snel, B. and Bork, P. 2006. Toward automatic reconstruction of a highly resolved tree of life. *Science*, 311, 1283-1287.

Clark, H. A., Hoyer, M., Philbert, M. A. and Kopelman, R. 1999. Optical nanosensors for chemical analysis inside single living cells. 1. fabrication, characterization, and methods for intracellular delivery of PEBBLE sensors. *Anal Chem*, 71, 4831-4836.

Coenye, T. and Nelis, H. J. 2010. *In vitro* and *in vivo* model systems to study microbial biofilm formation. *J Microbiol Methods*, 83, 89-105.

Cohen-Kashi, M., Deutsch, M., Tirosh, R., Rachmani, H. and Weinreb, A. 1997. Carboxyfluorescein as a fluorescent probe for cytoplasmic effects of lymphocyte stimulation. *Spectrochim Acta A*, 53, 1655-1661.

Colvin, K. M., Gordon, V. D., Murakami, K., Borlee, B. R., Wozniak, D. J., Wong, G. C. and Parsek, M. R. 2011. The Pel polysaccharide can serve a structural and protective role in the biofilm matrix of *Pseudomonas aeruginosa*. *PLoS Pathog*, 7, e1001264.

Colvin, K. M., Irie, Y., Tart, C. S., Urbano, R., Whitney, J. C., Ryder, C., Howell, P. L., Wozniak, D. J. and Parsek, M. R. 2012. The Pel and Psl polysaccharides provide *Pseudomonas aeruginosa* structural redundancy within the biofilm matrix. *Environ Microbiol*, 14, 1913-1928.

Conway, V. L., Hassen, K. P., Zhang, L., Seitz, W. R. and Gross, T. S. 1997. The influence of composition on the properties of pH-swellable polymers for chemical sensors. *Sens Actuators B*, 45, 1-9.

Cornelis, P. 2019. Putting an end to the Pseudomonas aeruginosa IQS controversy. *Microbiologyopen*, 9, e962.

Cortés, M. E., Bonilla, J. C. and Sinisterra, R. D. 2011. Biofilm formation, control and novel strategies for eradication. *Sci Against Microbial Pathog Commun Curr Res Technol Adv*, 2, 896–905.

Costa Oliveira, B. E., Cury, J. A. and Ricomini Filho, A. P. 2017. Biofilm extracellular polysaccharides degradation during starvation and enamel demineralization. *PLoS One*, 12, e0181168.

Cross, A. S., Sadoff, J. C., Iglewski, B. H. and Sokol, P. A. 1980. Evidence for the role of toxin A in the pathogenesis of infection with *Pseudomonas aeruginosa* in humans. *J Infect Dis*, 142, 538-546.

Crossley, K. B., Jefferson, K. K., Archer, G. L. and Fowler, V. G. 2009. *Staphylococci* in human disease, 2nd ed. Blackwell, West Sussex.

D'Urzo, N., Martinelli, M., Pezzicoli, A., De Cesare, V., Pinto, V., Margarit, I., Telford, J. L. and Maione, D. 2014. Acidic pH strongly enhances *in vitro* biofilm formation by a subset of hypervirulent st-17 *Streptococcus agalactiae* strains. *Appl Environ Microbiol*, 80, 2176–2185.

Daddaoua, A., Fillet, S., Fernandez, M., Udaondo, Z., Krell, T. and Ramos, J. L. 2012. Genes for carbon metabolism and the ToxA virulence factor in *Pseudomonas aeruginosa* are regulated through molecular interactions of PtxR and PtxS. *PLoS One*, 7, e39390.

Daddaoua, A., Krell, T. and Ramos, J. L. 2009. Regulation of glucose metabolism in *Pseudomonas*: the phosphorylative branch and entner-doudoroff enzymes are regulated by a repressor containing a sugar isomerase domain. *J Biol Chem*, 284, 21360-21368.

Daigle, D. M., Cao, L., Fraud, S., Wilke, M. S., Pacey, A., Klinoski, R., Strynadka, N. C., Dean, C. R. and Poole, K. 2007. Protein modulator of multidrug efflux gene expression in *Pseudomonas aeruginosa*. *J Bacteriol*, 189, 5441-5451.

Danaei, M., Dehghankhold, M., Ataei, S., Hasanzadeh Davarani, F., Javanmard, R., Dokhani, A., Khorasani, S. and Mozafari, M. R. 2018. Impact of particle size and polydispersity index on the clinical applications of lipidic nanocarrier systems. *Pharmaceutics*, 10.

Danese, P. N. 2002. Antibiofilm approaches: prevention of catheter colonization. *Chem Biol*, 9, 873–880.

Dasgupta, N., Arora, S. K. and Ramphal, R. 2004. The flagellar system of *Pseudomonas aeruginosa*. *In:* Ramos, J. L. (ed.) *In:* Pseudomonas. New York: Kluwer Academic/ Plenum Publishers. 675-698.

Davey, M. E., Caiazza, N. C. and O'Toole, G. A. 2003. Rhamnolipid surfactant production affects biofilm architecture in *Pseudomonas aeruginosa* PAO1. *J Bacteriol*, 185, 1027-1036.

Davey, M. E. and O'Toole, G. A. 2000a. Microbial biofilms: from ecology to molecular genetics. *Microbiol Mol Biol Rev*, 64, 847–867.

Davey, M. E. and O'Toole, G. A. 2000b. Microbial biofilms: from ecology to molecular genetics. *Microbiol Mol Biol Rev*, 64, 847-867.

Davies, D. G., Parsek, M. R., Pearson, J. P., Iglewski, B. H., Costerton, J. W. and Greenberg, E. P. 1998. The involvement of cell-to-cell signals in the development of a bacterial biofilm. *Science*, 280, 295-298.

Davies, S. K., Fearn, S., Allsopp, L. P., Harrison, F., Ware, E., Diggle, S. P., Filloux, A., McPhail, D. S. and Bundy, J. G. 2017. Visualizing antimicrobials in bacterial biofilms: Three-dimensional biochemical imaging using TOF-SIMS. *mSphere*, 2, 1-11.

Davis, S. and Ainsworth, P. 1989. The disinfectant action of low-temperature laundering. *J Consumer Stud Home Econ*, 13, 61-66.

De Kievit, T. R., Gillis, R., Marx, S., Brown, C. and Iglewski, B. H. 2001a. Quorum-sensing genes in *Pseudomonas aeruginosa* biofilms: their role and expression patterns. *Appl Environ Microbiol*, 67, 1865-1873.

De Kievit, T. R., Parkins, M. D., Gillis, R. J., Srikumar, R., Ceri, H., Poole, K., Iglewski, B. H. and Storey, D. G. 2001b. Multidrug efflux pumps: expression patterns and contribution to antibiotic resistance in *Pseudomonas aeruginosa* biofilms. *Antimicrob Agents Chemother*, 45, 1761-1770.

de Beer, D., Stoodley, P., Roe, F. and Lewandowski, Z. 1993. Effects of biofilm structures on oxygen distribution and mass transport. *Biotechnol Bioeng*, 43, 1131-1138.

de Kievit, T. R. and Iglewski, B. H. 2000. Bacterial Quorum Sensing in Pathogenic Relationships. *Infect and Immun*, 68, 4839–4849.

del Castillo, T., Duque, E. and Ramos, J. L. 2008. A set of activators and repressors control peripheral glucose pathways in *Pseudomonas putida* to yield a common central intermediate. *J Bacteriol*, 190, 2331-2339.

del Castillo, T. and Ramos, J. L. 2007. Simultaneous catabolite repression between glucose and toluene metabolism in *Pseudomonas putida* is channeled through different signaling pathways. *J Bacteriol*, 189, 6602-6610.

del Castillo, T., Ramos, J. L., Rodriguez-Herva, J. J., Fuhrer, T., Sauer, U. and Duque, E. 2007. Convergent peripheral pathways catalyze initial glucose catabolism in *Pseudomonas putida*: genomic and flux analysis. *J Bacteriol*, 189, 5142-5152.

Dénervaud, V., TuQuoc, P., Blanc, D., Favre-Bonte, S., Krishnapillai, V., Reimmann, C., Haas, D. and van Delden, C. 2004. Characterization of cell-to-cell signaling-deficient

Pseudomonas aeruginosa strains colonizing intubated patients. *J Clin Microbiol*, 42, 554-562.

Department of Health 2016. Health technical memorandum 01-04: decontamination of linen for health and social care: Management and provision. *In:* Health, D. O. (ed.).

Desai, A. S., Chauhan, V. M., Johnston, A. P., Esler, T. and Aylott, J. W. 2014. Fluorescent nanosensors for intracellular measurements: synthesis, characterization, calibration, and measurement. *Front Physiol*, 4, 1-15.

Déziel, E., Lépine, F., Milot, S., He, J., Mindrinos, M. N., Tompkins, R. G. and Rahme, L. G. 2004. Analysis of *Pseudomonas aeruginosa* 4-hydroxy-2-alkylquinolines (HAQs) reveals a role for 4-hydroxy-2-heptylquinoline in cell-to-cell communication. *Proc Natl Acad Sci U S A*, 101, 1339-1344.

Diggle, S. P., Crusz, S. A. and Cámara, M. 2007. Quorum sensing. *Curr Biol*, 17, R907-910.

Diggle, S. P. and Whiteley, M. 2020. Microbe Profile: *Pseudomonas aeruginosa*: opportunistic pathogen and lab rat. *Microbiology (Reading)*, 166, 30-33.

Dohmae, S., Okubo, T., Higuchi, W., Takano, T., Isobe, H., Baranovich, T., Kobayashi, S., Uchiyama, M., Tanabe, Y., Itoh, M. and Yamamoto, T. 2008. *Bacillus cereus* nosocomial infection from reused towels in Japan. *J Hosp Infect*, 69, 361-367.

Doig, P., Todd, T., Sastry, P. A., Lee, K. K., Hidges, R. S., Paranchych, W. and Irvin, R. T. 1988. Role of pili in adhesion of *Pseudomonas aeruginosa* to human respiratory epithelial cells. *Infect and Immun*, 56, 1641-1646.

Doll, K., Jongsthaphongpun, K. L., Stumpp, N. S., Winkel, A. and Stiesch, M. 2016. Quantifying implant-associated biofilms: Comparison of microscopic, microbiologic and biochemical methods. *J Microbiol Methods*, 130, 61-68.

Doyle, T. B., Hawkins, A. C. and McCarter, L. L. 2004. The complex flagellar torque generator of *Pseudomonas aeruginosa*. *J Bacteriol*, 186, 6341-6350.

Drahos, D. J., Hemming, B. C. and McPherson, S. 1986. Tracking recombinant organisms in the environment: β-galactosidase as a selectable non-antibiotic marker for fluorescent pseudomonads. *Nat Biotechnol*, 4, 439-443.

Dundas, A. A., Sanni, O., Dubern, J. F., Dimitrakis, G., Hook, A. L., Irvine, D. J., Williams, P. and Alexander, M. R. 2019. Validating a predictive structure-property relationship by discovery of novel polymers which reduce bacterial biofilm formation. *Adv Mater*, 31, e1903513.

Eberhard, A., Burlingame, A. L., Eberhard, C., Kenyon, G. L., Nealson, K. H. and Oppenheimer, N. J. 1981. Structural identification of autoinducer of luciferase. *Biochem*, 20, 2444-2449.

Efimenko, K., Finlay, J., Callow, M. E., Callow, J. A. and Genzer, J. 2009. Development and testing of hierarchically wrinkled coatings for marine antifouling. *ACS Appl Mater Interfaces*, 1, 1031-1040.

Egert, M., Höhne, H., List, M., Weide, M., Bockmühl, D. and Breves, R. 2010a. Microbial community composition of biofilms in domestic washing machines. *3rd joint conference of the German Society for Hygiene and Microbiology.* Hannover, Germany.

Egert, M., Schmidt, I., Bussey, K. and Breves, R. 2010b. A glimpse under the rim--the composition of microbial biofilm communities in domestic toilets. *J Appl Microbiol*, 108, 1167-1174.

El Badawy, A. M., Silva, R. G., Morris, B., Scheckel, K. G., Suidan, M. T. and Tolaymat, T. M. 2010. Surface charge-dependent toxicity of silver nanoparticles. *Environ Sci Technol*, 45, 283-287.

Elder, M. J., Stapleton, F., Evans, E. and Dart, J. K. 1995. Biofilm-related infections in ophtalmology. *Eye*, 9, 102-109.

Elias, A. F., Chaussee, M. S., McDowell, E. J. and Huntington, M. K. 2010. Community-based intervention to manage an outbreak of MRSA skin infections in a county jail. *J Correct Health Care*, 16, 205-215.

Elias, S. and Banin, E. 2012. Multi-species biofilms: living with friendly neighbors. *FEMS Microbiol Rev*, 36, 990-1004.

Elsutohy, M. M., Chauhan, V. M., Markus, R., Kyyaly, M. A., Tendler, S. J. B. and Aylott, J. W. 2017. Real-time measurement of the intracellular pH of yeast cells during glucose metabolism using ratiometric fluorescent nanosensors. *Nanoscale*, 9, 5904-5911.

Enomoto, R., Suzuki, C., Ohno, M., Ohasi, T., Futagami, R., Ishikawa, K., Komae, M., Nishino, T., Konishi, Y. and Lee, E. 2007. Cationic surfactants induce apoptosis in normal and cancer cells. *Ann N Y Acad Sci*, 1095, 1-6.

Entner, N. and Doudoroff, M. 1952. Glucose and gluconic acid oxidation of *Pseudomonas saccharophila*. *J Biol Chem*, 196, 853-862.

Essar, D. W., Eberly, L., Hadero, A. and Crawford, I. P. 1990. Identification and Characterization of Genes for a Second Anthranilate Synthase in *Pseudomonas aeruginosa:* Interchangeability of the Two Anthranilate Synthases and Evolutionary Implications. *J Bacteriol*, 172, 884-900.

European Union, T. E. P. a. t. C. o. t. 2012. Regulation (EU) No 528/2012 of the Eruopean Parliament and of the Council of 22 May 2012 concerning the making available on the market and use of biocidal products Text with EEA relevance. *Official Journal of the European Union L167*, 55, 1-123.

Feazel, L. M., Baumgartner, L. K., Peterson, K. L., Frank, D. N., Harris, J. K. and Pace, N. R. 2009. Opportunistic pathogens enriched in showerhead biofilms. *Proc Natl Acad Sci USA*, 106, 16393-16399.

Federle, M. J. and Bassler, B. L. 2003. Interspecies communication in bacteria. *J Clin Invest*, 112, 1291-1299.

Fejerskov, O., Scheie, A. A. and Manji, F. 1992. The effect of sucrose on plaque pH in the primary and permanent dentition of caries-inactive and -active Kenyan children. *J Dent Res*, 71, 25-31.

Feldman, M., Bryan, R., Rajan, S., Scheffler, L., Brunnert, S., Tang, H. and Prince, A. 1998. Role of flagella in pathogenesis of *Pseudomonas aeruginosa* pulmonary infection. *American Society for Microbiology*, 66, 43-51.

Fernandez-Barat, L., Ben-Aicha, S., Motos, A., Vila, J., Marco, F., Rigol, M., Munoz, L., Li Bassi, G., Ferrer, M. and Torres, A. 2018. Assessment of *in vivo* versus in *vitro* biofilm formation of clinical methicillin-resistant *Staphylococcus aureus* isolates from endotracheal tubes. *Sci Rep*, 8, 11906.

Finck-Barbançon, V., Goranson, J., Zhu, L., Sawa, T., Wiener-Kronish, J. P., Fleiszig, S. M. J., Wu, C., Mende-Mueller, L. and Frank, D. N. 1997. ExoU expression by *Pseudomonas aeruginosa* correlates with acute cytotoxicity and epithelial injury. *Mol Microbiol*, 25, 547-557.

Finkel, S. E. and Kolter, R. 2001. DNA as a nutrient: novel role for bacterial competence gene homologs. *J Bacteriol*, 183, 6288-6293.

Firestone, A. R., Imfeld, T., Schiffer, S. and Lutz, F. 1987. Measurement of interdental plaque pH in humans with an indwelling glass pH electrode following a sucrose rinse a long-term retrospective study. *Caries Res*, 21, 555-558.

Flemming, H. C. and Wingender, J. 2010. The biofilm matrix. *Nat Rev Microbiol*, 8, 623-633.

Fomsgaard, A., Conrad, R. S., Galanos, C., Shand, G. H. and Høiby, N. 1988. Comparative immunochemistry of lipopolysaccharides from typable and polyagglutinable *Pseudomonas aeruginosa* strains isolated from patients with cystic fibrosis. *J Clin Microbiol*, 26, 821-826.

Forier, K., Raemdonck, K., De Smedt, S. C., Demeester, J., Coenye, T. and Braeckmans, K. 2014. Lipid and polymer nanoparticles for drug delivery to bacterial biofilms. *J Control Release*, 190, 607-623.

Franklin, M. J., Chang, C., Akiyama, T. and Bothner, B. 2015. New technologies for studying biofilms. *Microbiol Spectr*, 3, 1-23.

Franklin, M. J., Nivens, D. E., Weadge, J. T. and Howell, P. L. 2011. Biosynthesis of the *Pseudomonas aeruginosa* extracellular polysaccharides, alginate, pel, and psl. *Front Microbiol*, 2, 1-16.

Friedman, L. and Kolter, R. 2004. Genes involved in matrix formation in *Pseudomonas aeruginosa* PA14 biofilms. *Mol Microbiol*, 51, 675-690.

Frimmersdorf, E., Horatzek, S., Pelnikevich, A., Wiehlmann, L. and Schomburg, D. 2010. How *Pseudomonas aeruginosa* adapts to various environments: a metabolomic approach. *Environ Microbiol*, 12, 1734-1747.

Fuhrer, T., Fischer, E. and Sauer, U. 2005. Experimental identification and quantification of glucose metabolism in seven bacterial species. *J Bacteriol*, 187, 1581-1590.

Fulaz, S., Hiebner, D., Barros, C. H. N., Devlin, H., Vitale, S., Quinn, L. and Casey, E. 2019. Ratiometric imaging of the *in situ* pH distribution of biofilms by use of fluorescent mesoporous silica nanosensors. *ACS Appl Mater Interfaces*, 11, 32679-32688.

Fux, C. A., Costerton, J. W., Stewart, P. S. and Stoodley, P. 2005. Survival strategies of infectious biofilms. *Trends Microbiol*, 13, 34-40.

Fuxman Bass, J. I., Russo, D. M., Gabelloni, M. L., Geffner, J. R., Giordano, M., Catalano, M., Zorreguieta, A. and Trevani, A. S. 2010. Extracellular DNA: a major proinflammatory component of *Pseudomonas aeruginosa* biofilms. *J Immunol*, 184, 6386-6395.

Gallagher, L. A., McKnight, S. L., Kuznetsova, M. S., Pesci, E. C. and Manoil, C. 2002. Functions required for extracellular quinolone signaling by *Pseudomonas aeruginosa*. *J Bacteriol*, 184, 6472-6480.

Gattlen, J., Amberg, C., Zinn, M. and Mauclaire, L. 2010. Biofilms isolated from washing machines from three continents and their tolerance to a standard detergent. *Biofouling*, 26, 873-882.

Gattlen, J., Zinn, M., Guimond, S., Körner, E., Amberg, C. and Mauclaire, L. 2011. Biofilm formation by the yeast *Rhodotorula mucilaginosa*: process, repeatability and cell attachment in a continuous biofilm reactor. *Biofouling*, 27, 979-991.

Gazze, S., Francis, L. and Van Keulen, G. 2016. The integration of nanoscale imaging and quantification of nanomechanical properties in microbiology. *Microbiol Today*, 43, 106-109.

Gellatly, S. L. and Hancock, R. E. 2013. *Pseudomonas aeruginosa*: new insights into pathogenesis and host defenses. *Pathog Dis*, 67, 159-173.

Gerba, C. P. and Kennedy, D. 2007. Enteric virus survival during household laundering and impact of disinfection with sodium hypochlorite. *Appl Environ Microbiol*, 73, 4425-4428.

Gilbert, P., Maira-Litran, T., McBain, M. J., Rickard, A. H. and Whyte, F. W. 2002. The physiology and collective recalcitrance of microbial biofilm communities. *Adv Microb Physiol*, 46, 203-256.

Giltner, C. L., Habash, M. and Burrows, L. L. 2010. *Pseudomonas aeruginosa* minor pilins are incorporated into type IV pili. *J Mol Biol*, 398, 444-461.

Giltner, C. L., Rana, N., Lunardo, M. N., Hussain, A. Q. and Burrows, L. L. 2011. Evolutionary and functional diversity of the *Pseudomonas type* IVa pilin island. *Environ Microbiol*, 13, 250-264.

Gloag, E. S., Turnbull, L., Huang, A., Vallotton, P., Wang, H., Nolan, L. M., Mililli, L., Hunt, C., Lu, J., Osvath, S. R., Monahan, L. G., Cavaliere, R., Charles, I. G., Wand, M. P., Gee, M. L., Prabhakar, R. and Whitchurch, C. B. 2013. Self-organization of bacterial biofilms is facilitated by extracellular DNA. *Proc Natl Acad Sci U S A*, 110, 11541-11546.

Gomila, M., Peña, A., Mulet, M., Lalucat, J. and García-Valdés, E. 2015. Phylogenomics and systematics in Pseudomonas. *Front Microbiol*, 6, 214.

González, J. E. and Keshavan, N. D. 2006. Messing with bacterial quorum sensing. *Microbiol Mol Biol Rev*, 70, 859-875.

Goodman, C. M., McCusker, C. D., Yilmaz, T. and Rotello, V. M. 2004. Toxicity of gold nanoparticles functionalized with cationic and anionic side chains. *Bioconjugate Chem*, 15, 897-900.

Gotoh, H., Zhang, Y., Dallo, S. F., Hong, S., Kasaraneni, N. and Weitao, T. 2008. *Pseudomonas aeruginosa*, under DNA replication inhibition, tends to form biofilms via Arr. *Res Microbiol*, 159, 294-302.

Govan, J. R. W. and Deretic, V. 1996. Microbial pathogenesis in cystic fibrosis: mucoid *Pseudomonas aeruginosa* and *Burkholderia cepacia*. *Microbiol Rev*, 60, 539–574.

Graber, M. L., Dilillo, D. C., Friedman, B. L. and Pastoriza-Munoz, E. 1986. Characteristics of fluoroprobes for measuring intracellular pH. *Anal Biochem*, 156, 202-212.

Gregori, G., Citterio, S., Ghiani, A., Labra, M., Sgorbati, S., Brown, S. and Denis, M. 2001. Resolution of viable and membrane-compromised bacteria in freshwater and marine waters based on analytical flow cytometry and nucleic acid double staining. *Appl Environ Microbiol*, 67, 4662-4670.

Gupta, P., Sarkar, S., Das, B., Bhattacharjee, S. and Tribedi, P. 2016. Biofilm, pathogenesis and prevention-a journey to break the wall: a review. *Arch Microbiol*, 198, 1-15.

Habimana, O., Steenkeste, K., Fontaine-Aupart, M. P., Bellon-Fontaine, M. N., Kulakauskas, S. and Briandet, R. 2011. Diffusion of nanoparticles in biofilms is altered by bacterial cell wall hydrophobicity. *Appl Environ Microbiol*, 77, 367-368.

Hall-Stoodley, L., Costerton, J. W. and Stoodley, P. 2004. Bacterial biofilms: from the natural environment to infectious diseases. *Nat Rev Microbiol*, 2, 95-108.

Hall-Stoodley, L. and Stoodley, P. 2009. Evolving concepts in biofilm infections. *Cell Microbiol*, 11, 1034-1043.

Hall, T. J., Wren, M. W., Jeanes, A. and Gant, V. A. 2009. Decontamination of laundry at low temperature with CuWB50, a novel copper-based biocidal compound. *Am J Infect Control*, 37, 478-483.

Hamood, A. N., Griswold, J. and Colmer, J. 1996. Characterization of elastase-deficient clinical isolates of *Pseudomonas aeruginosa*. *Infect and Immun*, 64, 3154-3160.

Hancock, R. E., Mutharia, L. M., Chan, L., Darveau, R. P., Speert, D. P. and Pier, G. B. 1983. *Pseudomonas aeruginosa* isolates from patients with cystic fibrosis: A class of serum-sensitive, nontypable strains deficient in lipopolysaccharide 0 side chains. *Infect and Immun*, 42, 170-177.

Hansen, S. K., Haagensen, J. A., Gjermansen, M., Jorgensen, T. M., Tolker-Nielsen, T. and Molin, S. 2007. Characterization of a *Pseudomonas putida* rough variant evolved in a mixed-species biofilm with *Acinetobacter* sp. strain C6. *J Bacteriol*, 189, 4932-4943.

Hardie, K. R. and Heurlier, K. 2008. Establishing bacterial communities by 'word of mouth': LuxS and autoinducer 2 in biofilm development. *Nat Rev Microbiol*, 6, 635-643.

Harimawan, A. and Ting, Y. P. 2016. Investigation of extracellular polymeric substances (EPS) properties of *P. aeruginosa* and *B. subtilis* and their role in bacterial adhesion. *Colloids Surf B Biointerfaces*, 146, 459-467.

Harmsen, M., Yang, L., Pamp, S. J. and Tolker-Nielsen, T. 2010. An update on *Pseudomonas aeruginosa* biofilm formation, tolerance, and dispersal. *FEMS Immunol Med Microbiol*, 59, 253-268.

Harrison, F. and Diggle, S. P. 2016. An *ex vivo* lung model to study bronchioles infected with *Pseudomonas aeruginosa* biofilms. *Microbiology (Reading)*, 162, 1755-1760.

Hassett, D. J., Cuppoletti, J., Trapnell, B., Lymar, S. V., Rowe, J. J., Yoon, S. S., Hilliard, G. M., Parvatiyar, K., Kamani, M. C., Wozniak, D. J., Hwang, S. H., McDermott, T. R. and Ochsner, U. A. 2002. Anaerobic metabolism and quorum sensing by *Pseudomonas aeruginosa* biofilms in chronically infected cystic fibrosis airways: rethinking antibiotic treatment strategies and drug targets. *Adv Drug Deliv Rev*, 54, 1425-1443.

Hejazi, A. and Falkiner, F. R. 1997. *Serratia marcescens*. *J Med Microbiol*, 46, 903-912.

Hewitt, C. J. and Nebe-Von-Caron, G. 2004. The application of multi-parameter flow cytometry to monitor individual microbial cell physiological state. *Adv Biochem Eng Biotechnol*, 89, 197-223.

Hidalgo, G., Burns, A., Herz, E., Hay, A. G., Houston, P. L., Wiesner, U. and Lion, L. W. 2009. Functional tomographic fluorescence imaging of pH microenvironments in microbial biofilms by use of silica nanoparticle sensors. *Appl Environ Microbiol*, 75, 7426-7435.

Hinton Jr, A. and Ingram, K. D. 2012. Influence of ethylenediamine-N,N'-disuccinic acid (Edds) concentration on the bactericidal activity of fatty acids *in vitro*. *Journal of Food Safety*, 32, 102-107.

Hitchener, B. J. and Egan, A. F. 1976. Outer-membrane damage in sublethally heated *Escherichia coli* K-12. *J Microbiol*, 23, 311-318.

Ho, Y. R., Li, C. M., Yu, C. H., Lin, Y. J., Wu, C. M., Harn, I. C., Tang, M. J., Chen, Y. T., Shen, F. C., Lu, C. Y., Tsai, T. C. and Wu, J. J. 2013. The enhancement of biofilm formation in Group B streptococcal isolates at vaginal pH. *Med Microbiol Immunol*, 202, 105-115.

Höckel, M., Knoop, C., Schlenger, K., Vorndran, B., Baußmann, E., Mitze, M., Knapstein, P. G. and Vaupel, P. 1993. Intratumoral pO_2 predicts survival in advanced cancer of the uterine cervix. *Radiother Oncol*, 26, 45-50.

Hoffman, L. R., D'Argenio, D. A., MacCoss, M. J., Zhang, Z., Jones, R. A. and Miller, S. I. 2005. Aminoglycoside antibiotics induce bacterial biofilm formation. *Nature*, 436, 1171-1175.

Hoge, R., Pelzer, A., Rosenau, F. and Wilhelm, S. 2010. Weapons of a pathogen: Proteases and their role in virulence of *Pseudomonas aeruginosa*. *In:* Méndez-Vilas, A. (ed.) *In:* Current research, technology and education topics in applied microbiology and microbial biotechnology. Badajoz: Formatex Research Center. 383-395.

Høiby, N., Bjarnsholt, T., Givskov, M., Molin, S. and Ciofu, O. 2010. Antibiotic resistance of bacterial biofilms. *Int J Antimicrob Agents*, 35, 322-332.

Holder, I. A. and Haidaris, C. G. 1979. Experimental studies of the pathogenesis of infections due to *Pseudomonas aeruginosa*: extracellular protease and elastase as *in vivo* virulence factors. *Can J Microbiol*, 25, 593-599.

Honisch, M., Stamminger, R. and Bockmuhl, D. P. 2014. Impact of wash cycle time, temperature and detergent formulation on the hygiene effectiveness of domestic laundering. *J Appl Microbiol*, 117, 1787-1797.

Hoogenboom, R. 2009. Poly(2-oxazoline)s: a polymer class with numerous potential applications. *Angew Chem Int Ed Engl*, 48, 7978-7994.

Hook, A. L., Chang, C. Y., Yang, J., Atkinson, S., Langer, R., Anderson, D. G., Davies, M. C., Williams, P. and Alexander, M. R. 2013. Discovery of novel materials with broad resistance to bacterial attachment using combinatorial polymer microarrays. *Adv Mater*, 25, 2542-2547.

Hook, A. L., Chang, C. Y., Yang, J., Luckett, J., Cockayne, A., Atkinson, S., Mei, Y., Bayston, R., Irvine, D. J., Langer, R., Anderson, D. G., Williams, P., Davies, M. C. and Alexander, M. R. 2012. Combinatorial discovery of polymers resistant to bacterial attachment. *Nat Biotechnol*, 30, 868-875.

Horev, B., Klein, M. I., Hwang, G., Li, Y., Kim, D., Koo, H. and Benoit, B. S. W. 2015. pH-activated nanoparticles for controlled topical delivery of farnesol to disrupt oral biofilm virulence. *ACS Nano*, 9, 2390–2404.

Hoštacká, A., Čižnár, I. and Štefcovičová, M. 2010. Temperature and pH affect the production of bacterial biofilm. *Folia Microbiol*, 55, 75-78.

Hunter, R. C. and Beveridge, T. J. 2005. Application of a pH-sensitive fluoroprobe (C-SNARF-4) for pH microenvironment analysis in *Pseudomonas aeruginosa* biofilms. *Appl Environ Microbiol*, 71, 2501-2510.

Hwang, G., Liu, Y., Kim, D., Sun, V., Aviles-Reyes, A., Kajfasz, J. K., Lemos, J. A. and Koo, H. 2016. Simultaneous spatiotemporal mapping of *in situ* pH and bacterial activity within an intact 3D microcolony structure. *Sci Rep*, 6, 32841.

Iglewski, B. H. 1996. Pseudomonas. *In:* Baron, S. (ed.) *In:* Medical Microbiology. 4 ed.: Galveston (TX): University of Texas Medical Branch at Galveston. Available: https://www.ncbi.nlm.nih.gov/books/NBK8326/.

Iglewski, B. H. and Kabat, D. 1975. NAD-dependent inhibition of protein synthesis by *Pseudomonas aeruginosa* toxin. *Proc Natl Acad Sci U S A*, 72, 2284-2288.

Iglewski, B. H., Liu, P. V. and Kabat, D. 1977. Mechanism of action of *Pseudomonas aeruginosa* exotoxin A: adenosine diphosphate-ribosylation of mammalian elongation factor 2 *in vitro* and in *vivo*. *American Society for Microbiology*, 15, 138-144.

Ikuma, K., Decho, A. W. and Lau, B. L. 2015. When nanoparticles meet biofilms-interactions guiding the environmental fate and accumulation of nanoparticles. *Front Microbiol*, 6, 591.

International Scientific Forum on Home Hygiene 2018. Containing the burden of infectious diseases is everyone's responsibility. A call for an integrated strategy for developing and promoting hygiene behaviour change in home and everyday life., *IFH White Paper*. Available: https://www.ifh-homehygiene.org/review/containing-burden-infectiousdiseases-everyones-responsibility-call-integrated-strategy.

IRI, W. G. B. 2020. Laundry detergent unit sales in the United States in 2019, by product type (in million units). Statista 2020.

Irie, Y., Borlee, B. R., O'Connor, J. R., Hill, P. J., Harwood, C. S., Wozniak, D. J. and Parsek, M. R. 2012. Self-produced exopolysaccharide is a signal that stimulates biofilm formation in *Pseudomonas aeruginosa*. *Proc Natl Acad Sci U S A*, 109, 20632-20636.

Iyer, R., Iken, B. and Damania, A. 2017. Genome of *Pseudomonas nitroreducens* DF05 from dioxin contaminated sediment downstream of the San Jacinto River waste pits reveals a broad array of aromatic degradation gene determinants. *Genom Data*, 14, 40-43.

Jacksch, S., Kaiser, D., Weis, S., Weide, M., Ratering, S., Schnell, S. and Egert, M. 2019. Influence of sampling site and other environmental factors on the bacterial community composition of domestic washing machines. *Microorganisms*, 8, 1-16.

Jackson, K. D., Starkey, M., Kremer, S., Parsek, M. R. and Wozniak, D. J. 2004. Identification of *psl,* a locus encoding a potential exopolysaccharide that is essential for *Pseudomonas aeruginosa* PAO1 biofilm formation. *J Bacteriol*, 186, 4466-4475.

Jaffar-Bandjee, M. C., Lazdunksi, A., Bally, M., Carrère, J., Chazalette, J. P. and Galabert, C. 1995. Production of elastase, exotoxin A, and alkaline protease in sputa during pulmonary exacerbation of cystic fibrosis in patients chronically infected by *Pseudomonas aeruginosa*. *J Clin Microbiol*, 33, 924–929.

Jahn, A., Griebe, T. and Nielsen, P. H. 1999. Composition of *Pseudomonas putida* biofilms: Accumulation of protein in the biofilm matrix. *Biofouling*, 14, 49-57.

Jarman, T. R., Deavin, L., Slocombe, S. and Righelato, R. C. 1978. Investigation of the effect of environmental conditions on the rate of exopolysaccharide synthesis in *Azotobacter vinelandii*. *J Gen Microbiol*, 107, 59-64.

Jefferson, K. K., Goldmann, D. A. and Pier, G. B. 2005. Use of confocal microscopy to analyze the rate of vancomycin penetration through *Staphylococcus aureus* biofilms. *Antimicrob Agents Chemother*, 49, 2467-2473.

Jennings, L. K., Storek, K. M., Ledvina, H. E., Coulon, C., Marmont, L. S., Sadovskaya, I., Secor, P. R., Tseng, B. S., Scian, M., Filloux, A., Wozniak, D. J., Howell, P. L. and Parsek, M. R. 2015. Pel is a cationic exopolysaccharide that cross-links extracellular DNA in the *Pseudomonas aeruginosa* biofilm matrix. *Proc Natl Acad Sci U S A*, 112, 11353-11358.

Jensen, P. O., Kolpen, M., Kragh, K. N. and Kuhl, M. 2017. Microenvironmental characteristics and physiology of biofilms in chronic infections of CF patients are strongly affected by the host immune response. *APMIS*, 125, 276-288.

Jesaitis, A. J., Franklin, M. J., Berglund, D., Sasaki, M., Lord, C. I., Bleazard, J. B., Duffy, J. E., Beyenal, H. and Lewandowski, Z. 2003. Compromised host defense on *Pseudomonas aeruginosa* biofilms: characterization of neutrophil and biofilm interactions. *J Immunol*, 171, 4329-4339.

Jeukens, J., Boyle, B., Kukavica-Ibrulj, I., Ouellet, M. M., Aaron, S. D., Charette, S. J., Fothergill, J. L., Tucker, N. P., Winstanley, C. and Levesque, R. C. 2014. Comparative genomics of isolates of a *Pseudomonas aeruginosa* epidemic strain associated with chronic lung infections of cystic fibrosis patients. *PLoS One*, 9, e87611.

Jin, Y., Yang, H., Qiao, M. and Jin, S. 2011. MexT regulates the type III secretion system through MexS and PtrC in *Pseudomonas aeruginosa*. *J Bacteriol*, 193, 399-410.

Jordana-Lluch, E., Garcia, V., Kingdon, A. D. H., Singh, N., Alexander, C., Williams, P. and Hardie, K. R. 2020. A simple polymicrobial biofilm keratinocyte colonization model for exploring interactions between commensals, pathogens and antimicrobials. *Front Microbiol*, 11, 291.

Joux, F. and Lebaron, P. 2000. Use of fluorescent probes to assess physiological functions of bacteria at single-cell level. *Microbes and Infection*, 2, 1523-1535.

Joyce, E., Phull, S. S., Lorimer, J. P. and Mason, T. J. 2003. The development and evaluation of ultrasound for the treatment of bacterial suspensions. A study of frequency, power and sonication time on cultured *Bacillus* species. *Ultrasonics Sonochemistry*, 10, 315-318.

Jucker, B. A., Harms, H. and Zehnder, A. J. B. 1996. Adhesion of the positively charged bacterium *Stenotrophomonas* (*Xanthomonas*) *maltophilia* 70401 to glass and teflon. *J Bacteriol*, 178, 5472-5479.

Junkins, A. D. and Doyle, M. P. 1992. Demonstration of exopolysaccharide production by enterohemorrhagic *Escherichia coli*. *Curr Microbiol*, 25, 9-17.

Junter, G. A., Thebault, P. and Lebrun, L. 2016. Polysaccharide-based antibiofilm surfaces. *Acta Biomater*, 30, 13-25.

Kadurugamuwa, J. L., Lam, J. S. and Beveridge, T. J. 1993. Interaction of gentamicin with the A band and B band lipopolysaccharides of *Pseudomonas aeruginosa* and its possible lethal effect. *Antimicrob Agents Chemother*, 37, 715-721.

Kagan, L. J., Aiello, A. E. and Larson, E. 2002. The role of the home environment in the transmission of infectious diseases. *J Commun Health*, 27, 247-267.

Kaiser, D. 2007. Bacterial swarming: A re-examination of cell-movement patterns. *Current Biology*, 17, R561-R570.

Kalia, V. C. 2013. Quorum sensing inhibitors: an overview. *Biotechnol Adv*, 31, 224-245.

Kanehisa, M. 2019. Toward understanding the origin and evolution of cellular organisms. *Protein Sci*, 28, 1947-1951.

Kanehisa, M. and Goto, S. 2000. KEGG: Kyoto Encyclopedia of Genes and Genomes. *Nucleic Acids Res*, 28, 27-30.

Kanehisa, M., Sato, Y., Furumichi, M., Morishima, K. and Tanabe, M. 2019. New approach for understanding genome variations in KEGG. *Nucleic Acids Res*, 47, D590-D595.

Karatzas, K. A., Webber, M. A., Jorgensen, F., Woodward, M. J., Piddock, L. J. and Humphrey, T. J. 2007. Prolonged treatment of *Salmonella enterica* serovar Typhimurium with commercial disinfectants selects for multiple antibiotic resistance, increased efflux and reduced invasiveness. *J Antimicrob Chemother*, 60, 947-955.

Katsikogianni, M. and Missirlis, Y. F. 2004. Concise review of mechanisms of bacterial adhesion to biomaterials and of techniques used in estimating bacteria-material interactions. *Eur Cell Mater*, 8, 37-57.

Kearns, D. B. 2010. A field guide to bacterial swarming motility. *Nat Rev Microbiol*, 8, 634-644.

Kim, M., Hatt, J. K., Weigand, M. R., Krishnan, R., Pavlostathis, S. G. and Konstantinidis, K. T. 2018. Genomic and transcriptomic insights into how bacteria withstand high concentrations of benzalkonium chloride biocides. *Appl Environ Microbiol*, 84, 1-15.

Kipnis, E., Sawa, T. and Wiener-Kronish, J. 2006. Targeting mechanisms of *Pseudomonas aeruginosa* pathogenesis. *Med Mal Infect*, 36, 78-91.

Kiratisin, P., Tucker, K. D. and Passador, L. 2002. LasR, a transcriptional activator of *Pseudomonas aeruginosa* virulence genes, functions as a multimer. *J Bacteriol*, 184, 4912-4919.

Kirner, S., Krauss, S., Sury, G., Lam, S. T., Ligon, J. M. and van Pée, K. H. 1996. The non-haem chloroperoxidase from *Pseudomonas fluorescens* and its relationship to pyrrolnitrin biosynthesis. *Microbiol*, 142, 2129-2135.

Klausen, M., Aaes-Jørgensen, A., Molin, S. and Tolker-Nielsen, T. 2003a. Involvement of bacterial migration in the development of complex multicellular structures in *Pseudomonas aeruginosa* biofilms. *Mol Microbiol*, 50, 61-68.

Klausen, M., Heydorn, A., Ragas, P., Lambertsen, L., Aaes-Jørgensen, A., Molin, S. and Tolker-Nielsen, T. 2003b. Biofilm formation by *Pseudomonas aeruginosa* wild type, flagella and type IV pili mutants. *Mol Microbiol*, 48, 1511-1524.

Kleinberg, I. 1970. Formation and accumulation of acid on the tooth aurface. *J Dent Res*, 49, 1300-1316.

Klockgether, J., Munder, A., Neugebauer, J., Davenport, C. F., Stanke, F., Larbig, K. D., Heeb, S., Schock, U., Pohl, T. M., Wiehlmann, L. and Tummler, B. 2010. Genome diversity of *Pseudomonas aeruginosa* PAO1 laboratory strains. *J Bacteriol*, 192, 1113-1121.

Kobayashi, N., Bauer, T. W., Tuohy, M. J., Fujishiro, T. and Procop, G. W. 2007. Brief ultrasonication improves detection of biofilm-formative bacteria around a metal implant. *Clin Orthop Relat Res*, 457, 210-213.

Koch, A. K., Reiser, J., Käppeli, O. and Fiechter, A. 1988. Genetic Construction of lactose-utilising strains of *Pseudomonas aeruginosa* and their application in biosurfactant production. *Nat Biotechnol*, 1335-1339.

Köhler, T., Curty, L. K., Barja, F., van Delden, C. and Pechère, J. C. 2000. Swarming of *Pseudomonas aeruginosa* is dependent on cell-to-cell signaling and requires flagella and pili. *J Bacteriol*, 182, 5990–5996.

Köhler, T., Michéa-Hamzehpour, M., Henze, U., Gotoh, N., Curty, L. K. and Pechère, J. C. 1997. Characterization of MexE–MexF–OprN, a positively regulated multidrug efflux system of *Pseudomonas aeruginosa*. *Mol Microbiol*, 23, 345-354.

Koo, H., Falsetta, M. L. and Klein, M. I. 2013. The exopolysaccharide matrix: a virulence determinant of cariogenic biofilm. *J Dent Res*, 92, 1065-1073.

Kossel 1908. Die experimentelle Bakteriologie und die Infektionskrankheiten mit besonderer Berücksichtigung der Immunitätslehre, 2 ed. Berlin, Wien, Urban und Schwarzenberg.

Kubota, H., Mitani, A., Niwano, Y., Takeuchi, K., Tanaka, A., Yamaguchi, N., Kawamura, Y. and Hitomi, J. 2012. *Moraxella* species are primarily responsible for generating malodor in laundry. *Appl Environ Microbiol*, 78, 3317-3324.

Kühl, M., Rickelt, L. F. and Thar, R. 2007. Combined imaging of bacteria and oxygen in biofilms. *Appl Environ Microbiol*, 73, 6289-6295.

Kulichikhin, K. Y., Aitio, O., Chirkova, T. V. and Fagerstedt, K. V. 2007. Effect of oxygen concentration on intracellular pH, glucose-6-phosphate and NTP content in rice (*Oryza sativa*) and wheat (*Triticum aestivum*) root tips: in vivo31P-NMR study. *Physiol Plant*, 129, 507-518.

Kunacheva, C. and Stuckey, D. C. 2014. Analytical methods for soluble microbial products (SMP) and extracellular polymers (ECP) in wastewater treatment systems: a review. *Water Res*, 61, 1-18.

Kung, V. L., Ozer, E. A. and Hauser, A. R. 2010. The accessory genome of *Pseudomonas aeruginosa*. *Microbiol Mol Biol Rev*, 74, 621-641.

Kus, J. V., Tullis, E., Cvitkovitch, D. G. and Burrows, L. L. 2004. Significant differences in type IV pilin allele distribution among *Pseudomonas aeruginosa* isolates from cystic fibrosis (CF) versus non-CF patients. *Microbiology*, 150, 1315-1326.

Kwon, S., Moon, E., Kim, T. S., Hong, S. and Park, H. D. 2011. Pyrosequencing demonstrated complex microbial communities in a membrane filtration system for a drinking water treatment plant. *Microbes Environ*, 26, 149-155.

Laarman, A. J., Bardoel, B. W., Ruyken, M., Fernie, J., Milder, F. J., van Strijp, J. A. and Rooijakkers, S. H. 2012. *Pseudomonas aeruginosa* alkaline protease blocks complement activation via the classical and lectin pathways. *J Immunol*, 188, 386-393.

Laitala, K. and Jensen, M. 2010. Cleaning effect of household laundry detergents at low temperatures. *Tenside Surf Det*, 47, 413-420.

Lakdawala, N., Pham, J., Shah, M. and Holton, J. 2011. Effectiveness of low-temperature domestic laundry on the decontamination of healthcare workers' uniforms. *Infect Control Hosp Epidemiol*, 32, 1103-1108.

Lalucat, J., Bennasar, A., Bosch, R., García-Valdés, E. and Palleroni, N. J. 2006. Biology of *Pseudomonas stutzeri*. *Microbiol Mol Biol Rev*, 70, 510-547.

Lam, J. S., MacDonald, L. A., Kropinski, A. M. and Speert, D. P. 1988. Characterization of non-typable strains of *Pseudomonas aeruginosa* from cystic fibrosis patients by means of monoclonal antibodies and SDS-polyacrylamide gel electrophoresis. *Serodiag Immun Infect Dis*, 2, 365-374.

Lam, J. S., Taylor, V. L., Islam, S. T., Hao, Y. and Kocincova, D. 2011. Genetic and functional diversity of *Pseudomonas aeruginosa* lipopolysaccharide. *Front Microbiol*, 2, 118.

Lamont, I. L., Konings, A. F. and Reid, D. W. 2009. Iron acquisition by *Pseudomonas aeruginosa* in the lungs of patients with cystic fibrosis. *Biometals*, 22, 53-60.

Langsrud, S. and Sundheim, G. 1997. Factors contributing to the survival of poultry associated *Pseudomonas* spp. exposed to a quaternary ammonium compound. *J Appl Microbiol*, 82, 705–712.

Langsrud, S., Sundheim, G. and Borgmann-Strahsen, R. 2003. Intrinsic and acquired resistance to quaternary ammonium compounds in food-related *Pseudomonas* spp. *J Appl Microbiol*, 95, 874-882.

Lányi, B. 1970. Serological properties of *Pseudomonas aeruginosa*. II. Type-specific thermolabile (flagellar) antigens. *Acta Microbiol Acad Sci Hung*, 17, 35-48.

Latifi, A., Foglino, M., Tanaka, K., Williams, P. and Lazdunksi, A. 1996. A hierarchical quorum-sensing cascade in *Pseudomonas aeruginosa* links the transcriptional activators LasR and RhlR (VsmR) to expression of the stationary-phase sigma factor RpoS. *Mol Microbiol*, 21, 1137-1146.

Latifi, A., Winson, K., Foglino, M., Bycroft, B. W., Stewart, G. S. A. B., Lazdunski, A. and Williams, P. 1995. Multiple homologues of LuxR and Luxl control expression of virulence determinants and secondary metabolites through quorum sensing in *Pseudomonas aeruginosa* PAO1. *Mol Microbiol*, 17, 333-343.

Lau, G. W., Hassett, D. J., Ran, H. and Kong, F. 2004a. The role of pyocyanin in *Pseudomonas aeruginosa* infection. *Trends Mol Med*, 10, 599-606.

Lau, G. W., Ran, H., Kong, F., Hassett, D. J. and Mavrodi, D. 2004b. *Pseudomonas aeruginosa* pyocyanin is critical for lung infection in mice. *Infect Immun*, 72, 4275-4278.

Lebeaux, D., Chauhan, A., Rendueles, O. and Beloin, C. 2013. From *in vitro* to *in vivo* models of bacterial biofilm-related infections. *Pathogens*, 2, 288-356.

Lee, D. G., Urbach, J. M., Wu, G., Liberati, N. T., Feinbaum, R. L., Miyata, S., Diggins, L. T., He, J., Saucier, M., Deziel, E., Friedman, L., Li, L., Grills, G., Montgomery, K., Kucherlapati, R., Rahme, L. G. and Ausubel, F. M. 2006. Genomic analysis reveals that *Pseudomonas aeruginosa* virulence is combinatorial. *Genome Biol*, 7, R90.

Lee, J., Wu, J., Deng, Y., Wang, J., Wang, C., Wang, J., Chang, C., Dong, Y., Williams, P. and Zhang, L. H. 2013. A cell-cell communication signal integrates quorum sensing and stress response. *Nat Chem Biol*, 9, 339-343.

Lee, J. and Zhang, L. 2015. The hierarchy quorum sensing network in *Pseudomonas aeruginosa*. *Protein Cell*, 6, 26-41.

Leid, J. G., Kerr, M., Selgado, C., Johnson, C., Moreno, G., Smith, A., Shirtliff, M. E., O'Toole, G. A. and Cope, E. K. 2009. Flagellum-mediated biofilm defense mechanisms of *Pseudomonas aeruginosa* against host-derived lactoferrin. *Infect Immun*, 77, 4559-4566.

Leive, L. 1965. Release of lipopolysaccharide by EDTA treatment of *E. coli*. *Biochem Biophys Res Commun*, 21, 290-296.

Lessie, T. G. and Neidhardt, F. C. 1967. Formation and operation of the histidine-degrading pathway in *Pseudomonas aeruginosa*. *J Bacteriol*, 93, 1800-1810.

Lewis, K. 2001. Riddle of biofilm resistance. *Antimicrob Agents Chemother*, 45, 999-1007.

Li, J., Zhang, K., Ruan, L., Chin, S. F., Wickramasinghe, N., Liu, H., Ravikumar, V., Ren, J., Duan, H., Yang, L. and Chan-Park, M. B. 2018. Block copolymer nanoparticles remove biofilms of drug-resistant gram-positive bacteria by nanoscale bacterial debridement. *Nano Lett*, 18, 4180-4187.

Li, L., Finnegan, M. B., S., Ö., Kim, Y., Lillehoj, P. B., Ho, C. M., Lux, R., Mito, R., Loewy, Z. and Shi, W. 2010. *In vitro* study of biofilm formation and effectiveness of antimicrobial treatment on various dental material surfaces. *Mol Oral Microbiol*, 25, 384-390.

Li, N., Wang, L., Yan, H., Wang, M., Shen, D., Yin, J. and Shentu, J. 2018. Effects of low-level engineered nanoparticles on the quorum sensing of *Pseudomonas aeruginosa* PAO1. *Environ Sci Pollut Res Int*, 25, 7049-7058.

Li, X.-Z. and Plésiat, P. 2016. Antimicrobial drug efflux pumps in *Pseudomonas aeruginosa*. *In:* Li, X.-Z. *E. A.* (ed.) *In:* Efflux-Mediated Antimicrobial Resistance in Bacteria. Springer International Publishing. 359-400.

Lin, P., Clash, C., Pearce, E. M. and Kwei, T. K. 1988. Solubility and miscibility of poly(ethyl oxazoline). 26, 603-619.

Lingström, P., Imfeld, T. and Birkheld, D. 1993. Comparison of three different methods for measurement of plaque-pH in humans after consumption of soft bread and potato chips. *J Dent Res*, 72, 865-870.

Lister, P. D., Wolter, D. J. and Hanson, N. D. 2009. Antibacterial-resistant *Pseudomonas aeruginosa*: clinical impact and complex regulation of chromosomally encoded resistance mechanisms. *Clin Microbiol Rev*, 22, 582-610.

Loughlin, M. F., Jones, M. V. and Lambert, P. A. 2002. *Pseudomonas aeruginosa* cells adapted to benzalkonium chloride show resistance to other membrane-active agents but not to clinically relevant antibiotics. *J Antimicrob Chemother*, 49, 631–639.

Luzar, M. A., Thomassen, M. J. and Montie, T. C. 1985. Flagella and motility alterations in *Pseudomonas aeruginosa* strains from patients with cystic fibrosis: Relationship to patient clinical condition. *Infect and Immun*, 50, 577-582.

Ma, H., Williams, P. L. and Diamond, S. A. 2013. Ecotoxicity of manufactured ZnO nanoparticles--a review. *Environ Pollut*, 172, 76-85.

Ma, L., Conover, M., Lu, H., Parsek, M. R., Bayles, K. and Wozniak, D. J. 2009. Assembly and development of the *Pseudomonas aeruginosa* biofilm matrix. *PLoS Pathog*, 5, e1000354.

Ma, L., Jackson, K. D., Landry, R. M., Parsek, M. R. and Wozniak, D. J. 2006. Analysis of *Pseudomonas aeruginosa* conditional psl variants reveals roles for the Psl polysaccharide in adhesion and maintaining biofilm structure postattachment. *J Bacteriol*, 188, 8213-8221.

Ma, L., Lu, H., Sprinkle, A., Parsek, M. R. and Wozniak, D. J. 2007. *Pseudomonas aeruginosa* Psl is a galactose- and mannose-rich exopolysaccharide. *J Bacteriol*, 189, 8353-8356.

Magennis, E. P., Hook, A. L., Williams, P. and Alexander, M. R. 2016. Making silicone rubber highly resistant to bacterial attachment using thiol-ene grafting. *ACS Appl Mater Interfaces*, 8, 30780-30787.

Makabenta, J. M. V., Nabawy, A., Li, C. H., Schmidt-Malan, S., Patel, R. and Rotello, V. M. 2020. Nanomaterial-based therapeutics for antibiotic-resistant bacterial infections. *Nat Rev Microbiol*, 1-14.

Makin, S. A. and Beveridge, T. J. 1996a. The influence of A-band and B-band lipopolysaccharide on the surface characteristics and adhesion of *Pseudomonas aeruginosa* to surfaces. *Micobiol*, 142, 299-307.

Makin, S. A. and Beveridge, T. J. 1996b. *Pseudomonas aeruginosa* PAO1 ceases to express serotype-specific lipopolysaccharide at 45°C. *J Bacteriol*, 178, 3350-3352.

Mann, E. E. and Wozniak, D. J. 2012. *Pseudomonas* biofilm matrix composition and niche biology. *FEMS Microbiol Rev*, 36, 893-916.

Marr, A. K., Overhage, J., Bains, M. and Hancock, R. E. W. 2007. The Lon protease of *Pseudomonas aeruginosa* is induced by aminoglycosides and is involved in biofilm formation and motility. *Microbiology*, 153, 474-482.

Marty-Teysset, C., Posthuma, C., Lolkema, J. S., Schmitt, P., Divies, C. and Kinings, W. N. 1996. Proton motive force generation by citrolactic fermentation in *Leuconostoc mesenteroides*. *J Bacteriol*, 178, 2178-2185.

Marvin, H. J. P., ter Beest, M. B. A. and Witholt, B. 1989. Release of outer membrane fragments from wild-type *Escherichia coli* and from several *E. coli* lipopolysaccharide mutants by EDTA and heat shock treatments. *J Bacteriol*, 171, 5262-5267.

Mavrodi, D. V., Bonsall, R. F., Delaney, S. M., Soule, M. J., Phillips, G. and Thomashow, L. S. 2001. Functional analysis of genes for biosynthesis of pyocyanin and phenazine-1-carboxamide from *Pseudomonas aeruginosa* PAO1. *J Bacteriol*, 183, 6454-6465.

Mc Cay, P. H., Ocampo-Sosa, A. A. and Fleming, G. T. 2010. Effect of subinhibitory concentrations of benzalkonium chloride on the competitiveness of *Pseudomonas aeruginosa* grown in continuous culture. *Microbiology*, 156, 30-38.

McDonnell, G. and Russell, A. D. 1999. Antiseptics and disinfectants: Activity, action, and resistance. *Clin Microbiol Rev*, 12, 147–179.

McMahon, M. A., Blair, I. S., Moore, J. E. and McDowell, D. A. 2007. Habituation to sub-lethal concentrations of tea tree oil (*Melaleuca alternifolia*) is associated with reduced susceptibility to antibiotics in human pathogens. *J Antimicrob Chemother*, 59, 125-127.

McPhee, J. B., Lewenza, S. and Hancock, R. E. 2003. Cationic antimicrobial peptides activate a two-component regulatory system, PmrA-PmrB, that regulates resistance to polymyxin B and cationic antimicrobial peptides in *Pseudomonas aeruginosa*. *Mol Microbiol*, 50, 205-217.

Mero, A., Pasut, G., Dalla Via, L., Fijten, M. W., Schubert, U. S., Hoogenboom, R. and Veronese, F. M. 2008. Synthesis and characterization of poly(2-ethyl 2-oxazoline)-conjugates with proteins and drugs: suitable alternatives to PEG-conjugates? *J Control Release*, 125, 87-95.

Messiaen, A. S., Forier, K., Nelis, H., Braeckmans, K. and Coenye, T. 2013. Transport of nanoparticles and tobramycin-loaded liposomes in *Burkholderia cepacia* complex biofilms. *PLoS One*, 8, e79220.

Meyer, J. M., Stintzi, A., De Vos, D., Cornelis, P., Tappe, R., Taraz, K. and Budzikiewicz, H. 1997. Use of siderophores to type pseudomonads: the three *Pseudomonas aeruginosa* pyoverdine systems. *Micobiol*, 143, 35-43.

Michalska, M. and Wolf, P. 2015. *Pseudomonas* Exotoxin A: optimized by evolution for effective killing. *Front Microbiol*, 6, 963.

Midgley, M. 1987. An efflux system for cationic dyes and related compounds in *Escherichia coli*. *Microbiol Sci*, 4, 125-127.

Mikulskis, P., Hook, A., Dundas, A. A., Irvine, D., Sanni, O., Anderson, D., Langer, R., Alexander, M. R., Williams, P. and Winkler, D. A. 2018. Prediction of broad-spectrum pathogen attachment to coating materials for biomedical devices. *ACS Appl Mater Interfaces*, 10, 139-149.

Miller, R. V. and Ku, C. M. C. 1978. Characterization of *Pseudomonas aeruginosa* mutants deficient in establishment of lysogeny. *J Bacteriol*, 134, 875-883.

Moken, M. C., McMurry, L. M. and Levy, S. B. 1997. Selection of multiple-antibiotic-resistant (Mar) mutants of *Escherichia coli* by using the disinfectant pine oil: roles of the *mar* and *acrAB* loci. *Antimicrob Agents Chemother*, 41, 2770–2772.

Moradali, M. F., Ghods, S. and Rehm, B. H. 2017. *Pseudomonas aeruginosa* Lifestyle: A Paradigm for Adaptation, Survival, and Persistence. *Front Cell Infect Microbiol*, 7, 39.

Moreadith, R. W., Viegas, T. X., Bentley, M. D., Harris, J. M., Fang, Z., Yoon, K., Dizman, B., Weimer, R., Rae, B. P., Li, X., Rader, C., Standaert, D. and Olanow, W. 2017. Clinical development of a poly(2-oxazoline) (POZ) polymer therapeutic for the treatment of Parkinson's disease – Proof of concept of POZ as a versatile polymer platform for drug development in multiple therapeutic indications. *European Polymer Journal*, 88, 524-552.

Morelle, B., Salmon, J. M., Vigo, J. and Viallet, P. 1994. Measurement of intracellular magnesium concentration in 3T3 fibroblast with the fluorescent indicator Mag-indo-1. *Anal Biochem*, 218, 170-176.

Moreno, E. C. and Margolis, H. C. 1988. Composition of human plaque fluid. *J Dent Res*, 67, 1181-1189.

Moriarty, T. F., Elborn, J. S. and Tunney, M. M. 2007. Effect of pH on the antimicrobial susceptibility of planktonic and biofilm-grown clinical *Pseudomonas aeruginosa* isolates. *Br J Biomed Sci*, 64, 101-104.

Morita, R. Y. 1975. Psychrophilic bacteria. *Bacteriol Rev*, 39, 144-167.

Moskowitz, S. M., Brannon, M. K., Dasgupta, N., Pier, M., Sgambati, N., Miller, A. K., Selgrade, S. E., Miller, S. I., Denton, M., Conway, S. P., Johansen, H. K. and Hoiby, N. 2012. PmrB mutations promote polymyxin resistance of *Pseudomonas aeruginosa* isolated from colistin-treated cystic fibrosis patients. *Antimicrob Agents Chemother*, 56, 1019-1030.

Moyer, C. L. and Morita, R. Y. 2007. Psychrophiles and psychrotrophs. *In:* Encyclopedia of Life Sciences. John Wiley & Sons. 1-6.

Mukamolova, G. V., Turapov, O. A., Kazarian, K., Telkov, M., Kaprelyants, A. S., Kell, D. and Young, M. 2002. The *rpf* gene of *Micrococcus luteus* encodes an essential secreted growth factor. *Mol Microbiol*, 46, 611-621.

Mulcahy, H., Charron-Mazenod, L. and Lewenza, S. 2008. Extracellular DNA chelates cations and induces antibiotic resistance in *Pseudomonas aeruginosa* biofilms. *PLoS Pathog*, 4, e1000213.

Munk, S., Johansen, C., Stahnke, L. H. and Adler-Nissen, J. 2001. Microbial survival and odor in laundry. *J Surfactants Deterg*, 4, 385-394.

Murtough, S. M., Hiom, S. J., Palmer, M. and Russell, A. D. 2001. Biocide rotation in the healthcare setting: is there a case for policy implementation? *J Hosp Infect*, 48, 1-6.

Müsken, M., Di Fiore, S., Römling, U. and Häussler, S. 2010. A 96-well-plate-based optical method for the quantitative and qualitative evaluation of *Pseudomonas aeruginosa* biofilm formation and its application to susceptibility testing. *Nat Protoc*, 5, 1460-1469.

Nagai, K., Murata, T., Ohta, S., Zenda, H., Ohnishi, M. and Hayashi, T. 2003. Two different mechanisms are involved in the extremely high-level benzalkonium chloride resistance of a *Pseudomonas fluorescens* strain. *Microbiol Immunol*, 47, 709-715.

Nealson, K. H., Platt, T. and Hasting, W. 1970. Cellular control of the synthesis and activity of the bacterial luminescent system. *J Bacteriol*, 104, 313-322.

Nebe-von-Caron, G., Stephens, P. J., Hewitt, C. J., Powell, J. R. and Badley, R. A. 2000. Analysis of bacterial function by multi-colour fluorescence flow cytometry and single cell sorting. *J Microbiol Methods*, 42, 97-114.

Ng, F. M. W. and Dawes, E. A. 1973. Chemostat studies on the regulation of glucose metabolism in *Pseduomonas aeruginosa* by citrate. *Biochem*, 132, 129-140.

Nguyen, D. M., Mascola, L. and Bancroft, E. 2005. Recurring methicillin-resistant *Staphylococcus aureus* infections in a football team. *Emerg Infect Dis*, 11.

Niehaus, F., Gabor, E., Wieland, S., Siegert, P., Maurer, K. H. and Eck, J. 2011. Enzymes for the laundry industries: tapping the vast metagenomic pool of alkaline proteases. *Microb Biotechnol*, 4, 767-776.

Nielsen, A. T., Tolker-Nielsen, T., Barken, K. B. and Molin, S. 2000. Role of commensal relationships on the spatial structure of a surface-attached microbial consortium. *Environ Microbiol*, 2, 59-68.

Nix, I. D., Frontzek, A. and Bockmühl, D. P. 2015. Characterization of microbial communities in household washing machines. *Tenside Surf Det*, 52, 432-440.

Nostro, A., Cellini, L., Di Giulio, M., D'Arrigo, M., Marino, A., Blanco, A. R., Favaloro, A., Cutroneo, G. and Bisignano, G. 2012. Effect of alkaline pH on staphylococcal biofilm formation. *APMIS*, 120, 733-742.

O'Toole, G. A. 2011. Microtiter dish biofilm formation assay. *J Vis Exp*, 1-2.

O'Toole, G. A. and Kolter, R. 1998. Flagellar and twitching motility are necessary for *Pseudomonas aeruginosa* biofilm development. *Mol Microbiol*, 30, 295-304.

O'Toole, J., Sinclair, M. and Leder, K. 2009. Transfer rates of enteric microorganisms in recycled water during machine clothes washing. *Appl Environ Microbiol*, 75, 1256-1263.

O'Malley, Y. Q., Reszka, K. J., Rasmussen, G. T., Abdalla, M. Y., Denning, G. M. and Britigan, B. E. 2003. The *Pseudomonas* secretory product pyocyanin inhibits catalase activity in human lung epithelial cells. *Am J Physiol Lung Cell Mol Physiol*, 285, L1077–L1086.

Ochsner, U. A. and Reiser, J. 1995. Autoinducer-mediated regulation of rhamnolipid biosurfactant synthesis in *Pseudomonas aeruginosa*. *Proc Natl Acad Sci U S A*, 92, 6424-6428.

Odumosu, O., Nicholas, D., Yano, H. and Langridge, W. 2010. AB toxins: a paradigm switch from deadly to desirable. *Toxins (Basel)*, 2, 1612-1645.

Oh, K. B., Miyazawa, H., Naito, T. and Matsuoka, H. 2001. Purification and characterization of an autoregulatory substance capable of regulating the morphological transition in *Candida albicans*. *Proc Natl Acad Sci USA*, 98, 4664-4668.

Oh, S., Kurt, Z., Tsementzi, D., Weigand, M. R., Kim, M., Hatt, J. K., Tandukar, M., Pavlostathis, S. G., Spain, J. C. and Konstantinidis, K. T. 2014. Microbial community degradation of widely used quaternary ammonium disinfectants. *Appl Environ Microbiol*, 80, 5892-5900.

Okuda, J., Hayashi, N., Arakawa, M., Minagawa, S. and Gotoh, N. 2013. Type IV pilus protein PilA of *Pseudomonas aeruginosa* modulates calcium signaling through binding the calcium-modulating cyclophilin ligand. *J Infect Chemother*, 19, 653-664.

Ophir, T. and Gutnick, D. L. 1994. A role for exopolysaccharides in the protection of microorganisms from desiccation. *Appl Environ Microbiol*, 60, 740-745.

Ostuni, E., Chapman, E. G., Liang, M. N., Meluleni, G., Pier, G. B., Ingber, D. and Whitesides, G. M. 2001. Self-assembled monolayers that resist the adsorption of proteins and the adhesion of bacterial and mammalian cells. *Langmuir*, 17, 6336-6343.

Overly, C. C., Lee, K. D., Berthiaume, E. and Hollenbeck, P. J. 1995. Quantitative measurement of intraorganelle pH in the endosomal-lysosomal pathway in neurons by using ratiometric imaging with pyranine. *Proc Natl Acad Sci USA*, 92, 3156-3160.

Oyama, J., Lera-Nonose, D., Ramos-Milare, A., Padilha Ferreira, F. B., de Freitas, C. F., Caetano, W., Hioka, N., Silveira, T. G. V. and Lonardoni, M. V. C. 2019. Potential of Pluronics® P-123 and F-127 as nanocarriers of anti-*Leishmania* chemotherapy. *Acta Trop*, 192, 11-21.

Pakula, C. and Stamminger, R. 2010. Electricity and water consumption for laundry washing by washing machine worldwide. *Energ Effic*, 3, 365-382.

Pal, A. and Paul, A. K. 2008. Microbial extracellular polymeric substances: central elements in heavy metal bioremediation. *Indian J Biotechnol*, 48, 49-64.

Panova, A. A., Pantano, P. and Walt, D. R. 1997. *In situ* fluorescence imaging of localized corrosion with a pH-sensitive imaging fiber. *Anal Chem*, 69, 1635-1641.

Paranchych, W., Sastry, P. A., Frost, L. S., Carpenter, M., Armstrong, G. D. and Watts, T. H. 1997. Biochemical studies on pili isolated from *Pseudomonas aeruginosa* strain PA0. *Can J Microbiol*, 25, 1175-1181.

Park, K. D., Kim, Y. S., Han, D. K., Kim, Y. H., Lee, E. H. B., Suh, H. and Choi, K. S. 1998. Bacterial adhesion on PEG modified polyurethane surfaces. *Biomaterials*, 19, 851-859.

Patel, S. N., Murray-Leonard, J. and Wilson, A. P. 2006. Laundering of hospital staff uniforms at home. *J Hosp Infect*, 62, 89-93.

Patriquin, G. M., Banin, E., Gilmour, C., Tuchman, R., Greenberg, E. P. and Poole, K. 2008. Influence of quorum sensing and iron on twitching motility and biofilm formation in *Pseudomonas aeruginosa*. *J Bacteriol*, 190, 662-671.

Pedroza, C. J., Flórez, A. M., Ruiz, O. S. and Orduz, S. 2014. Enzymatic hydrolysis of molecules associated with bacterial quorum sensing using an acyl homoserine lactonase from a novel *Bacillus thuringiensis* strain. *Antonie Van Leeuwenhoek*, 105, 253-264.

Penketh, A., Pitt, T., Roberts, D., Hodson, M. E. and Batten, J. C. 1982. The relationship of phenotype changes in *Pseudomonas aeruginosa* to the clinical condition of patients with cystic fibrosis. *Am Rev Respir Dis*, 127, 605-608.

Perenich, T. A. and Wilkinson, R. P. 1993. Bacterial survival on fabrics laundered in cold water. *J Consumer Stud Home Econ*, 17, 57-65.

Persat, A., Inclan, Y. F., Engel, J. N., Stone, H. A. and Gitai, Z. 2015. Type IV pili mechanochemically regulate virulence factors in *Pseudomonas aeruginosa*. *Proc Natl Acad Sci U S A*, 112, 7563-7568.

Pesci, E. C., Milbank, J. B. J., Pearson, J. P., McKnight, S., Kende, A. S., Greenberg, E. P. and Iglewski, B. H. 1999. Quinolone signaling in the cell-to-cell communication system of *Pseudomonas aeruginosa*. *Proc Natl Acad Sci U S A*, 96, 11229–11234.

Pesci, E. C., Pearson, J. P., Seed, P. C. and Iglewski, B. H. 1997. Regulation of *las* and *rhl* Quorum Sensing in *Pseudomonas aeruginosa*. *J Bacteriol*, 179, 3127-3132.

Peterson, B. W., He, Y., Ren, Y., Zerdoum, A., Libera, M. R., Sharma, P. K., van Winkelhoff, A. J., Neut, D., Stoodley, P., van der Mei, H. C. and Busscher, H. J. 2015. Viscoelasticity of biofilms and their recalcitrance to mechanical and chemical challenges. *FEMS Microbiol Rev*, 39, 234-245.

Petrova, O. E. and Sauer, K. 2009. A novel signaling network essential for regulating *Pseudomonas aeruginosa* biofilm development. *PLoS Pathog*, 5, e1000668.

Peulen, T. O. and Wilkinson, K. J. 2011. Diffusion of nanoparticles in a biofilm. *Environ Sci Technol*, 45, 3367-3373.

Pillar, C. M. and Hobden, J. A. 2002. *Pseudomonas aeruginosa* exotoxin A and keratitis in mice. *IOVS*, 43, 1437-1444.

Pirmoradi, F. N., Jackson, J. K., Burt, H. M. and Chiao, M. 2011. A magnetically controlled MEMS device for drug delivery: design, fabrication, and testing. *Lab Chip*, 11, 3072-3080.

Price, C. T., Singh, V. K., Jayaswal, R. K., Wilkinson, B. J. and Gustafson, J. E. 2002. Pine oil cleaner-resistant *Staphylococcus aureus*: reduced susceptibility to vancomycin and oxacillin and involvement of SigB. *Appl Environ Microbiol*, 68, 5417-5421.

Promega 2019. BacTiter-Glo™ Microbial Cell Viability Assay. Available: https://www.promega.de/products/cell-health-assays/cell-viability-and-cytotoxicity-assays/bactiter_glo-microbial-cell-viability-assay/?catNum=G8230#protocols.

Qian, Z., Sagers, R. D. and Pitt, W. G. 1997. The effect of ultrasonic frequency upon enhanced killing of *P. aeruginos*a biofilms. *Ann Biomed Eng*, 25, 69-76.

Qurashi, A. W. and Sabri, A. N. 2012. Bacterial exopolysaccharide and biofilm formation stimulate chickpea grwoth and soil aggregation under salt stress. *Braz J Microbiol*, 1183-1191.

Ramsing, N. B., Kühl, M. and Jørgensen, B. B. 1993. Distribution of sulfate-reducing bacteria, O_2, and H_2S in photosynthetic biofilms determined by oligonucleotide probes and microelectrodes. *Appl Environ Microbiol*, 59, 3840-3849.

Rani, S. A., Pitts, B. and Stewart, P. S. 2005. Rapid diffusion of fluorescent tracers into *Staphylococcus epidermidis* biofilms visualized by time lapse microscopy. *Antimicrob Agents Chemother*, 49, 728-732.

Rappé, M. S. and Giovannoni, S. J. 2003. The uncultured microbial majority. *Annu Rev Microbiol*, 57, 369-394.

Rasamiravaka, T., Labtani, Q., Duez, P. and El Jaziri, M. 2015. The formation of biofilms by *Pseudomonas aeruginosa*: a review of the natural and synthetic compounds interfering with control mechanisms. *Biomed Res Int*, 2015, 1-17.

Raschle, P. 1983. Einfluss der Waschtemperatur auf den Keimgehalt der Wäsche. *Textilveredlung*, 18, 37-40.

Rashid, M. H. and Kornberg, A. 2000. Inorganic polyphosphate is needed for swimming, swarming, and twitching motilities of *Pseudomonas aeruginosa*. *Proc Natl Acad Sci U S A*, 97, 4885–4890.

Ravichandran, A., Ramachandran, M., Suriyanarayanan, T., Wong, C. C. and Swarup, S. 2015. Global regulator MorA affects virulence-associated protease secretion in *Pseudomonas aeruginosa* PAO1. *PLoS One*, 10, 1-17.

Rayner, J., Veeh, R. and Flood, J. 2004. Prevalence of microbial biofilms on selected fresh produce and household surfaces. *Int J Food Microbiol*, 95, 29-39.

Rehberg, L., Frontzek, A., Melhus, A. and Bockmuhl, D. P. 2017. Prevalence of beta-lactamase genes in domestic washing machines and dishwashers and the impact of laundering processes on antibiotic-resistant bacteria. *J Appl Microbiol*, 123, 1396-1406.

Rice, L. B. 2008. Federal funding for the study of antimicrobial resistance in nosocomial pathogens: no ESKAPE. *J Infect Dis*, 197, 1079-1081.

Rickard, A. H., Palmer, R. J., Jr., Blehert, D. S., Campagna, S. R., Semmelhack, M. F., Egland, P. G., Bassler, B. L. and Kolenbrander, P. E. 2006. Autoinducer 2: a concentration-dependent signal for mutualistic bacterial biofilm growth. *Mol Microbiol*, 60, 1446-1456.

Roberts, A. E., Kragh, K. N., Bjarnsholt, T. and Diggle, S. P. 2015. The limitations of *in vitro* experimentation in understanding biofilms and chronic infection. *J Mol Biol*, 427, 3646-3661.

Rocchetta, H. L., Burrows, L. L. and Lam, J. S. 1999. Genetics of O-antigen biosynthesis in *Pseudomonas aeruginosa*. *Microbiol Mol Biol Rev*, 63, 523-553.

Rocha, A. J., Barsottini, M. R. d. O., Rocha, R. R., Laurindo, M. V., Moraes, F. L. L. d. and Rocha, S. L. d. 2019. *Pseudomonas aeruginosa*: Virulence factors and antibiotic resistance genes. *Brazilian Archives of Biology and Technology*, 62, 1-15.

Roosjen, A., Van der Mei, H. C., Busscher, H. J. and Norde, W. 2004. Microbial adhesion to poly(ethylene oxide) brushes: influence of polymer chain length and temperature. *Langmuir*, 20, 10949-10955.

Russell, A. D. 1998. Bacterial resistance to disinfectants: present knowledge and future problems. *J Hosp Infect*, 43, S57-S68.

Russell, A. D. 2002. Introduction of biocides into clinical practice and the impact on antibiotic-resistant bacteria. *J Appl Microbiol Symposium Supplement*, 92, 121S–135S.

Russell, A. D. 2004. Bacterial adaptation and resistance to antiseptics, disinfectants and preservatives is not a new phenomenon. *J Hosp Infect*, 57, 97-104.

Russell, A. D., Tattawasart, U., Maillard, J. Y. and Furr, J. R. 1998. Possible link between bacterial resistance and use of antibiotics and biocides. *Antimicrob Agents Chemother*, 42, 2151.

Ryu, J. H. and Beuchat, L. R. 2004. Factors affecting production of extracellular carbohydrate complexes by *Escherichia coli* O157:H7. *Int J Food Microbiol*, 95, 189-204.

Sahle-Demessie, E. and Tadesse, H. 2011. Kinetics and equilibrium adsorption of nano-TiO2 particles on synthetic biofilm. *Surface Science*, 605, 1177-1184.

Sajid, M., Ilyas, M., Basheer, C., Tariq, M., Daud, M., Baig, N. and Shehzad, F. 2015. Impact of nanoparticles on human and environment: review of toxicity factors, exposures, control strategies, and future prospects. *Environ Sci Pollut Res Int*, 22, 4122-4143.

Salmanpour, M., Tamaddon, A., Yousefi, G. and Mohammadi-Samani, S. 2017. "Grafting-from" synthesis and characterization of poly (2-ethyl-2-oxazoline)-b-poly (benzyl L-glutamate) micellar nanoparticles for potential biomedical applications. *Bioimpacts*, 7, 155-166.

Salton, M. R. J. 1968. Lytic agents, cell permeability, and monolayer penetrability. *J Gen Physiol*, 52, 277S–252S.

Sánchez-Clemente, R., Igeño, M. I., Población, A. G., Guijo, M. I., Merchán, F. and Blasco, R. 2018. Study of pH changes in media during bacterial growth of several environmental strains. *Proceedings*, 2, 1-5.

Sarkar, D., Mallick, A., Haldar, B. and Chattopadhyay, N. 2010. Ratiometric spectroscopic response of pH sensitive probes: An alternative strategy for multidimensional sensing. *Chem Phys Lett*, 484, 168-172.

Sato, H., Frank, D. W., Hillard, C. J., Feix, J. B., Pankhaniya, R. R., Moiyama, K., Finck-Barbançon, V., Buchaklian, A., Lei, M., Long, R. M., Wiener-Kronish, J. and Sawa, T. 2003. The mechanism of action of the *Pseudomonas aeruginosa*-encoded type III cytotoxin, ExoU. *EMBO*, 22, 2959-2969.

Sauer, K., Camper, A. K., Ehrlich, G. D., Costerton, J. W. and Davies, D. G. 2002. *Pseudomonas aeruginosa* sisplays multiple phenotypes during development as a biofilm. *J Bacteriol*, 184, 1140-1154.

Schaber, J. A., Carty, N. L., McDonald, N. A., Graham, E. D., Cheluvappa, R., Griswold, J. A. and Hamood, A. N. 2004. Analysis of quorum sensing-deficient clinical isolates of *Pseudomonas aeruginosa*. *J Med Microbiol*, 53, 841-853.

Schimmelbusch, C. 1993. Volkmanns Sammlung Klinischer Vorträge. 62, 312-328.

Schmithausen, R. M., Sib, E., Exner, M., Hack, S., Rösing, C., Ciorba, P., Bierbaum, G., Savin, M., Bloomfield, S. F., Kaase, M., Jacobshagen, A., Gemein, S., Gebel, J., Engelhart, S. and Exner, D. 2019. The washing machine as a reservoir for transmission of extended-spectrum-beta-lactamase (CTX-M-15)-producing *Klebsiella oxytoca* ST201 to newborns. *Appl Environ Microbiol*, 85, 1-11.

Schurek, K. N., Sampaio, J. L., Kiffer, C. R., Sinto, S., Mendes, C. M. and Hancock, R. E. 2009. Involvement of *pmrAB* and *phoPQ* in polymyxin B adaptation and inducible resistance in non-cystic fibrosis clinical isolates of *Pseudomonas aeruginosa*. *Antimicrob Agents Chemother*, 53, 4345-4351.

Schuster, M. and Greenberg, E. P. 2007. Early activation of quorum sensing in *Pseudomonas aeruginosa* reveals the architecture of a complex regulon. *BMC Genomics*, 8, 287.

Shah, P. C., Krajden, S., Kane, J. and Summerbell, R. C. 1988. Tinea corpis caused by *Microsporum canis*: report of a nosocomial outbreak. *Eur J Epidermiol*, 4, 33-38.

Sheane, C. A. 2000. Secondary wash benefits of TAED integrated laundry detergent formulations. *Riv Ital Sostanze Gr*, 77, 365-369.

Shephard, J., McQuillan, A. J. and Bremer, P. J. 2008. Mechanisms of cation exchange by *Pseudomonas aeruginosa* PAO1 and PAO1 *wbpL*, a strain with a truncated lipopolysaccharide. *Appl Environ Microbiol*, 74, 6980-6986.

Shi, L., Gunther, S., Hubschmann, T., Wick, L. Y., Harms, H. and Muller, S. 2007. Limits of propidium iodide as a cell viability indicator for environmental bacteria. *Cytometry A*, 71, 592-598.

Silo-Suh, L., Suh, S. J., Phibbs, P. V. and Ohman, D. E. 2005. Adaptations of *Pseudomonas aeruginosa* to the cystic fibrosis lung environment can include deregulation of *zwf,* encoding glucose-6-phosphate dehydrogenase. *J Bacteriol*, 187, 7561-7568.

Simpson, J. A., Smith, S. E. and Dean, R. T. 1989. Scavenging by alginate of free radicals released by macrophages. *Free Radic Biol Med*, 6, 347-353.

Singh, N., Romero, M., Travanut, A., Monteiro, P. F., Jordana-Lluch, E., Hardie, K. R., Williams, P., Alexander, M. R. and Alexander, C. 2019. Dual bioresponsive antibiotic and quorum sensing inhibitor combination nanoparticles for treatment of *Pseudomonas aeruginosa* biofilms in vitro and ex vivo. *Biomater Sci*, 1-13.

Singh, P. K., Parsek, M. R., Greenberg, E. P. and Welsh, M. J. 2002. A component of innate immunity prevents bacterial biofilm development. *Nature*, 417, 552-555.

Singhal, N., Kumar, M., Kanaujia, P. K. and Virdi, J. S. 2015. MALDI-TOF mass spectrometry: an emerging technology for microbial identification and diagnosis. *Front Microbiol*, 6, 791.

Smith, A. C. and Hussey, M. A. 2005. Gram stain protocol. *American Society for Microbiology* [Online]. Available: https://www.asmscience.org/content/education/protocol/protocol.2886.

Smith, E. E., Buckley, D. G., Wu, Z., Saenphimmachak, C., Hoffman, L. R., D'Argenlo, D. A., Miller, S. I., Ramsey, B. W., Speert, D. P., Moskowitz, S. M., Burns, J. L., Kaul, R. and Olson, M. V. 2006. Genetic adaptation by *Pseudomonas aeruginosa* to the airways of cystic fibrosis patients. *Proc Natl Acad Sci U S A*, 103, 8487-8492.

Solé, M., Rius, N. and Lorén, J. G. 2000. Rapid extracellular acidification induced by glucose metabolism in nonproliferating cells of *Serratia marcescens*. *Internal Microbiol*, 3, 39–43.

Søndergaard, R. V., Henriksen, J. R. and Andresen, T. L. 2014. Design, calibration and application of broad-range optical nanosensors for determining intracellular pH. *Nat Protoc*, 9, 2841-2858.

Sorensen, R. U. and Joseph, F. 1993. Phenazine pigments in *Pseudomonas aeruginosa* infection. *In:* Camper, M., Bendinelli, M. & Friedman, H. (eds.) *In: Pseudomonas aeruginosa* as an Opportunistic Pathogen. New York: Plenum Press.

Spoering, A. L. and Gilmore, M. S. 2006. Quorum sensing and DNA release in bacterial biofilms. *Curr Opin Microbiol*, 9, 133-137.

Standaert, S. M., Hutcheson, R. H. and Schaffner, W. 1994. Nosocomial transmission of *Salmonella gastroenteritis* to laundry workers in a nursing home. *Infect Control Hosp Epidemiol*, 15, 22-26.

Stanier, R. Y., Palleroni, N. J. and Doudoroff, M. 1966. The aerobic Pseudomonads: a taxonomic study. *J Gen Microbiol*, 43, 159-271.

Statistisches Bundesamt 2017. Statistisches Jahrbuch Deutschland, 1st ed. Wiesbaden, Germany.

Stewart, P. S. 2003. Diffusion in Biofilms. *Journal of Bacteriology*, 185, 1485-1491.

Stewart, P. S. and Franklin, M. J. 2008. Physiological heterogeneity in biofilms. *Nat Rev Microbiol*, 6, 199-210.

Stiefel, P., Schmidt-Emrich, S., Maniura-Weber, K. and Ren, Q. 2015. Critical aspects of using bacterial cell viability assays with the fluorophores SYTO9 and propidium iodide. *BMC Microbiol*, 15, 36.

Stocks, S. M. 2004. Mechanism and use of the commercially available viability stain, BacLight. *Cytometry A*, 61, 189-195.

Stoodley, P., Cargo, R., Rupp, C. J., Wilson, S. and Klapper, I. 2002a. Biofilm material properties as related to shear-induced deformation and detachment phenomena. *J Ind Microbiol Biotechnol*, 29, 361-367.

Stoodley, P., De Beer, D. and Lappin-Scott, H. M. 1997. Influence of eletric fields and pH on biofilm structure as related to the bioelectric effect. *Antimicrob Agents Chemother*, 41, 1876–1879.

Stoodley, P., Sauer, K., Davies, D. G. and Costerton, J. W. 2002b. Biofilms as complex differentiated communities. *Annu Rev Microbiol*, 56, 187-209.

Stover, C. K., Pham, X. Q., Erwin, A. L., Mizoguchi, S. D., Warrener, P., Hickey, M. J., Brinkman, F. S. L., Hufnagle, W. O., Kowalik, D. J., Lagrou, M., Garber, R. L., Goltry, L., Tolentino, E., Westbrock-Wadman, S., Yuan, Y., Brody, L. L., Coulter, S. N., Folger, K. R., Kas, A., Larbig, K. D., Lim, R., Smith, K., Spencer, D., Wong, G. K. S., Wu, Z., Paulsen, I. T., Reizer, J., Saier, M. H., Hancock, R. E. W., Lory, S. and Olson, M. V. 2000. Complete genome sequence of *Pseudomonas aeruginosa* PAO1, an opportunistic pathogen. *Nature*, 406, 959-964.

Strathmann, M., Wingender, J. and Flemming, H. C. 2002. Application of fluorescently labelled lectins for the visualization and biochemical characterization of polysaccharides in biofilms of *Pseudomonas aeruginosa*. *J Microbiol Methods*, 50, 237-248.

Subedi, D., Vijay, A. K., Kohli, G. S., Rice, S. A. and Willcox, M. 2018. Comparative genomics of clinical strains of *Pseudomonas aeruginosa* strains isolated from different geographic sites. *Sci Rep*, 8, 15668.

Suh, S. J., Runyen-Janecky, L. J., Maleniak, T. C., Hager, P., MacGregor, C. H., Zielinski-Mozny, N. A., Phibbs, P. V. and West, S. E. H. 2002. Effect of *vfr* mutation on global gene expression and catabolite repression control of *Pseudomonas aeruginosa*. *Microbiol*, 148, 1561–1569.

Sun, H., Almdal, K. and Andresen, T. L. 2011. Expanding the dynamic measurement range for polymeric nanoparticle pH sensors. *Chem Commun (Camb)*, 47, 5268-5270.

Sun, H., Andresen, T. L., Benjaminsen, R. V. and Almdal, K. 2009. Polymeric nanosensors for measuring the full dynamic pH range of endosomes and lysosomes in mammalian cells. *J Biomed Nanotechnol*, 5, 676-682.

Sun, S. J., Liu, H. J., Weng, C. H., Lai, C. F., Ai, L. Y., Liu, Y. C. and Zhu, H. 2016. The response of *Serratia marcescens* JG to environmental changes by quorum sensing system. *Arch Microbiol*, 198, 585-590.

Sun, W. C., Gee, K. R., Klaubert, D. H. and Haugland, R. P. 1997. Synthesis of fluorinated fluoresceins. *J Org Chem*, 62, 6469-6475.

Sundheim, G., Langsrud, S., Heir, E. and Holck, A. L. 1998. Bacterial resistance to disinfectants containing quaternary ammonium compounds. *Int Biodeterior Biodegradation*, 41, 235-239.

Sutherland, I. W. 1999. Polysaccharases for microbial exopolysaccharides. *Carbohydr Polym*, 38, 319-328.

Takenaka, S., Pitts, B., Trivedi, H. M. and Stewart, P. S. 2009. Diffusion of macromolecules in model oral biofilms. *Appl Environ Microbiol*, 75, 1750-1753.

Takeuchi, K., Hasegawa, Y., Ishida, H. and Kashiwagi, M. 2012. Identification of novel malodour compounds in laundry. *Flavour Frag J*, 27, 89-94.

Tauhardt, L., Frant, M., Pretzel, D., Hartlieb, M., Bücher, C., Hildebrand, G., Schröter, B., Weber, C., Kempe, K., Gottschaldt, M., Liefeith, K. and Schubert, U. S. 2014. Amine end-functionalized poly(2-ethyl-2-oxazoline) as promising coating material for antifouling applications. *J Mater Chem B*, 2, 4883-4893.

Tedjo, C., Neoh, K. G., Kang, E. T., Fang, N. and Chan, V. 2007. Bacteria-surface interaction in the presence of proteins and surface attached poly(ethylene glycol) methacrylate chains. *J Biomed Mater Res A*, 82, 479-491.

Teng, A. 2000. The detergent market. *Happi*, 37, 72.

Terpe, K., Kerkhoff, K., Pluta, E. and Jendrossek, D. 1999. Relationship between succinate transport and production of extracellular poly(3-hydroxybutyrate) depolymerase in *Pseudomonas lemoignei*. *Appl Environ Microbiol*, 65, 1703–1709.

Terpstra, P. M. 1998. Domestic and institutional hygiene in relation to sustainability. Historical, social and environmental implications. *Int Biodeterior Biodegradation*, 41, 169-175.

Teughels, W., Van Assche, N., Sliepen, I. and Quirynen, M. 2006. Effect of material characteristics and/or surface topography on biofilm development. *Clin Oral Impl Res*, 17, 68–81.

Tezel, U. and Pavlostathis, S. G. 2015. Quaternary ammonium disinfectants: microbial adaptation, degradation and ecology. *Curr Opin Biotechnol*, 33, 296-304.

Tezel, U., Tandukar, M., Martinez, R. J., Sobecky, P. A. and Pavlostathis, S. G. 2012. Aerobic biotransformation of n-tetradecylbenzyldimethylammonium chloride by an enriched *Pseudomonas* spp. community. *Environ Sci Technol*, 46, 8714-8722.

Thermo Fisher Scientific 2010a. Fluorophores and their amine-reactive derivatives. *In:* The Molecular Probes™ Handbook: A Guide to Fluorescent Probes and Labeling Technologies. Available: www.thermofisher.com.

Thermo Fisher Scientific 2010b. pH indicators. *In:* The Molecular Probes™ Handbook: A Guide to Fluorescent Probes and Labeling Technologies. Available: www.thermofisher.com.

Tinh, N. T., Dung, N. V., Trung, C. T. and Thuy, V. T. 2013. *In vitro* characterization of a recombinant AHL-lactonase from *Bacillus cereus* isolated from a striped catfish (*Pangasianodon hypophthalmus*) pond. *Indian J Microbiol*, 53, 485-487.

Tiwari, N. P. and Campbell, J. J. R. 1869. Enzymatic control of the metabolic activity of *Pseudomonas aeruginosa* grown in glucose or succinate media. *Biochimica et Biophysica Acta*, 192, 395-401.

Toder, D. S., Ferrell, S. J., Nezezon, J. L., Rust, L. and Iglewski, B. H. 1994. *lasA* and *lasB* Genes of *Pseudomonas aeruginosa*: Analysis of Transcription and Gene Product Activity. *Infect and Immun*, 62, 1320-1327.

Tolker-Nielsen, T., Brinch, U. C., Ragas, P. C., Andersen, J. B., Jacobsen, C. S. and Molin, S. 2000. Development and dynamics of *Pseudomonas* sp. biofilms. *J Bacteriol*, 182, 6482–6489.

Toutain, C. M., Zegans, M. E. and O'Toole, G. A. 2005. Evidence for two flagellar stators and their role in the motility of *Pseudomonas aeruginosa*. *J Bacteriol*, 187, 771-777.

Trevors, J. T. 2012. Can dead bacterial cells be defined and are genes expressed after cell death? *J Microbiol Methods*, 90, 25-28.

Tribedi, P., Gupta, A. D. and Sil, A. K. 2015. Adaptation of *Pseudomonas* sp. AKS2 in biofilm on low-density polyethylene surface: an effective strategy for efficient survival and polymer degradation. *Bioresources and Bioprocessing*, 2, 1-10.

Tricot, C., Vander Wauven, C., Wattiez, R., Falmagne, P. and Stalon, V. 1994. Purification and properties of a succinyltransferase from *Pseudomonas aeruginosa* specific for both arginine and ornithine. *Eur J Biochem*, 224, 853-861.

Uroz, S., Chhabra, S. R., Cámara, M., Williams, P., Oger, P. and Dessaux, Y. 2005. *N*-Acylhomoserine lactone quorum-sensing molecules are modified and degraded by *Rhodococcus erythropolis* W2 by both amidolytic and novel oxidoreductase activities. *Microbiol*, 151, 3313-3322.

Usher, L. R., Lawson, R. A., Geary, I., Taylor, C. J., Bingle, C. D., Taylor, G. W. and Whyte, M. K. 2002. Induction of neutrophil apoptosis by the *Pseudomonas aeruginosa* exotoxin pyocyanin: a potential mechanism of persistent infection. *J Immunol*, 168, 1861-1868.

Valentini, M. and Lapouge, K. 2013. Catabolite repression in *Pseudomonas aeruginosa* PAO1 regulates the uptake of C4 -dicarboxylates depending on succinate concentration. *Environ Microbiol*, 15, 1707-1716.

Van Delden, C. and Iglewski, B. H. 1998. Cell-to-cell signaling and *Pseudomonas aeruginosa* infections. *Emerg Infect Dis*, 4, 551-560.

Vasseur, P., Vallet-Gely, I., Soscia, C., Genin, S. and Filloux, A. 2005. The *pel* genes of the *Pseudomonas aeruginosa* PAK strain are involved at early and late stages of biofilm formation. *Microbiology (Reading)*, 151, 985-997.

Vasudevan, R. 2014. Biofilms: microbial cities of scientific significance. *Journal of Microbiology & Experimentation*, 1, 1-16.

Večeř, J., Holoubek, A. and Sigler, K. 2001. Fluorescence behavior of the pH-sensitive probe carboxy SNARF-1 in suspension of liposomes. *Photochem Photobiol*, 74, 8-13.

Vendeville, A., Winzer, K., Heurlier, K., Tang, C. M. and Hardie, K. R. 2005. Making 'sense' of metabolism: autoinducer-2, LuxS and pathogenic bacteria. *Nat Rev Microbiol*, 3, 383-396.

Villaverde, S., Mirpuri, R. G., Lewandowski, Z. and Jones, W. L. 1997. Physiological and chemical gradients in a *Pseudomonas putida* 54G biofilm degrading toluene in a flat plate vapor phase bioreactor. *Biotechnol Bioeng*, 56, 361-371.

Vojcic, L., Pitzler, C., Korfer, G., Jakob, F., Ronny, M., Maurer, K. H. and Schwaneberg, U. 2015. Advances in protease engineering for laundry detergents. *N Biotechnol*, 32, 629-634.

Vroom, J. M., De Grauw, K. J., Cerritsen, H. C., Bradshaw, D. J., Marsh, P. D., Watson, G. K., Birmingham, J. J. and Allison, C. 1999. Depth penetration and detection of pH gradients in biofilms by two-photon excitation microscopy. *Appl Environ Microbiol*, 65, 3502-3511.

Wan, N., Wang, H., Ng, C. K., Mukherjee, M., Ren, D., Cao, B. and Tang, Y. J. 2018. Bacterial metabolism during biofilm growth investigated by ^{13}C tracing. *Front Microbiol*, 9, 2657.

Wang, H., Li, L., Tong, Q. and Yan, M. 2011. Evaluation of photochemically immobilized poly(2-ethyl-2-oxazoline) thin films as protein-resistant surfaces. *ACS Appl Mater Interfaces*, 3, 3463-3471.

Wang, L. H., He, Y., Gao, Y., Wu, J. E., Dong, Y. H., He, C., Wang, S. X., Weng, L. X., Xu, J. L., Tay, L., Fang, R. X. and Zhang, L. H. 2004. A bacterial cell-cell communication signal with cross-kingdom structural analogues. *Mol Microbiol*, 51, 903-912.

Wang, Y., Gao, L., Rao, X., Wang, J., Yu, H., Jiang, J., Zhou, W., Wang, J., Xiao, Y., Li, M., Zhang, Y., Zhang, K., Shen, L. and Hua, Z. 2018. Characterization of *lasR*-deficient clinical isolates of *Pseudomonas aeruginosa*. *Sci Rep*, 8, 13344.

Wang, Y., Liu, E., Sun, X., Huang, P., Long, H., Wang, H., Yu, X., Zheng, C. and Huang, Y. 2013. Pluronic L61 as a long-circulating modifier for enhanced liposomal delivery of cancer drugs. *Polymer Chemistry*, 4, 1-5.

Wang, Z., Shen, Y. and Haapasalo, M. 2014. Dental materials with antibiofilm properties. *Dent Mater*, 30, e1-16.

Wattam, A. R., Davis, J. J., Assaf, R., Boisvert, S., Brettin, T., Bun, C., Conrad, N., Dietrich, E. M., Disz, T., Gabbard, J. L., Gerdes, S., Henry, C. S., Kenyon, R. W., Machi, D., Mao, C., Nordberg, E. K., Olsen, G. J., Murphy-Olson, D. E., Olson, R., Overbeek, R., Parrello, B., Pusch, G. D., Shukla, M., Vonstein, V., Warren, A., Xia, F., Yoo, H. and Stevens, R. L. 2017. Improvements to PATRIC, the all-bacterial Bioinformatics Database and Analysis Resource Center. *Nucleic Acids Res*, 45, D535-D542.

Wei, Q. and Ma, L. Z. 2013. Biofilm matrix and its regulation in *Pseudomonas aeruginosa*. *Int J Mol Sci*, 14, 20983-21005.

Welser, K., Adsley, R., Moore, B. M., Chan, W. C. and Aylott, J. W. 2011. Protease sensing with nanoparticle based platforms. *Analyst*, 136, 29-41.

West, S. A., Diggle, S. P., Buckling, A., Gardner, A. and Griffin, A. S. 2007. The social lives of microbes. *Annu Rev Ecol Evol Syst*, 38, 53-77.

Whitchurch, C. B., Beatson, S. A., Comolli, J. C., Jakobsen, T., Sargent, J. L., Bertrand, J. J., West, J., Klausen, M., Waite, L. L., Kang, P. J., Tolker-Nielsen, T., Mattick, J. S. and Engel, J. N. 2005. *Pseudomonas aeruginosa fimL* regulates multiple virulence functions by intersecting with Vfr-modulated pathways. *Mol Microbiol*, 55, 1357-1378.

Whitchurch, C. B., Tolker-Nielsen, T., Ragas, P. and Mattick, J. S. 2002. Extracellular DNA required for bacterial biofilm formation. *Science*, 295, 1487.

Whitehead, N. A., Barnard, A. M. L., Slater, H., Simpson, N. J. L. and Salmond, G. P. C. 2001. Quorum-sensing in Gram-negative bacteria. *FEMS Microbiol Rev*, 25, 365-404.

Whiteley, M., Lee, K. M. and Greenberg, E. P. 1999. Identification of genes controlled by quorum sensing in *Pseudomonas aeruginosa*. *Proc Natl Acad Sci U S A*, 96, 13904-13909.

Whiting, P. H., Midgley, M. and Dawes, E. A. 1976. The regulation of transport of glucose, gluconate and 2-oxogluconate and of glucose catabolism in *Pseudomonas aeruginosa*. *Biochem J*, 154, 6S9-669.

Wilke, M. S., Heller, M., Creagh, A. L., Haynes, C. A., McIntosh, L. P., Poole, K. and Strynadka, N. C. J. 2008. The crystal structure of MexR from *Pseudomonas aeruginosa* in complex with its antirepressor ArmR. *Proc Natl Acad Sci U S A*, 105, 14832-14837.

Williams, P. 2007. Quorum sensing, communication and cross-kingdom signalling in the bacterial world. *Microbiology (Reading)*, 153, 3923-3938.

Williams, P. and Camara, M. 2009. Quorum sensing and environmental adaptation in *Pseudomonas aeruginosa:* a tale of regulatory networks and multifunctional signal molecules. *Curr Opin Microbiol*, 12, 182-191.

Williamson, K. S., Richards, L. A., Perez-Osorio, A. C., Pitts, B., McInnerney, K., Stewart, P. S. and Franklin, M. J. 2012. Heterogeneity in *Pseudomonas aeruginosa* biofilms includes expression of ribosome hibernation factors in the antibiotic-tolerant subpopulation and hypoxia-induced stress response in the metabolically active population. *J Bacteriol*, 194, 2062-2073.

Wilson, J. A., Loveday, H. P., Hoffman, P. N. and Pratt, R. J. 2007. Uniform: an evidence review of the microbiological significance of uniforms and uniform policy in the prevention and control of healthcare-associated infections. Report to the Department of Health (England). *J Hosp Infect*, 66, 301-307.

Wilson, R., Skyes, D. A., Watson, D., Rutman, A., Taylor, G. W. and Cole, P. J. 1988a. Measurement of *Pseudomonas aeruginosa* phenazine pigments in sputum and assessment of their contribution to sputum sol toxicity for respiratory epithelium. *Infect and Immun*, 56, 2515-2517.

Wilson, R., Sykes, D. A., Watson, D., Rutman, A., Taylor, G. W. and Cole, P. J. 1988b. Measurement of *Pseudomonas aeruginosa* phenazine pigments in sputum and assessment of their contribution to sputum sol toxicity for respiratory rpithelium. *Infect and Immun*, 56, 2515-2517.

Wilton, M., Charron-Mazenod, L., Moore, R. and Lewenza, S. 2016. Extracellular DNA acidifies biofilms and induces aminoglycoside resistance in *Pseudomonas aeruginosa*. *Antimicrob Agents Chemother*, 60, 544-553.

Winson, M. K., Camara, M., Latifi, A., Foglino, M., Chhabra, S. R., Daykin, M., Bally, M., Chapon, V., Salmond, G. P. C., Bycroft, B. W., Lazdunksi, A., Stewart, G. S. A. B. and Williams, P. 1995. Multiple N-acyl-L-homoserine lactone signal molecules regulate production of virulence determinants and secondary metabolites in *Pseudomonas aeruginosa*. *Proc Natl Acad Sci U S A*, 92, 9427-9431.

Winsor, G. L., Griffiths, E. J., Lo, R., Dhillon, B. K., Shay, J. A. and Brinkman, F. S. 2016. Enhanced annotations and features for comparing thousands of *Pseudomonas* genomes in the Pseudomonas genome database. *Nucleic Acids Res*, 44, D646-653.

Winstanley, C., Langille, M. G., Fothergill, J. L., Kukavica-Ibrulj, I., Paradis-Bleau, C., Sanschagrin, F., Thomson, N. R., Winsor, G. L., Quail, M. A., Lennard, N., Bignell, A., Clarke, L., Seeger, K., Saunders, D., Harris, D., Parkhill, J., Hancock, R. E., Brinkman, F. S. and Levesque, R. C. 2009. Newly introduced genomic prophage islands are critical determinants of *in vivo* competitiveness in the Liverpool Epidemic Strain of *Pseudomonas aeruginosa*. *Genome Res*, 19, 12-23.

Winzer, K. and Williams, P. 2001. Quorum sensing and the regulation of virulence gene expression in pathogenic bacteria. *Int J Med Microbiol*, 291, 131-143.

Witter, L. D. 1961. Psychrophilic bacteria - A review. *J Dairy Sci*, 44, 983-1015.

Woddle, M. C., Engbers, C. M. and Zalipsky, S. 1994. New amphipatic polymer-lipid conjugates forming long-circulating reticuloendothelial system-evading liposomes. *Bioconjugate Chem*, 5, 493-496.

Xiong, M. H., Bao, Y., Yang, X. Z., Zhu, Y. H. and Wang, J. 2014. Delivery of antibiotics with polymeric particles. *Adv Drug Deliv Rev*, 78, 63-76.

Xu, H. S., Roberts, N., Singleton, F. L., Attwell, R. W., Grimes, D. J. and Colwell, R. R. 1982. Survival and viability of nonculturable *Escherichia coli* and *Vibrio cholerae* in the estuarine and marine environment. *Microb Ecol*, 8, 313-323.

Yahr, T. L., Vallis, A. J., Hancock, M. K., Barbieri, J. T. and Frank, D. W. 1998. ExoY, an adenylate cyclase secreted by the *Pseudomonas aeruginosa* type III system. *Proc Natl Acad Sci U S A*, 95, 13899-13904.

Yang, L., Nilsson, M., Gjermansen, M., Givskov, M. and Tolker-Nielsen, T. 2009a. Pyoverdine and PQS mediated subpopulation interactions involved in *Pseudomonas aeruginosa* biofilm formation. *Mol Microbiol*, 74, 1380-1392.

Yang, L., Tolker-Nielsen, T. and Molin, S. 2009b. *Pseudomonas aeruginosa quorum-sensing - A factor in biofilm development, and an antipathogenic drug target.* Technical University of Denmark.

Yates, E. A., Philipp, B., Buckley, C., Atkinson, S., Chhabra, S. R., Sockett, R. E., Goldner, M., Dessaux, Y., Cámara, M., Smith, H. and Williams, P. 2002. *N*-acylhomoserine lactones undergo lactonolysis in a pH-, temperature-, and acyl chain length-dependent manner during growth of *Yersinia pseudotuberculosis* and *Pseudomonas aeruginosa*. *Infect Immun*, 70, 5635-5646.

Yildiz, F. H. and Schoolnik, G. K. 1999. *Vibrio cholerae* O1 El Tor: Identification of a gene cluster required for the rugose colony type, exopolysaccharide production, chlorine resistance, and biofilm formation. *Proc Natl Acad Sci U S A*, 96, 4028–4033.

Yokoseki, T., Kutsukake, K., Ohnishi, K. and Iino, T. 1995. Functional analysis of the flagellar genes in the *fliD* operon of *Salmonella typhimurium*. *Micobiol*, 141, 1715-1722.

Yumoto, I., Yamazaki, K., Hishinuma, M., Nodasaka, Y., Suemori, A., Nakajima, K., Inoue, N. and Kawasaki, K. 2001. *Pseudomonas alcaliphila* sp. nov., a novel facultatively psychrophilic alkaliphile isolated from seawater. *Int J Syst Evol Microbiol*, 51, 349-355.

Zalar, P., Novak, M., de Hoog, G. S. and Gunde-Cimerman, N. 2011. Dishwashers -a man-made ecological niche accommodating human opportunistic fungal pathogens. *Fungal Biol*, 115, 997-1007.

Zalipsky, S., Hansen, C. B., Oaks, J. M. and Allen, T. M. 1995. Evaluation of blood clearance rates and biodistribution of poly(2-oxazoline)-grafted liposomes. *J Pharm Sci*, 85, 133-137.

Zaltsman, N., Ionescu, A. C., Weiss, E. I., Brambilla, E., Beyth, S. and Beyth, N. 2017. Surface-modified nanoparticles as anti-biofilm filler for dental polymers. *PLoS One*, 12, e0189397.

Zhang, J., Brown, J., Scurr, D. J., Bullen, A., MacLellan-Gibson, K., Williams, P., Alexander, M. R., Hardie, K. R., Gilmore, I. S. and Rakowska, P. D. 2020. Cryo-OrbiSIMS for 3D molecular imaging of a bacterial biofilm in its native state. *Anal Chem*, 92, 9008-9015.

Zhang, L. H. 2003. Quorum quenching and proactive host defense. *Trends Plant Sci*, 8, 238-244.

Zhang, W., Shi, Y., Chen, Y., Ye, J., Sha, X. and Fang, X. 2011. Multifunctional pluronic P123/F127 mixed polymeric micelles loaded with paclitaxel for the treatment of multidrug resistant tumors. *Biomaterials*, 32, 2894-2906.

Zhang, X., Wang, L. and Levänen, E. 2013. Superhydrophobic surfaces for the reduction of bacterial adhesion. *RSC Advances*, 3, 1-18.

Zhang, Y. and Miller, R. M. 1994. Effect of a *Pseudomonas* rhamnolipid biosurfactant on cell hydrophobicity and biodegradation of octadecane. *Appl Environ Microbiol*, 60, 2101-2106.

Appendices

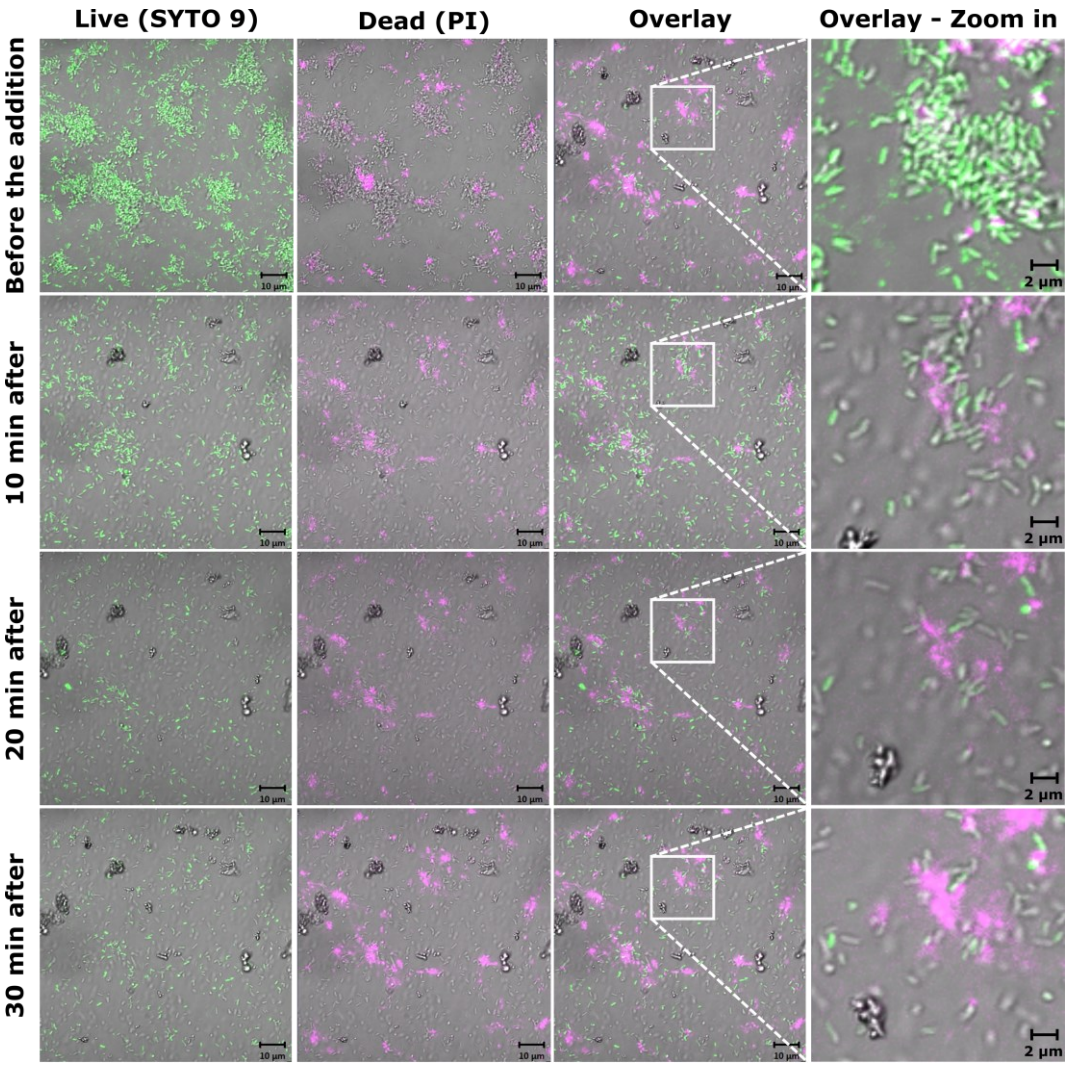
Appendix A Base formulations of laundry products

Appendix Table A: Base formulations of laundry products.

Product	Ingredients	Inclusion level (%)	Function
Liquid detergent	Sodium linear alkylbenzene sulphonate (Na LAS)	5.8	Surfactant
	Sodium lauryl ether sulphonate (SLES) 3EO	4.4	Surfactant
	Alcohol ethoxylate C12-C18-7EO	4.4	Surfactant
	Fatty acid (C12-C18), sodium salts	0.9	Surfactant, rheology control
	Glycerol	2	Solvent, rheology control
	Triethanolamine (TEA)	8.8	pH adjustment, rheology control
	Citric acid	1	pH adjustment
	Methylisothiazolinone/ Benzothiazolinone	0.02	Preservatives
	Demineralised water	to 100	Solvent
Powder detergent	Sodium linear alkylbenzene sulphonate (Na LAS)	20	Surfactant
	Alcohol ethoxylate C12-C18-7EO	8	Surfactant
	Sodium silicate	2	Builder, flow aid
	Sodium sulphate	45	Filler, electrolyte
	Sodium carbonate	20	Alkalinity adjustment
	Sodium carboxymethylcellulose (SCMC)	1	Soil antiredeposition polymer
	Minors	to 100	Processing aid polymers, perfume, optical whitener, moisture

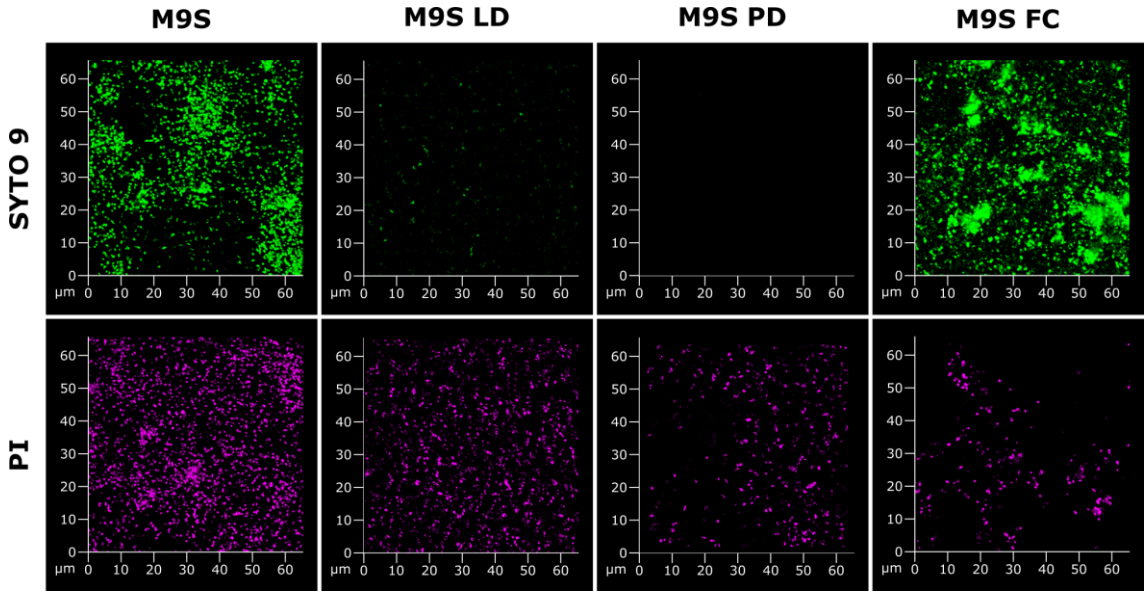
Fabric conditioner	C16-18 Triethanolamine Esterquat (TEA-quat)	4.7	Softener
	Fatty alcohol (C12-C18)	0.4	Co-surfactant, rheology control
	Minors	0.08	Processing aid polymers, perfume, optical whitener, moisture
	Water	to 100	Solvent

Appendix B Addition of powder detergent to an established biofilm of PAO1-N.



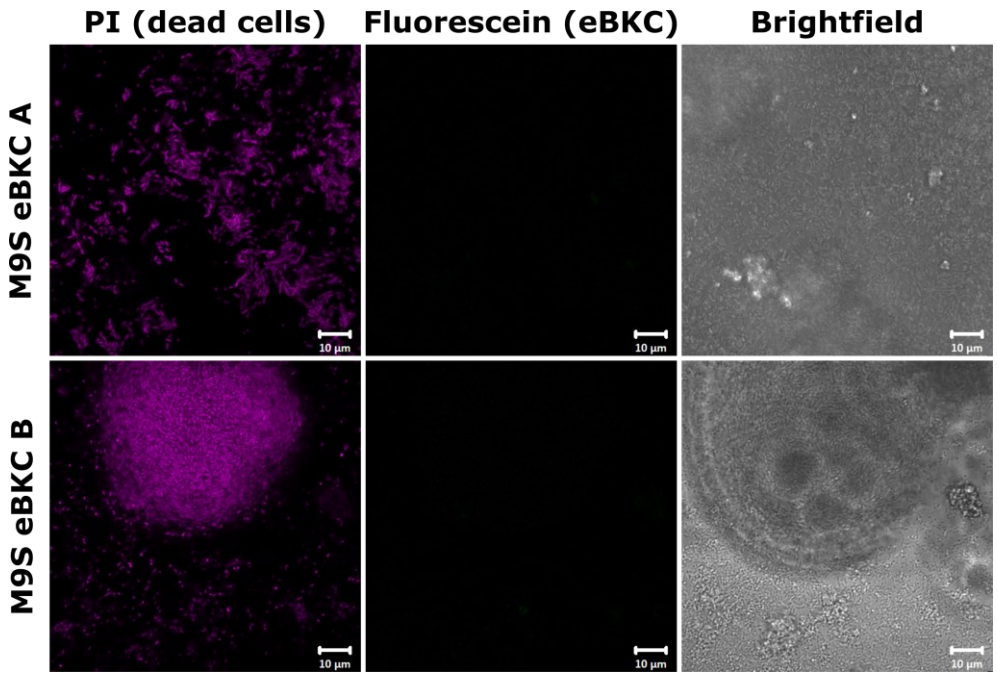
Appendix Figure A: Representative images of PAO1-N cells stained with SYTO 9 show slight loss of fluorescence signal over time when powder detergent is added to the cells. PAO1-N was inoculated into an 8-well glass bottom chamber at an OD_{600} of 0.05 in M9S. The cells were incubated at 37°C under static conditions for 48 h. Live cells were stained with SYTO 9 (green) and dead cells with PI (magenta) and images were taken with a Zeiss CLSM and a 63x objective. M9S containing powder detergent was added to the established biofilm to give a final concentration of 2 mg mL^{-1} and imaged every 5 min over a period of 30 min. Representative 2D images before the addition as well as 10 min, 20 min, and 30 min after the addition are presented. Right panel shows a zoom-in view of the square indicated in the overlay images.

Appendix C Single dye staining (SYTO 9 and PI) of biofilms grown in M9S with or without the addition of liquid detergent, powder detergent, or fabric conditioner.



Appendix Figure B: Representative images of PAO1-N show reduction of viable cells when grown statically in M9S with liquid or powder detergent, whereas no reduction is apparent for the addition of fabric conditioner for biofilms either stained with SYTO 9 or PI. PAO1-N was inoculated into an 8-well glass bottom chamber at an OD_{600} of 0.05 in M9S containing no supplement, liquid detergent (LD, 2.9 mg mL^{-1}), powder detergent (PD, 2 mg mL^{-1}), or fabric conditioner (FC, 2.9 mg mL^{-1}). The cells were incubated at 37°C under static conditions for 48 h. Live cells were stained with SYTO 9 (green, top panel) or dead cells with PI (magenta, bottom panel). Images shown represent different biofilms stained with either SYTO 9 or PI. Z-stack images were taken with a Zeiss CLSM using a 63x objective and 3D top view images are presented.

Appendix D CLSM imaging of biofilms grown with eBKC A or eBKC B does not reveal any fluorescein signal of the eBKC samples.



Appendix Figure C: Representative images of PAO1-N grown with eBKC A or eBKC B do not show any fluorescein signal of the eBKC samples. PAO1-N was inoculated into an 8-well glass bottom chamber at an OD_{600} of 0.05 in M9S containing eBKC A (top, 0.51 mg mL^{-1}) or eBKC B (bottom. 0.55 mg mL^{-1}). The cells were incubated at 37°C under static conditions for 48 h. Dead cells were stained with PI (magenta). Z-stack images were taken with a Zeiss CLSM using a 63x objective and 3D top view images are presented.

Appendix E Size and ζ-potential of encapsulated BKC samples.

Appendix Table B: Size and ζ-potential of encapsulated BKC samples used in this study.

eBKC sample	Size (µm)	ζ-potential (mV)
A	12	35.2
B	11	32.3
C	15	31.5
D	17	30.2
E	14	35.3
F	13	33.9
G	17	32.5
H	18	32.7
I	16	-24.3